Université de Montréal

Les racines cachées de la phytoremédiation :

Décryptage métabolomique des mécanismes d'exsudation racinaire pour la tolérance à l'arsenic

Par

Adrien Frémont

Département de sciences biologiques, Faculté des arts et sciences

Thèse présentée en vue de l'obtention du grade de Philosophiae Doctor (Ph.D.)

en sciences biologiques

Janvier 2024

Université de Montréal

Département de Sciences Biologiques,

Faculté des Arts et des Sciences

Cette thèse intitulée

Les racines cachées de la phytoremédiation :

Décryptage métabolomique des mécanismes d'exsudation racinaire pour la tolérance à l'arsenic

Présentée par

Adrien Frémont

A été évaluée par un jury composé des personnes suivantes

Geneviève Lajoie

Présidente-rapporteure

Frédéric Pitre

Directeur de recherche

Jacques Brisson

Co-directeur

Pierre-Luc Chagnon

Membre du jury

Sébastien Roy

Examinateur externe

Résumé

Les sols représentent une ressource non renouvelable qui soutient 95% de la production alimentaire mondiale. Cependant, les sols sont de plus en plus impactés par la pollution chimique anthropique, menaçant la santé humaine et l'environnement. Parmi les polluants les plus répandus dans les sols, l'arsenic est aussi l'un des plus dommageables pour la santé humaine, touchant près de 200 millions de personnes dans le monde. Pour limiter la contamination des sols, les approches conventionnelles de remédiation reposent principalement sur l'excavation et l'enfouissement des sols contaminés, mais sont incompatibles avec les grandes surfaces concernées par la contamination chimique, pouvant s'étendre sur des millions d'hectares. Une solution novatrice utilise les plantes et les microorganismes associés pour extraire, dégrader ou stabiliser les contaminants *in situ* dans une approche dite de phytoremédiation. L'exsudation d'une grande diversité de métabolites des racines dans le sol environnant serait un mécanisme essentiel qui permet aux plantes de tolérer et de détoxifier les contaminants du sol. Cependant, l'environnement chimique de la rhizosphère et les interactions complexes entre les exsudats racinaires et les contaminants restent largement inconnus. L'objectif de cette thèse est de faire progresser la compréhension de l'exsudation racinaire en réponse à la contamination et de son impact sur le devenir de l'arsenic dans la rhizosphère.

Le **Chapitre 1** rapporte un nouveau système de croissance à petite échelle, hautement reproductible, développé pour capturer et caractériser les exsudats racinaires. En utilisant une analyse métabolomique non ciblée basée sur la chromatographie liquide couplée à la spectrométrie de masse, l'espèce légumineuse *Lupinus albus* a été examinée pour identifier les différences significatives dans l'exsudation d'un large spectre de composés dans la rhizosphère. Cette approche a révélé les classes prédominantes de composés exsudés et leurs variations en réponse à la contamination, notamment les coumarines, connues pour être impliquées dans les stratégies d'acquisition de nutriments chez les plantes, ainsi que l'exsudation inattendue de phytochélatines, connues pour participer à la complexation et à la détoxification intracellulaire de l'arsenic. Pour confirmer l'exsudation des phytochélatines, une expérience supplémentaire a été menée et a permis de valider l'exsudation des phytochélatines comme mécanisme potentiel de tolérance à l'arsenic dans la rhizosphère.

Le **Chapitre 2** examine plus en détail les mécanismes d'exsudation des phytochélatines et leurs interactions avec l'arsenic chez *Lupinus albus*. Grâce à l'inhibition chimique des principales voies de synthèse et d'exsudation des phytochélatines, ce chapitre fournit les premières observations de l'exsudation active de complexes arsenic-phytochélatine chez les plantes, pouvant jouer un rôle

critique dans la détoxification de l'arsenic. À partir de ces observations, le chapitre 2 propose une révision du modèle actuel d'efflux d'arsénite des racines et met en évidence l'exsudation de complexes arsenic-phytochélatine comme mécanisme jusque-là inconnu de détoxification chez les plantes.

Dans le **Chapitre 3**, les différentes stratégies employées en réponse à la contamination à l'arsenic chez *Lupinus albus* et *Salix miyabeana* sont explorées en profondeur par différents essais en pots et à plus grande échelle, directement sur le terrain. Ces deux espèces, illustrant différents traits fonctionnels importants pour la phytoremédiation, révèlent des adaptations distinctes ainsi que des stratégies d'exsudation conservées en réponse à l'arsenic. Les résultats présentés dans ce chapitre révèlent en particulier le rôle central de l'exsudation de phytochélatines dans la rhizosphère de ces deux espèces, pourtant éloignées phylogénétiquement. Notamment, la découverte de complexes phytochélatine-arsenic dans la rhizosphère des deux espèces souligne l'importance des mécanismes extracellulaires dans la détoxification de l'arsenic chez les plantes. De plus, les mesures sur le terrain soutiennent les implications de l'exsudation des phytochélatines en tant qu'adaptation à l'exposition à l'arsenic en conditions réelles. En résumé, ce chapitre fournit de nouvelles perspectives sur l'interaction complexe entre les plantes et les sols lors de la phytoremédiation de l'arsenic.

Dans l'ensemble, cette thèse présente de nouvelles stratégies d'exsudation chez deux espèces phytoremédiatrices majeures et apporte de nouvelles connaissances sur la façon dont l'investissement de ressources dans la rhizosphère peut aider les plantes à tolérer, voire à surmonter, l'effet de la pollution anthropique sur l'environnement. Comprendre ces interactions naturelles est essentiel pour aider à concevoir des stratégies de gestion durables des terres, visant à réduire l'impact à long terme des activités humaines sur les sols.

Mots-clés : Arsenic; complexes arsenic phytochélatine; efflux; phytochélatine; phytoremédiation; pollution; rhizosphère; exsudats racinaires; santé du sol; *Lupinus albus* (lupin blanc); *Salix miyabeana* (saule); métabolomique; tolérance au stress.

Abstract

Soils represent a non-renewable resource supporting 95% of global food production. However, soils face increasing threats from anthropogenic chemical pollution, creating an environmental burden impacting human and environmental health worldwide. Arsenic is one of the most widespread soil contaminants, thought to affect over 200 million people globally and posing substantial threats to public health. To limit contamination of soils, conventional remediation approaches rely on soil excavation and burial, but are incompatible with the extensive problem of soil contamination, often impacting millions of hectares. An innovative solution is to use phytoremediation to harness plants' natural abilities to extract or degrade soil contaminants. The exudation of a wide diversity of metabolites from roots into the surrounding soil is thought to be an essential mechanism used by plants to modify challenging soil environments. However, the extent and variation of root exudation remains largely uncharacterised for many important crops. The objective of this thesis is to advance the understanding of root exudation in response to contamination and how it impacts the fate of arsenic in the rhizosphere.

Chapter 1 reports a novel small-scale but highly reproducible growth system developed to capture and characterise root exudates. Using untargeted liquid chromatography-tandem mass spectrometry-based metabolomic analysis, the leguminous crop white lupin (*Lupinus albus*) was scrutinised to identify significant differences in exuded compounds within the rhizosphere. This approach revealed the predominant classes of exuded compounds in response to contamination, including coumarins, known to be involved in plant nutrient acquisition strategies, as well as unexpected phytochelatin exudation, known to participate in intracellular arsenic complexation and detoxification. A validatory experiment was conducted and confirmed the exudation of phytochelatins as a potential arsenic tolerance mechanism for rhizosphere detoxification.

Chapter 2 further investigates the mechanisms of phytochelatin exudation and their interactions with arsenic in *Lupinus albus*. Through chemical inhibition of key root exudates synthesis and exudation mechanisms, this chapter provides the first evidence that plants actively exude arsenic-phytochelatin complexes, which may function as a critical step for arsenic detoxification and tolerance. From this evidence, Chapter 2 provides a tentative revision of the current model of arsenite efflux from roots and demonstrates that arsenic-phytochelatin exudation may be an active mechanism conferring arsenic tolerance.

In **Chapter 3**, the different strategies employed in response to arsenic contamination in *Lupinus albus* and *Salix miyabeana* were extensively scrutinised in larger-scale pot and field trials, to capture the diversity of rhizosphere metabolites within constructed and real-world soils. These species, illustrating different important functional traits for phytoremediation, revealed distinct as well as more conserved root exudate adaptations to arsenic. Most importantly, the findings presented in this chapter reveal a conserved and pivotal role for extracellular phytochelatin exudation in the rhizosphere of these distantly related phytoremediating species. The discovery of phytochelatin-arsenic complexes in the rhizosphere of both species underscores the importance of extracellular mechanisms in plant arsenic detoxification. Furthermore, field assessments supported the real-world implications of phytochelatin exudation as an adaptive response to arsenic exposure. In summary, this chapter provides novel insights into the complex interplay between plants and soils in arsenic phytoremediation.

Overall, this thesis presents novel exudation strategies in two major phytoremediation species and brings new knowledge on how investment of resources in the rhizosphere can help plants tolerate, or even overcome, the effect of anthropogenic pollution upon the natural environment. Understanding these mechanisms is vital to devise sustainable land management strategies to reduce the long-term impact of human activity on soils around the world.

Keywords: Arsenic; arsenic phytochelatin complexes; efflux; phytochelatin; phytoremediation; pollution; rhizosphere; root exudates; soil health; *Lupinus albus* (white lupin); *Salix miyabeana* (willow); metabolomics; stress tolerance.

Table des matières

Liste des tableaux

Liste des figures

Introduction

Chapitre 1

Chapitre 2

Chapitre 3

Conclusion

Figures supplémentaires

Chapitre 1

Chapitre 2

Chapitre 3

Liste des sigles et abréviations

5OP: 5-Oxoproline

ABC: ATP-binding cassette

As(III): Arsénite

As(V): Arséniate

BSO: L-buthionine sulfoximine

CySSG: Cysteineglutathione disulfide

DA: Differentially abundant

ETM: Elément traces métalliques

FC: Fold change

FBMN: Feature-based molecular networking

GNPS: Global Natural Products Social Molecular Networking

GS-As-PC2: Glutathione-arsenic-phytochelatin 2 complex

GSH: Glutathione

GSSG: Glutathione disulfide

ISCF: Inventaire des sites contaminés fédéraux

iso-oxPC$_3$: Oxidised phytochelatin 3 isomer

LSIP: Liste des substances d'intérêt prioritaire

MELCC: ministère de l'Environnement et de la lutte contre les changements climatiques

NIP: Nodulin26-like Intrinsic Protein

OA: Organic acids

oxPC$_2$: Oxidized phytochelatin 2

oxPC$_3$: Oxidized phytochelatin 3

PC_2: Phytochelatin 2

PC_3: Phytochelatin 3

PCs: Phytochelatins

PCA: Principal component analysis

PERMANOVA: Permutational multivariate analysis of variance

RT: Retention time

Remerciements

Pendant ce travail de thèse j'ai eu besoin du soutien de beaucoup de personnes qui m'ont aidé sans relâche pendant toutes ces années. Je voudrais donc les remercier pour leur aide et pour m'avoir supporté alors que j'avais la tête, pas dans les nuages, mais dans les exsudats racinaires…

Je remercie tous les collègues du laboratoire Pitre, ceux que j'ai côtoyés tout au long de mon parcours et ceux que je n'ai fait que croiser. Un grand merci à mon directeur Frédéric pour ta jovialité et ton soutien tout au long de cette thèse, et pour avoir été une source d'optimisme bien utile. Merci à Nicholas pour avoir été un mentor hors pairs et pour m'avoir enseigné l'art de faire de la bonne science, j'espère avoir bien tout retenu ! Merci à Eszter d'avoir été la meilleure collègue de bureau, de labo, de terrain, et d'être une amie exceptionnelle. Merci pour tes retours toujours « on point » sur mes tentatives, parfois ratées, pour faire des figures simples à comprendre. Merci Ariane, Adèle, Ahmed, la « dream team » du labo avec qui j'ai eu beaucoup de plaisir à travailler toutes ces années. Merci à Emmanuel Gonzalez pour avoir su faire parler les p-values. Et merci aux stagiaires, Isabelle, Bruno, Mathilde, dédiés à leur travail et qui m'ont offert une aide précieuse.

Merci à mon co-directeur Jacques Brisson et toute son équipe, Patrick, Benoit, pour votre soutien et les sorties labo-camping, labo-bar, et les 5 à 7 bien agréables ! Définitivement le laboratoire du savoir vivre ! Merci aussi aux collègues de thèse pour les discussions et les conseils, Andrew, Simon, Kym, Vanessa, Maxime. Merci à toutes les personnes que j'ai croisées à l'IRBV et qui font fonctionner cette belle institution. Merci Dave, l'homme de toutes les situations. Merci Nicolas Boivin à qui je crois avoir rendu tout ce que je lui ai emprunté… enfin je crois… Merci à Joan Laur pour ton aide et la motivation que tu m'as transmise. Merci à Noémie Legault et Christophe Duong Lefebvre pour l'aide sur le terrain. Et un grand merci à l'équipe du secrétariat, votre bonne humeur va me manquer.

Enfin, merci infiniment à ma famille qui m'a toujours soutenu. Merci Erick et Isabelle pour votre amour sans faille et merci de croire en moi. Merci à ma sœur Élodie d'être ma meilleure complice depuis toujours. Merci à ma partenaire de vie et d'aventures Lucie, on ne peut pas rêver mieux pour se lancer dans un avenir qui nous réserve tant de belles surprises.

Je tiens aussi à exprimer ma gratitude envers les organismes et institutions suivants pour leur soutien financier indispensable à la réalisation de ce projet de recherche : la Chaire de recherche en phytotechnologie, Hydro-Québec, le conseil de recherches en sciences naturelles et en génie du Canada (CRSNG), Mitacs, ainsi que le département des sciences biologiques et l'institut de recherche en biologie végétale (IRBV).

“There are few studies more fascinating, and at the same time more neglected, than those of the teeming populations that exist in the dark realms of the soil. We know too little of the threads that bind the soil organisms to each other and to their world, and to the world above.”

Rachel Carson, Silent Spring. 1962

Introduction

Le problème global de la contamination des sols

Les sols, définis comme les gaz, les matières solides et l'eau contenus dans la couverture meuble de la croûte terrestre supérieure, représentent un élément essentiel de la vie sur Terre. Ils abritent 59% de la diversité du vivant, allant de la bactérie, aux mammifères (Anthony et al., 2023) et ils sont une composante primordiale des cycles biogéochimiques, stockant plus de 4 100 gigatonnes de carbone, équivalent à près de cinq fois la quantité de carbone atmosphérique (Le Quéré et al., 2018). Du point de vue des sociétés humaines, les sols représentent une ressource non renouvelable dont dépend 95% de la production alimentaire mondiale (Rodríguez Eugenio et al., 2018) ce qui place la protection des sols au centre des objectifs de développement durable fixés par les Nations Unies, dont 8 des 17 objectifs dépendent d'un environnement pédologique sain (Hou et al., 2020).

Cependant, malgré l'importance cruciale des sols et de leurs fonctions, il est estimé que 33 % des terres sont modérément à fortement dégradées en raison de l'érosion, de la salinisation, du compactage, de l'acidification et de la pollution chimique (FAO & ITPS, 2015). La contamination chimique des sols est un problème d'envergure planétaire qui touche particulièrement les terres agricoles. Bien qu'il n'existe pas encore de système harmonisé de surveillance globale de leur dégradation, de récents rapports dressent un portrait non exhaustif de la contamination des sols dans certaines parties du monde. Ainsi, en Europe, il est estimé que près de 2,8 million de sites présentent une contamination des sols (Payá Pérez & Rodríguez Eugenio, 2018) et qu'environ 137 000 km^2 de terres agricoles, soit 6,24% du total de terres cultivées en Europe sont potentiellement contaminées aux métaux lourds (Tóth et al., 2016). En Chine, il est estimé que près de 20 millions d'hectares de terres agricoles sont contaminés par des métaux lourds, ce qui représente environ 20% des terres agricoles chinoises (Mahar et al., 2016). L'Amérique du nord et le Canada n'échappent pas à ce constat. Au Canada, un total de 23 663 sites contaminés ont été identifiés (ISCF, Conseil du Trésor du Canada, 2016), et à elle seule, la province du Québec répertorie plus de 5 500 sites contaminés et 223 sites miniers abandonnés, créant un fardeau environnemental et financier estimé à plus d'un milliard de dollars (Répertoire des terrains contaminés, MELCC, 2023).

La phytoremédiation

Ce constat mondial alarmant encourage de nombreux projets de réhabilitation des terres pour limiter les impacts de la pollution sur la santé et l'environnement. Au Canada, au cours des 20 dernières

années, 1 040 sites contaminés ont été réhabilités, et depuis 2020, plus d'un milliard de dollars ont été investis pour l'assainissement de 1 316 sites contaminés supplémentaires (PASCF, Environnement et Changement climatique Canada, 2023). Cependant, compte tenu de l'importance des surfaces concernées par la pollution chimique des sols (plusieurs dizaine de millions d'hectares), les technologies conventionnelles de décontamination par excavation suivie de l'enfouissement ou du traitement des sols contaminés ne peuvent à elles seules répondre à la demande grandissante de réhabilitation des terres (Gerhardt et al., 2017). Il est alors crucial d'explorer des techniques alternatives plus écologiques, économiquement viables et capables de restaurer la santé des sols à long terme. Cette nécessité met en évidence le potentiel des technologies comme la phytoremédiation qui exploitent les capacités naturelles des plantes et des microorganismes associés aux racines pour dégrader, extraire ou stabiliser les contaminants du sol (Pilon-Smits, 2005).

Diversité des pollutions chimiques

Pour atteindre les objectifs de décontamination souhaités, les approches de phytoremédiation doivent être finement adaptées au type de contamination, qui ne se limite généralement pas à la présence d'un seul contaminant isolé mais se caractérise souvent par un mélange complexe et hétérogène de contaminants de diverses natures, créant un cocktail toxique aux propriétés variables (Rodríguez Eugenio et al., 2018). Il existe deux grandes catégories de contaminants, classés selon la présence ou non de carbone. D'un côté, les contaminants inorganiques, dépourvus de carbone, regroupent certains éléments du tableau périodique, dont divers métaux et métalloïdes, aussi appelés éléments traces métalliques (ETMs), comme le cadmium (Cd), le zinc (Zn) ou l'arsenic (As). De l'autre, les contaminants organiques, ou xénobiotiques, comportent plusieurs atomes de carbones, parfois organisés en chaines comme dans le cas des hydrocarbures pétroliers. On y retrouve aussi certains pesticides comme le Dichlorodiphényltrichloroéthane (DDT) ou des solvants industriels comme le toluène. Au sein d'un même site pollué, il est courant de retrouver un mélange de ces deux catégories de contaminants. Par exemple, la pollution liée aux déchets pétroliers peut déposer un mélange d'hydrocarbures et d'ETMs comme l'arsenic, cadmium, cobalt, chrome, cuivre, plomb et zinc (Robichaud et al., 2019). D'autres encore, comme les déchets miniers, déposent généralement un mélange toxique de contaminants uniquement inorganiques, comme l'As, Zn ou le Cd (Vázquez et al., 2008).

Les différentes approches de phytoremédiation

L'une des approches les plus efficaces en phytoremédiation utilise l'action combinée des plantes et des microorganismes qui lui sont associés pour la dégradation des contaminants organiques (Pilon-

Smits, 2005). Cette approche, appelée phytodégradation (Figure 1), permet de réduire, et dans certains cas d'éliminer totalement, certains contaminants comme les explosifs ou les hydrocarbures (Cary et al., 2021; Robichaud et al., 2019). Grâce à leurs capacités métaboliques, leur permettant d'utiliser une grande diversité de substrats pour en tirer de l'énergie, les microorganismes sont les principaux acteurs de la dégradation des contaminants organiques (Correa-García et al., 2018). Pour maximiser son efficacité il est donc nécessaire d'optimiser les associations plantes-microorganismes (Bell et al., 2014). Par exemple, la combinaison de l'espèce *Medicago sativa,* inoculée avec des rhizobactéries fixatrices d'azote et des champignons mycorhiziens arbusculaires permet de réduire la présence de polychlorobiphényles (PCB) de 44%, contre 8% pour la plante seule sur un terrain pollué (Teng et al., 2010).

Contrairement aux contaminants organiques qui peuvent être dégradés par l'action des microorganismes, les contaminants inorganiques ne peuvent pas être dégradés (Pilon-Smits, 2005). Ainsi, la phytoremédiation d'un terrain contaminé aux ETMs doit favoriser l'implantation d'espèces capables d'accumuler une grande quantité métaux et capables de produire une grande quantité de biomasse, dans une approche dite de phytoextraction (Figure 1). Par exemple, il est estimé qu'il faudrait des cultures avec un facteur de bioconcentration en métaux de 20 et une production de biomasse de 10 tonnes par hectare pour parvenir à une réduction significative des contaminants en 10 ou 20 ans (Peuke & Rennenberg, 2005). Cependant, il n'existe pas de plante possédant ces deux caractéristiques et la phytoextraction reste un processus lent, qui nécessite souvent plusieurs dizaines d'années pour réduire significativement la contamination (Bhargava et al., 2012). Certaines recherches se tournent alors vers la complémentarité fonctionnelle entre espèces couramment utilisées en phytoremédiation comme *Salix miyabeana* ou *Medicago sativa* (Brereton et al., 2020; Desjardins et al., 2018) ou encore le développement de variétés transgéniques pour optimiser l'absorption et la translocation des contaminants inorganiques et une forte production de biomasse (Cao et al., 2019).

Une troisième approche de phytoremédiation vise à stabiliser la contamination dans les sol et les racines, évitant ainsi la propagation des contaminants dans l'environnement (Pilon-Smits, 2005). Cette approche de phytostabilisation (Figure 1) est notamment utilisée sur d'anciens terrains miniers pour éviter la migration des contaminants inorganiques vers les eaux souterraines, (Dary et al., 2010; Sylvain et al., 2016; Vázquez et al., 2006a). Ainsi, l'espèce légumineuse *Lupinus albus*, ou lupin blanc, est souvent utilisée pour la phytostabilisation de l'As (Fresno et al., 2018; Vázquez et al., 2006a), pour sa capacité à fixer l'As dans ses racines et le sol qui les entoure (Fresno et al., 2016, 2017).

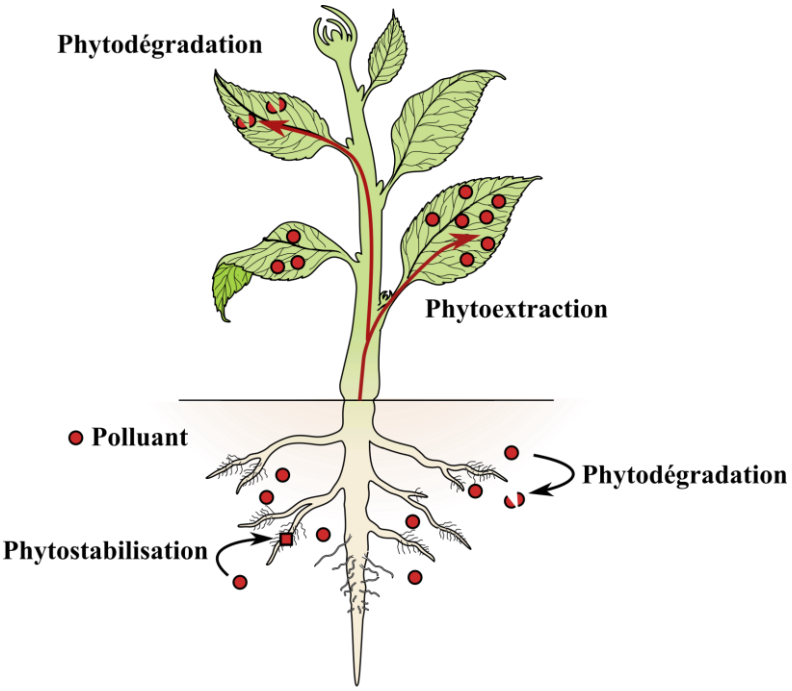

Figure 1 Modèle simplifié illustrant les principaux mécanismes de phytoremédiation dans les plantes et dans la rhizosphère.
Ceux-ci incluent la phytodégradation, qui consiste à dégrader les contaminants organiques dans les tissus de la plante ou dans la rhizosphère (aussi appelé rhizodégradation) ; la phytoextraction qui prend avantage de la capacité de certaines espèces à extraire et accumuler de grandes quantités de contaminants dans les parties aériennes ; la phytostabilisation qui favorise l'immobilisation de formes neutralisées des contaminants autour ou dans les racines. Schéma inspiré de Pilon-Smits, (2005)

La pollution à l'arsenic

Échelle de la pollution à l'arsenic

L'As est l'un des contaminants les plus préoccupants pour les risques liés à son accumulation dans les eaux souterraines et les produits de l'agriculture (Rodríguez Eugenio et al., 2018). Au Canada, il est classé comme carcinogène avéré sans seuil et est inscrit dans le groupe 1 de la liste des substances d'intérêt prioritaire pour sa toxicité et ses risques accrus de pénétration dans l'environnement (LSIP1, 1994). Un empoisonnement chronique à l'arsenic peut en effet causer des dommages importants à l'ensemble des organes du corps humain, causant cancers, neuropathies et maladies cardio-vasculaires (Rahaman et al., 2021). Naturellement présent, il prend la 20ème place des éléments les plus abondants de la croute terrestre, à des concentrations allant de 1,5 à 3 mg kg^{-1} (Mandal & Suzuki, 2002) et menace la santé de plus de 200 millions d'êtres humains dans le monde (Podgorski & Berg, 2020). Cependant, en plus de cette occurrence naturelle, les activités humaines telles que les industries minières et

agricoles ont participé à sa libération à grande échelle dans le sol et les eaux de surface à des concentrations largement supérieures à celles recommandées dans la plupart des pays (Patel et al., 2023). Ces normes limitent par exemple la concentration en arsenic pour une utilisation résidentielle à 12 mg kg^{-1} au Canada (Provoost et al., 2006). Cependant, dans les années 1950, l'As était massivement utilisé comme pesticide ou herbicide, pour ses activités de biocide non sélectif. La production mondiale annuelle d'« arsenic blanc » ou trioxyde d'As pour l'agriculture s'élevait alors à 37 000 tonnes, dont plus de la moitié était utilisée aux États Unis (Mandal & Suzuki, 2002), avant son interdiction dans les années 1990 (ATSDR, 2007).

Effet de l'As sur les plantes

Une fois libéré dans l'environnement, l'As inorganique existe sous deux niveaux d'oxydation majoritaires. La forme principale dans les sols aérobies est l'arséniate (AsO_4^{3-}), noté As(V). Cette forme est un analogue structurel du phosphate (PO_4^{3-}) qui comme l'As(V) possède une structure tétraédrique de taille similaire (Zhang & Selim, 2008). L'arséniate entre ainsi en compétition avec le phosphate dans diverses réactions métaboliques essentielles. Premièrement, chez les plantes, l'As(V) emprunte les transporteurs de phosphate inorganique pour pénétrer les cellules et entre en compétition avec la nutrition en phosphate (Asher & Reay, 1979; Esteban et al., 2003; Ullrich-Eberius et al., 1989). Une fois à l'intérieur des cellules, l'As(V) peut aussi interférer avec les nombreuses réactions essentielles mettant en jeu le phosphate, comme la synthèse d'ATP ou d'ADN, et remplace le phosphate dans les réactions de phosphorylation (Finnegan & Chen, 2012). Dans les sols anaérobies, par exemple dans les sols inondés comme les rizières, l'arsénite [As(III)] est majoritaire (Ma et al., 2008). Cette forme réduite pénètre les racines via les aquaporines Nodulin26-like Intrinsic Proteins (NIPs) (Bienert et al., 2008) et contrairement à l'As(V), l'As(III) n'est pas l'analogue d'un élément essentiel du métabolisme. En effet, l'As(III) doit sa toxicité à sa forte affinité pour les groupements thiols des acides aminés comme la cystéine, et interfère notamment avec la structure secondaire de certaines protéines, pouvant les rendre inactives (Finnegan & Chen, 2012).

Mécanismes de défense

Mécanismes d'efflux

Au cours de l'évolution, les plantes ont élaboré diverses stratégies leur permettant de tolérer des niveaux d'As(III) et d'As(V) plus ou moins élevés. La première étape de défense des plantes en présence d'As(V) dans les racines consiste à réduire 96-100% de l'As(V) en As(III) (Liu et al., 2010). Les premières études ont rapporté l'implication de la protéine ACR2 pour la réduction de l'As chez

les plantes, homologues des réductases d'As(V) identifiées chez la levure (Dhankher et al., 2006), et plus récemment la protéine HAC (High Arsenic Content) chez *Arabidopsis thaliana* puis *Oriza sativa* (Chao et al., 2014; Shi et al., 2016). Une fois réduit, la majorité (60-80%) de l'As(III) peut être rejeté des racines vers l'extérieur, permettant à la plante de réduire la charge toxique présente dans ses racines (Xu et al., 2007; Zhao, et al., 2010a). Cet efflux d'As(III) par les racines est en partie opéré par les transporteurs aquaporines Lsi1, mais d'autres transporteurs sont probablement impliqués, car seul 15-20% de l'efflux total d'As(III) peut être expliqué par les seuls transporteurs Lsi1 (Zhao, et al., 2010a).

Mécanismes de complexation

L'autre fraction d'As(III) qui n'est pas expulsée hors des racines peut être directement détoxifiée grâce à la formation de complexes non toxiques avec les groupements thiols de certains peptides riches en cystéine, comme le glutathion (GSH) ou les phytochélatines (PC). Les PCs sont des oligomères de GSH, lui-même composé de trois acides aminés, l'acide glutamique (Glu), la cystéine (Cys) et la glycine (Gly). Les PCs sont produites par l'ajout successif de GSH par la phytochélatine synthase pour former la structure $[\gamma\text{-Glu-Cys}]_n$-Gly (**Figure 2**), avec n généralement compris entre 2 et 11 (Grill et al., 1989). Premièrement identifiées chez la levure à fission *Schizosaccharomyces pombe* (Kondo et al., 1985), les PCs sont retrouvées chez la plupart des plantes, et certains microorganismes comme les diatomées, certains champignons et chez le nématode *Caenorhabditis elegans* (Clemens, 2006). La synthèse de PCs est rapidement induite par la présence de métaux tels que l'As ou le Cd et se régule par une boucle de rétroaction négative ; les ions AsO_3^{3-}ou Cd^{2+} activent la PC synthase et les PC produites forment des complexes avec les ions activateurs, ce qui termine la réaction (Grill et al., 1989). Ainsi, chez *Arabidopsis thaliana*, jusqu'à 60% de l'As(III) présent dans les racines est complexé sous forme de As(III)-PC_3, As(III)-PC_4, et As(III)-$(PC_2)_2$ (Liu et al., 2010) (**Figure 2**). Les complexes PC-As une fois formés dans la cellule sont transportés dans les vacuoles par des transporteurs de type ATP-binding cassette (ABC), identifiés chez *Oriza sativa* (OsABCC1) et *Arabidopsis thaliana* (AtABCC1, AtABCC2) et localisés sur le tonoplaste (Song et al., 2010; Song, et al., 2014). Les plantes dépourvues de PC synthase ou des transporteurs responsables de leur chargement vers les vacuoles sont extrêmement sensibles à l'As(III) ce qui démontre l'importance de ce mode de détoxification de l'As chez les plantes (Liu et al., 2010; Song et al., 2010).

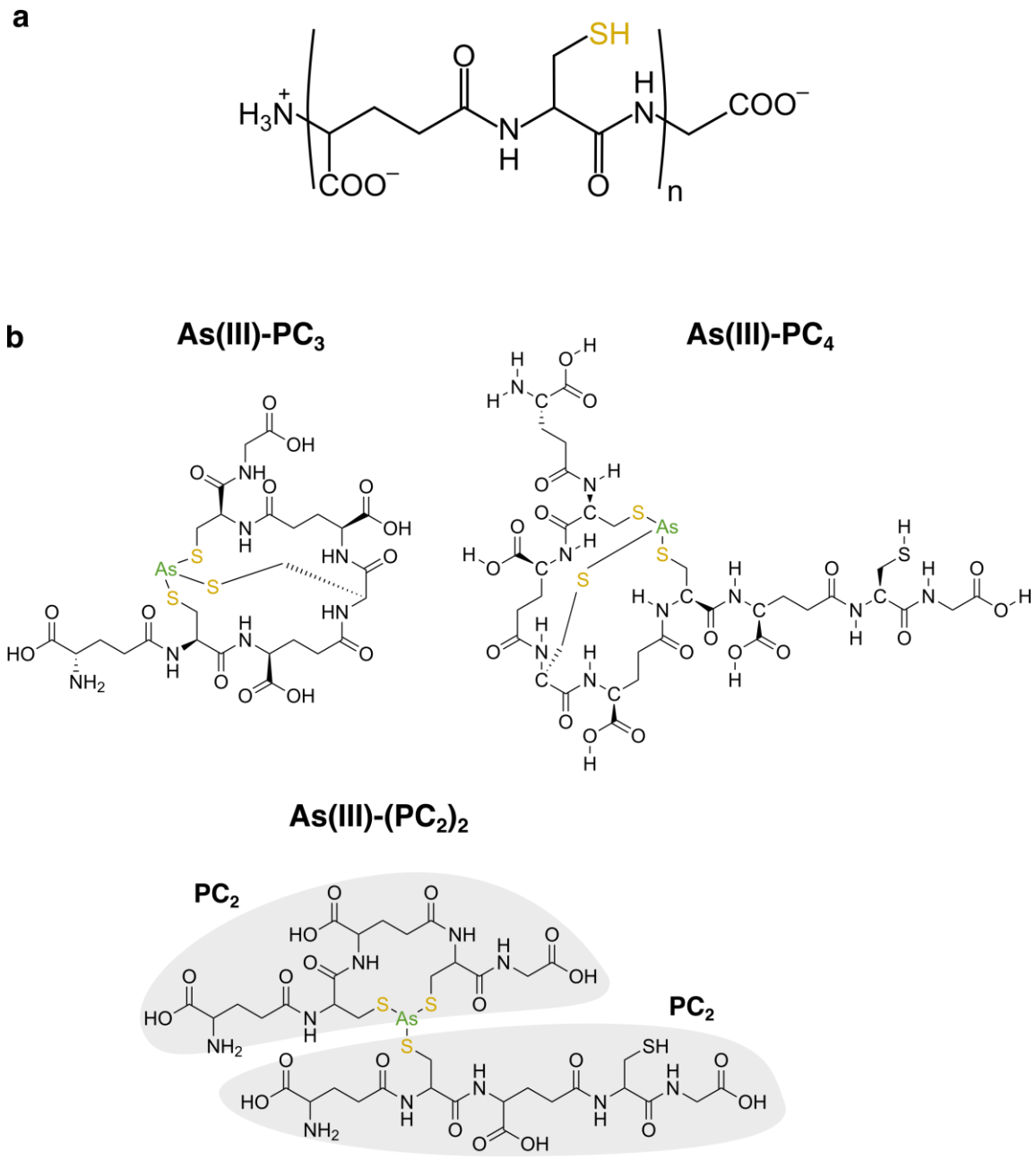

Figure 2 Structure des phytochélatines et des principaux complexes arsenic-phytochélatines. Les PCs sont formés de résidus de glutathionne assemblés en chaines plus ou moins longues. Les groupements thiols (SH) des cystéines possèdent une forte affinité pour l'arsenite et trois groupements thiols peuvent former un complexe avec un ion arsenite. **a** Structure générique d'une molécule de PC. Le motif interne peut se répéter pour former des phytochélatines de taille variable. **b** Exemples de structures connues de complexes As-PC, montrant un complexe As-PC_3, As-PC_4 et As-$(PC_2)_2$ où 2 molécules de PC_2 forment un complexe avec un arsenic.

Les stratégies de défense : exclusion et hyperaccumulation

La plupart des plantes appuient leur stratégie de tolérance à l'As sur la réduction d'As(V) en As(III), l'efflux de celui-ci vers le milieu extérieur via les aquaporines, la complexation de la fraction intracellulaire restante avec les PCs, et la séquestration des complexes formés par l'action des transporteurs ABCC vers les vacuoles (Li et al., 2016). Ce mode de tolérance s'apparente grandement à la stratégie d'exclusion aussi très répandue dans le cas d'autres métaux comme le nickel (Ni), Zn, ou Cd, où les mécanismes physiologiques des plantes dites excluantes visent à minimiser la translocation des éléments toxiques vers les parties aériennes (Krämer, 2010). Celui-ci est en opposition avec la stratégie d'hyperaccumulation employée chez certaines espèces, plus rares (<0,2 % des angiospermes), chez lesquelles la machinerie physiologique permet de diriger de grandes quantités de métaux vers les parties aériennes qui peuvent atteindre des concentrations de plusieurs milliers de mg par kg (Bhargava et al., 2012; Krämer, 2010). Dans le cas de l'As et plus particulièrement de l'espèce hyperaccumulatrice *Pteris vittata*, sa capacité à accumuler jusqu'à 20 000 mg kg^{-1} d'As dans ses parties aériennes (frondes) (Ma et al., 2001), repose sur une chaine de mécanismes physiologiques optimisée pour le transport de l'As du sol vers les parties aériennes (H. Yan et al., 2022) tout en limitant la production de phytochélatines, ce qui empêche l'immobilisation de l'As dans les racines (Zhao et al., 2003) (**Figure 3**). L'une des applications concrètes de ces recherches pour la phytoremédiation de l'As serait le développement de variétés de plantes transgéniques qui combineraient les traits d'espèces hyperaccumulatrices, une production importante de biomasse et une croissance rapide (Zhu & Rosen, 2009). Par exemple, l'insertion du transporteur de phosphate provenant de *Pteris vittata* PvPht1;3 dans des plants transgéniques de tabac permet d'augmenter la concentration en As jusqu'à 81% dans les feuilles en comparaison au phénotype sauvage (Cao et al., 2019). De même, chez *Arabidopsis thaliana,* l'extinction par interférence ARN du gène ACR2, en partie responsable de la réduction de l'As(V) en As(III), permet d'augmenter l'accumulation d'As de 10 à 16 fois dans les parties aériennes des plantes transgéniques, en éliminant la production d'As(III), contournant ainsi son immobilisation dans les racines par les PCs (Dhankher et al., 2006). Ces recherches pourraient également conduire à améliorer les capacités excluantes de certaines espèces, notamment des plantes d'intérêt agronomique, pour limiter l'accumulation d'As dans les parties comestibles (Zhao et al., 2009). Ainsi, des plants mutants d'*Oriza sativa* n'exprimant pas les transporteurs Lsi1 et Lsi2 qui permettent l'influx d'As(III) dans les racines et son transport vers le xylème accumulent jusqu'à 63% moins d'As dans les grains (Ma et al., 2008).

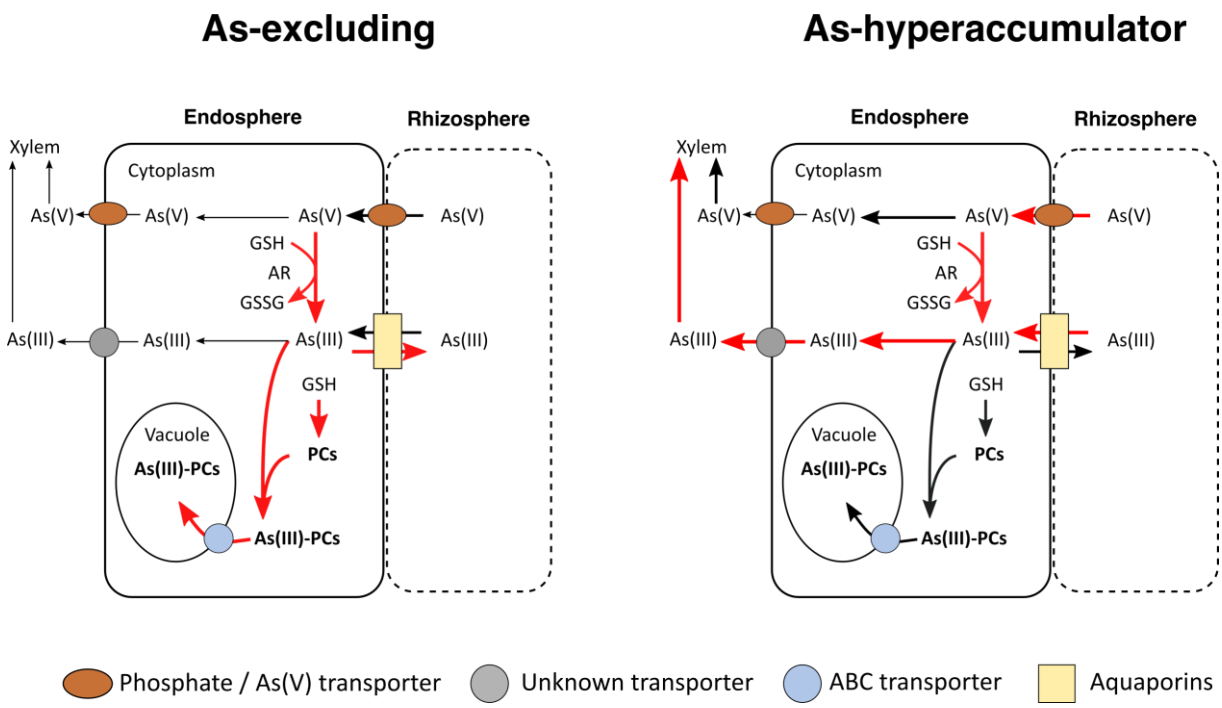

Figure 3 Transport et métabolisation de l'As dans les cellules racinaires.
Plantes excluantes *vs* plantes hyperaccumulatrices. Les plantes excluantes favorisent la prise en charge de l'arsenite dans la cellule par les phytochélatines, dont les complexes sont chargés dans les vacuoles par des transporteurs de type ABC. Les plantes hyperaccumulatrices en revanche, favorisent l'export d'arsenite vers le xylème et sa translocation vers les parties aériennes. Schéma modifié de Li et al., (2016) et Zhao et al., (2009). Les flèches représentent les principales les voies d'entrée, de transport, et du métabolisme de l'arsenic. Les flèches rouges indiquent les voies favorisées pour chacune des stratégies décrites.

Rôles de la rhizosphère

Au-delà des processus physiologiques intracellulaires de défense à l'As discutés plus haut, les processus biochimiques ayant lieu dans la fine couche de sol qui entoure les racines, la rhizosphère, pourraient avoir une influence cruciale sur le sort de contaminants comme l'As dans l'environnement (Fitz & Wenzel, 2002). En effet, l'une des principales adaptations qui permet aux plantes de s'adapter à leur environnement souterrain est l'exsudation racinaire d'une grande diversité de métabolites, pouvant altérer la biodisponibilité de certains métaux dans la rhizosphère (Dessureault-Rompré et al., 2008; Martínez-Alcalá et al., 2010) et qui pourrait renfermer des outils précieux pour la phytoextraction ou la phytostabilisation de l'As (Fresno et al., 2017; Podar & Maathuis, 2022).

Composition des exsudats racinaires

Les exsudats racinaires renferment une grande diversité de métabolites primaires comme des sucres, acides aminés et acides organiques, ainsi qu'un mélange complexe et encore mal connu de composés du métabolisme secondaire, comme ceux issus des voies métaboliques des alcaloïdes, des terpénoïdes ou des shikimates et phénylpropanoïdes (Badri & Vivanco, 2009; Strehmel et al., 2014; van Dam & Bouwmeester, 2016). Représentant jusqu'à 40 % du carbone fixé par la photosynthèse (Badri & Vivanco, 2009), l'exsudation racinaire engendre un coût significatif pour la plante et pourrait être perçue comme une perte et un paradoxe évolutif (Lambers et al., 2009). Mais l'exsudation racinaire permet en réalité aux plantes de mieux tolérer les environnements difficiles, en y modifiant les conditions physico-chimiques, tels que le pH ou le potentiel redox (Figure 4), en solubilisant les éléments essentiels à leur croissance, et en créant un environnement favorable au développement d'une grande diversité de microorganismes, tout en favorisant l'établissement de relations mutualistes entre certains microorganismes et la plante hôte (Akiyama et al., 2005; Bais et al., 2006; Cesco et al., 2010; Dakora & Phillips, 2002; Neumann et al., 2009; Römheld et al., 1984).

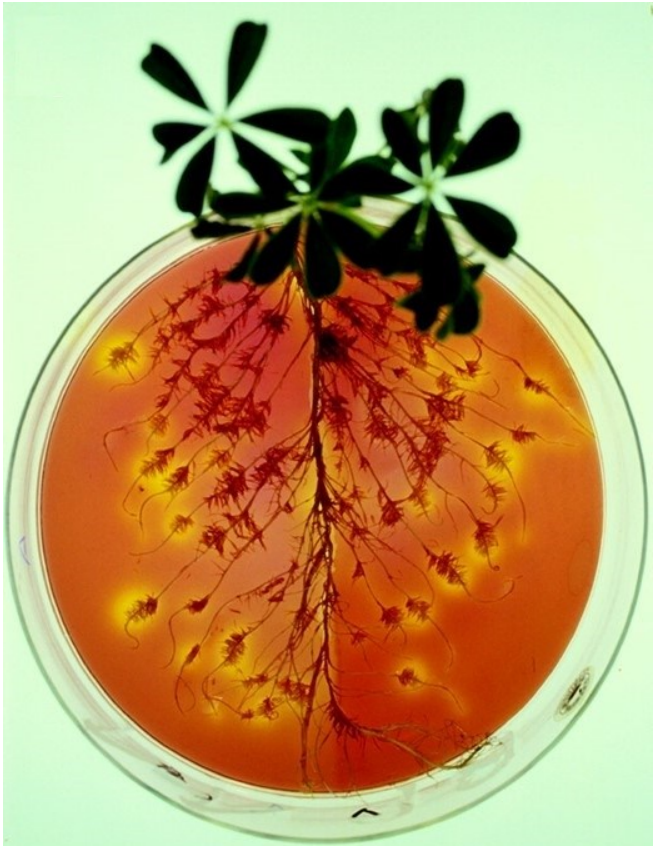

Figure 4 Effet des exsudats racinaires du lupin blanc sur le le pH de la rhizosphère.
Photos de racines de lupin blanc cultivé en hydroponique et mises au contact d'un mélange d'agarose et de pourpre de bromocrésol. Les zones décolorées autour des racines correspondent à une chute de pH induite par les racines. Extrait de F. Yan et al. (2002)

Réponse des exsudats aux stimuli abiotiques

Dans les environnements limités en certains nutriments essentiels pour la plante, comme le phosphate (P) ou le fer (Fe), les plantes ont développé des stratégies d'exsudation racinaire qui permettent de libérer les fractions de nutriments indisponibles pour les rendre accessibles aux racines. Par exemple, chez certaines espèces efficaces pour l'acquisition de P, comme *Lupinus albus* (Lambers et al., 2013), une limitation en P induit l'exsudation de protons (H^+) et d'acides organiques comme, l'acide citrique, oxalique ou encore l'acide malique, abaissant significativement le pH, tout en libérant le phosphate adsorbé aux particules du sol. En effet, dans la rhizosphère, les acides organiques se lient aux oxydes de fer, d'aluminium (Al) ou de calcium (Ca) qui retiennent une grande quantité de P, créant un échange de ligant qui a pour effet de remettre en solution cette fraction de P indisponible pour la plante (Lambers et al., 2006). Dans le cas d'une déficience en Fe, les Poaceae exsudent des acides aminés non-protéiques, appelés phytosiderophores, pour complexer et solubiliser les fractions non solubles de Fe (Dakora & Phillips, 2002). Une autre adaptation pour l'acquisition du Fe, présente particulièrement chez certaines Fabacées, utilise la libération de flavonoïdes, tels que la daidzéine, la génistéine ou le coumestrol, qui par leurs activités réductrices et chélatrices peuvent augmenter la biodisponibilité du Fe (Cesco et al., 2010).

Réponse des exsudats aux stimuli biotiques

À mesure que l'on s'approche des racines, les communautés microbiennes sont de moins en moins diverses et diffèrent significativement d'un sol dépourvu de racines (Edwards et al., 2015). Ceci indique une sélection progressive des microorganismes, le sol agissant comme un « réservoir de semences » dans lequel chaque espèce végétale puise les communautés microbiennes qui lui sont les mieux adaptées (Reinhold-Hurek et al., 2015). D'une part, les exsudats racinaires, riches en composés labiles comme les sucres, les acides organiques ou les acides aminés, offrent un substrat pour le développement microbien et façonnent l'assemblage des communautés en fonction des préférences métaboliques qui leur sont propres (Sasse et al., 2017). Ainsi, chez *Avena barbata*, certains exsudats comme le tryptophane, ou l'acide nicotinique, montrent une métabolisation microbienne rapide, favorisant le développement dans la rhizosphère des microorganismes dits copiotrophes, enrichis aux détriments d'oligotrophes à la croissance plus lente (López et al., 2023; Zhalnina et al., 2018). D'autre part, certains exsudats racinaires montrent des propriétés antimicrobiennes et exercent une forte pression de sélection sur les communautés rhizosphériques (Haichar et al., 2014). Chez *Solanum lycopersicum* et *Glycine max*, certains triterpènes glycosylés de type saponines possèdent des propriétés antimicrobiennes qui ralentissent le développement de certaines souches microbiennes et

avantagent les microorganismes capables d'utiliser les saponines comme source de C (Fujimatsu et al., 2020; Nakayasu et al., 2021). Les exsudats racinaires présentent aussi une diversité de signaux chimiques qui témoigne d'une coévolution entre plantes et microorganismes bénéfiques, comme l'illustre le rôle des exsudats racinaires dans l'établissement des bactéries fixatrices d'azote et des champignons mycorhiziens. Par exemple, l'exsudation de lutéoline, un flavonoïde produit chez *Medicago sativa*, induit l'expression de gènes de nodulation chez une bactérie fixatrice d'azote du genre *Rhizobium* (Peters et al., 1986). Par ailleurs, une classe de terpénoïdes, connus pour induire la germination de la plante parasite striga, les strigolactones, sont aussi reconnues par les champignons mycorhiziens comme signaux de la présence de racines et entrainent la ramification des hyphes (Akiyama et al., 2005)

Réponse à la contamination

Grâce à leurs diverses fonctions chélatrices ou qui augmentent la solubilité d'éléments essentiels pour les plantes, les exsudats racinaires jouent aussi un rôle majeur dans les interactions entre les plantes et les contaminants, particulièrement les contaminants inorganiques tels que le Zn et l'Al (Chen et al., 2017). En réponse à des concentrations d'Al toxiques pour les plantes, certaines espèces exsudent de grandes quantités d'acides organiques (Ma et al., 2001). Chez *Triticum aestivum*, le transporteur ALMT1 (aluminum-activated malate transporter) est responsable de l'exsudation d'acide malique, un chélateur d'Al, ce qui lui confère une résistance à l'Al par une stratégie d'exclusion (Sasaki et al., 2004). Dans le cas du Zn, l'exsudation de nicotianamine, un acide aminé non protéinogène, permet à l'espèce *Arabidopsis halleri* de complexer la fraction de Zn biodisponible et de tolérer des concentrations importantes par un mécanisme d'exclusion des complexes Zn-nicotianamine hors des racines (Tsednee et al., 2014).

Dans le cas de l'As, la majorité des études sur les rôles de l'exsudation racinaire se sont concentrées sur l'hyperaccumulatrice *Pteris vittata* (Das et al., 2017; X. Liu et al., 2017; Tu et al., 2004; Wu et al., 2018). Chez cette espèce, les acides organiques exsudés en réponse à l'As semblent jouer un rôle pour la solubilisation des fractions non solubles d'As (Wu et al., 2018). De plus, en présence d'arsenic l'exsudation racinaire semble participer au modelage de communautés microbiennes efficaces pour le recyclage d'éléments essentiels comme le S, N et P, participant au développement de *Pteris* sur les sols riches en As (Das et al., 2017). Chez les plantes excluantes comme *Lupinus albus*, les exsudats racinaires pourraient aussi jouer un rôle majeur déterminant le devenir de l'As dans la rhizosphère. Pour développer la recherche dans cette direction, il est nécessaire de développer des

méthodes avancées de capture et de caractérisation des exsudats racinaires. Ceci permettrait de révéler la diversité des stratégies d'adaptation à l'As liées aux exsudats chez différentes espèces.

Les défis de la caractérisation des exsudats racinaires

La rhizosphère, qui s'étend sur quelques millimètres autour des racines, représente un environnement souterrain difficile à explorer en raison de la diversité des sols et de l'activité foisonnante des microorganismes qui s'y développent. Cette zone constitue une frontière complexe pour la recherche, tant dans les domaines de l'écologie, de l'agriculture que de la phytoremédiation (Ahkami et al., 2017; Chen et al., 2017; Faucon et al., 2017). L'échantillonnage des exsudats racinaires pose notamment un défi technique, souvent surmonté par la simplification du milieu de croissance à l'aide de méthodes telles que la culture hydroponique ou aéroponique (Oburger & Schmidt, 2016). Ces approches offrent l'avantage d'un accès non destructif aux racines, d'un échantillonnage simplifié des exsudats racinaires, de l'estimation des taux d'exsudation, ainsi que du contrôle exhaustif et précis des concentrations de nutriments ou de contaminants (Oburger & Jones, 2018). Cependant, les techniques de culture hydroponiques font abstraction de l'impact des interactions entre le sol et les racines qui, par rétroaction, modulent l'architecture racinaire et ultimement, altèrent l'exsudation (Sasse et al., 2020).

Plusieurs méthodes ont été développées pour permettre la collecte d'exsudats racinaires à partir de racines non altérées. L'une d'elles utilise des « rhizo-box » conçues pour isoler les racines dépourvues de sol sans les perturber et d'en extraire une solution de capture chargée en exsudats (Oburger et al., 2013). Celle-ci offre l'avantage d'un échantillonnage non destructif mais demande l'installation d'un système expérimental complexe (Oburger & Jones, 2018). D'autres méthodes simples à mettre en œuvre permettent d'extraire les exsudats racinaires présents dans la gaine racinaire ou « rhizosheath » (Pang et al., 2018; Ryan et al., 2012). Cette gaine de sol qui adhère aux racines se forme notamment grâce à la libération de mucilages par les racines et concentre une grande partie des processus rhizosphériques (McCully, 1999; Pang et al., 2017). Cette méthode, qui par simplification peut être désignée sous le terme d'« extraction de la rhizosphère » (Neumann & Römheld, 2007), a l'avantage de s'adapter à tous types de sols, du plus simple comme le sable de silice, qui limite l'adsorption des exsudats sur les particules du sol, au plus complexe, comme les sols naturels (Sasse et al., 2020). Cependant, les frontières de l'étude de l'exsudation racinaire ne résident pas uniquement dans les techniques de capture mais aussi dans la caractérisation chimique de l'extrême diversité des molécules qui la composent.

La diversité des métabolites spécialisées produites par les plantes est de l'ordre de 100 000 à 1 000 000 de métabolites produites dans le règne végétal, résultant d'une longue évolution et d'une adaptation à

diverses niches écologiques (Maeda & Fernie, 2021). Bien que les exsudats racinaires ne représentent qu'une fraction de cette vaste diversité métabolique végétale, la rhizosphère peut néanmoins contenir des milliers de métabolites différents. Ceux-ci incluent à la fois les composés produits par le métabolisme microbien appelés « natural products », et ceux provenant de la matière organique du sol (Pétriacq et al., 2017). Ainsi, il a été montré qu'en conditions axéniques, les plantes libèrent dans la rhizosphère une diversité significativement différente de métabolites qu'en présence de microorganismes (McLaughlin et al., 2023). En effet, les microorganismes peuvent éliciter une réponse exsudative de la plante, et réciproquement, la plante peut induire une réponse métabolique chez les microbes, dans ce qui est considéré comme un dialogue moléculaire rhizosphérique (Haldar & Sengupta, 2015; X. Wang et al., 2023).

Les approches contemporaines visant à caractériser ce milieu complexe reposent principalement sur la séparation chromatographique des métabolites présents dans les échantillons d'exsudats, suivie de leur détection et identification de façon non ciblée par spectrométrie de masse (van Dam & Bouwmeester, 2016). Après plus d'un siècle de développement depuis son invention en 1920, la spectrométrie de masse est devenue l'outil prédominant pour la caractérisation des métabolites de faible poids moléculaire, suscitant un regain d'intérêt pour sa capacité à offrir une lecture directe de l'état d'un système biologique (Aksenov et al., 2017). Englobée sous le terme de métabolomique, cette technologie est complémentaire aux techniques de métagénomique et métatranscriptomique par sa capacité à décrypter les produits de l'expression des gènes et de leurs interactions avec l'environnement (Aksenov et al., 2017). Cependant, les méthodes computationnelles développées pour la métabolomique n'ont pas suivi le même essor que celles dédiées à la métagénomique et à la métatranscriptomique. Le plus souvent, seule une petite fraction (<10%) des milliers de signatures spectrales (ou « features ») générées dans l'analyse métabolomique d'un environnement sont traduites en informations biologiques (da Silva et al., 2015). De nombreux outils bioinformatiques visent à combler ce manque par des approches toujours plus poussées, appuyées notamment par des réseaux collaboratifs globaux de partage d'informations spectrales telles que GNPS (Wang et al., 2016) (**Figure 5**). Ou encore s'appuient sur le développement de l'intelligence artificielle et particulièrement de l'apprentissage profond, pour l'identification *de novo* de molécules inconnues, uniquement à partir de leurs signatures spectrales (Cai et al., 2023). Ainsi, aujourd'hui ces outils permettent l'identification et l'annotation d'une part toujours plus importante des molécules présentes dans un milieu et tendent de plus en plus vers la caractérisation exhaustive des métabolites qui modèlent l'environnement de la rhizosphère (Elser et al., 2023; Lai et al., 2021; McLaughlin et al., 2023).

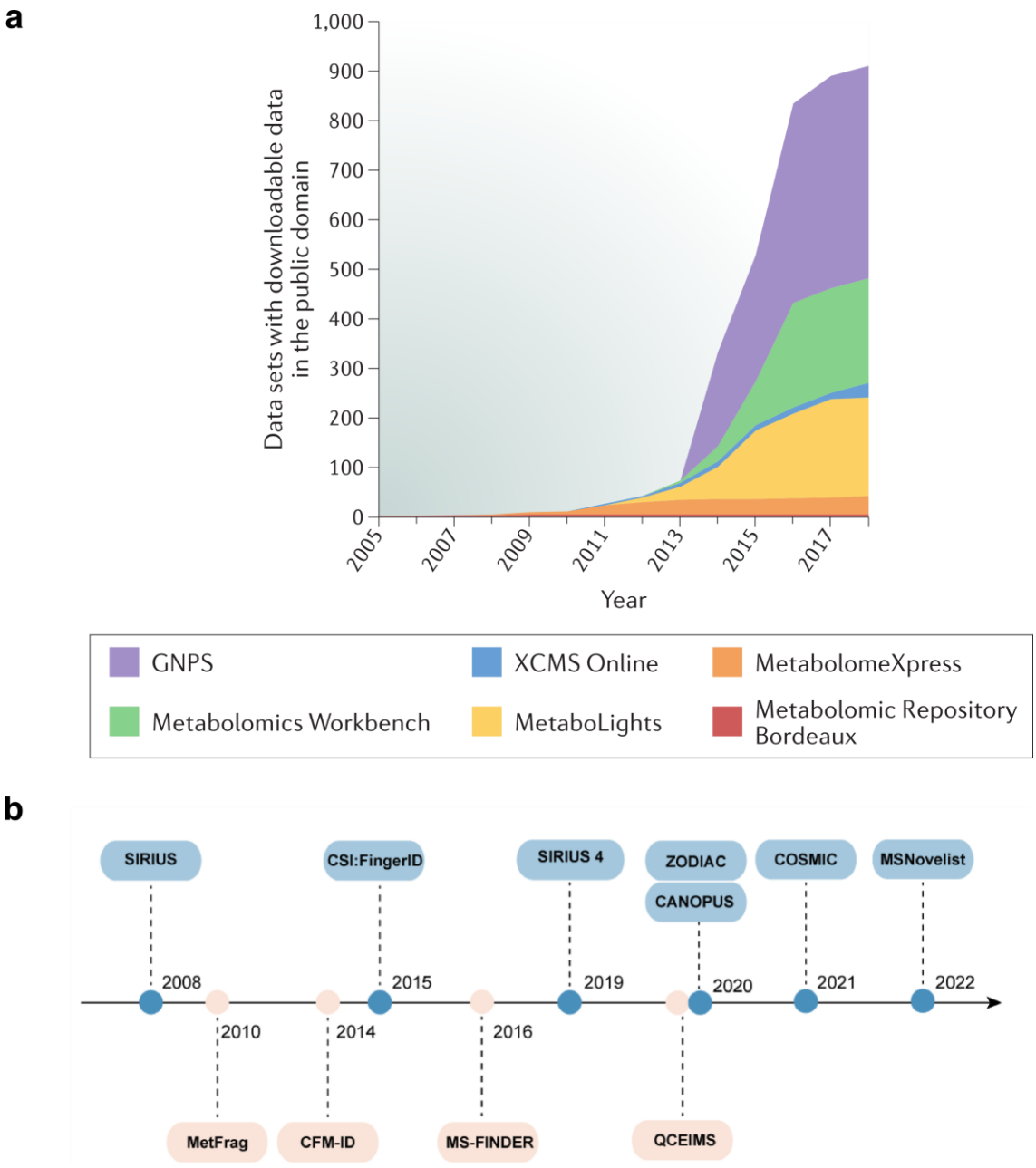

Figure 5 Évolution temporelle du développement d'outils computationnels en spectrométrie de masse.

a Utilisation croissante du partage des données de métabolomique pour faciliter l'identification de métabolites à partir des spectres. **b** Développement massif des outils de bioinformatique permettant l'identification *de novo* de métabolites inconnus. Extraits de Aksenov et al. (2017) et Cai et al. (2023). GNPS : Global Natural Products Social Molecular Networking

Objectifs de la thèse

La rhizosphère s'établit à l'échelle du millimètre dans la zone d'influence des racines. Mais à l'échelle d'une plantation, cette zone peut représenter la majorité de l'environnement souterrain, et est reconnue comme l'un des principaux moteurs des processus de décontamination. Malgré son importance, la rhizosphère reste une boite noire, aux fonctions façonnant les cycles biogéochimiques, mais dont les rouages moléculaires commencent seulement à se laisser apercevoir, notamment grâce aux avancées dans les méthodes d'analyse de son environnement chimique et biologique. **Pour cette thèse, mon objectif est de comprendre et de décrire les mécanismes d'interaction à l'échelle moléculaire entre les exsudats racinaires et la contamination dans la rhizosphère.** Pour ce faire, je me suis concentré sur l'arsenic comme modèle de contamination, pour son caractère ubiquitaire et encore aujourd'hui, menaçant l'environnement et la santé de plusieurs centaines de millions d'êtres humains. Le travail de recherche présenté ici s'articule en trois objectifs principaux, chacun présenté dans un chapitre sous forme de publication scientifique revue par les pairs, ou de manuscrits soumis, ou en voie d'être soumis pour publication.

La capture de la rhizosphère et la caractérisation des métabolites exsudées par les racines est souvent décrite comme l'une des principales limites à leur étude, principalement pour son caractère difficile d'accès et la complexité chimique de ce microenvironnement. Dans le **Chapitre 1**, mon objectif est de mettre en place une méthode de culture et d'échantillonnage des exsudats racinaires pour établir le portrait de l'exsudation en réponse à l'arsenic chez le lupin blanc (*Lupinus albus*), une espèce modèle pour la phytostabilisation de l'arsenic. Pour m'affranchir des obstacles méthodologiques, j'ai développé un système de croissance et une méthodologie d'extraction qui permet de capturer les exsudats en utilisant du sable de silice comme substrat inerte. Après de nombreux essais, cette méthode s'est imposée pour sa capacité à limiter les dommages causés aux racines et éliminant les problèmes d'interférence du sol, tout en gardant les caractéristiques physiques d'un sol naturel. Après extraction et concentration des extraits de rhizosphère, j'ai utilisé la chromatographie liquide couplée à un spectromètre de masse pour établir le profil des molécules présentes avec une résolution de pointe. En comparant les abondances de chaque molécule exsudée, avec ou sans arsenic, j'ai pu mettre à jour certaines adaptations exsudatives jusque-là inconnues, qui pourraient participer à la tolérance du lupin à l'arsenic et à ses capacités de plante stabilisatrice.

Sur la base d'une meilleure compréhension des adaptations exsudatives du lupin face à l'arsenic et de l'optimisation des méthodes de capture des exsudats racinaires, le **Chapitre 2** se concentre ensuite sur la caractérisation des mécanismes d'exsudation et des produits de l'interaction entre les exsudats

racinaires du lupin et l'arsenic dans la rhizosphère. Ainsi, dans le Chapitre 2, j'utilise des inhibiteurs chimiques pour interrompre la synthèse et le transport de certains exsudats de défense du lupin. En parallèle, j'utilise la spectrométrie de masse pour la caractérisation *in vitro* puis *in planta* des produits de l'interaction entre l'arsenic et certains exsudats du lupin. Mis ensemble, ces résultats offrent une compréhension approfondie d'un nouveau mécanisme d'exsudation et de détoxification de l'arsenic chez le lupin, validant ainsi certaines hypothèses émises dans le Chapitre 1.

Les résultats décrits dans le Chapitre 1 et le Chapitre 2 découlent d'expériences en milieu contrôlé et font abstraction de la complexité des interactions pouvant avoir lieu dans les sols complexes en présence de microorganismes. De plus, ils n'abordent pas les adaptations exsudatives pouvant être présentes chez d'autres espèces d'intérêt en phytoremédiation. Dans le **Chapitre 3**, l'objectif est de répondre à ce manque, tout d'abord en mettant en place une expérience en serre qui incorpore un sol organique avec l'ajout de compost, et qui introduit une nouvelle espèce d'importance centrale en phytoremédiation pour ses capacités de croissance rapide et de tolérance aux contaminants, le saule *Salix miyabeana*. Enfin, le Chapitre 3 permet une incursion dans le « monde réel » en explorant l'exsudation racinaire du saule en réponse à la contamination, directement sur un terrain de phytoremédiation mis en place dans la région de Montréal. Pour répondre aux objectifs de ce dernier Chapitre, j'ai utilisé une suite d'outils de bioinformatique que nous avons développée au sein du laboratoire pour permettre la caractérisation approfondie de l'environnement complexe de la rhizosphère et de la diversité des métabolites qui la composent. Ce chapitre offre tout d'abord une vue d'ensemble de l'exsudation racinaire chez ces deux espèces. Il dévoile ensuite les réponses exsudatives à l'arsenic spécifiques à chaque espèce et leur réponse commune. Enfin, les adaptations du saule à l'arsenic, initialement décrites en serre, sont confrontées à la complexité du terrain, mettant en évidence les adaptations préservées lors du passage d'un système contrôlé à un système complexe soumis aux variations naturelles de l'environnement. Ces résultats montrent la diversité des mécanismes rhizosphériques de défense contre l'arsenic, ainsi que les adaptations conservées chez deux espèces éloignées d'un point de vue évolutif, offrant des perspectives pour de nouvelles stratégies de phytoremédiation de l'arsenic.

Chapitre 1 – Enrichissement de phytochélatines et de coumarines dans les exsudats racinaires du lupin blanc exposé à l'arsenic.

Phytochelatin and coumarin enrichment in root exudates of arsenic-treated white lupin

Adrien Frémont[1], Eszter Sas[1], Mathieu Sarrazin[2], Emmanuel Gonzalez[3,4], Jacques Brisson[1], Frédéric Emmanuel Pitre[1,5], Nicholas James Beresford Brereton[1]

[1] University of Montreal – Institut de Recherche en Biologie Végétale (IRBV), 4101 Sherbrooke St. E, Montreal, QC H1X 2B2, Canada

[2] Collège de Maisonneuve – CÉPROCQ, 6220 Sherbrooke St. E, Montréal, QC H1N 1C1, Canada

[3] Canadian Centre for Computational Genomics (C3G) - Department of Human Genetics, McGill University, 740 Dr. Penfield avenue, Montreal, QC H3A 0G1, Canada.

[4] Microbiome Research Platform - McGill Interdisciplinary Initiative in Infection and Immunity (MI4), Genome Centre, McGill University, Montreal, QC, Canada

[5] Montreal Botanical Garden - 4101 Sherbrooke St. E, Montreal, QC H1X 2B2, Canada

Publié dans Plant, Cell & Environment, 45(3), 936-954.

https://doi.org/10.1111/pce.14163

Abstract

Soil contamination with toxic metalloids, such as arsenic, can represent a substantial human health and environmental risk. Some plants are thought to tolerate soil toxicity using root exudation, however, the nature of this response to arsenic remains largely unknown. Here, white lupin plants were exposed to arsenic in a semi-hydroponic system and their exudates were profiled using untargeted liquid chromatography tandem mass spectrometry. Arsenic concentrations up to 1 ppm were tolerated and led to accumulation of 12.9 μg As g^{-1} dry weight (DW) and 411 μg As g^{-1} DW in aboveground and belowground tissues, respectively. From 193 exuded metabolites, 34 were significantly differentially abundant due to 1 ppm arsenic, including depletion of glutathione disulphide and enrichment of phytochelatins and coumarins. Significant enrichment of phytochelatins in exudates of arsenic-treated plants was further confirmed using exudate sampling with strict root exclusion. The chemical tolerance toolkit in white lupin included nutrient acquisition metabolites as well as phytochelatins, the major intracellular metal-binding detoxification oligopeptides which have not been previously reported as having an extracellular role. These findings highlight the value of untargeted metabolite profiling approaches to reveal the unexpected and inform strategies to mitigate anthropogenic pollution in soils around the world.

Keywords: *Lupinus albus* (white lupin); Root exudates; Arsenic; Phytoremediation; Metabolomics; Stress tolerance; Phytochelatin; Rhizosphere.

Introduction

High arsenic concentrations can be naturally present in soil and groundwater but are also generated from anthropogenic industrial and agricultural activities (Han et al., 2003; Matschullat, 2000) which can damage the environment and cause risk to human health (Naujokas et al., 2013). In Canada, more than 7,000 arsenic and other metal(loid)-contaminated sites are listed as highly concerning by the Canadian government (Federal Contaminated Sites Inventory, 2019; First Priority Substances List, 1988), but remediation is often hampered due to the high economic cost of conventional methods involving soil removal and burial. Some plants have evolved efficient arsenic tolerance mechanisms allowing them to colonise soils which are naturally high in arsenic concentrations (Meharg & Hartley-Whitaker, 2002), including translocation and accumulation into aerial biomass, as well as stabilisation of arsenic in roots and soils (Raab et al., 2007). One way in which arsenic contaminated soils could be rejuvenated is to exploit these natural plant mechanisms for phytoremediation, the in-situ rehabilitation of soils by arsenic extraction or phytostabilisation , as a sustainable alternative to more conventional remediation strategies (Pilon-Smits, 2005).

In aerobic soils, arsenic primarily occurs as the arsenate As(V) oxyanion (AsO_4^{3-}) which is an analogue of the phosphate oxyanion (PO_4^{3-}) and can be taken up by roots through phosphate transporters (Asher & Reay, 1979; Ullrich-Eberius et al., 1989). Once inside root cells, over 90% of As(V) can be reduced to As(III) by endogenous arsenate reductases (Chao et al., 2014; Dhankher et al., 2006). In anaerobic soils, arsenic primarily occurs as arsenite As(III), and can directly enter roots through aquaporins (Ma et al., 2008). Within root cells, As(III) can be translocated to other organs (Wang et al., 2018), extruded back into the soil (Xu et al., 2007; Zhao, et al., 2010b), or form complexes with thiol (-SH) groups of oligopeptides, such as glutathione (γ-glutamate-cysteine-glycine: GSH) and phytochelatins ([γ-glutamate-cysteine]$_n$-glycine: PC_n), which can then be loaded into the vacuoles via ABC-type transporters (Li et al., 2016; Mishra et al., 2017; Raab et al., 2004; Schmöger et al., 2000; Song, Yamaki, et al., 2014). As(III)-thiol complexation and compartmentalisation in the vacuoles are considered as the main mechanisms for arsenic detoxification and stabilisation in the roots of non-hyperaccumulating plant species (Zhao et al., 2009). Efflux of As(III) back into the soil is known to occur rapidly in *Arabidopsis thaliana* and other non-hyperaccumulating species; while there is evidence that aquaporins play a partial role, explaining up to 20% of As(III) efflux (F.-J. Zhao, Ago, et al., 2010b), the major mechanisms explaining As(III) efflux in non-hyperaccumulators remain to be elucidated (Li et al., 2016; Zhao, et al., 2010a).

Interactions within the rhizosphere (the plant-soil interface) may also influence the fate of arsenic in contaminated soil as the bioavailability of metal(loid)s in soils can be strongly altered by plants (Dessureault-Rompré et al., 2008; Fresno et al., 2016, 2017; Martínez-Alcalá et al., 2010). Plant influence on biochemistry within the rhizosphere is thought to be driven mainly through root exudation, which underlies important processes of nutrient acquisition and may also influence arsenic bioavailability (Fitz & Wenzel, 2002). However, despite the growing interest in understanding these mechanisms, relatively few studies have explored the interactions between root exudates and arsenic, partly due to the challenges in characterising complex chemical mixtures within the rhizosphere (Oburger & Jones, 2018).

Root exudates are mainly composed of low molecular weight compounds such as carbohydrates, amino acids, phenolics, saponins, fatty acids, and organic acids (OA) such as oxalate, malate and citrate, as well as other diverse and largely uncharacterised plant secondary metabolites (Strehmel et al., 2014; Tsuno et al., 2018; van Dam & Bouwmeester, 2016), which are known to collectively influence nutrient acquisition and interactions with microbes in the rhizosphere (Badri & Vivanco, 2009; Dakora & Phillips, 2002). OA exudates can alter the phosphate (P) soil bioavailability through ligand exchange, particularly in P-efficient crops such as white lupin (Dinkelaker et al., 1989; Neumann & Römheld, 1999; Wen et al., 2019). Phenolics such as flavonoids and coumarins are thought to help plants acquire Fe through Fe(III) oxides reduction and complexation mechanisms (Cesco et al., 2010; Chen et al., 2017; Schmid et al., 2014). Studies have suggested that recruitment and establishment of plant beneficial microorganisms is mediated by root exudates, such as genistein, an isoflavonoid involved in the symbiotic association of legumes and nitrogen fixing bacteria (Kosslak et al., 1987; C.-W. Liu & Murray, 2016; Schmidt, 1994). Similarly, saponins could help shape complex rhizosphere microbial communities and provide protection from pathogens and competing plants (Fujimatsu et al., 2020; Nakayasu et al., 2021; Oleszek & Jurzysta, 1987; Tsuno et al., 2018).

Despite the diversity of exuded compounds, only OAs are known to directly neutralise contaminants in the rhizosphere (Chen et al., 2017; Kochian, 1995; Lin & Aarts, 2012). Exuded OAs, such as oxalate, malate, citrate and nicotianamine can potentially form stable and non-phytotoxic complexes with metal(loid)s, and have been associated with tolerance to aluminium in *Phaseolus vulgaris* (Miyasaka et al., 1991; Ryan et al., 2001), cadmium in *Solanum lycopersicum* (X. F. Zhu et al., 2011) and zinc in *Arabidopsis halleri* (Tsednee et al., 2014). For arsenic, research has focussed on the arsenic hyperaccumulator *Pteris vittata* (Ma et al., 2001), which uses OA exudation to indirectly solubilise arsenic from As minerals and increase arsenic uptake (Das et al., 2017; Liu et al., 2017; Tu et al., 2004;

Wu et al., 2018). However, less is known of root exudate adaptations to arsenic in non-hyperaccumulating species. For instance, some species of ferns and trees show a reduction in exuded OAs, amino acids and carbohydrates in the presence of arsenic (Johansson et al., 2008; Tu et al., 2004), while others have increased OA exudation (Mei et al., 2021). The extent and variation of root exudation in response to arsenic has yet to be examined in detail and plant species beyond *Pteris vittata* may possess unknown exudation mechanisms in response to arsenic.

To address this, the leguminous crop *Lupinus albus* (white lupin), with high tolerance to arsenic, high phosphate acquisition efficiency as well as extensive root exudation of organic acids and phenolics (Lambers et al., 2013; Vázquez et al., 2009; Weisskopf, Tomasi, et al., 2006) was subjected to a range of As(III) and As(V) concentrations within a controlled growth environment designed to capture exudates. Untargeted metabolite profiling was then used to elucidate the exudation response to successfully tolerated levels of arsenic.

Methods

Experimental design, plant growth and arsenic quantification

White lupin seeds (*Lupinus albus* L. cv. AMIGA) were surface sterilised in consecutive baths of 70 % ethanol, 1% sodium hypochlorite and sterile Milli-Q water. Seeds were germinated on sterile moist filter paper and seedlings were transferred to 7.6 × 15.2 cm 25 µm nylon mesh growth pouches containing 700 mL of washed and autoclaved silica sand as a growth medium (**Figure 1**). Plants were supplied twice a week with 65 mL Hoagland nutrient solution (1600 µM N, 200 µM P, 605 µM K, 400 µM Ca, 100.2 µM S, 100 µM Mg, 5 µM Cl, 2.5 µM B, 0.2 µM Mn, 0.2 µM Zn, 0.05 µM Cu, 0.05 µM Mo, 4.5 µM Fe) prepared with Milli-Q water and adjusted to pH 6 with sodium hydroxide 10%, when leachate was also collected beneath each growth pouch. Growth chamber conditions were LED lighting with photosynthetic light density of 150 µmol m^{-2} s^{-1}, a light / dark period of 18/6 hours, temperature of 24.4 ± 0.2 / 22.5 ± 0.1 °C, and 71.3 ± 2 / 76.3 ± 2 % relative humidity.

After 21 days of growth, plants were either left as controls or exposed to one of five concentrations of either arsenite As(III), or arsenate As(V) added as sodium (meta)arsenite $NaAsO_2$ or sodium heptahydrate arsenate $Na_2HAsO_4.7H_2O$. Treatments were applied five times at 2–3-day intervals until plants were harvested after 35 days of growth. Arsenic (element) concentrations were: 0 mg L^{-1} (control), 0.05 mg L^{-1} (0.7 µM), 0.1 mg L^{-1} (1.3 µM), 0.5 mg L^{-1} (6.7 µM), 1 mg L^{-1} (13.3 µM) and 5 mg L^{-1} (66.7 µM) and were prepared in Hoagland nutrient solution. A randomised block design was

used with five replicate plants for each dose and each arsenic form (5 blocks, 60 plants in total). Unplanted controls were also included with the same treatments.

Signs of canopy toxicity and transpiration were monitored during growth, while root morphology, biomass production and arsenic concentrations were measured at harvest. Transpiration per plant (mL day $^{-1}$) was estimated as the difference of water loss in planted and unplanted control pots by day (Gu et al., 1996). Shoots and roots were separated, roots were scanned (Epson, V750 PRO) and the images processed with WinRHIZO (Regent Instruments Inc., update 2017a) for root surface area (RSA) measurements. Shoots and roots were then oven-dried at 105°C for 48h and weighed. For total As quantification, dried shoots and roots, as well as reference material (NIST #1573a tomato leaf, for quality control), were ground and digested in nitric acid using a block digester for 6h at 120°C and analysed by ICP-MS, following the methods described in Courchesne et al. (2017).

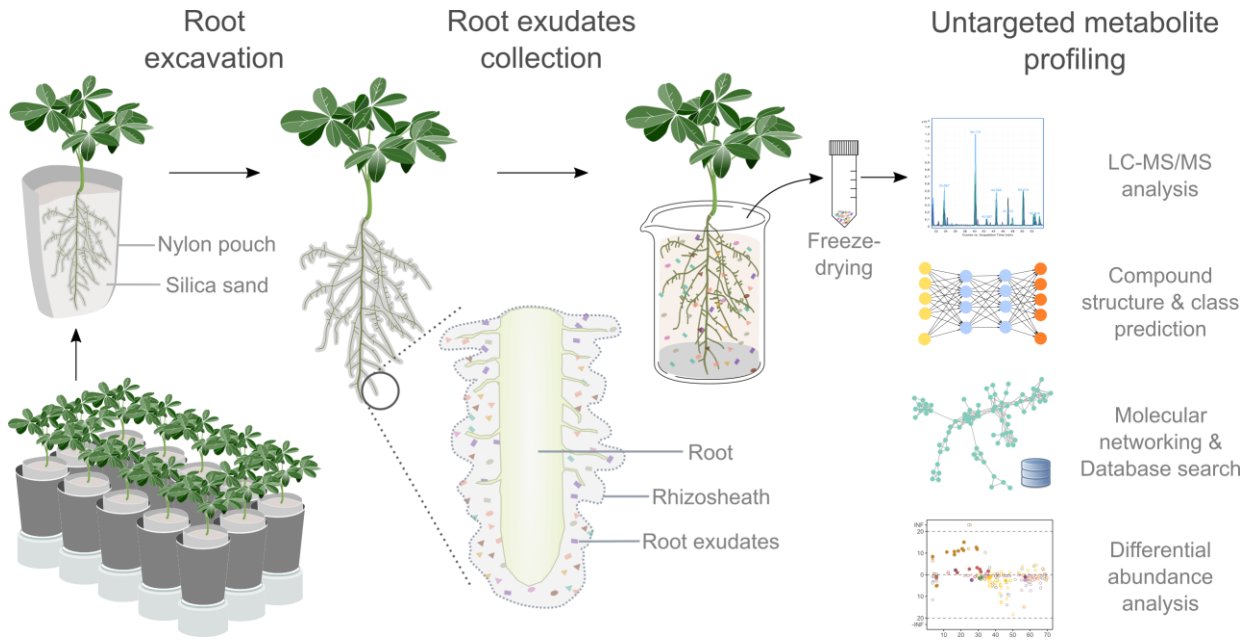

Figure 1 Root exudates analysis pipeline
Schematic view of an experimental block where each plant is excavated from the nylon pouch and the root system, with the rhizosheath containing root exudates, is dipped in water for 1 min to collect exudates. The trap solution is then freeze-dried to concentrate the analytes before LC-MS/MS analysis. Annotation steps include compound structure and class prediction using SIRIUS (Dührkop et al., 2019) and Feature-Based Molecular Networking in the GNPS environment (Nothias et al., 2020). Compound abundance (peak area) of plants treated with arsenic were compared to control plants to identify enriched and depleted exudates due to arsenic treatment.

Root exudate collection

Root exudate collection was performed based on Pearse et al. (2007), Ryan et al. (2012) and Wen et al. (2019), with minor modifications. Briefly, the nylon mesh growth pouches were cut open and loose sand was carefully removed from root systems to leave the attached rhizosheath. Root systems with the rhizosheath were then soaked in 40 mL Milli-Q water for 1 min with gentle circular shaking to capture exudates (**Figure 1**). Despite care taken to minimize root damage, the possibility that some exudates may originate from cellular damage cannot be excluded. Unplanted controls were extracted in the same conditions, by soaking ~20 grams of sand collected from each unplanted pot, replicating a similar amount of sand extracted from rhizosheaths. The trap solutions were then lyophilised and stored at -70°C. All lyophilised extracts were resuspended in 800 µL of Milli-Q water and filtered with 0.2 µm centrifuge filters prior to exudate profiling (InnoSep™ Spin, NY).

Validation of phytochelatin exudation used isolated exudates from belowground fractions to discount direct leaching from damaged root cells to the trap solution. The same experimental conditions were replicated but plants were only subjected to either 0.5 ppm arsenate or left as controls. Four different exudate sampling approaches were used: 1. standard rhizosphere extraction (RE) performed as described above, 2. rhizosheath (RS) extraction, 3. bulk soil (BS) extraction, and 4. root exclusion (RX) extraction. The RS was isolated by careful collection of the sand attached to the root surface with a soft brush. BS comprised sand that was not attached to the root surface and was easily separated from the root system. RX samples, designed to strictly exclude root fragments, were collected using five heat-sealed 2.5 × 6 cm 25 µm nylon mesh pockets which were filled with sand and included in growth pouches before planting. At harvest, the nylon pockets were cut open and sand free from direct contact with roots, was collected. RS and RX sampling used 10 plants each, while the same 10 plants were used for RE and BS (30 plants in total). All samples were then extracted for root exuded metabolite profiling as described above.

Low molecular weight organic acids analysis

Organic acids analysis was performed by HPLC on a Shimadzu SCL-10AVP equipped with an SIL-10AXL autosampler, LC-10VP pump, CTO-10ASvp Column Oven, RID-10A and SPD-10AV VP UV/Vis Detector at 254 nm. Organic acids from exudates or standards of citric acid and malic acid were separated using an AMINEX HPX-87H with isocratic elution of 0.005 M H_2SO_4 at 0.6 mL min^{-1} and column temperature of 65°C, based on Grierson (1992).

Liquid chromatography-tandem mass spectrometry (LC-MS/MS) analysis

Chromatographic separation was performed using an Agilent 1260 Infinity system, where 10 µL of exudate sample was injected onto a Zorbax Eclipse Plus C18 column (4.6 x 100 mm, 3.5 µm) at 30°C. Mobile phase was solvent A (water, 5% v/v methanol, 0.1% v/v formic acid) and solvent B (methanol, 0.1% formic acid) with a flow rate of 0.4 mL min^{-1} and an 80-minute elution gradient: 100% v/v A hold for 20 min, then a linear increase from 0% to 100% v/v B over 50 min and 100% v/v B hold for 10 min.

Untargeted full-scan (100-1300 Da) MS1 acquisition was performed on biological samples (60 samples and 40 samples for phytochelatin validation) and controls (12 unplanted controls, and 5 blanks prepared from Milli-Q water) using an Agilent Q-TOF 6530B mass spectrometer equipped with an Agilent Jet Stream ion source operating in negative ion mode [ESI(-)]. Gas temperature was 300°C, drying gas flow was 5 L min^{-1}, and the nebulizer pressure was 45 psig. Sheath gas temperature was 250°C with a gas flow of 11 L min^{-1}. MS2 acquisition was performed on 12 representative samples (based on MS1 analysis) and blanks (samples extraction solvent and mobile phase). Tandem mass spectra were acquired with a collision energy of 20 and 35 V.

After LC-MS acquisition, raw data were processed using MZmine 2.37 (Pluskal et al., 2010). Background noise cut-off was set to an intensity threshold of 1000 for MS1 and 500 for MS2. Chromatogram building was performed with a 10-ppm mass accuracy and a minimum peak intensity of 10,000. Extracted ion chromatograms were deconvoluted using MZmine minimum search algorithm. Isotope peaks were grouped with 10 ppm mass tolerance and 0.2 min retention time tolerance. Between samples feature alignment was performed with 10 ppm mass tolerance (weighing for 80%) and 0.8 min retention time tolerance (weighing for 20%). Features which contained >1 isotope peak, and which occurred in >2 samples were retained. Gaps in the feature matrix were filled with 0.2 min retention time tolerance and 5 ppm mass tolerance. Features eluting in < 0.2 min retention time windows and which peak shape correlated by >85% (Pearson correlation from MZmine metaCorrelate algorithm) were assigned to a feature group and used for curation of adducts, complex formation, and in-source fragments, using the ion identity networking module in MZmine (Schmid et al., 2020). Features detected in > 2 blank samples were removed from the dataset, while those detected in > 6 unplanted controls were flagged. MS2 spectra were matched to a precursor ion from the MS1 chromatogram within 0.02 m/z and 0.2 min retention time windows. MS2 spectra from 20 and 35 eV collision energies matched to the same precursor ion were merged into a single consensus spectrum and their intensities summated. All retained features were between 3.5- 69.8 min retention time (RT) and 115 to 1087 m/z.

Untargeted metabolite annotation

MS2 fragmentation spectra were annotated using feature-based molecular networking from the Global Natural Product Social Molecular Network (GNPS) platform (Nothias et al., 2020), as well as SIRIUS (version 4.5.3; Dührkop et al., 2019) for *in silico* formula, structure (Dührkop et al., 2015) and chemical class (Dührkop et al., 2020) prediction. Features annotation was further refined using the Plant Metabolic Network compound database of all available leguminous species (https://plantcyc.org/) (Caspi et al., 2018) and the public phytochelatin database PyCDB (Dennis et al., 2019) (https://kuppal.shinyapps.io/pycdb/), based on exact mass similarities (< 5 ppm) and characteristic delta *m/z* of common adducts. For a limited number of features, annotation was confirmed from retention time and fragmentation spectra matching against standards (± 1 min RT, cosine > 0.9). Standards included phytochelatin 2 (Anaspec, USA, CA), glutathione (Alfa Aesar Co., Inc.), glutathione disulphide (ACROS Organics) and genistein (Sigma-Aldrich). Features with ambiguous annotation were annotated by best matching CANOPUS (Dührkop et al., 2020) predicted chemical class using ClassyFire taxonomy (Djoumbou Feunang et al., 2016). Annotation of each feature is categorised into four levels of metabolite identification, as proposed standards for minimum reporting in metabolomics experiments (Sumner et al., 2007). Unless categorised as level 1 identification (identified from standards), all annotation should be considered as putative even when confirmed using database matched MS2 fragmentation patterns, as untargeted identification methodologies and database records are subject to change.

Statistical analysis

All statistical tests were performed using R, version 4.0.2 (R Core Team, 2020). Comparisons of two groups were performed using Student's t-test and multiple groups comparisons were performed with ANOVA followed by Tukey HSD post-hoc test ($\alpha < 0.05$). For differential abundance analysis of metabolic features, two groups comparisons were performed using Mann-Whitney U test with Benjamini-Hochberg correction, and multiple groups comparisons were performed using the non-parametric Kruskal-Wallis test [FSA package in R, (Ogle et al., 2020)], followed by Games-Howell post-hoc test with Benjamini-Hochberg FDR correction [UFS package in R, (Peters, 2018)]. Diversity of features within exudate samples was estimated using Shannon and inverse Simpson indices (Schweiger et al., 2018), which account for both relative intensities and evenness between treatments. Unsupervised classification was estimated based on feature relative intensities using Bray-Curtis dissimilarity and the principal coordinates analysis (PCoA) ordination method. Dispersion ellipses used standard deviation for each treatment group. Significant distance was evaluated between the

groups using the permutational multivariate analysis of variance (PERMANOVA) with Benjamini-Hochberg correction and permutations set to 9999. Diversity and multivariate analysis were performed within the vegan R package (Oksanen et al., 2019).

Results

Physiological response to arsenic

White lupin transpiration, above- and belowground biomass, RSA, and above- and belowground As concentration did not significantly vary between plants when comparing As(III) to As(V) form at any specific concentration (t-test, $p > 0.05$; Supplementary file 1). When comparing the different As concentrations to controls (discounting form), transpiration of plants treated with 0.05, 0.1, 0.5 and 1 ppm As did not significantly vary from controls, with a mean transpiration of 7 ± 0.5 mL day $^{-1}$ after the first As application (day 25) and 7.3 ± 0.7 mL day $^{-1}$ before harvest (day 32), but some necrotic lesions were observed on leaves of plants treated with 1 ppm before harvest (**Figure 2**). Plants treated with 5 ppm As had a mean transpiration of 3.5 ± 0.3 mL day $^{-1}$ after the first As application and a mean of 1.6 ± 0.2 mL day $^{-1}$ before harvest, both of which were significantly lower than controls and other treatments (Tukey HSD, $\alpha < 0.05$). The first treatment with 5 ppm As also induced necrotic lesions in older leaves, which progressed to complete necrosis and abscission before harvest.

Mean aboveground dry weight was not significantly altered by 0.05, 0.1 and 0.5 ppm As when compared to control plants at a mean of 387.1 ± 16.3 mg, but was significantly lower in plants receiving 1 ppm and 5 ppm As, at 307.6 ± 17 and 132.2 ± 10 mg, respectively (**Figure 2**). Belowground dry weight and RSA were not significantly altered by 0.05, 0.1, 0.5 and 1 ppm As compared to controls at a mean of 169.5 ± 15.5 mg and 143.5 ± 12.8 cm^2, but was significantly lower in plants receiving 5 ppm As, with 91.8 ± 8.6 mg and 52.4 ± 4 cm^2 (Tukey HSD, $\alpha < 0.05$).

Mean As concentrations in aboveground biomass of plants treated with 0.05, 0.1 and 0.5 ppm As were 1.7 ± 0.2, 2.4 ± 0.2, 7.3 ± 0.6 µg As g^{-1} dry weight (DW), respectively, and did not significantly differ from controls concentration of 0.3 ± 0.01 µg As g^{-1} DW (**Figure 2**). However, As concentrations were significantly higher than controls in aboveground biomass of plants treated with 1 ppm and 5 ppm As, with mean concentrations of 12.9 ± 1.9 and 46.9 ± 7.2 µg As g^{-1} DW, respectively (Tukey HSD, $\alpha < 0.05$). In belowground biomass, As concentrations were 11.7 ± 1 and 23.6 ± 1.2 µg As g^{-1} DW in plants treated with 0.05 and 0.1 ppm As, respectively, and increased in plants treated with 0.5 ppm, 1 ppm and 5 ppm As, to concentrations of 171 ± 13.1, 411 ± 32.9, and 578.3 ± 34.8 µg As g^{-1} DW, which were significantly higher than 1.1 ± 1.1 µg As g^{-1} DW in controls (Tukey HSD, $\alpha < 0.05$).

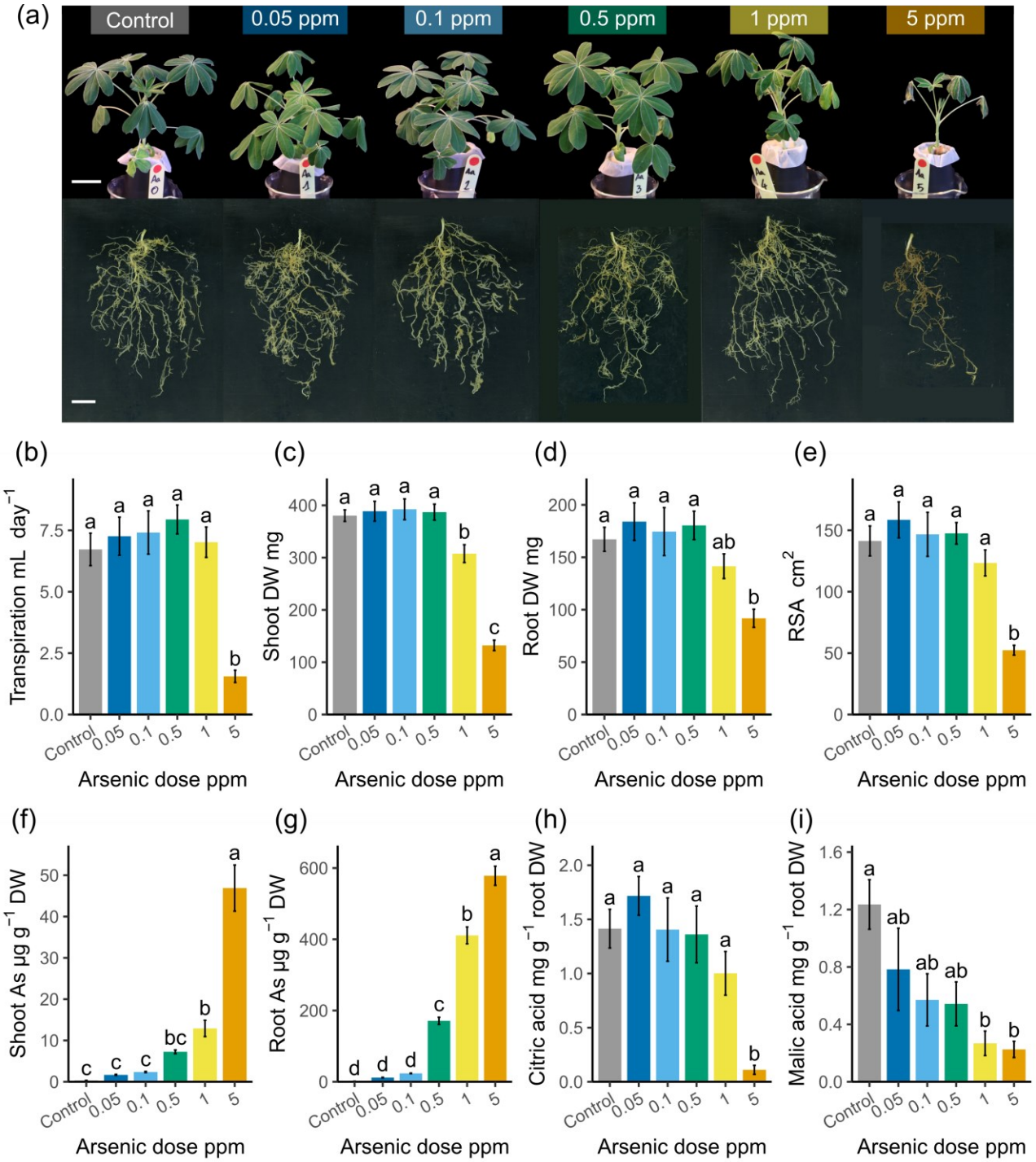

Figure 2 White lupin physiological parameters in response to arsenic

(a) Representative plant aboveground (top) and belowground (bottom) photographs before harvest in response to treatment (scale bars: 3 cm). Arsenic effect on (b) transpiration at harvest, (c, d) aboveground and belowground biomass, (e) root system area (RSA), (f, g) shoot and root arsenic concentrations, (h, i) root exudation of citric acid and malic acid. Data are means ± standard error (n = 10). Different letters indicate significant differences (Tukey HSD, $\alpha < 0.05$).

Organic acid exudation

Citric acid accumulation in the rhizosphere did not significantly vary in plants treated with 0.05, 0.1, 0.5 and 1 ppm As compared to controls, with a mean of 1.4 ± 0.2 mg citric acid g^{-1} root DW, but was significantly lower in plants receiving 5 ppm arsenic with 0.1 ± 0.04 mg citric acid g^{-1} root DW (Tukey HSD, $\alpha < 0.05$, **Figure 2**). Malic acid concentrations in the rhizosphere of plants treated with 0.05, 0.1 and 0.5 ppm As were 0.8 ± 0.3, 0.6 ± 0.2, 0.5 ± 0.2 mg malic acid g^{-1} root DW, respectively, and did not significantly differ from the concentration of controls with 1.2 ± 0.2 mg malic acid g^{-1} root DW. However, malic acid concentrations were significantly lower in plants receiving 1 and 5 ppm arsenic compared to controls, with mean concentrations of 0.3 ± 0.1 and 0.2 ± 0.1 mg malic acid g^{-1} root DW, respectively (Tukey HSD, $\alpha < 0.05$).

Root exudate untargeted metabolite profile

The number of initial features per exudate sample ranged from 323 to 1200. After alignment and quality control, which included removal of one sample as an extreme outlier, a total of 245 features were retained as shared across >2 of the 59 root exudate samples (**Figure 3**). Of the 245 retained features, 82 were annotated as compounds, 80 annotated to a predicted chemical superclass, class, or subclass, and 52 annotated as adducts, multimers and in-source fragments of identified metabolites (not considered in differential abundance analysis), while 31 features remained unknown (Supplementary file 1).

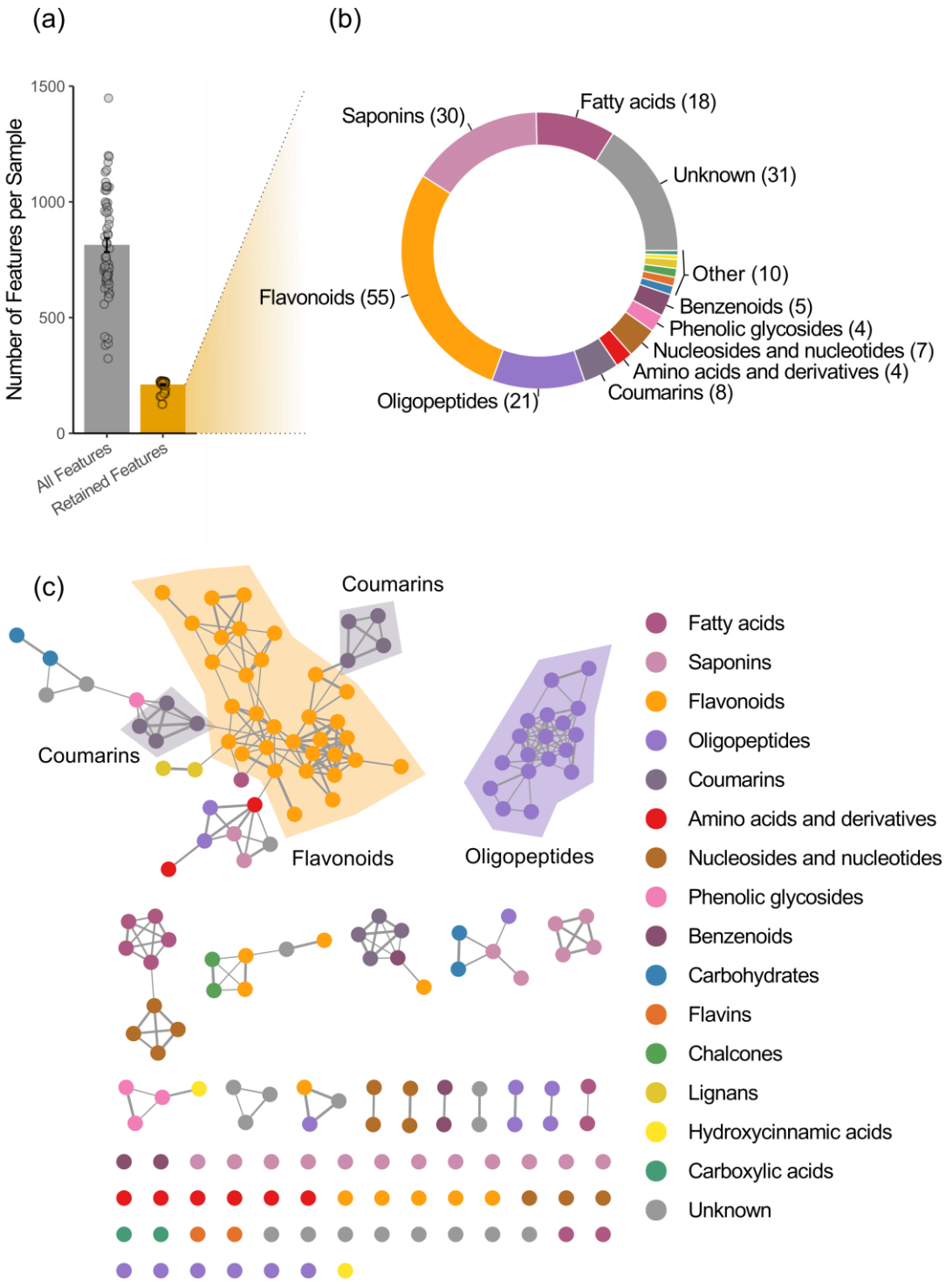

Figure 3 Overview of untargeted metabolite profile of white lupin root exudates

(a) Quality control of untargeted LC-MS features. Each point represents a sample and bars represent means ± standard error (n = 60 plants) before and after quality control filtering. (b) Number of compounds identified in the different chemical classes. (c) Molecular network based on MS2 spectra similarities (cosine > 0.4) computed in the GNPS environment (Nothias et al., 2020) and plotted in Cytoscape, major cluster groups are circled. Full annotation of each feature is available in Supplementary file 1.

In total, root exudate features from controls and As exposed white lupin plants belonged to 15 predicted chemical classes, including: fatty acids, saponins, flavonoids, oligopeptides, coumarins, amino acids and derivatives, nucleosides and nucleotides, phenolic glycosides, benzenoids, carbohydrates, flavins, chalcones, lignans, hydroxycinnamic acids and carboxylic acids (**Figure 3**). Features with available fragmentation spectra were grouped into molecular networks based on spectral similarity (cosine score > 0.4). This revealed 17 delimited subnetworks (clusters): the largest contained 55 features, the majority of which were flavonoids and coumarins and the second largest contained 18 features which were all oligopeptides (**Figure 3**). Forty-nine features did not cluster and were classified mostly as saponins or unknown features.

Using all 245 features across all samples, unsupervised analysis on Bray Curtis distances suggests samples separate by As dose and not by As form (**Figure 4**, Supplementary file 1). Permutational multivariate analysis of variance (PERMANOVA) revealed significantly greater variance between As doses than within dose ($p < 0.05$) and no significant difference between As(III) and As(V). Shannon and InvSimpson indices were used as a measure of feature diversity within samples; treatment with 5ppm As significantly reduced both diversity indices compared to controls (Tukey HSD, $\alpha < 0.05$), while As form did not significantly alter either diversity indices.

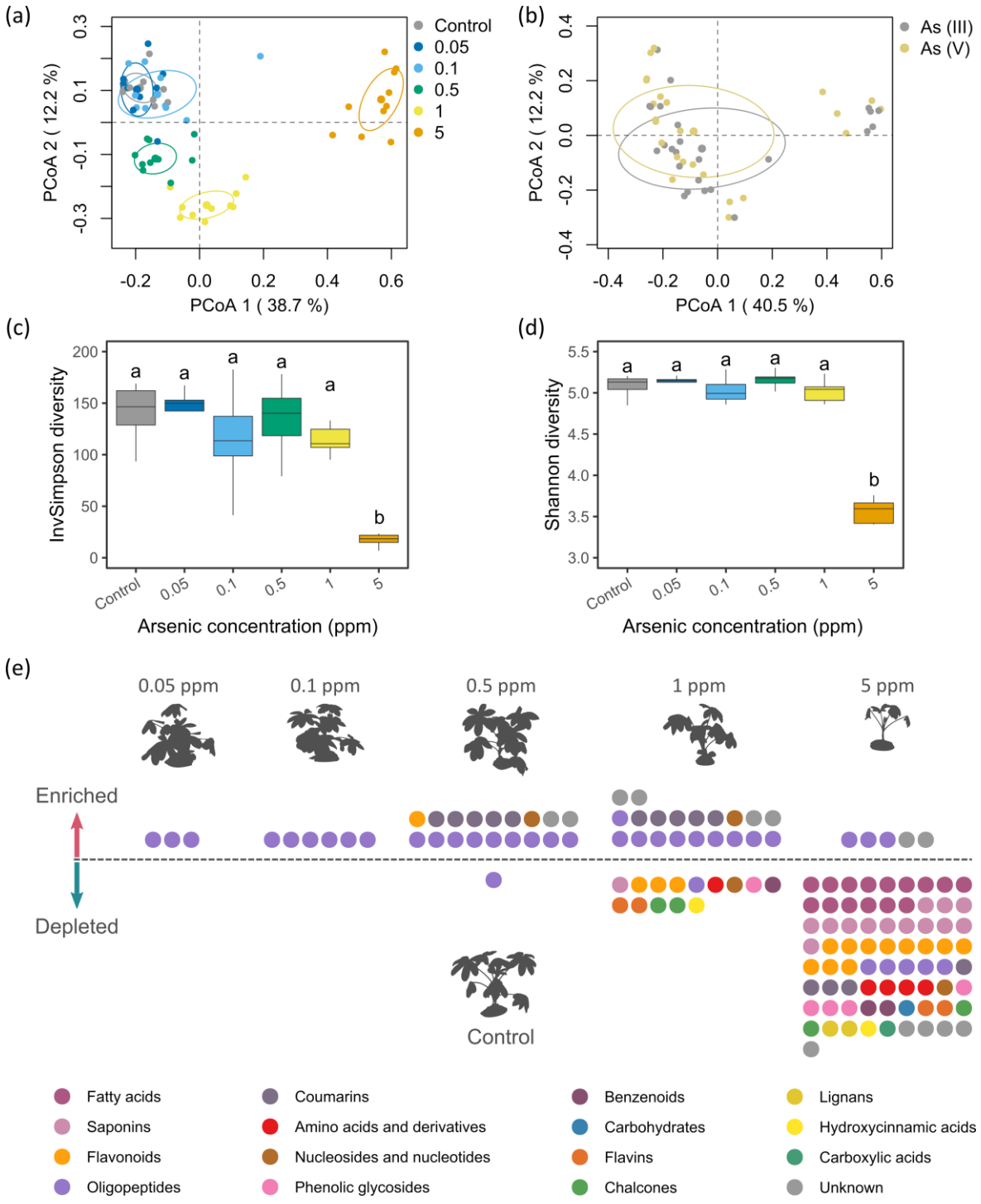

Figure 4 Alterations in white lupin root exudate profiles in response to arsenic
(a,b) PCoA of sample dissimilarity based on Bray-Curtis distances including standard deviation ellipses for treatment with arsenic doses or arsenic forms. (c,d) Shannon and InvSimpson diversity indices comparison between arsenic treatments, different letters indicate significant differences (Tukey HSD, $\alpha < 0.05$). (e) Significantly enriched and depleted features in the different arsenic concentrations compared to controls, each point represents one feature, coloured by chemical class.

Differential abundance analysis comparing As(III) and As(V) forms, within each As dose, revealed 11 significantly differentially abundant features (Supplementary file 1). Of these, 10 varied significantly at 0.1 ppm As and one feature varied significantly at 1 ppm As. Comparison between As doses (discounting form) to controls revealed a total of 93 significantly differentially abundant features in at least one As dose, with 73 depleted and 22 enriched (**Figure 4**). No significantly depleted features were detected at 0.05 or 0.1 ppm As, whereas one significantly depleted feature was detected at 0.5 ppm As, 14 at 1 ppm As and 73 at 5 ppm As. Significantly enriched features included three at 0.05 ppm As, six at 0.1 ppm As, 18 at 0.5 ppm As, 20 at 1 ppm As, and 5 at 5 ppm As.

Metabolites significantly altered between arsenic forms

Of the 11 features significantly differentially abundant between As forms, 10 were lower in 0.1 ppm As(III) compared to 0.1 ppm As(V), and were putatively classified as six saponins, one flavonoid glycoside, one amino acid derivative, as well as two features that were unknown (Supplementary file 1). At 1 ppm, one feature, putatively classified as a disaccharide, was significantly higher in As(III) compared to As(V). No significant differences were identified in exudates of plants treated with As(III) compared to As(V) at 0.05, 0.5 or 5 ppm As. Due to this similarity, As(III) and As(V) treated plants are used collectively for differential analysis comparing exudate response of As doses to controls (although additional pair-wise comparisons are available in Supplementary file 1).

Metabolites significantly altered by 5 ppm arsenic

The 73 features significantly depleted in response to 5 ppm As compared to controls were putatively classified into 15 chemical classes (**Figure 4**). The five largest depleted chemical classes were fatty acids (15), saponins (13), flavonoids (11), oligopeptides (5) and coumarins (4). The fatty acids included, trihydroxy octadecadienoic acids, trihydroxy octadecenoic acids and octadecynedioic acids, as well as one saccharolipid, licoagroside B (Supplementary file 1). The saponins included pisumsaponin II and soyasaponin I. Flavonoids included apigenin 6,8-digalactoside, apigenin 7-O-glucosylglucoside, apigenin 7-O-glucoside, dihydrokaempferol 7-glucoside and genistein glucoside. Oligopeptides included glutathione disulphide (GSSG). Coumarins included two chromenone glycoside derivatives. Other putative compounds included the amino acid, tryptophan, two flavins, riboflavin and lumiflavin, the phenolic glycosides p-coumaric acid glucoside and ferulic acid glucoside, the hydroxycinnamic acid, p-coumaric acid and the nucleoside uridine, while five significantly depleted features were unknown.

Of the five features enriched in response to 5 ppm As, three were classified as putative oligopeptides, including cysteineglutathione disulphide (CySSG), two yet-to-be-characterised compounds predicted as sulphur-containing gamma-glutamyl peptides (Feat_66, Feat_84, supp data), while the remaining two features were unknown (**Figure 4**, Supplementary file 1).

Features significantly altered by 0.05, 0.1, 0.5 and 1 ppm arsenic

There was no significant depletion of exuded features in treatments with 0.05 and 0.1 ppm As when compared to controls. Treatment with 0.5 ppm and 1 ppm As led to significant depletion of one and 14 features, respectively. The depleted feature in 0.5 ppm As treated plants was the oligopeptide GSSG, which was also depleted in response to 1 ppm, along with 13 other features from nine chemical classes: flavonoids (3), flavins (2), chalcones (2), amino acid derivatives (1), benzenoids (1), hydroxycinnamic acids (1), nucleosides (1), phenolic glycosides (1) and saponins (1) (**Figure 4** and **Figure 5**).

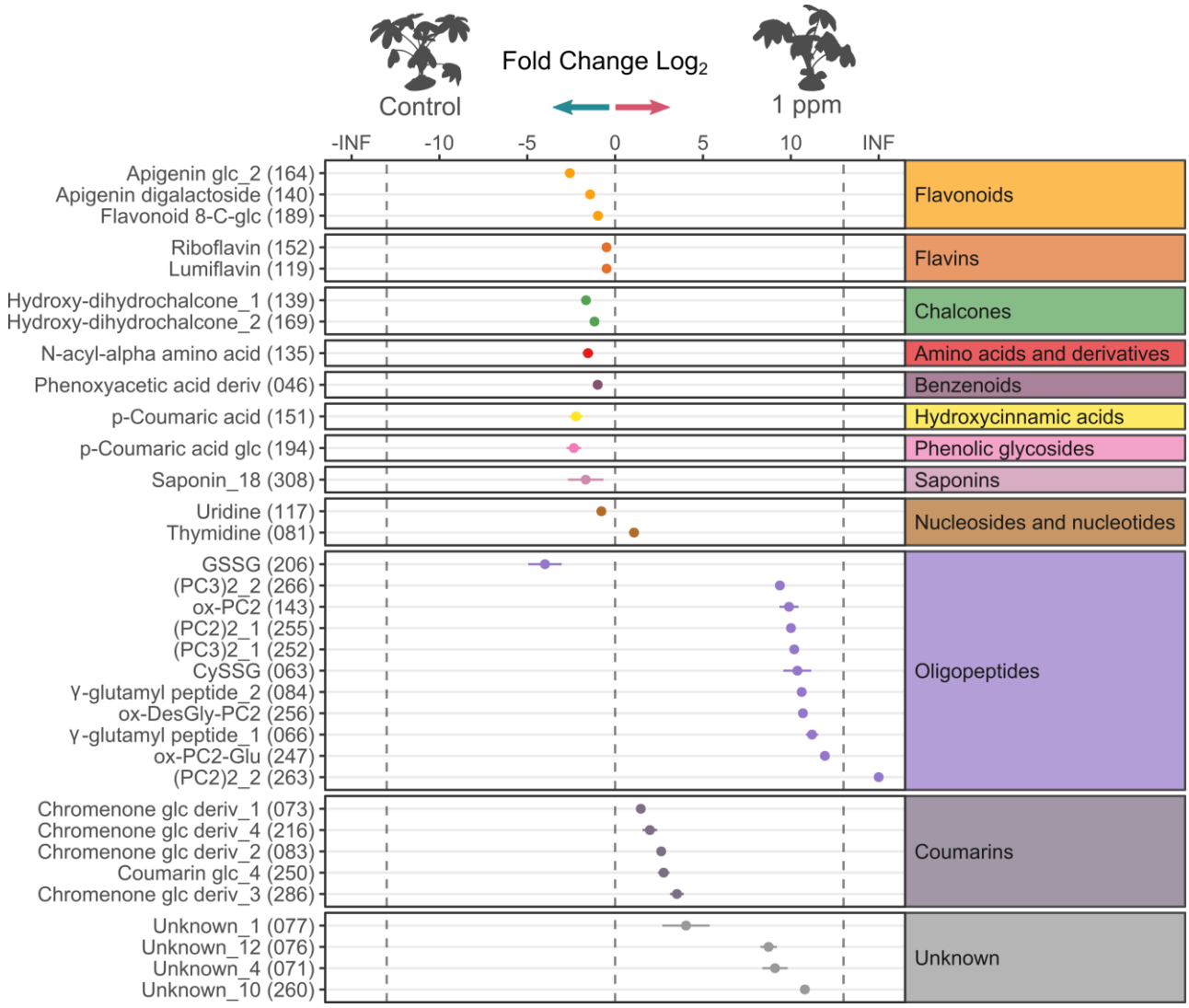

Figure 5 Differentially abundant exudates between plants treated with 1 ppm arsenic
Significantly differentially abundant exudates in 1 ppm arsenic compared to controls, annotated, and grouped by putative compound classes (Supplementary file 1 includes full annotation, feature unique ID is indicated in brackets). Statistical significance was determined using the non-parametric Kruskal-Wallis test, followed by Games-Howell post-hoc test using a Benjamini-Hochberg correction (FDR adjusted $p < 0.05$). Data are mean fold change (FC $\log_2$) of peak intensities from significantly different exudates between arsenic-treated and control plants, ± standard error (n = 10). The dashed lines indicate "infinite" fold change, where the exudate had detectable signal in only one condition.

Exuded features significantly enriched in response to treatment with 0.05, 0.1, 0.5 and 1 ppm As when compared to controls belonged to four chemical classes, oligopeptides (10), coumarins (5), flavonoids (1), and nucleosides (1), while four features were unknown (**Figure 4**, **Figure 5**, Supplementary file 1). Treatment with 0.05 ppm As significantly enriched three putative oligopeptides: oxidised phytochelatin 2 (ox-PC_2), oxidised phytochelatin 2 with the glycine residue substituted for glutamic

acid (ox-PC_2-Glu) as well as one uncharacterised sulphur-containing gamma-glutamyl peptide (Feat_66, Supplementary file 1). Treatment with 0.1 ppm As also significantly enriched the common features ox-PC_2, ox-PC_2-Glu and the gamma-glutamyl peptide (Feat_66) along with three additional oligopeptides, oxidised PC_2 with a terminal glycine deletion (ox-DesGly-PC_2), one dimer of phytochelatin 3 (with three S-S bonds, $(PC_3)_2$), and one gamma-glutamyl peptide (Feat_84, isomer of Feat_66). Treatment with 0.5 ppm As significantly enriched, five coumarins, including four chromenone glycoside derivatives and one coumarin glycoside, one uncharacterised flavonoid, the nucleoside thymidine, the same oligopeptides ox-PC_2, ox-PC_2-Glu, ox-DesGly-PC_2, gamma-glutamyl peptides (Feat_66, Feat_84), the phytochelatin 3 dimer $(PC_3)_2$, as well as another phytochelatin 3 dimer, two phytochelatin 2 dimers (with two S-S bonds, $(PC_2)_2$), and two unknown features (Supplementary file 1). Treatment with 1 ppm As significantly enriched the same five coumarins, the nucleoside thymidine and the oligopeptides ox-PC_2, ox-PC_2-Glu, ox-DesGly-PC_2, gamma-glutamyl peptides (Feat_66, Feat_84), the two phytochelatin 3 dimers $(PC_3)_2$, two phytochelatin 2 dimers $(PC_2)_2$, cysteineglutathione disulphide (CySSG), and four unknown features (**Figure 5**). All enriched oligopeptides, except for $(PC_3)_2$, clustered into a single subnetwork (oligopeptide cluster; **Figure 6**) with similar fragmentation spectra (cosine score > 0.4) and which contained only one depleted metabolite, GSSG.

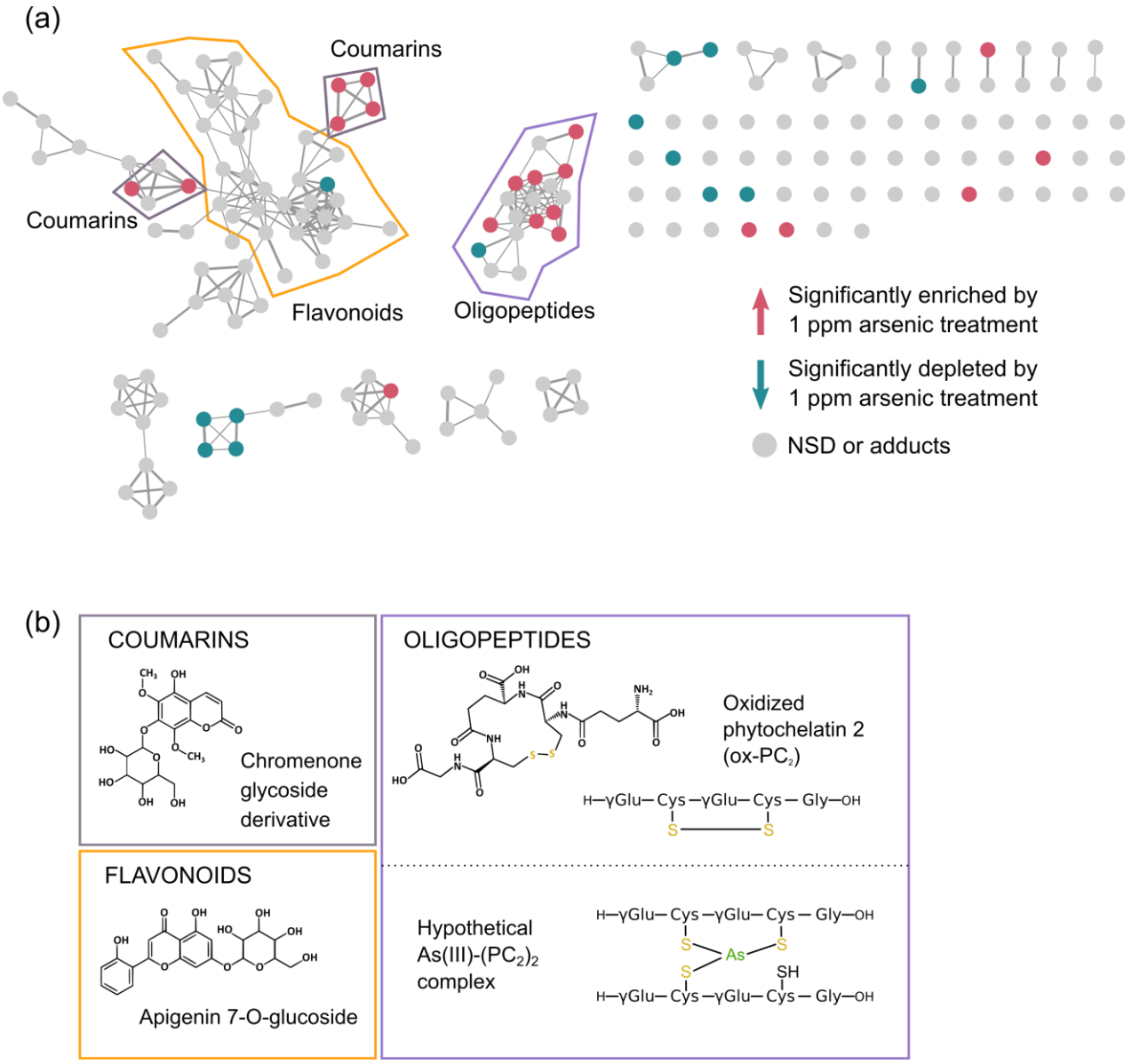

Figure 6 Molecular network and representative molecular structure of differentially abundant exudates in 1 ppm arsenic

(a) Molecular network of feature MS2 spectra similarities (cosine > 0.4) computed in the GNPS environment (Nothias et al., 2020) and plotted in Cytoscape, major cluster groups are circled. Each significantly differentially abundant exudate is coloured by direction of significant change after 1 ppm arsenic treatment compared to controls (enriched in red, depleted in blue, NSD = non-significant difference). (b) Example molecular structures from major cluster groups from exudates, and hypothetical As(III)-(PC2)2 complex adapted from Schmöger et al. (2000).

Phytochelatins exudation validation

To further confirm exudation of phytochelatins, plants were treated with 0.5 ppm As or were left as controls, and different belowground fractions were sampled, including: root exclusion (RX), which

was strictly isolated from direct contact with roots, rhizosheath (RS), bulk soil (BS) and rhizosphere (RE) as the standard exudate sampling approach (**Figure 7**). A total of 351 features were detected as shared across >2 exudate samples.

The phytochelatins and glutathione derivatives: ox-PC_2, ox-PC_2-Glu, ox-DesGly-PC_2, the two isomers of $(PC_2)_2$ and CySSG, were all significantly enriched in the RX belowground fraction from As-treated plants compared to controls (**Figure 7**), while only one phytochelatin 3 dimer $(PC_3)_2$ was detected in RX and did not significantly differ from controls. Conversely, GSSG was significantly depleted in the RX belowground fraction of As-treated plants compared to controls. Ox-PC_2, other PC variants and glutathione derivatives were also significantly increased in other belowground fractions when compared to controls, including the repeated standard rhizosphere extraction (RE), the rhizosheath (RS) and the bulk soil (BS) (Supplementary file 1).

Direct comparison between RE, RS, BS and RX belowground fractions of As-treated plants revealed ox-PC_2, ox-PC_2-Glu and ox-DesGly-PC_2 were higher in RE fractions when compared to RS fractions, which were higher compared to BS and RX fractions (**Figure 7**), consistent with an expected diffusion gradient. The two isomers of $(PC_3)_2$ were significantly higher in RE compared to BS and RX belowground fractions, but did not significantly differ between RS, BS and RX. GSSG and the two isomers of $(PC_2)_2$ were higher in RE and RS fractions compared to BS and RX fractions, while CySSG remained stable between all belowground fractions.

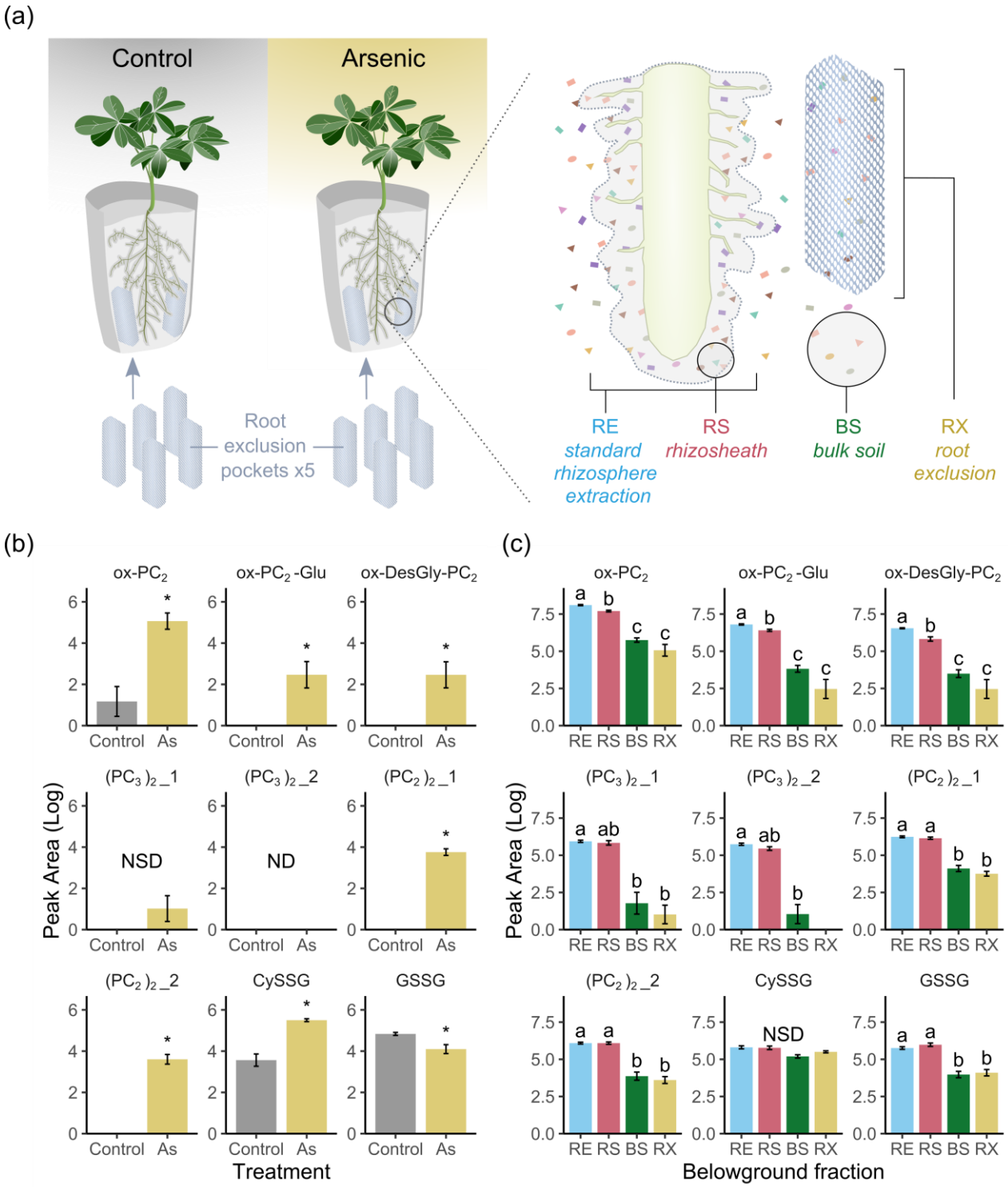

Figure 7 Validation of phytochelatin exudation

(a) Schematic of the rhizosphere of arsenic-treated and control plants illustrating different belowground fractions sampled for exudate profiling: Standard rhizosphere extraction (RE), rhizosheath (RS) extraction, bulk soil (BS) extraction, and root exclusion (RX) extraction. RX samples were collected using nylon mesh pockets filled with sand and included in growth pouches before planting which strictly exclude root penetration. (b) Phytochelatin and glutathione derivatives abundance (Log_{10} peak area) in RX belowground fraction from controls and arsenic-treated plants.

Asterisks indicate significant difference from controls (Mann-Whitney U test, FDR adjusted $p < 0.05$). (c) Phytochelatin and glutathione derivatives abundance (Log_{10} peak area, normalised based on dry weight of extracted material) comparing the different belowground fractions of arsenic-treated plants. Data are means ± standard error (n = 5 plants), different letters indicate significant difference (Games-Howell test, FDR adjusted $p < 0.05$). NSD = non-significant difference, ND = non detected.

Discussion

Physiological response to arsenic

The absence of observed toxicity symptoms in canopy morphology, transpiration and biomass production in plants subjected to arsenic at concentrations of 0.05, 0.1 and 0.5 ppm suggests short-term tolerance to arsenic in white lupin within the semi-hydroponic system (**Figure 1** and **Figure 2**). Visible toxicity symptoms on leaves after 11 days of treatment indicates a chronic toxic effect of 1 ppm arsenic, and similar symptoms after only four days of treatment indicate acute toxicity of 5 ppm arsenic. The leaf lesions in plants subjected to 5 ppm arsenic are characteristic of arsenic-induced oxidative stress (Sharma, 2012) and coincided with a sharp decrease in transpiration and biomass production, consistent with impaired photosynthesis and primary metabolism due to arsenic cellular toxicity (Tripathi et al., 2012). Although arsenite As(III) and arsenate As(V) can have distinct degrees of phytotoxicity (Finnegan & Chen, 2012), they had similar effects on white lupin, potentially due to one form being rapidly converted to the other, as observed in rice and tomato by Xu et al. (2007), where > 90% of As(V) was reduced into As(III) in the presence of plant roots. Treated plants significantly accumulated arsenic in both belowground and aboveground tissues, regardless of the arsenic form applied, in similar concentrations as those observed in hydroponically grown white lupin from Vázquez et al. (2005). The proportion of arsenic accumulated in roots was substantially higher than in shoots, with 76-94% of the total arsenic retained in root systems. Preferential arsenic accumulation in roots was also highlighted in Vázquez et al. (2006a, 2005), providing evidence that white lupin may be a good candidate for immobilising arsenic within contaminated soils (a process termed “phytostabilisation”).

These results indicate that white lupin successfully tolerated concentrations up to 0.5 ppm of arsenic, had partial tolerance to 1 ppm arsenic and was sensitive to 5 ppm arsenic. This agrees with Moreno-Jiménez et al. (2010) where white lupin tolerated concentrations of 0.5 ppm As, which corresponded to the bioavailable arsenic from highly contaminated soil. White lupin response to arsenic is thought

to involve root exudation of compounds, such as citric acid (Fresno et al., 2017). Here, citric acid and malic acid, the two main OAs found in root exudates of P-deficient white lupin (Neumann & Römheld, 1999; Pearse et al., 2007), were significantly reduced by high arsenic treatment, and were unaffected by tolerable arsenic levels. This suggests that white lupin might not use OA exudation to alter arsenic solubility directly within the rhizosphere, contrary to hyperaccumulating species such as *Pteris vittata* (Das et al., 2017; Liu et al., 2017; Tu et al., 2004). As the full range of exuded compounds in response to arsenic is largely unknown but could influence the fate of soil arsenic, exuded compounds were profiled and compared.

Root exudation is significantly altered in response to arsenic

Accurate exudate profiling is challenging due to the difficultly of sampling undamaged roots, the low concentrations, metabolite sorption onto soil particles, potential microbial interactions as well as other interfering soil constituents (Oburger & Jones, 2018). Semi-hydroponic silica sand cultivation systems, such as that used here (Pang et al., 2018; Pearse et al., 2007; Ryan et al., 2012; Sasse et al., 2020; **Figure 1**), enabled root exudates to be sampled from whole root systems for untargeted metabolite profiling. Overall, 245 exuded metabolites were repeatedly observed across multiple plants and arsenic drove significant and substantial changes in their abundance (based on peak intensities) when compared to untreated controls (**Figure 4**).

The form of arsenic had limited impact on exudation, with no significant differentially abundant metabolites detected between As(III) and As(V) at 0.05, 0.5 or 5 ppm. Only ten metabolites identified as differentially abundant when comparing As(III) to As(V) at 0.1 ppm, including a relative reduction in saponins due to As(III), and one differentially abundant metabolite at 1ppm. Saponins are commonly found in exudates of *Glycine max* and *Solanum lycopersicum,* where they are thought to alter rhizosphere microbial communities (Fujimatsu et al., 2020; Nakayasu et al., 2021). As comparative studies of As(III) and As(V) effects on plant metabolism are scarce (Tripathi et al., 2012), any direct role of altered saponin exudation or indirect interaction with rhizospheric microbiota is unclear.

Conversely, substantial differences in exudation profiles were induced between different arsenic doses when compared to untreated controls, with 93 differentially abundant metabolites in at least one dose when arsenic treatment (regardless of form) was compared to controls. The large proportion (78%) of differentially abundant metabolites significantly depleted in response to 5 ppm only (**Figure 4**) can likely be explained by a general decrease in metabolism and exudation, reflecting the physiological symptoms of arsenic sensitivity at this toxic concentration (**Figure 2**). In contrast, treatments with 0.05, 0.1, 0.5 and 1ppm arsenic led to a more balanced shift in exuded metabolites, particularly in

treatments with 0.5 ppm and 1 ppm (**Figure 4**), which were tolerated or partially tolerated by white lupin. The depletion of certain metabolites may reflect the action of intracellular arsenic toxicity but could also be a response aimed at decreasing arsenic sensitivity through a redirection of resources and switch from constitutive exudation to tolerance exudation. The corresponding significant enrichment of specific metabolites due to 0.5 and 1 ppm arsenic treatment likely represents the metabolites facilitating or directly acting towards neutralisation of arsenic.

Exudation profile of arsenic toxicity in white lupin

The toxicity response of white lupin to 5 ppm arsenic included a general decrease in metabolite exudation compared to controls (**Figure 4**, Supplementary file 1). These compounds were largely fatty acids, saponins and flavonoids, and are likely the constitutive white lupin root exudates associated to rhizosphere functions. For instance, the depleted fatty acids found here, such as trihydroxy octadecadienoic acids, have been reported in exudates of several species (da Silva Lima et al., 2014; Strehmel et al., 2014) including in white lupin (Lucas García et al., 2001), and can facilitate root penetration, nutrient exchange, and microbial dynamics at the root soil interface as constituents of mucilage (McCully, 1999; Read et al., 2003). Other depleted fatty acids, such as octadecenoic acids, can be found in root hairs of *Glycine max* (a relative of lupin within Fabaceae), where they are thought to be involved in interactions with symbiotic rhizobacteria (Brechenmacher et al., 2010). Saponins have also recently been identified in root exudates of *Glycine max* (Tsuno et al., 2018) and at high concentrations in roots of *Panax notoginseng* in arsenic contaminated soils (Zu et al., 2018). Additionally, some saponins have been shown to protect mammalian cells from arsenic (Manna et al., 2007) and have been used as a biosurfactant to treat arsenic contaminated soils (Gusiatin, 2014). Flavonoids are commonly found in root exudates of white lupin and other species (Cesco et al., 2012) where they can have diverse functions. Amongst the flavonoids depleted in high arsenic here, apigenin glucoside is thought to be involved in legume-rhizobia interactions (Brechenmacher et al., 2010) and isoflavonoids such as genistein glucosides, have been found in white lupin rhizosphere as having antimicrobial activities and possible roles in Cu detoxification and P acquisition (Jung et al., 2003; Weisskopf, Abou-Mansour, et al., 2006; Weisskopf, Tomasi, et al., 2006). Alongside the symptoms of arsenic toxicity observed with 5 ppm arsenic (**Figure 2**), the depletion of these metabolites are therefore consistent with a reduction in root exudate functions, such as shaping soil physicochemical conditions through mucilage formation, improved nutrient acquisition, defence, as well as recruitment and maintenance of a healthy rhizosphere microbiome (Badri & Vivanco, 2009).

Although most exuded compounds were depleted in 5 ppm arsenic-treated white lupin, the arsenic toxicity also led to significant enrichment in three oligopeptides, cysteineglutathione disulphide (CySSG), and two sulphur-containing gamma-glutamyl peptides (Feat_66, Feat_84; Supplementary file 1) which clustered with CySSG within the oligopeptide cluster (**Figure 3**). Glutathione-derived sulphur-containing peptides such as these can be strongly induced during oxidative stress and metalloid response (Finnegan & Chen, 2012) and are consistent with the extreme toxicity of high arsenic concentrations.

Exudation profile of arsenic tolerance in white lupin

Metabolites that were depleted in response to tolerated, or partially tolerated, levels of arsenic (0.5 and 1 ppm As) included, flavonoids, flavins, chalcones, amino acid derivatives, benzenoids, hydroxycinnamic acids, nucleosides, phenolic glycosides and saponins. Depletion in these diverse exudate molecular classes, which occurred mostly in response to 1 ppm arsenic, resembled the toxicity response to 5 ppm arsenic (**Figure 4**) and supports the physiological symptoms interpreted as partial tolerance of white lupin to 1 ppm arsenic (**Figure 2**). A common response to 0.5 and 1 ppm arsenic was the significant depletion in glutathione disulphide (GSSG). Previous research has provided evidence that GSSG can reduce translocation of metals such as cadmium to aboveground tissue (Nakamura et al., 2013). GSSG is the oxidised form of glutathione (GSH), a compound with high intracellular antioxidant activity (Jozefczak et al., 2012) which can form As(III)-GSH complexes like arsenotriglutahione in roots (Delnomdedieu et al., 1994; Raab et al., 2004, 2005). A reduction in GSSG within exudates after arsenic treatment could therefore be due to increased demand for GSH *in planta* for arsenic partitioning and compartmentalisation. Depleted intracellular levels of GSH due to arsenic have also previously been observed in lupin leaves, stems and roots, following the increased synthesis of phytochelatins (Vázquez et al., 2005). As GSH is difficult to capture in exudates due to high reactivity (Giustarini et al., 2016), the significant depletion of GSSG is an important clue suggesting a general redirection of the glutathione pathway towards increased synthesis and enrichment of arsenic tolerance exudates.

Enriched metabolites in root exudates due to arsenic belonged to four molecular classes, including ten oligopeptides, five coumarins, one nucleoside, and one uncharacterised flavonoid. The nucleoside thymidine, a DNA constituent, has been shown to have exudate function as a growth substrate for rhizosphere microorganisms in *Avena barbata* (Zhalnina et al., 2018) and as a metabolite involved in response to P deficiency in *Glycine max* (Tawaraya et al., 2014). Enriched coumarins included four chromenone glycoside derivatives (**Figure 5**, Supplementary file 1), previously identified in root

extracts from *Glycine max* (Zanzarin et al., 2020). The coumarin pathway was reported as upregulated in response to Fe limitation in white lupin (Venuti et al., 2019) and some coumarins from *Arabidopsis* root exudates were shown to complex Fe (Schmid et al., 2014) but coumarins have not previously been associated to arsenic response, and their role in root exudates remain unclear. Arsenic is thought to cause Fe limitation in plants (Shaibur et al., 2009), therefore, enriched coumarin exudation could have a role in Fe nutrition during arsenic exposure to maintain lupin health.

Ten metabolites of the oligopeptide class were significantly enriched in response to tolerated levels of arsenic, and clustered to suggest related molecular structures (**Figure 3** and **Figure 6**). Most of the enriched oligopeptides were identified as phytochelatins (PCs) or GSH-derived oligopeptides. As PC synthesis requires two GSH to form one phytochelatin 2 molecule (PC_2) (Grill et al., 1989; Scheller et al., 1987), the general enrichment of PCs within exudates could explain the depleted levels of total GSH (detected here as GSSG) in arsenic-treated plants due to a major shift in the glutathione pathway. The most abundant (based on peak intensities) form of exuded PCs was ox-PC_2, which is a major intracellular metal(loid) detoxification metabolite in plants, including white lupin, and is commonly identified in cells responding to different heavy metals and metal(loid)s such as lead, mercury, cadmium and arsenic (Cobbett & Goldsbrough, 2002; Vázquez et al., 2005). The two PCs, ox-PC_2-Glu and ox-DesGly-PC_2, have not previously been reported as detected in white lupin but are known metal(loid)-induced intracellular metabolites in tissues of other crops, such as rice (*sativa*) (Lemos Batista et al., 2014) and sunflower (*Helianthus annuus*) (Raab et al., 2005). To our knowledge, phytochelatins have not previously been reported in root exudates in any plant species.

Phytochelatins exudation validation

To further confirm white lupin PC exudation in response to arsenic, an independent experiment was performed to strictly exclude roots from exudate samples (**Figure 7**). After arsenic treatment with 0.5 ppm, ox-PC_2, other PC variants, ox-PC_2-Glu, ox-DesGly-PC_2, ox-$(PC_2)_2$ and GSH-derivative CySSG were significantly enriched in the root exclusion (RX) fraction, which ensured complete separation of roots or roots fragments from the extracted sand using 25-micron nylon mesh pockets. Using the RX approach, the experimental results confirm the exudation of ox-PC_2, other PC variants and glutathione derivatives into the rhizosphere as opposed to these metabolites originating from root cell damage and leaching of intracellular metabolites during sampling.

All PCs decreased gradually from the surface of the roots (RE and RS) into the bulk soil (BS and RX) (**Figure 7**) in line with expected diffusion gradients of exuded compounds through soils (Dessureault-Rompré et al., 2006; Oburger et al., 2013) and confirms that the root zone of influence upon the soil,

often considered as a definition of the rhizosphere, is spatially limited. A noteworthy exception was CySSG; present in similar abundance across all compartments, which suggests a high diffusion rate through the rhizosphere and is consistent with its short chromatographic retention time (3 min) due to strong polarity.

The diversity of PC variants enriched in exudates or arsenic treated plants suggests that white lupin could deploy an arsenal of detoxification metabolites directly in the rhizosphere (with roughly 53% of internal PC_2 levels exuded into the rhizosphere based on peak area per plant, Supplementary file 1). The major intracellular arsenic detoxification strategy in plants is thought to be the binding of As(III) to sulfhydryl (-SH) groups of PC cysteine residues in the cytoplasm to form a less toxic As(III)-PC complex (Schmöger et al., 2000). Complexation of arsenic with PC_2 has been directly observed in plants extracts, under specific buffer conditions, demonstrating the effective binding of one As(III) to three thiol (-SH) from two PC_2 molecules to form As(III)-$(PC_2)_2$ complexes (Raab et al., 2004; Schmöger et al., 2000; **Figure 6**). A similar arsenic detoxification mechanism by PCs could therefore operate within the rhizosphere directly to immobilise arsenic and reduce uptake into roots. Another hypothesis is that As(III)-$(PC_2)_2$ complexes are exuded (efflux) from roots as a mechanism to exclude arsenic in a similar manner as intracellular compartmentalisation in plant vacuoles. Non-complexed arsenite efflux through channels of the NIP subfamily of plant aquaporins has been reported in several species but only explains up to 20% of total As(III) efflux from roots into the soil in non-hyperaccumulators, where 50-100% of intracellular As(III) is complexed with thiols (Bienert et al., 2008; Li et al., 2016; Ma et al., 2008; Zhao et al., 2009; Zhao et al., 2010b). Interestingly, Song et al. (2014) reported the expression of rice ABC-type transporters, responsible for As(III)-PC loading into the vacuole, within the plasma membrane of the root epidermis, providing a route for efflux of As(III)-PC complexes into the rhizosphere.

Conclusions

Untargeted metabolite profiling revealed white lupin has a distinctive root exudate response to arsenic. The exudation profile associated with successful tolerance of high arsenic concentrations included unexpected compounds, such as coumarins, several yet-to-be-characterised molecules and a diverse suite of phytochelatins, exudation that was further confirmed through repeated growth trials and strict exclusion of roots from sampled growth medium. These findings provide evidence that an extracellular arsenic tolerance mechanism mediated by phytochelatins exists in white lupin which has the potential to explain the successful tolerance of excluder species. This improved understanding of how plants

can adapt to, and potentially alter, metal(loid) challenged soil environments can help inform sustainable strategies to help mitigate environmental pollution.

Acknowledgments

We gratefully acknowledge the financial support provided from NSERC/Hydro-Québec Industrial Research Chair in Phytotechnology, MITACS, NSERC Strategic Project Grant (STPGP-506680-17), Natural Resources Canada Forest Innovation Program Grant (CWFC1718-018 and CWFC1920-104), ECCC Environmental Damage Fund (EDF-PQ-2020b012) and NSERC Discovery Grant (FEP RGPIN-2017-05452). We would like to thank Annie-Claude Martel for kindly providing use of CEPROCQ's laboratory equipment and Dr. Benjamin Péret for graciously providing white lupin seeds. A special thank you is extended to Kymberly Newton, Aleena Massenet, Susan Boucher, and Loup Sénizergues for their kind support during harvest.

Supplementary information

All the data supporting the results, as well as supplementary file 1 are publicly available in MassIVE repository: MSV000087512. Accessible at: https://massive.ucsd.edu/ProteoSAFe/static/massive.jsp

Supplementary figure

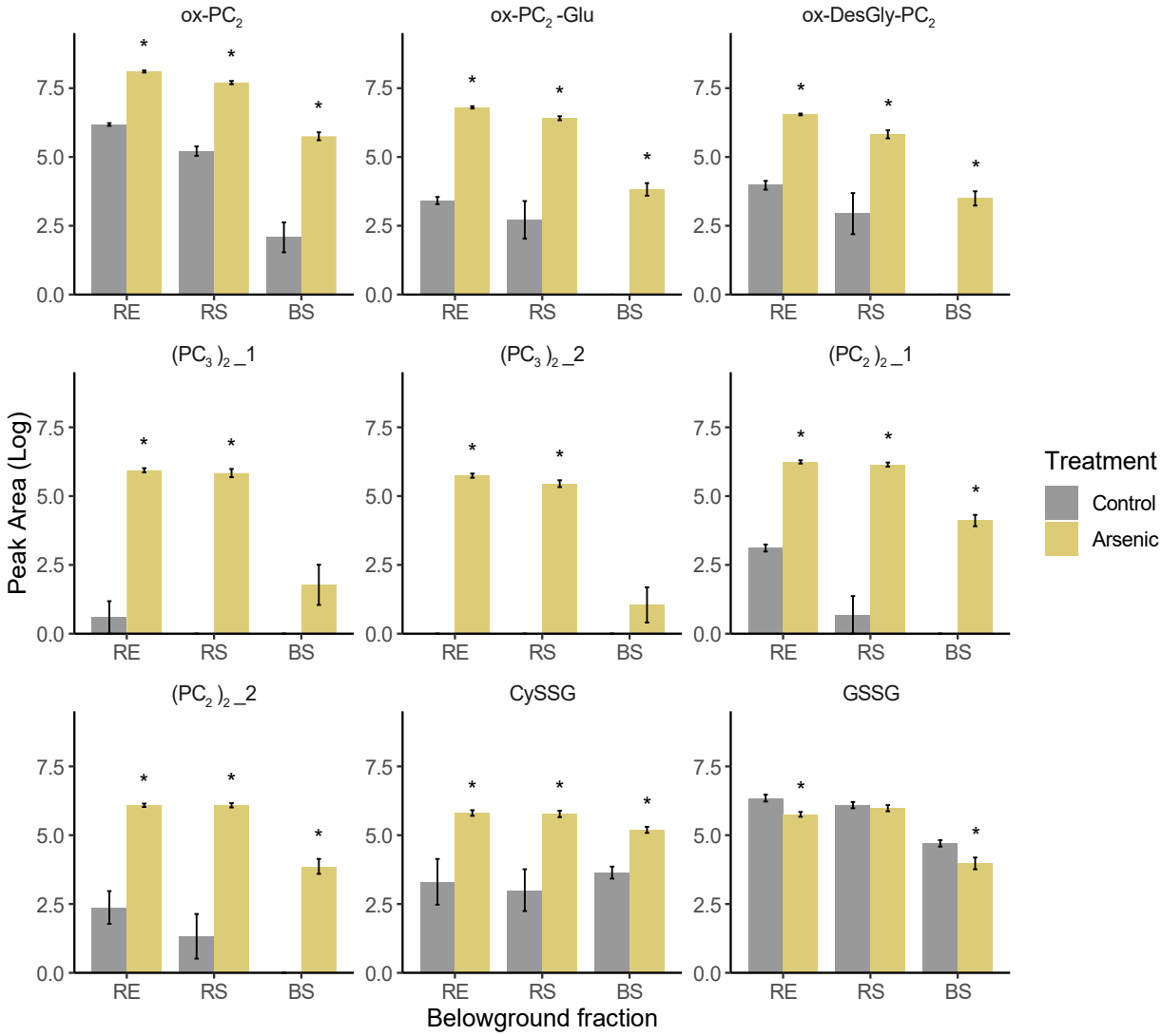

Figure S1 Abundance (Logged peak area) of PC and GSH derived compounds in the different belowground fraction comparing controls and arsenic-treated plants.
Asterisks indicate significant difference from controls (Mann-Whitney U test, FDR correction, $p < 0.05$)

Chapitre 2 – Le stress à l'arsenic induit l'exsudation active de complexes arsenic-phytochélatine des racines de *Lupinus albus*

Arsenic stress triggers active exudation of arsenic-phytochelatin complexes from *Lupinus albus* roots

Adrien Frémont[1], Eszter Sas[1], Mathieu Sarrazin[2], Jacques Brisson[1], Frédéric Emmanuel Pitre[1,3], Nicholas James Beresford Brereton[4]

[1] Institut de recherche en biologie végétale, Université de Montréal, 4101 Sherbrooke Est, Montréal, QC H1X 2B2, Canada

[2] Collège de Maisonneuve CÉPROCQ, 6220 Sherbrooke Est, Montréal, Québec, Canada

[3] Montreal Botanical Garden, 4101 Sherbrooke Est, Montreal, Québec, Canada

[4] School of Biology and Environmental Science, University College Dublin, Belfield, Dublin 4, Ireland

Under review in Journal of Experimental Botany

Abstract

Arsenic contamination of soils threatens the health of millions globally through accumulation in crops. While plants detoxify arsenic via phytochelatin (PC) complexation and efflux of arsenite from roots, arsenite efflux mechanisms are not fully understood. Here, white lupin (*Lupinus albus*) was grown in semi-hydroponics and exudation of glutathione (GSH) derivatives and PCs in response to arsenic was scrutinised using LC-MS/MS. Inhibiting synthesis of PC precursor GSH with L-buthionine sulfoximine (BSO) or ABC transporters with vanadate drastically reduced (>22%) GSH-derivative and PC_2 exudation, but not PC_3 exudation. This was accompanied by arsenic hypersensitivity in plants treated with BSO and moderate sensitivity with vanadate treatment. Investigating arsenic-phytochelatin (As-PC) complexation revealed two distinct As-PC complexes, As bound to GSH and PC_2 (GS-As-PC_2) and As bound to PC_3 (As-PC_3), in exudates of As-treated lupin. Vanadate inhibited As-PC exudation, while BSO inhibited both the synthesis and exudation of As-PC complexes. These results demonstrate the critical role of GSH derivatives and PC exudation in lupin arsenic tolerance and reveal As-PC exudation as a new mechanism of active arsenic efflux in plants. Overall, this study provides insight into rhizosphere arsenic detoxification and highlights the potential for As-PC exudation to mitigate pollution and reduce arsenic accumulation in crops.

Highlight

Active root exudation of arsenic-phytochelatin complexes in white lupin provides evidence of a new mechanism of arsenic efflux in plants, providing novel pathways for phytoremediation and food safety.

Keywords: *Lupinus albus*; arsenic; arsenic phytochelatin complexes; phytochelatin; phytoremediation; pollution; rhizosphere; root exudates; soil health

Introduction

Arsenic is a major soil contaminant affecting environment and human health. Contamination of soil and groundwater is widespread, with elevated arsenic concentrations resulting from natural weathering and biological activity, as well as anthropogenic activities such as mining and agriculture (Patel et al., 2023). With an estimated 2.8 million contaminated sites in Europe and 20 million hectares of farmland affected by heavy metals in China, extensive soil pollution is putting substantial pressure on agricultural soils (FAO & ITPS, 2015). As plants readily take up mobile arsenic from the soil and translocate it to aboveground tissues, dietary intake presents a major exposure route to humans, potentially threatening millions with a range of adverse health effects from arsenic poisoning (Zhao et al., 2010a). Therefore, understanding the specific processes governing arsenic bioavailability, uptake, and detoxification in plants is critical for developing mitigation strategies. One crucial plant-soil interaction thought to help plants adapt to and influence arsenic-challenged soil is the release of diverse metabolites from roots (root exudates) which can markedly impact soil chemistry and microbiota to influence contaminant tolerance (Podar & Maathuis, 2022). However, the molecular mechanisms underlying root exudate-mediated arsenic detoxification are not fully elucidated.

In aerobic soils, plants predominantly encounter arsenic in the form of arsenate [As(V)] which enters roots through phosphate transporters (Asher & Reay, 1979; Ullrich-Eberius et al., 1989), while arsenite [As(III)] is most prevalent in anaerobic soils and enters roots through aquaporin channels (Bienert et al., 2008). Arsenic detoxification and tolerance mechanisms have been largely studied in the hyperaccumulating species *Pteris vittata* (Lombi et al., 2002; Ma et al., 2001; Su et al., 2008) in which arsenate taken up from the soil through phosphate transporters is reduced to arsenite in the roots and rapidly translocated to aboveground tissues, where free arsenite is sequestered in vacuoles (Zhao et al., 2009). In contrast, non hyperaccumulating species preferentially eliminate up to 90 % of internally reduced arsenite back into the external medium, partly through aquaporin channels but also through yet-to-be identified pathways (Zhao et al., 2010b), while the remaining intracellular arsenite is complexed with phytochelatins (Schmöger et al., 2000).

Phytochelatins (PC_n) are oligomers derived from glutathione (GSH) and comprised of $(\gamma\text{-glutamylcysteinyl})_n$ glycine units, typically with n between 2 and 11. PCs can form stable complexes with arsenic through coordination with cysteine thiol groups, including As-PC_3, As-$(PC_2)_2$ and GS-As-PC_2 (Raab et al., 2004), and play a critical role in arsenic detoxification and stabilisation in plants. Liu et al., (2010) found up to 70% of intracellular arsenite bound to PCs in *Arabidopsis thaliana* roots. Mutants deficient in PC synthesis, such as *cad1-3*, exhibit 10- to 20-fold greater sensitivity to arsenate

compared to wild-type plants (Ha et al., 1999). Furthermore, inhibition of the PC precursor GSH using L-buthionine sulfoximine (BSO) induces arsenic hypersensitivity across diverse plant species (Meharg & Hartley-Whitaker, 2002).

The ultimate phase of arsenic detoxification in non-hyperaccumulating plants is thought to occur through ATP-dependent vacuolar loading of arsenic-phytochelatin complexes, mediated by ABC transporters localised to the tonoplast, as evidenced by inhibition of arsenic-phytochelatin vacuolar sequestration with ABC transport inhibitor vanadate (Song et al., 2010). However, recent evidence also points to extracellular roles of PCs in arsenic detoxification. Phytochelatin 2 was found in root exudates of *Lupinus albus*, suggesting arsenic complexation in the rhizosphere or PC complex-mediated efflux of arsenite directly from roots (Frémont et al., 2022). Elucidating the mechanisms and roles of PC exudation is important for harnessing the potential of root exudates to mitigate arsenic environmental and health damage, yet a number of challenging methodological hurdles need to be overcome.

Current methods for capturing root exudates largely utilise hydroponic and aeroponic cultivation systems. While these substrate-free growth methods provide easy access to roots and root exudates, they lack the physical properties of soils that influence root architecture and physiology (Oburger & Jones, 2018). Soil-like substrates such as silica sand may offer advantages, providing mechanical support and resistance to root growth that feedback to modulate root morphology and exudate composition, while still maintaining inert properties to limit interference from soil organic particles (Sasse et al., 2020). Beyond experimental limitations, chemical characterisation of root exudates also faces several hurdles, particularly due to the intricate chemical interactions occurring between arsenic and root exudates, which may produce transient compounds critical for arsenic detoxification (Bluemlein et al., 2009). Analytical approaches like LC-MS/MS have enabled detection of previously unknown metal-organic complexes involved in metal detoxification in the rhizosphere, such as zinc-nicotianamine (Tsednee et al., 2014). Therefore, coupling physiologically relevant growth systems with selective, high-resolution analytical techniques may shed light on specialised plant exudation mechanisms for arsenic detoxification and tolerance.

In this research, the root exudation tolerance mechanisms of arsenic-exposed lupins were investigated. Using targeted LC-MS/MS and in vitro arsenic complexation assay, phytochelatins and arsenic-phytochelatin complexes levels were assessed in the endosphere and in exudates. Chemical inhibition of glutathione synthesis with BSO and ABC transporter-mediated exudation with vanadate was then

used to elucidate the mechanisms involved in As-PC complex exudation and their influence on the fate of arsenic in the rhizosphere.

Materials and methods

Plant growth and experimental design

Seeds of white lupin (*Lupinus albus* L. cv. AMIGA) were surface sterilised by sequential immersion in 70% ethanol, 1% sodium hypochlorite, and sterile Milli-Q water. Sterilised seeds were germinated on moist filter paper for 3 days, after which seedlings were transferred to growth pouches (7.6 x 15.2 cm) containing 700 ml sterile silica sand, for a total of 30 plants divided into 5 blocks (**Figure 1A**). Plants were supplied twice weekly with 65 ml Hoagland nutrient solution (pH 6.0) containing the following concentrations: 1,600 µM N, 200 µM P, 605 µM K, 400 µM Ca, 100 µM S, 100 µM Mg, 5 µM Cl, 2.5 µM B, 0.2 µM, 0.2 µM Zn, 0.05 µM Cu, 0.05 µM Mo, 4.5 µM Fe. Growth chamber conditions were 18 h photoperiod under LED lighting (150 µmol m^{-2} s^{-1}) at 25°C. After 22 days, plants were either kept as untreated controls or subjected to BSO or vanadate inhibitor treatments (n=10 each) prepared in Hoagland solution: 0.5 mM L-buthionine sulfoximine (BSO) (>99% Thermo Fisher Scientific, Cat# AC235520010), a GSH synthesis inhibitor (Liu et al., 2010), and 1 mM vanadate (Sodium Orthovanadate, >99% Thermo Fisher Scientific, Cat# AC205330500) an ABC-type transporter inhibitor (Song et al., 2014). Three days after the initial inhibitor treatment, plants were subjected to a second inhibitor treatment and further divided into + or – arsenate groups with the addition of 13 µM arsenate ($Na_2HAsO_4 \cdot 7H_2O$, Sodium hydrogen arsenate heptahydrate, >98%, Thermo Fisher Scientific, Cat# AAA1827536), resulting in six treatments (n=5 each): control, arsenate, BSO, arsenate + BSO, vanadate, and arsenate + vanadate (**Figure 1A**). Unplanted controls were also included for each treatment (n=5 each). Stomatal conductance was measured at day 27 and 28 on the abaxial surface of the youngest fully expanded leaf (Vezza et al., 2018) using a porometer (LI-600, LI-COR Biosciences). Shoot and root morphology, as well as biomass, were assessed at the time of harvest (28 days).

Root exudate collection and root metabolite extraction

Root exudates were collected following the procedure of Frémont et al. (2022). Briefly, nylon mesh growth pouches were opened and loose sand was gently removed, leaving intact root systems with attached rhizosheaths. Root systems were then immersed in 40 mL Milli-Q water for 10 seconds with gentle circular agitation to collect exudates (**Figure 1B**). Although care was taken to minimise root damage, some exudates may have originated from cellular injury. For unplanted controls, 20 g of sand

from each unplanted pot was extracted under identical conditions to mirror the quantity of sand obtained from rhizosheaths. Solutions were lyophilised and stored at -70°C. All lyophilised extracts were resuspended in 800 µL Milli-Q water and 0.1% formic acid, filtered through 0.2 µm centrifuge filters (InnoSep Spin, Canadian Life Sciences) at 10,000 x g for 30 seconds, transferred to HPLC vials and kept at 4°C before LC-MS/MS analysis within 24 h.

After rhizosphere extraction, whole root systems went through 5 additional wash cycles in Milli-Q water with strong vortexing at maximum speed to recover root samples devoid of rhizosphere residues for endosphere metabolite extraction. Root samples were dried of residual water using absorbing paper, immediately frozen in liquid nitrogen, lyophilised, and kept at -70°C. Root samples were ground using a mortar and pestle and 50 mg of dried material was extracted in 1 mL Milli-Q water + 0.1% formic acid for 15 minutes with ultrasonication at 4°C. Endosphere extracts were then centrifuged at 4°C at 20,000 x g for 2 minutes, the supernatant transferred to 0.2 µm centrifuge filters, centrifuged at 10,000 x g for 30 seconds, transferred to HPLC vials and kept at 4°C before LC-MS/MS analysis within 24 h.

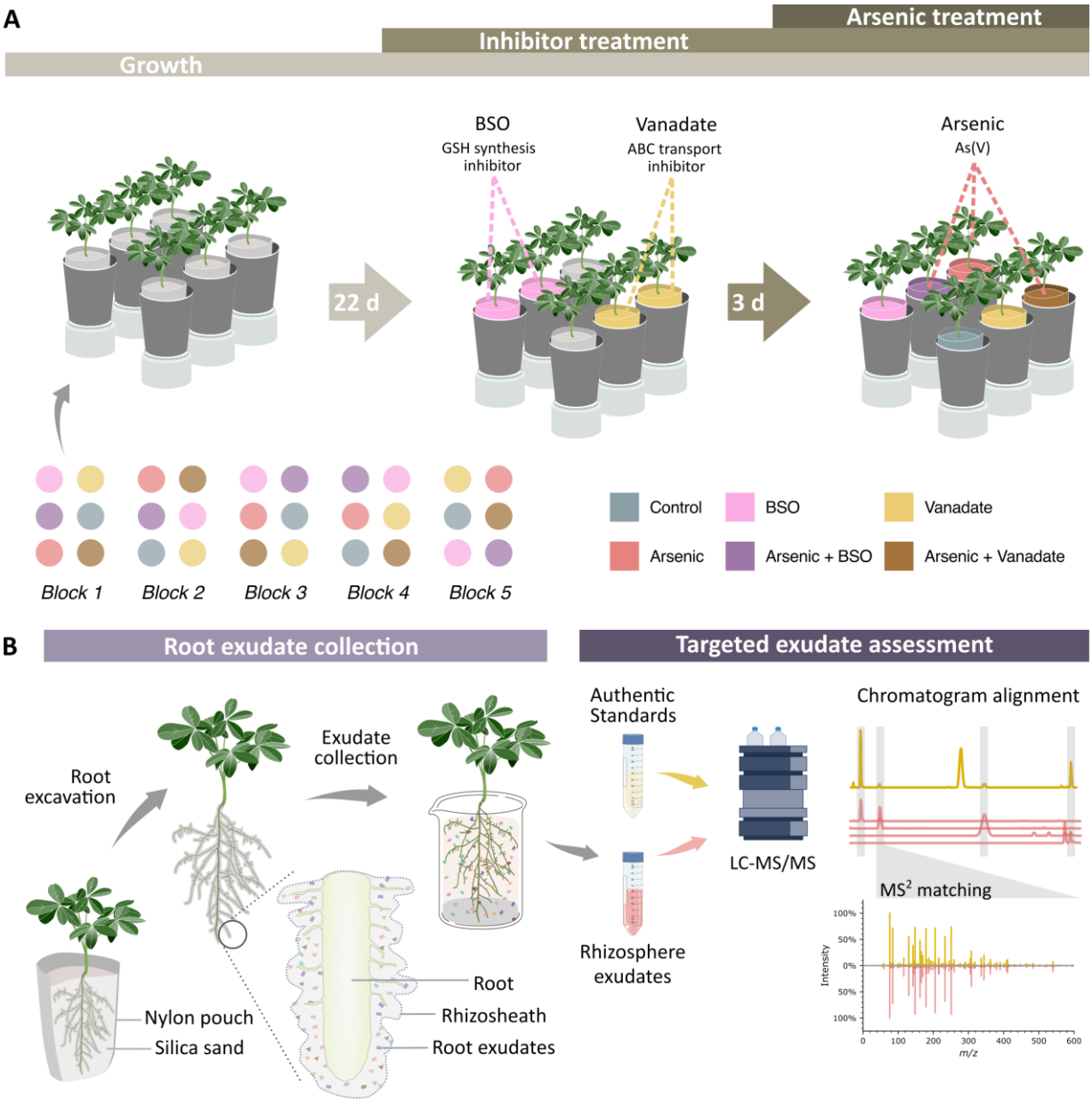

Figure 1 Experimental design and workflow for collecting and analysing root exudates.
(A) Experimental design (n = 5, illustrated; total plants = 30), with each plant grown for 22 days before inhibitors, arsenic, and co-treatments. **(B)** Exudate capture workflow, adapted from Frémont et al. (2022). Plants were extracted from nylon pouches with rhizosheaths intact, then briefly dipped in water to collect exudates. Exudate solutions were concentrated by freeze-drying before LC-MS/MS. Exudate metabolites were identified by comparing LC-MS/MS chromatograms and retention times to commercial standards and synthesised compounds (Table S1), with definitive ID based on matching MS^2 spectra to authentic standards.

Liquid chromatography-tandem mass spectrometry (LC-MS/MS) analysis

Targeted metabolite profiling was performed using an Agilent 1,260 Infinity HPLC system coupled to an Agilent 6530 Q-TOF mass spectrometer with Jet Stream ionisation source. Chromatographic separation utilised a Zorbax Eclipse Plus C18 column (4.6 x 100 mm, 3.5 μm) at 30°C with a 0.4 mL/min flow rate. The 80 min gradient consisted of solvent A (5% methanol, 0.1% formic acid in water) and solvent B (methanol, 0.1% formic acid), starting at 100% A for 20 min, increasing linearly to 100% B over 50 min, then holding at 100% B for 10 min. Biological samples (n=30), unplanted controls (n=15), and Milli-Q water blanks (n=5) were analysed in ESI+ mode. MS^2 fragmentation used a precursor ion inclusion list at 20 and 35 eV collision energy (Table S1) and was performed on 3 samples per treatment (n= 18). Source parameters included 300°C gas temperature, 5 L/min drying gas, 45 psig nebulizer pressure, 250°C sheath gas temperature, and 11 L/min sheath gas flow.

LC-MS raw data were processed in MZmine 3.4.14 (Schmid et al., 2023). Background noise was filtered at intensity thresholds of 800 for MS^1 and 10 for MS^2. Chromatograms were constructed within 10 ppm mass accuracy and minimum peak intensity of 800. Extracted ion chromatograms were deconvoluted using MZmine's minimum search algorithm. Isotope peaks were grouped within 10 ppm mass tolerance and 0.1 min retention time tolerance. Features were aligned across samples within 15 ppm mass tolerance (75% weighting) and 0.2 min retention time tolerance (25% weighting). Features containing MS^2 spectra were retained. Gaps in the feature matrix were filled within 0.8 min retention time and 5 ppm mass tolerances. MS^2 spectra were matched to precursor ions within 0.02 m/z and 0.2 min retention time windows. MS^2 spectra acquired at 20 and 35 V collision energies were merged into consensus spectra after summing their intensities.

Targeted metabolite annotation

Targeted features were annotated as glutathione (GSH), glutathione disulfide (GSSG), phytochelatins (PCs) and their arsenic (As) complexes based on matching retention times and MS^2 spectra (cosine > 0.9) to those of authentic standards analysed under identical LC-MS/MS conditions (**Figure 1B**). Standards were prepared from commercially obtained phytochelatin 2 (PC_2) and phytochelatin 3 (PC_3) (Anaspec, Fremont, CA, USA), GSH (Alfa Aesar Co., Inc., Ward Hill, MA, USA) and GSSG (ACROS Organics, Geel, Belgium). Oxidised PCs were generated via spontaneous oxidation during sample preparation. As-PC complexes were synthesised following Schmied-Tobies et al. (2014) by incubating PC_2, PC_3 and GSH standards (100 μM) with arsenite at various thiol (SH):As molar ratios (3:1, 1:3, 1:6) in 0.1% formic acid. To synthesise As-GS_3 complex, GSH alone was incubated with As (III) at a

1:6 SH:As molar ratio. See Supporting Information Table S1 for the full list of ions produced from As-PC *in vitro* complexation and their corresponding chemical formulas.

Statistical analysis

One-way analysis of variance (ANOVA) followed by Tukey's honest significant difference (HSD) *post hoc* test was used to determine treatment effects when data met assumptions of normality and homogeneity of variance. For non-normal or heteroscedastic data, the non-parametric Kruskal-Wallis test followed by Dunn's *post hoc* test was used for multiple comparisons. P values were adjusted for false discovery rate control using the Benjamini-Hochberg method (Benjamini & Hochberg, 1995). Pairwise comparisons were performed using T-tests when data met assumptions of normality and homogeneity of variance and Mann-Whitney U tests for non-normal or heteroscedastic data. All analyses were conducted in R v.4.3.1 (R Core Team, 2020).

Results

Physiological response

Lupin plants (*Lupinus albus*) were grown for 26 d and left as either untreated as controls, or subjected to treatments with arsenic (As), L-buthionine sulfoximine (BSO), As + BSO, vanadate, As + vanadate. Stomatal conductance (g_s) was measured at 24 and 48 h post-treatment. After 24 h, neither As nor inhibitor treatments significantly affected g_s, except for a significant decrease from 0.25 ± 0.043 to 0.04 ± 0.01 mol m^{-2} s^{-1} with As + BSO compared to As alone ($P<0.05$, ANOVA, Tukey's HSD; **Figure 2B**). By 48 h, no significant effects on g_s were observed for As, BSO or vanadate alone. However, As + BSO significantly reduced g_s to undetectable levels compared to 0.12 ± 0.026 mol m^{-2} s^{-1} in controls and 0.18 ± 0.036 mol m^{-2} s^{-1} in As-treated plants, and wilting was observed, while As + vanadate significantly decreased g_s to 0.03 ± 0.01 mol m^{-2} s^{-1} compared to As alone, without any observable morphological effects (**Figure 2A, B**). At harvest (28 d), only As + BSO reduced shoot fresh biomass compared to controls, from 3,596 ± 305 mg FW in controls to 2,501 ± 98 mg FW in As + BSO ($P<0.05$, ANOVA, Tukey's HSD).

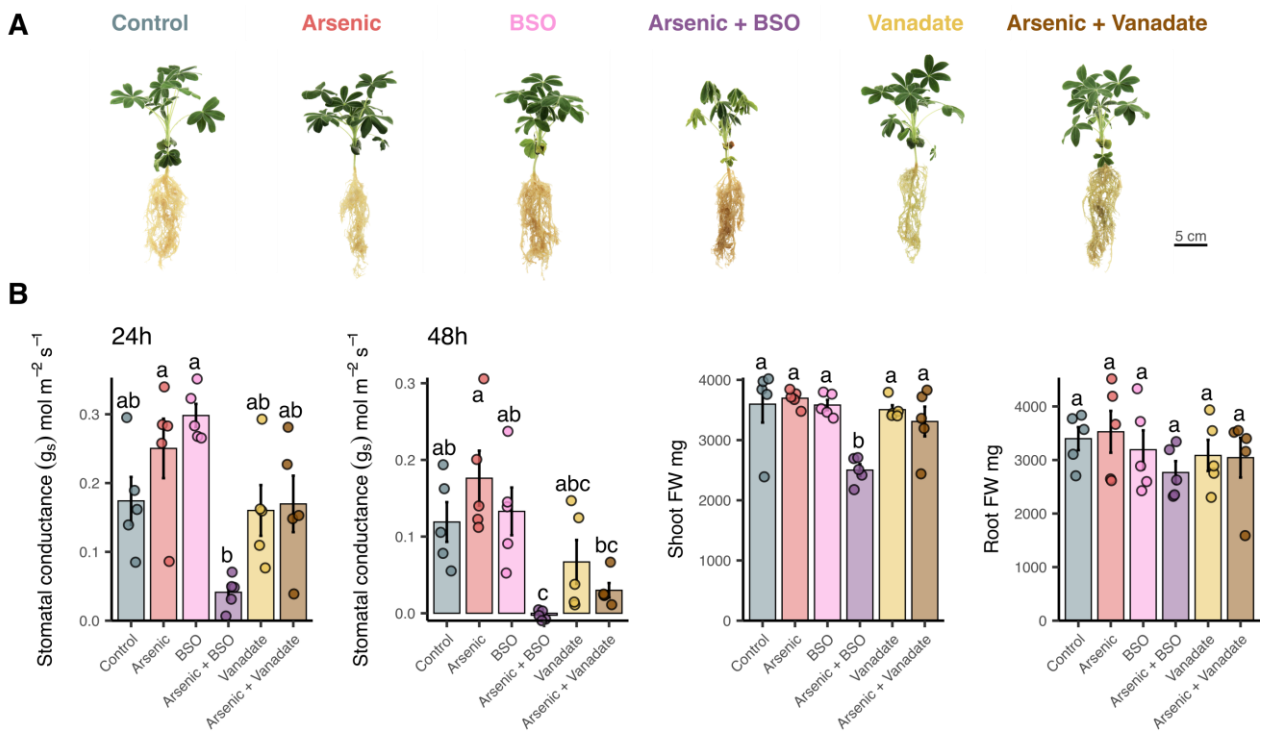

Figure 2 Physiological responses of white lupin to inhibitors, arsenic, and co-treatments. **(A)** Representative photographs of whole plants at harvest for each treatment. **(B)** Stomatal conductance (gs) at 24 h and 48 h after treatments and shoot and root fresh weight (FW) biomass. Data show means ± SE (n=5). Different letters indicate significant differences between treatments (ANOVA, Tukey HSD test, $P < 0.05$).

Targeted analysis of glutathione and phytochelatin exudates

To evaluate the metabolic response of lupin to arsenic, root tissue (endosphere) extracts and rhizosphere exudates from arsenic-treated plants were analysed using LC-MS/MS and compared to authentic standards. Six major glutathione-derived compounds and phytochelatins (PCs) were measured: glutathione (GSH), glutathione disulfide (GSSG), phytochelatin 2 (PC_2), oxidised phytochelatin 2 ($oxPC_2$), phytochelatin 3 (PC_3) and two isomers of oxidised phytochelatin 3 ($oxPC_3$, iso-$oxPC_3$). The endosphere contained GSH, GSSG, both reduced and oxidised forms of PC_2, but only $oxPC_3$ (**Figure 3A**). Exudates contained GSH, GSSG, $oxPC_2$ and $oxPC_3$. $OxPC_2$ was most prominent in both the endosphere and rhizosphere of arsenic-treated plants.

In comparing endosphere of control and arsenic-treated plants, GSH levels were not significantly different, while GSSG was depleted in As-treated roots (**Figure 3B**). PC_2 was detected in As-treated plants but not in controls, while PC_3 was not detected. $OxPC_2$ and $oxPC_3$ were enriched in As-treated roots compared to controls, with iso-$oxPC_3$ not detected in controls (**Figure 3B**). In exudates, GSH did

not significantly vary between controls and As-treated plants, while GSSG was significantly depleted (**Figure 3C**). Exuded $oxPC_2$ and $oxPC_3$ were enriched in As-treated plants compared to controls, with $oxPC_2$ the most enriched compound, and iso-$oxPC_3$ absent in untreated controls (**Figure 3C**).

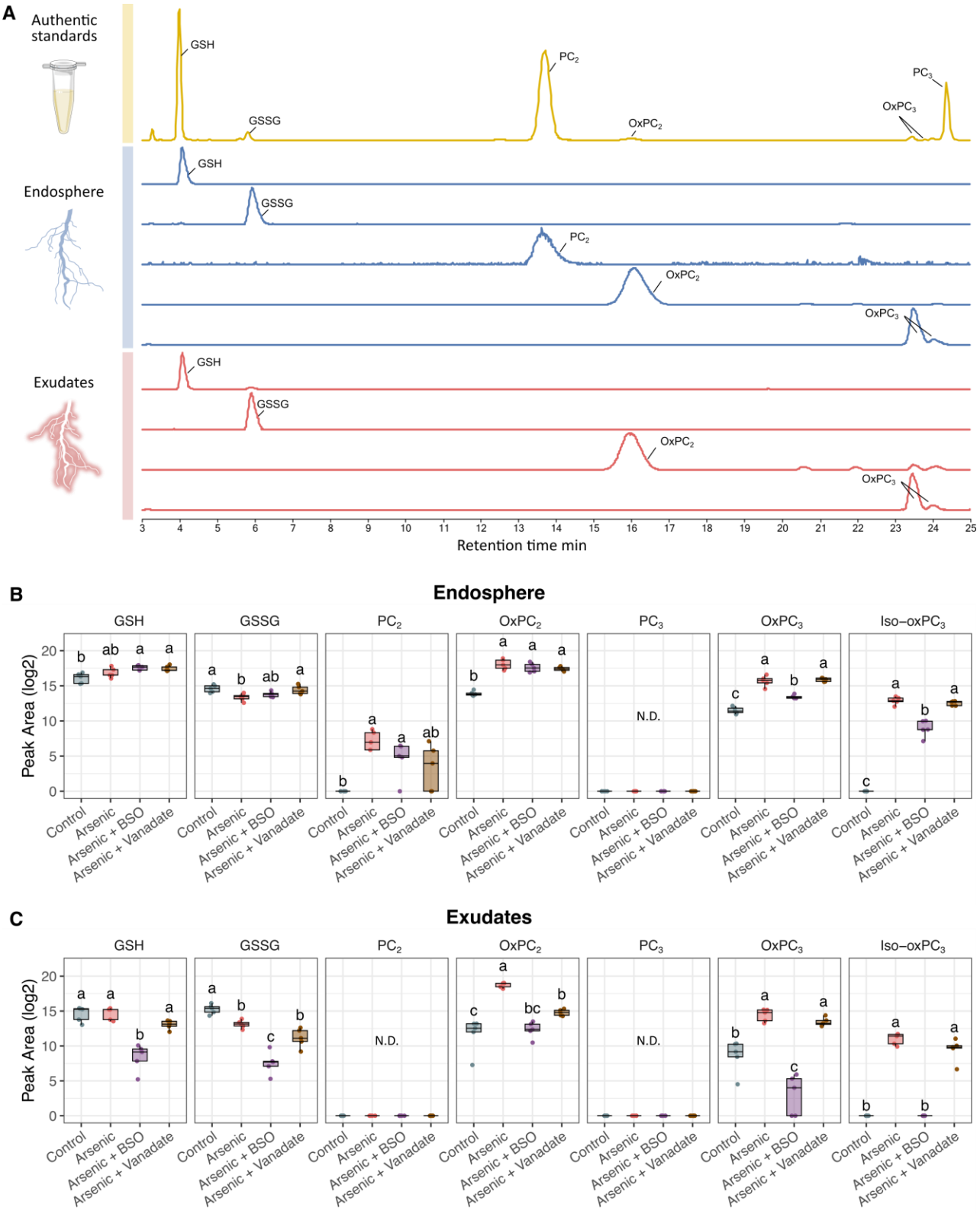

Figure 3 Glutathione derivatives and phytochelatins in endosphere and root exudates in response to treatment. (A)

Base peak chromatogram of glutathione (GSH) and phytochelatin (PC) standards (yellow) and extracted ion chromatograms of GSH (*m/z*: 308.09107; [M+H]+), oxidised glutathione (GSSG) (*m/z*: 613.15862; [M+H]+) and PC_2 (*m/z*: 540.14152; [M+H]+), oxidised phytochelatin 2 ($oxPC_2$) (*m/z*: 538.12685; [M+H]+), $oxPC_3$ and its isomer (iso-$oxPC_3$) (*m/z*: 770.17546; [M+H]+) detected in endosphere (blue) and exudates (red) of As-treated lupin plants, with definitive ID based on matching retention time and MS^2 spectra. **(B)** GSH derivatives and PC abundance (Log2 peak area) in endosphere (root extracts) from controls and treated plants. **(C)** GSH derivatives and PC abundance in exudates from controls and treated plants. For all boxplots the bottom and top of the boxes correspond to the lower and upper quartiles and the center line marks the median (n = 5). Different letters indicate significant differences between treatments (ANOVA, Tukey HSD test, $P < 0.05$). Full factorial plots including all six treatments are presented in **Figure S1**.

Inhibition of arsenic response

In the endosphere, co-treatment with As + BSO did not significantly alter levels of GSH, GSSG, PC_2 and $oxPC_2$ compared to As alone (**Figure 3B**). However, $oxPC_3$ and iso-$oxPC_3$ were significantly depleted with As + BSO co-treatment compared to As alone. Compared to controls, GSH, PC_2, $oxPC_2$, $oxPC_3$ and iso-$oxPC_3$ were significantly enriched in As + BSO co-treatment, while GSSG did not significantly vary. Co-treatment with As + vanadate resulted no significant change in levels of GSH, PC_2, $oxPC_2$, $oxPC_3$ and iso-$oxPC_3$ compared to As alone but induced a significant enrichment of GSSG. Compared to control, As + vanadate significantly increased GSH, $oxPC_2$, $oxPC_3$ and iso-$oxPC_3$ but did not significantly affect levels of GSSG or PC_2.

In exudates, co-treatment with As + BSO significantly reduced As response of the thiol-containing compounds, with GSH, GSSG and $oxPC_3$ being depleted compared to both control and As treatment, while $oxPC_2$ and iso-$oxPC_3$ returned to control levels (**Figure 3C**). Co-treatment with As + vanadate did not significantly alter GSH, GSSG, $oxPC_3$ and iso-$oxPC_3$ levels compared to As-treatment, but did significantly deplete levels of $oxPC_2$. Compared to controls, As + vanadate co-treatment resulted in similar levels of GSH and a significantly depleted level of GSSG, as well as significantly increased levels of $oxPC_2$, $oxPC_3$ and iso-$oxPC_3$ (**Figure 3C**).

Targeted analysis of arsenic-phytochelatin complexes in exudates

To evaluate the potential for detecting arsenic-phytochelatin (As-PC) complexes in the endosphere and root exudates, an *in vitro* experiment was conducted in which arsenite As(III) was incubated in 0.1 M formic acid with standards of GSH, PC_2, and PC_3, either individually or in combinations at varying thiol:arsenic molar ratios. Liquid chromatography-tandem mass spectrometry (LC-MS/MS) revealed

six chromatographic peaks present only with As addition, corresponding to five distinct As-PC complexes and their isomers (**Figure 4A**, Table S1).

By re-analysing endosphere and exudate samples with these *in vitro*-derived spectra (**Figure 4A**), two As-PC complexes were identified in both endosphere and exudates: GS-As-PC_2, which comprised one molecule of GSH and one molecule of PC_2 coordinated to As(III) through their three thiol groups, and As-PC_3, in which As(III) is coordinated to the three thiol groups of one PC_3 molecule (**Figure 4B**). GS-As-PC_2 and As-PC_3 were absent from control endosphere and exudate samples and As-PC_3 was the most prevalent As complex in As-treated endosphere and exudates (**Figure 4C, D**).

In the endosphere, addition of BSO significantly reduced levels of both GS-As-PC_2 and As-PC_3 compared to As treatment alone, while vanadate had no significant effect on endosphere GS-As-PC_2 and As-PC_3 levels compared to As treatment alone (**Figure 4C**). However, both the application of BSO and the application of vanadate eliminated all GS-As-PC_2 from exudates, while As-PC_3 exudation was only partially reduced with BSO, and almost eliminated with vanadate, with only one outlier with detectable As-PC_3 (**Figure 4C, D**).

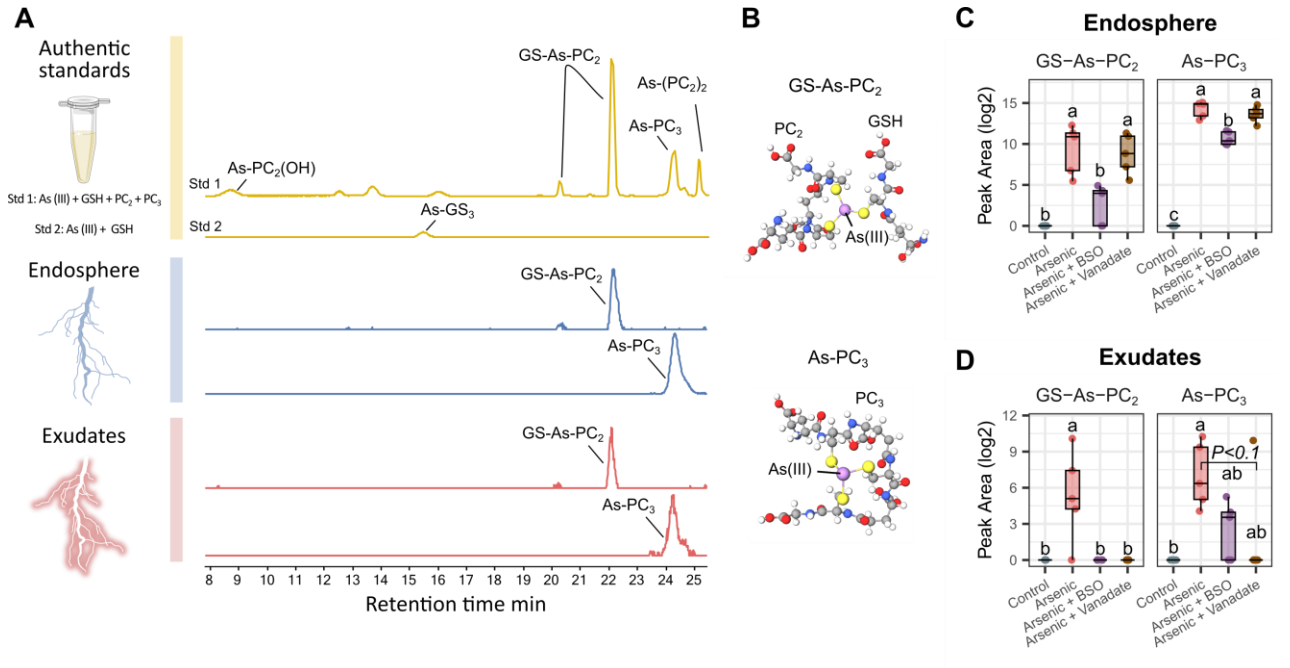

Figure 4 Arsenic-phytochelatin complexes in endosphere and root exudates in response to treatments. (A) Base peak chromatogram of synthesised arsenic-phytochelatin complex (As-PC) standards (yellow) and extracted ion chromatograms of glutathione-arsenic-phytochelatin 2 complex (GS-As-PC_2) (m/z: 460.06593; [M+2H]2+), and arsenic-phytochelatin 3 complex (As-PC_3) (m/z: 844.09144; [M+H]+) detected in endosphere (blue) and exudates (red) of arsenic-treated lupin plants, with definitive ID based on matching retention time and MS^2 spectra (**Figure S2**). **(B)** Proposed structures of As-PCs in arsenic-treated lupin, adapted from Schmied-Tobies et al. (2014). 3D models generated using MolView (https://molview.org/). **(C)** Abundance (Log2 peak area) of As-PCs in root endosphere from control and treated plants. **(D)** As-PC abundance in exudates from control and treated plants. For all boxplots the bottom and top of the boxes correspond to the lower and upper quartiles and the centre line marks the median (n = 5). Different letters indicate significant differences between treatments (ANOVA, Tukey HSD test; Kruskal-Wallis, Dunn's test; p.adj < 0.05). Full factorial plots including all six treatments are presented in **Figure S2**.

Discussion

Combination of metabolic inhibitors and arsenic disrupts lupin arsenic tolerance

Arsenic (As) alone had no significant effect on stomatal conductance or biomass in lupin, which confirms tolerance to short-term exposure to 13 µM As(V) as previously observed (Frémont et al., 2022; Vázquez et al., 2005). Similarly, the application of inhibitors without arsenic treatment did not affect physiological parameters compared to control, except for a small non-significant increase in stomatal conductance 24 h after L-buthionine sulfoximine (BSO) treatment, indicating physiological functions were largely maintained during inhibitor treatment. However, co-treatment with As and

BSO, which inhibits glutathione (GSH) synthesis (Liu et al., 2010), substantially reduced both stomatal conductance and biomass, particularly after 48 h with complete loss of stomatal conductance and wilting (**Figure 2**). This acute sensitivity to As + BSO co-treatment resembles the response previously reported with much higher (5×) As concentrations (Frémont et al., 2022), underscoring the protective role of GSH and derivatives in mitigating arsenic toxicity in lupin. Additionally, co-treatment with As and vanadate, an ATP-dependent membrane transport inhibitor (Song, Mendoza-Cózatl, et al., 2014), decreased stomatal conductance at 48 h, highlighting vanadate-induced As sensitivity and suggesting the involvement of active transmembrane transport in lupin As detoxification.

Targeted exudates assessment reveals critical roles of glutathione-derived metabolites and phytochelatin synthesis and exudation in lupin arsenic tolerance

In a previous study, Frémont et al., (2022) reported the presence of PCs in exudates of arsenic-treated lupin plants. Since PCs are major arsenic detoxification metabolites in plants (Cobbett & Goldsbrough, 2002), the exudation of PCs and their GSH precursor were examined here to gain insight into their mechanisms of exudation, interactions with arsenic and roles in As detoxification. With the exception of GSH, which was unchanged, all measured GSH-derivatives and PCs in endosphere and exudates exhibited significant and substantial responses to As addition compared to controls (**Figure 3**). Oxidised glutathione (GSSG) decreased by 8% in the endosphere and 17% in arsenic-treated exudates. Since GSH is challenging to capture in exudates owing to its high reactivity (Giustarini et al., 2016), the significant GSSG depletion is an important clue indicating a general shift of the glutathione pathway towards increased PC synthesis in response to arsenic (Frémont et al., 2022; Vázquez et al., 2005). Oxidised PCs ($oxPC_2$ and $oxPC_3$) increased in abundance by >30% in the endosphere and >60% in exudates, confirming the enriched synthesis and exudation of $oxPC_2$ in response to As reported by Frémont et al., (2022) and the novel detection of $oxPC_3$ in lupin exudates.

Surprisingly, while As + BSO co-treatment significantly decreased GSH exudation, it did not decrease GSH levels in the endosphere (**Figure 3B**), contradictory with the target role of BSO as endogenous GSH synthesis inhibitor (Liu et al., 2010). One possible explanation for this could be the reduction of GSH exudation, compensating for the BSO-mediated reduction in endogenous GSH synthesis in order to maintain GSH levels within roots. Different responses between endosphere and exudates were also observed for GSSG and $oxPC_2$, which remained unchanged in the endosphere but were drastically reduced in exudates upon addition of As + BSO co-treatment (**Figure 3C**), confirming the reduced GSH availability affects exudation of metabolites downstream from GSH, such as GSSG, and PCs. On the other hand, the significant depletion of $oxPC_3$ in the endosphere and in exudates with As + BSO

co-treatment indicates decreased PC_3 synthesis and exudation. As PC_3 is a product of the stepwise condensation of γ-Glu-Cys moieties to PC_2 itself and of the growing phytochelatin chain, its synthesis is dependent on the availability of both PC_2 and GSH (Grill et al., 1989), which is likely strongly compromised with the addition of As + BSO. Overall, the severe disruption of lupin As tolerance with As + BSO (**Figure 2**) suggests inhibiting GSH synthesis likely disrupted PC production and exudation, which compromised essential As detoxification mechanisms such as the chelation of As(III) into non-toxic As-PCs complexes.

Inhibition of ATP-dependant membrane transport with vanadate effectively reduced exudate levels of $oxPC_2$ by more than 22% but did not influence endogenous synthesis (**Figure 3**). This indicates active transport and exudation of $oxPC_2$ across membranes likely involves (ATP-dependant) ABC transporters, analogous to those involved in As-PC complex loading into vacuoles in *Arabidopsis thaliana* (Song et al., 2010). However, unaltered levels of $oxPC_3$ in endosphere and exudates after As + vanadate treatment suggests a different exudation route may exist for these compounds. Collectively, although plasma membrane ABC transport appears important to facilitate $oxPC_2$ exudation, this alone may not fully explain the observed As-sensitivity with As-vanadate co-treatment (**Figure 2**) but likely represents one of multiple arsenic detoxification mechanisms conferring lupin As-tolerance, which potentially include As-PC complex exudation.

Phytochelatin-arsenic complexes exudation provides a new route for arsenic efflux and detoxification in lupin

Characterising arsenic-phytochelatin (As-PC) complexes in plant matrices presents several analytical challenges (Bluemlein et al., 2008, 2009) and is even more difficult in complex extracellular environments like the rhizosphere. To target specific As-PCs in the endosphere and the rhizosphere, As-PC complexes were first synthesised in vitro from GSH, PC_2, and PC_3 and analysed using liquid chromatography-tandem mass spectrometry (LC-MS/MS; **Figure 4A**). Five distinct As-PC species were detected, representing all known As-PC coordination schemes from these three compounds (Bluemlein et al., 2009; Schmied-Tobies et al., 2014). A targeted search for these complexes in endosphere and exudates of As treated plants revealed the presence of two As-PC complexes (**Figure 4A, B**), indicating rhizosphere As complexation, or As-complex exudation from roots, may act as a yet unknown As-detoxification mechanism in lupin.

Using this As-PC complex fingerprint, complexation in the rhizosphere was also explored after the use of detoxification inhibitors. By disrupting GSH synthesis, BSO also interrupted or drastically reduced As-PC in the endosphere and in exudates (**Figure 4C, D)**, indicating that arsenic detoxification through

As-PC complex formation relies on the availability of GSH for PC synthesis and As binding (Grill et al., 1989). Conversely, vanadate treatment had no effect on endosphere As-PC levels but abolished As-PC complexes in exudates (**Figure 4C, D**), likely due to inactivation of target membrane ABC-type transporters. This provides evidence of As-PC exudation as an active process, potentially occurring via ATP-dependant ABC transporters, similar to those plants use for As-PC vacuolar loading and sequestration (Song et al., 2010) (**Figure 5**). This new route for As detoxification in lupin may provide an additional mechanism beyond the current understanding of As(III) efflux from roots, of which approximately 20% is explained by NIP transporter-mediated efflux of free As(III), while the remaining 80% is still unaccounted for (Zhao et al., 2010b). While there is some evidence of increased unbound As(III) efflux when PC production is compromised (Liu et al., 2010), to our knowledge, this is the first investigation and report of As-phytochelatin complexes in exudates and characterisation of the exudation mechanisms involved.

These findings indicate As-PC complexes may contribute to As(III) efflux from roots, providing a new As detoxification and tolerance mechanism in plants. Future work should explore the specificity of transporters involved, quantify the rate of As-PC efflux from lupin roots and other plant species, and investigate the potential exudation of other heavy metal complexes. Elucidating this potential new detoxification pathway may have useful applications for phytoremediation as well as inform strategies aimed at reducing arsenic accumulation in food crops.

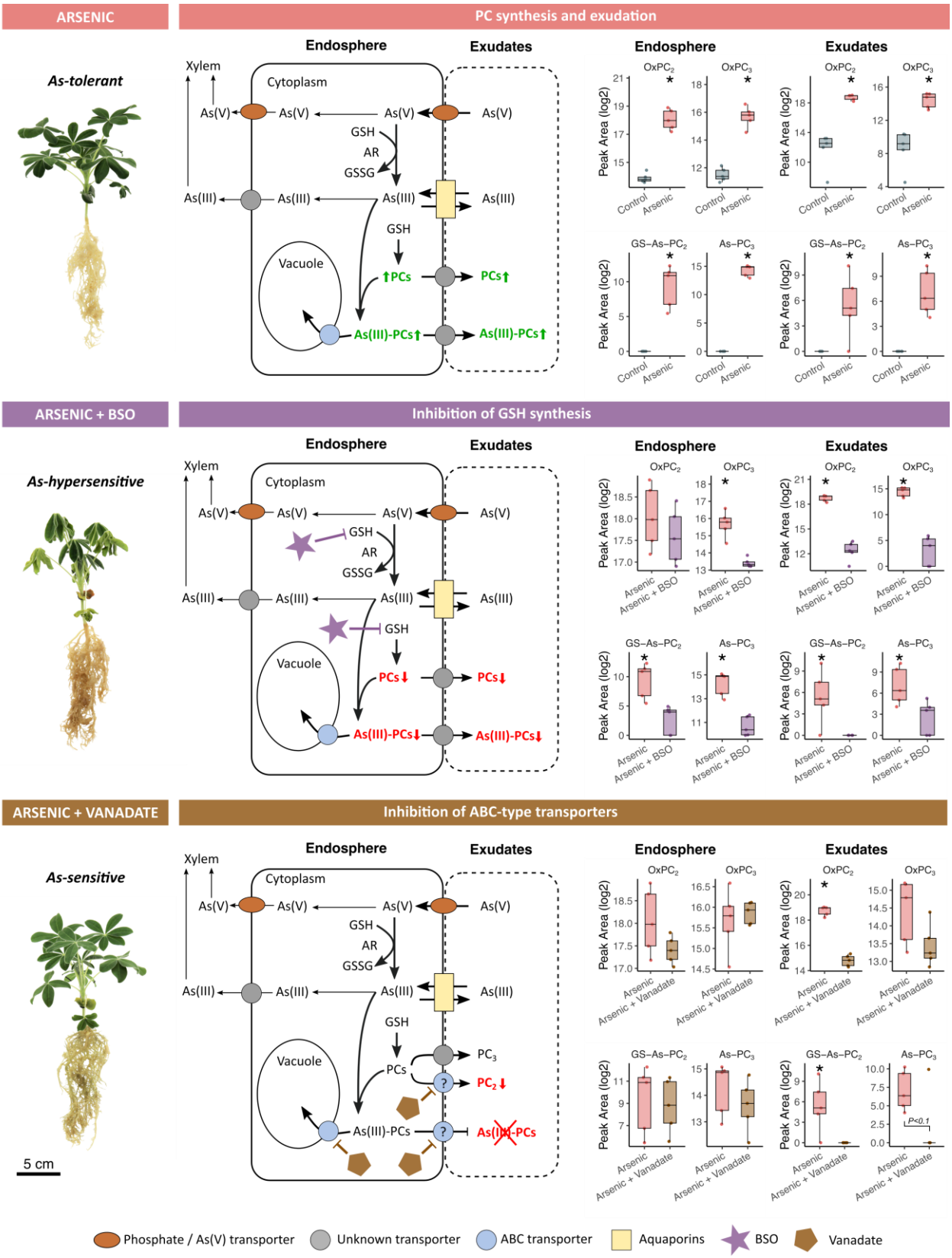

Figure 5 Arsenic treated Lupinus albus plants after chemical inhibition and corresponding putative detoxification models.

Adapted from Li et al. (2016). Arrows indicate demonstrated or putative arsenic metabolic and transport pathways, while question marks highlight knowledge gaps. For all boxplots the bottom and

top of the boxes correspond to the lower and upper quartiles and the centre line marks the median (n = 5); asterisks denote significant differences ($P<0.05$; T-test or Mann-Whitney U test). Abbreviations: ABC: ATP-binding cassette transporter; AR: arsenate reductase; GSSG: glutathione disulfide; GSH: glutathione; PC: phytochelatins.

Acknowledgements

We gratefully acknowledge the financial support provided from NSERC Discovery Grant (FEP RGPIN-2017-05452), MITACS (IT23193), NSERC/Hydro-Québec Industrial Research Chair in Phytotechnology, and the UCD Ad Astra Fellowship Programme. We would like to thank Dr. Benjamin Péret for graciously providing white lupin seeds. A special thank you is extended to Ariane Lafrenière for her kind support during harvest.

Supplementary information

All primary data to support the findings of this study were deposited to MassIVE and are openly available at [http://massive.ucsd.edu; MSV000093078]. Spectra from As-PC in vitro complexation were added as new library entries on the Global Natural Products Social Molecular Networking (GNPS) platform (https://gnps.ucsd.edu), and spectra IDs are listed in Supplementary Information Table S1.

Supplementary table

Table S1 Glutathione, phytochelatin, and arsenic-phytochelatin species identified from standards and in vitro complexation assay using liquid chromatography-tandem mass spectrometry (LC-MS/MS).
This list was used for targeted analysis of exudate and endosphere samples via LC-MS/MS. Global Natural Products Social Molecular Networking (GNPS) spectrum IDs correspond to new entries in the GNPS open spectral libraries (accessible at **https://library.gnps2.org/**).

Precursor m/z	Adduct	Mean RT (min)	Compound name	Molecular formula	GNPS Spectrum ID
308.092	[M+H]+	3.5	GSH	C10H17N3O6S	-
613.160	[M+H]+	5.6	GSSG	C20H32N6O12S2	-
630.049	[M+H]+	8.6	As-PC_2(OH)	C18H28AsN5O11S2	CCMSLIB00010011905
540.143	[M+H]+	13.4	PC_2	C18H29N5O10S2	CCMSLIB00010011902
497.583	[M+2H]2+	15.0	$As(GS)_3$	C30H48AsN9O18S3	CCMSLIB00010011946
994.157	[M+H]+	15.0	$As(GS)_3$	C30H48AsN9O18S3	CCMSLIB00010011947
538.127	[M+H]+	15.7	oxPC_2	C18H27N5O10S2	CCMSLIB00010011944
460.067	[M+2H]2+	20.1	GS-As-PC_2	C28H43AsN8O16S3	-
919.125	[M+H]+	20.1	GS-As-PC_2	C28H43AsN8O16S3	-
919.125	[M+H]+	22.0	GS-As-PC_2	C28H43AsN8O16S3	CCMSLIB00010173329
460.067	[M+2H]2+	22.0	GS-As-PC_2	C28H43AsN8O16S3	CCMSLIB00010173330
844.092	[M+H]+	24.1	As-PC_3	C26H38AsN7O14S3	CCMSLIB00010011906
422.550	[M+2H]2+	24.2	As-PC_3	C26H38AsN7O14S3	CCMSLIB00010011906
770.178	[M+H]+	23.3	oxPC_3	C26H39N7O14S3	CCMSLIB00010011945
772.192	[M+H]+	24.3	PC_3	C26H41N7O14S3	CCMSLIB00010127002
576.092	[M+2H]2+	25.2	$As(PC_2)_2$	C36H55AsN10O20S4	CCMSLIB00010011949
1151.175	[M+H]+	25.4	$As(PC_2)_2$	C36H55AsN10O20S4	CCMSLIB00010011948

Supplementary figures

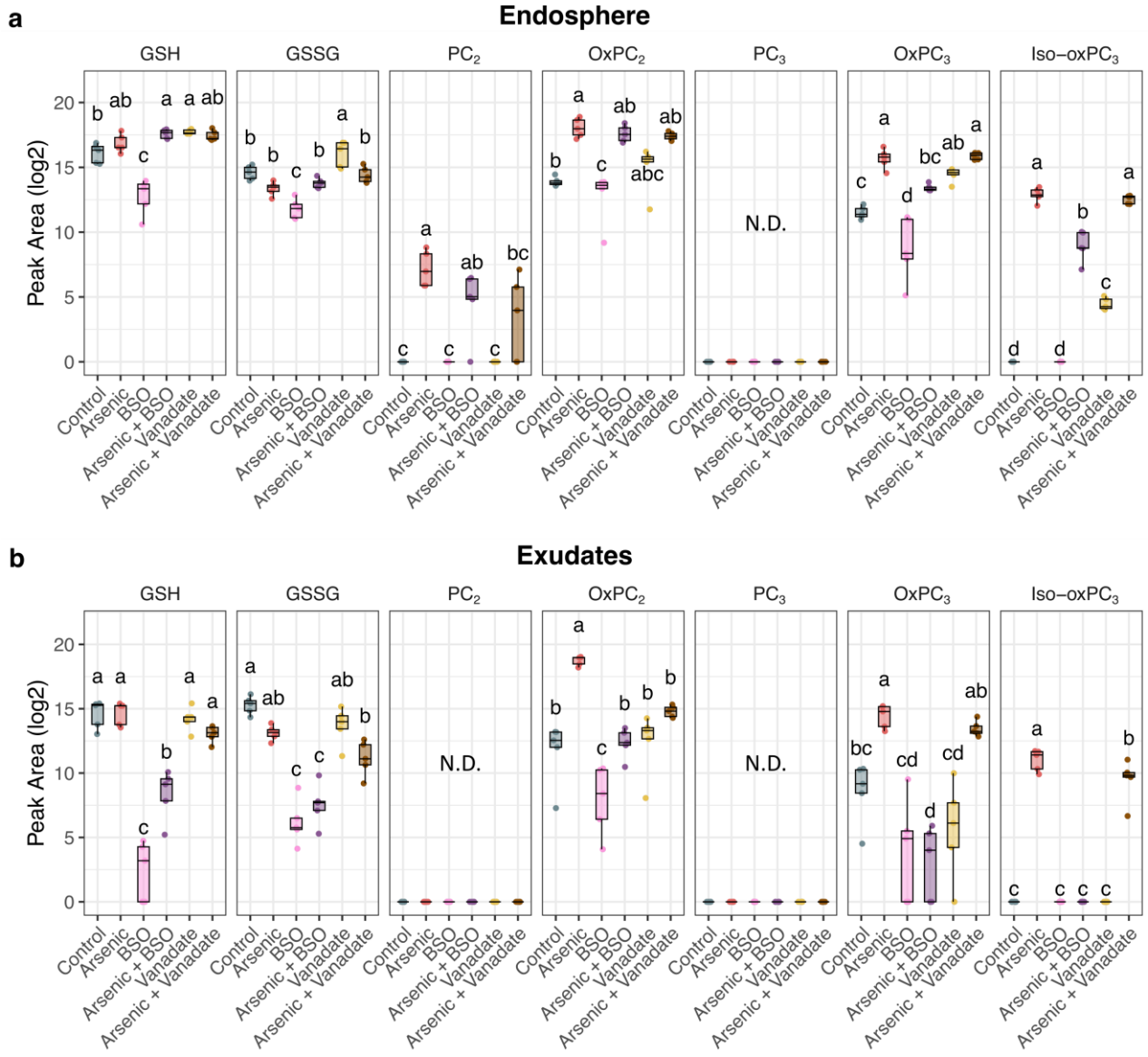

Figure S1 GSH derivatives and PCs in endosphere and root exudates in response to treatment. **a** PC and GSH derivatives abundance (Log2 peak area) in endosphere (root extracts) from controls and treated plants. **b** PC and GSH derivatives abundance in exudates from controls and treated plants. For all boxplots the bottom and top of the boxes correspond to the lower and upper quartiles and the center line marks the median (n = 5). Different letters indicate significant differences between treatments (ANOVA, Tukey HSD test, $P < 0.05$).

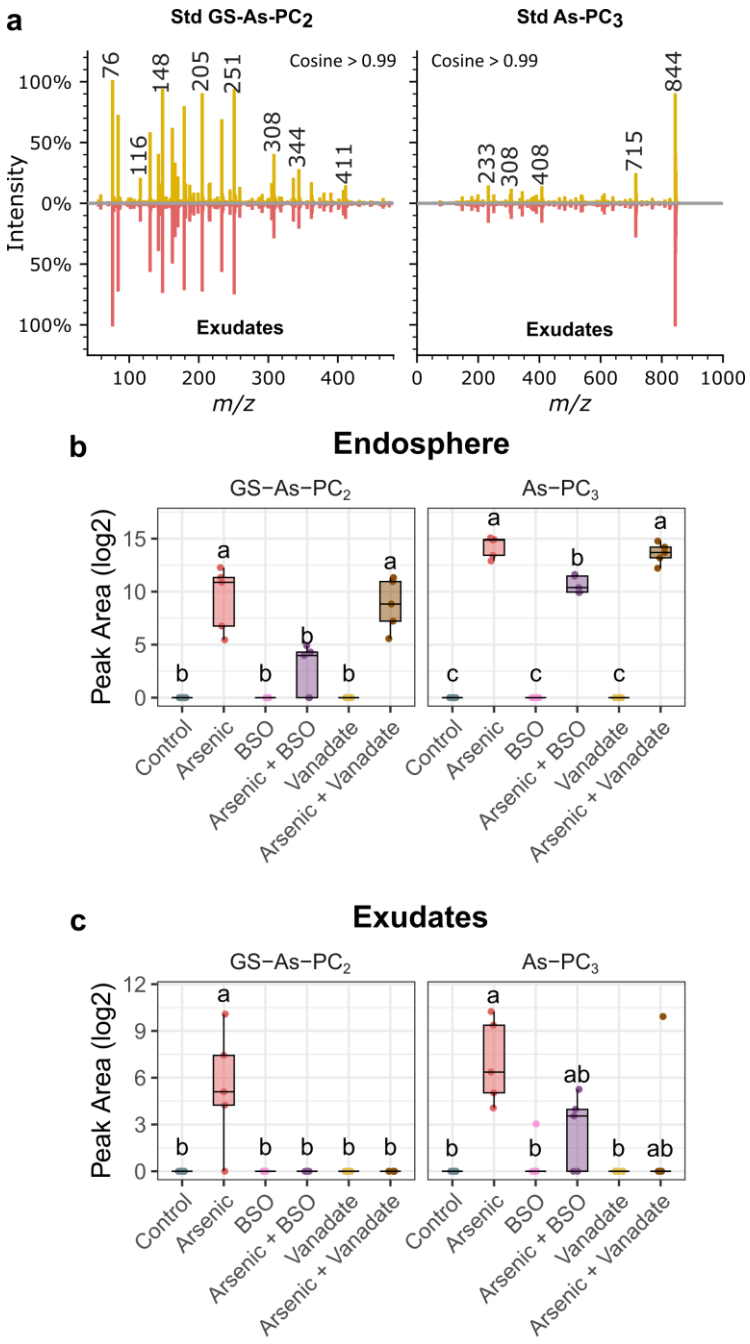

Figure S2 Arsenic-phytochelatin (As-PC) complexes in the root endosphere and exudates in response to treatments.

a Mirror plots comparing As-PCs synthesized in vitro to those detected in exudates. Matching tandem mass spectrometry (MS/MS) spectra with cosine scores >0.9 were used to confirm metabolite identities. **b** Abundance (Log2 peak area) of As-PCs in root endosphere from control and treated plants. **b** As-PC abundance in exudates from control and treated plants. For all boxplots the bottom and top of the boxes correspond to the lower and upper quartiles and the center line marks the median (n = 5). Different letters indicate significant differences between treatments (ANOVA, Tukey HSD test; Kruskal-Wallis, Dunn's test; p.adj < 0.05).

Chapitre 3 – Le métabolome de la rhizosphère pendant le stress à l'arsenic révèle des mécanismes d'exsudation racinaire divergents chez le lupin et le saule

Rhizosphere metabolomic landscape of arsenic stress reveals divergent root exudate strategies in lupin and willow

Adrien Frémont[1], Eszter Sas[1], Emmanuel Gonzalez[2,3], Mathieu Sarrazin[4], Jacques Brisson[1], Frédéric Emmanuel Pitre[1,5], Nicholas James Beresford Brereton[6]

[1] University of Montreal – Institut de Recherche en Biologie Végétale (IRBV), 4101 Sherbrooke St. E, Montreal, QC H1X 2B2, Canada

[2] Canadian Centre for Computational Genomics (C3G) - Department of Human Genetics, McGill University, 740 Dr. Penfield avenue, Montreal, QC H3A 0G1, Canada.

[3] Microbiome Research Platform - McGill Interdisciplinary Initiative in Infection and Immunity (MI4), Genome Centre, McGill University, Montreal, QC, Canada

[4] Collège de Maisonneuve – CÉPROCQ, 6220 Sherbrooke St. E, Montréal, QC H1N 1C1, Canada

[5] Montreal Botanical Garden - 4101 Sherbrooke St. E, Montreal, QC H1X 2B2, Canada

[6] School of Biology and Environmental Science, University College Dublin, Belfield, Dublin 4, Ireland

Manuscrit en préparation pour soumission

Abstract

Phytoremediation of major global soil pollutants, such as arsenic, is thought to involve root exudation of metabolites to modify challenging rhizosphere conditions. However, the influence of exudates on the rhizosphere during a response to arsenic remains largely uncharacterised for many important crops. Using untargeted metabolomics with differential abundance analysis and exhaustive annotation, the metabolomic profiles of the root endosphere, rhizosphere and bulk soil were scrutinised in two arsenic-tolerant phytoremediation plants – the leguminous species *Lupinus albus* and the fast-growing tree *Salix miyabeana*, and arsenic-responsive exudates were identified. Treated plants tolerated up to 60 μM arsenic in pot trials, preferentially accumulating up to 39× more arsenic in roots than leaves. Comparing belowground compartments suggested 930 and 1,503 rhizospheric metabolites are directly exuded by lupin and willow, respectively. Arsenic treatment significantly altered a total of 6,865 rhizosphere metabolites in both species. Lupin increased exudation of flavonoids and coumarins, including luteolin glycoside and dihydroxy-dimethoxy-coumarins. Willow reduced exudation of phenolic acids, cinnamic acids and proanthocyanidins, which accumulated in the endosphere. This revealed distinct tolerance strategies involving potential arsenic chelation by coumarins in lupin and suppressed exudation of possible metal-mobilising phenolics in willow. Moreover, both species commonly exuded phytochelatins (PC) and phytochelatin-arsenic complexes, like As-PC_3, representing a novel, potentially generalised phytoremediation mechanism in plants. A willow field trial was assessed to test if this root exudation mechanism was present outside controlled conditions, and confirmed detection of oxidized PC_2 in the rhizosphere, even against a complex metabolomic background. These findings provide insight into divergent and conserved exudate approaches for arsenic tolerance in plants and could inform new strategies for the efficient removal of contaminants in polluted soils around the world.

Keywords: *Lupinus albus* (white lupin); *Salix miyabeana* (willow); Root exudates; Arsenic; Phytoremediation; Metabolomics; Stress tolerance; Phytochelatin; Rhizosphere.

Introduction

Anthropogenic activities have led to widespread arsenic contamination of agricultural soils, mines and brownfield sites worldwide (Patel et al., 2023). With over 200 million people potentially exposed to arsenic toxicity through contaminated food and water, urgent action is imperative to mitigate this critical threat to human and environmental health (Podgorski & Berg, 2020; Zhao et al., 2010). One solution to enhance environmental arsenic remediation is to leverage the abilities of plants to detoxify arsenic and other contaminants through phytoremediation (Bell et al., 2014; Tripathi et al., 2007). The basis of these adaptations are intimately linked to the rhizosphere, the hotspot of biochemical activity surrounding plant roots (Podar & Maathuis, 2022). However, unravelling the complex molecular root-soil interactions that facilitate arsenic tolerance and detoxification remains an exciting frontier in rhizosphere research.

In aerobic soils, arsenic exists primarily as arsenate [As(V)] (AsO_4^{3-}), an analogue of phosphate (PO_4^{3-}), which can enter plant roots via phosphate transporters (Asher & Reay, 1979; Ullrich-Eberius et al., 1989), while arsenite As(III) prevails under anaerobic conditions and enters roots through Nodulin26-like Intrinsic Proteins (NIPs) aquaporins (Bienert et al., 2008). Within plant roots, most arsenate is reduced to arsenite by arsenate reductases (Dhankher et al., 2006). This enables extrusion of up to 90% of root arsenite back into the rhizosphere, partly via NIPs transporters (Zhao et al., 2010a), while up to 70% of the remaining arsenite can be immobilised directly in roots through phytochelatin (PC) synthesis (Liu et al., 2010). Phytochelatins are glutathione oligomers that confer arsenic tolerance by complexing arsenite via thiol coordination and subsequent vacuole sequestration (Schmöger et al., 2000; Song et al., 2010). Most plants species rely on reduction into As(III) and complexation with PCs to limit aboveground arsenic accumulation and toxicity, in a metal-excluding fashion, which contrasts the specialised arsenic metabolism and transport of hyperaccumulators like *Pteris vittata*, which allows arsenic accumulation of up to 6,000 mg kg^{-1} arsenic aboveground (Lombi et al., 2002; Yan et al., 2022).

As the first point of contact between roots and soil, the unique biochemistry of the rhizosphere may also impact arsenic fate. The rhizosphere harbours extensive metabolic diversity, largely thought to be due to plant exudation (van Dam & Bouwmeester, 2016). These root exudates represent only a fraction of the large repertoire of plant metabolites biosynthesised through the largely conserved central carbon metabolic pathways and highly diversified specialised metabolic pathways, such as those generating terpenoids, phenylpropanoids, and alkaloids (Maeda & Fernie, 2021). Plants tightly regulate root exudation through enzymes and membrane transporters, varying with developmental stage, genotype,

and in response to biotic and abiotic stimuli (Chaparro et al., 2013; Kawasaki et al., 2021; Korenblum et al., 2022; McLaughlin et al., 2023). *Arabidopsis thaliana* grown under sterile conditions can release hundreds of metabolites, but these differ substantially when microorganisms are present, as plant roots interact with microbes in a chemical crosstalk, triggering metabolic responses which can modulate the rhizosphere metabolome (Korenblum et al., 2020; Strehmel et al., 2014). Similarly, abiotic factors such as P or Fe availability elicit exudation of organic acids and coumarins as a mechanism for nutrient mobilisation, complexation and uptake (Robe et al., 2021; Stringlis et al., 2018; Wen et al., 2019; Ziegler et al., 2016). These tripartite plant-soil-microbe interactions result in a unique and complex biochemical microenvironment, potentially harbouring distinct metabolic signatures compared to those produced by plants or microbes alone. This complex rhizosphere metabolome is critical for key rhizosphere functions like the mobilisation of nutrients and may also participate in detoxifying contaminants like arsenic.

Most studies on root exudation in response to arsenic have focused on the hyperaccumulator *Pteris vittata*. Altered exudation and shifts in root microbiome composition in the presence of arsenic in this species revealed mechanisms of arsenic mobilisation through organic acid exudation and microbial siderophore production (Das et al., 2017; Ghosh et al., 2011). In the non-hyperaccumulating phytoremediation crop white lupin (*Lupinus albus*), recent work demonstrated a substantial change in root exudation when exposed to arsenic, with lupin secreting phytochelatins from roots (Frémont et al., 2022). This suggests arsenic detoxification via arsenic-phytochelatin complexation may occur in the rhizosphere of non-hyperaccumulating species. Other crops used in field-scale phytoremediation trials, such as willow (*Salix spp.*), may possess additional unknown root exudate-mediated arsenic tolerance strategies, as implied by the high plasticity of willow root microbiomes and transcriptomes in response to contamination (Brereton et al., 2020; Gonzalez et al., 2018; Yanitch et al., 2017; Yergeau et al., 2018). Changes involve altered metabolite transporter genes, including ABC (ATP-binding cassette) and SWEET2 (Sugars Will Eventually Be Exported) transporters, reflecting intense below-ground crosstalk. However, disentangling the intricate chemical root-arsenic interactions in these species remains challenging, chiefly due to constraints in high-throughput methods for comprehensively characterising complex rhizosphere chemical environments.

Modern LC-MS-based metabolomics instrumentation and computational tools provide a platform for high-throughput characterisation of complex environments. However, due to the massive amount of metabolomics data these tools generate, only a small proportion of spectra are commonly annotated and assessed (Aksenov et al., 2017; da Silva et al., 2015; Elser et al., 2023). This limitation has driven

the rapid development of computational tools to transform the thousands of spectra typically produced from a single LC-MS/MS run into chemical knowledge (Cai et al., 2023). One approach utilises spectral grouping algorithms for molecular networking and rapid mining of MS/MS spectral libraries embedded within the Global Natural Products Social Molecular Networking ecosystem (GNPS) (M. Wang et al., 2016). For instance, Feature-Based Molecular Networking (FBMN) can group previously unidentified metabolites into molecular families, thus providing information about structural diversity within complex samples (Nothias et al., 2020), while other recent tools like microbeMASST leverage community-sourced spectral databases of pure microbial culture to map metabolites to their potential microbial producers (Zuffa et al., 2023). Another approach develops *in silico* fragmentation and substructure prediction directly from mass spectra. For instance, the SIRIUS metabolite annotation pipeline includes tools such as CSI:Finger ID and CANOPUS, which use artificial intelligence-powered structural prediction from spectra to improve annotation (Dührkop et al., 2019, 2020). However, systematically integrating reliable annotation from multiple, rapidly improving, tools remains a challenge (Elser et al., 2023).

To unravel the intricate molecular interactions between roots and soil that facilitate arsenic tolerance during phytoremediation, we hypothesised that phylogenetically distinct phytoremediation species assemble unique rhizosphere metabolomes, which underpin species-specific adaptations conferring arsenic tolerance. To test this, an untargeted metabolomics approach integrating comprehensive metabolite annotation was employed to delineate the metabolite partitioning between the endosphere and rhizosphere microenvironments of two phylogenetically distinct species, *Lupinus albus* and *Salix miyabeana*. Differential abundance analysis was then used to elucidate the rhizosphere metabolite responses under arsenic-treated and untreated conditions and define species-specific and shared rhizosphere adaptations to arsenic stress. The identified rhizosphere metabolite adaptations were further validated in a real-world phytoremediation field trial. Collectively, these molecular root-soil adaptations facilitating arsenic tolerance could inform the development of targeted phytoremediation solutions to address the global challenge of arsenic contamination.

Methods

Greenhouse and field trial experimental design

Lupin (*Lupinus albus* L., cv. AMIGA) and willow plants (*Salix miyabeana* cv. SX. 67) were grown in the greenhouse (conditions in Methods S1) for eight and seven weeks, respectively, before being either left as controls or exposed to 60 µM arsenate As(V) added as sodium heptahydrate arsenate $Na_2HAsO_4 \cdot 7H_2O$. Treatments consisted of 1 L of arsenic solution prepared in Hoagland nutrient

solution or 1L of Hoagland solution alone, applied twice a week over two weeks for lupin and four weeks for willow before plants were harvested. A randomized block design was used with six replicate plants for each species and treatment (6 blocks, 24 plants in total). Fully replicated unplanted controls (12 pots) were also included with the same treatments. Plant measurements and arsenic quantification procedures are detailed in Methods S1.

To validate the greenhouse findings under real-world field conditions, a willow (*Salix miyabeana* cv. SX. 64) phytoremediation field trial was established in May 2021 in the Montreal region, Canada (45°40′29.5″N, 74°24′44.3″W), which presented arsenic contamination as well as other trace metal contaminants (**Figure S1**). Prior to planting, one uncontaminated control plot (16.5 m × 40 m) and one contaminated plot (16.5 m × 40 m) were delimited based on soil contaminant concentrations. Planting procedures and contaminant quantification are detailed in Methods S1.

Metabolomic greenhouse and field trial sampling

For metabolomic sampling, greenhouse plants were unpotted and root segments (~10 cm long) were collected from the main root, while bulk soil was sampled from unplanted pots by taking two soil cores, at a depth of 5 to 10 cm below the surface, randomly located in the pot and directly processed as described below.

Field metabolomic sampling was performed in September 2021, after four months of growth. Fine roots and associated rhizosphere soil were sampled from 12 randomly selected willow trees from the control and contaminated plots (n = 6 per plot). Two 20 cm × 20 cm × 20 cm soil cubes (8000 cm^3 each) were carefully excavated at opposite sides, 20 cm away from the main stem, and lateral root segments were collected at a depth of 10-20 cm. Bulk soil samples were sampled between planted rows nearest to each sampled tree (n = 6 per plot) and consisted of three soil cores collected at 10 cm depth mixed together. All samples were kept on ice in the field before extraction in the laboratory following the procedures described below.

Extraction of endosphere, rhizosphere and bulk soil metabolites

The rhizosphere extraction used the procedures from Swenson et al., (2015), Edwards et al. (2015) and Xun et al. (2023) with modifications. Briefly, root segments from the greenhouse or field were gently shaken to remove loose soil and retain only the rhizosheath (**Figure 1**). Approximately two grams of endosphere plus rhizosphere material were placed in a 50 mL centrifuge tube and vortexed for 10 sec in 40 ml of trap solution (ultrapure water + 0.1% formic acid) to detach rhizosphere soil. The root segments were removed from the tubes and kept for endosphere treatment. The trap solution containing

rhizosphere extracts was kept on ice before centrifugation at 4°C and 5,000 G for 5 minutes. The supernatant was recovered and kept frozen at -70°C until sample processing, while the soil pellet was removed. After rhizosphere extraction, the root segments went through 5 additional wash cycles in ultrapure water with strong vortexing at maximum speed to recover endosphere samples devoid of rhizosphere residues. Endosphere samples were then dried from residual water using absorbing paper, immediately frozen in liquid nitrogen, and kept at -70°C before sample processing. Bulk soil core material was homogenised, and 2 g extracted following the same procedure as for rhizosphere soil, *i.e.*, 10 sec vortex in 40 ml of trap solution, centrifugation, supernatant recovery and freezing at -70°C until sample processing.

Endosphere samples were ground in liquid nitrogen to extract 150 mg of fresh material in 450 µL milliQ water + 0.1% formic acid for 15 minutes with ultrasonication at 4°C to recover endosphere water-soluble metabolites. The trap solution containing rhizosphere and bulk soil extracts was lyophilized (Alpha 1-4 LSCplus, Martin Christ, Osterode am Harz, Germany). The dried extracts were resuspended in 400 µL of ultrapure water with 0.1% formic acid. The endosphere, rhizosphere and bulk soil extracts were then centrifuged at 4°C and 20,000 g for 2 min. The supernatants were transferred to 0.2 µm centrifuge filters (InnoSep^{TM} Spin, Canadian Life Sciences, Peterborough, ON, Canada), centrifuged at 10,000 g for 30 s, and the filtrates transferred to HPLC vials for storage at 4°C. Liquid chromatography-tandem mass spectrometry (LC-MS/MS) analysis was performed on the samples within 24 h (Methods S1). Extraction blanks were also included with the same preparation steps.

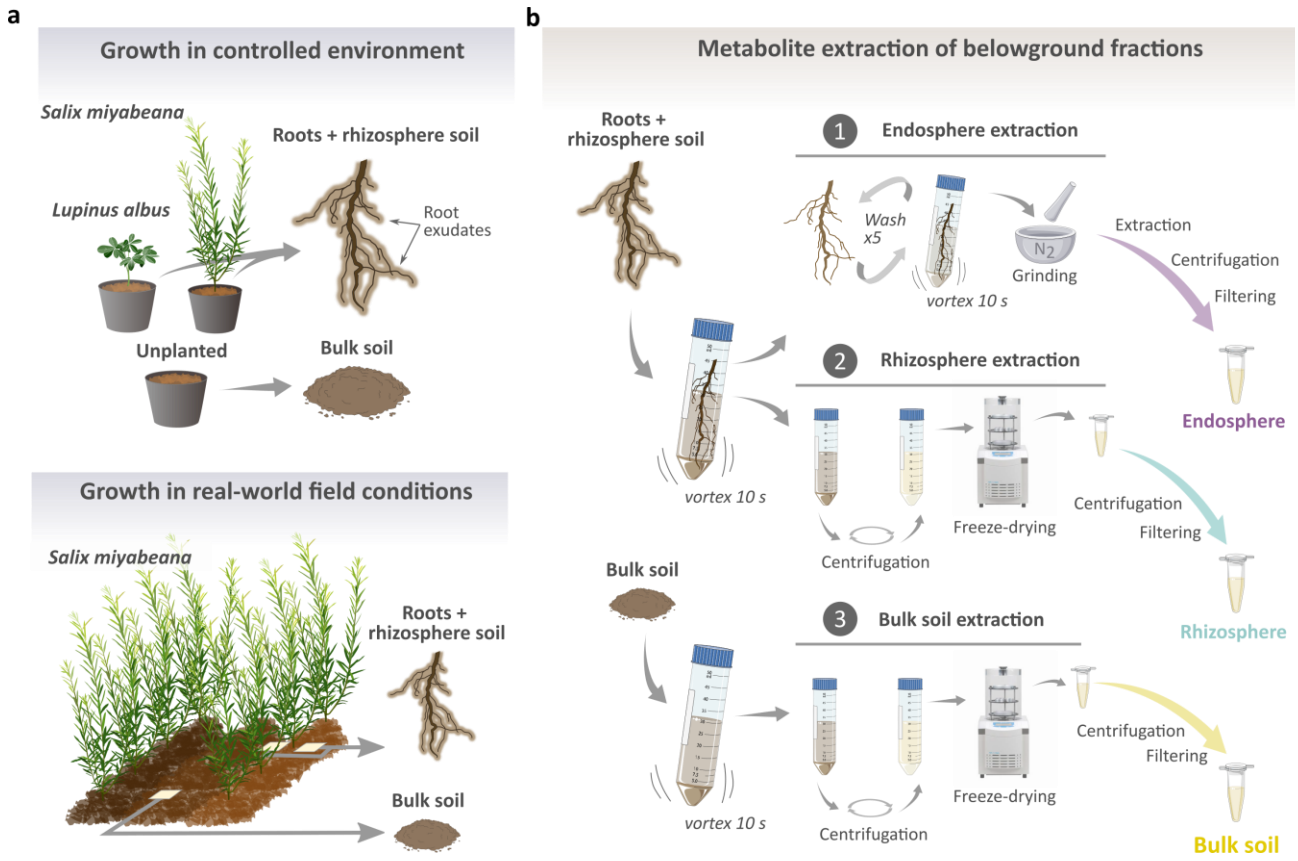

Figure 1 Overview of sampling procedures for root endosphere, rhizosphere, and bulk soil metabolomic analyses.

a Root fragments of lupin and willow were collected from plants grown in a greenhouse or field phytoremediation trial. **b** Root fragments with attached rhizosheath soil were vortexed in a trap solution to separate roots and adhering rhizosphere soil. Separated root fragments were then washed repeatedly to remove soil particles before endosphere metabolite extraction (1). To obtain rhizosphere metabolites, the trap solution containing rhizosphere soil was centrifuged to keep only water-soluble metabolites and concentrated via freeze-drying (2). For bulk soil, samples were taken from unplanted pots or inter-row areas in the field trial, then extracted following the same procedure used for the rhizosphere samples (3).

Untargeted metabolite data processing

LC-MS raw data were converted to .mzML files using MSConvert and subsequently processed in batch mode with MZmine 3.4.14 (Schmid et al., 2023) (Method S1). The resulting features abundance matrices (*.csv) were imported into R for quality control and statistical analyses. In parallel, MS2 spectra (*.mgf) were imported into the GNPS environment for feature-based molecular networking (FBMN) analysis (Method S1) and spectral annotation using SIRIUS.

Statistical analysis

For metabolomic differential abundance analysis, each pairwise comparison was first evaluated for minimum occurrence and structural zeros (He et al., 2014). Metabolomic data has high sparsity (*i.e.* a high proportion of zeros), which can impede the detection of significant features (Huang & Wang, 2022). To account for high sparsity, features lacking sufficient occurrence across biological replicates (plants) to represent the group being statistically compared were excluded (Gonzalez et al., 2019): Only features detected in more than 3 samples (occurrence ≥ 4) in at least one experimental group (6 replicate plants) were retained for statistical differential abundance analysis. Secondly, features absent in one sample group (occurrence ≤ 1) but present in the other (occurrence ≥ 4) (structural zeros) were *de facto* called as differentially abundant (DA) (Kaul et al., 2017). After processing for minimum occurrence and structural zeros, feature intensities were $\log_2$ transformed using *decostand* function in vegan R package (Oksanen et al., 2019) and normalised using EigenMS in R (Karpievitch et al., 2014) (**Figure 2**). Differential abundance analysis of features was tested with either Student's T, Welch's T or Mann-Whitney U, based on normality and variance ($p<0.01$).

After controlling for false discovery rate (Benjamini & Hochberg, 1995), features with adjusted p values < 0.05 were considered significantly differentially abundant (DA). All statistical analyses were performed in R (R Core Team, 2020) using shapiro.test(), bartlett.test(), t.test(), t.test(var.equal = FALSE), wilcox.test() and p.adjust(method="BH") functions.

Untargeted metabolite annotation

Annotation of unknown features was performed using a bespoke pipeline (**Figure 2**) integrating searches across multiple databases and advanced *in silico* tools, as well as in-depth curation of DA features. Unsupervised annotation is performed by querying features against a set of MS^2 and MS^1 databases, including all databases available in the GNPS environment (*e.g.*, GNPS, MoNA, MassBank, ReSpect) (Wang et al., 2016) as well as bespoke experiment- and organism-specific databases (PlantCys (Hawkins et al., 2021), NPAtlas (van Santen et al., 2022), PhytochelatinDB (Dennis et al., 2019)). In parallel, unsupervised annotation used *in silico* prediction with SIRIUS (Dührkop et al., 2019), combining raw formula and substructure elucidation with CSI:FingerID (Dührkop et al., 2015), as well as compound class annotation with CANOPUS (Dührkop et al., 2020) using the Natural Products Classifier ontology (Kim et al., 2021). Annotated compounds then undergo annotation integration and tool prioritisation to generate a list of putative compounds from combined cheminformatic tools, as either high confidence (MS^2 hit and consensus between tools) or low confidence annotation (MS^1 hit or ambiguity between tools). Annotation refinement using both data-driven and knowledge-based approaches is then used to further improve annotation of DA compounds.

Data-driven curation uses feature-based ion identity molecular networking (Schmid et al., 2021) with cosine metrics of spectral similarity to enhance annotation within molecular family clusters and resolve annotation ambiguities. Knowledge-driven curation takes advantage of published compound lists and spectra from comparable experiments and plant species not deposited in public databases to improve annotation. This exhaustive annotation enables the comprehensive assessment of metabolomic data at the metabolite and class level through unsupervised annotation and provides in-depth biological insights using the higher confidence annotation of DA compounds. For annotation confidence assessment, each putative compound is assigned with a confidence level (1-5) based on Sumner et al. (2007) (see Methods S1; Supplementary Data S1) following best reporting practices from Alseekh et al. (2021). However, all annotations remain putative and subject to change as database records and annotation strategies improve. Procedures for identification of microbe-derived metabolites and arsenic complexes are detailed in Methods S1.

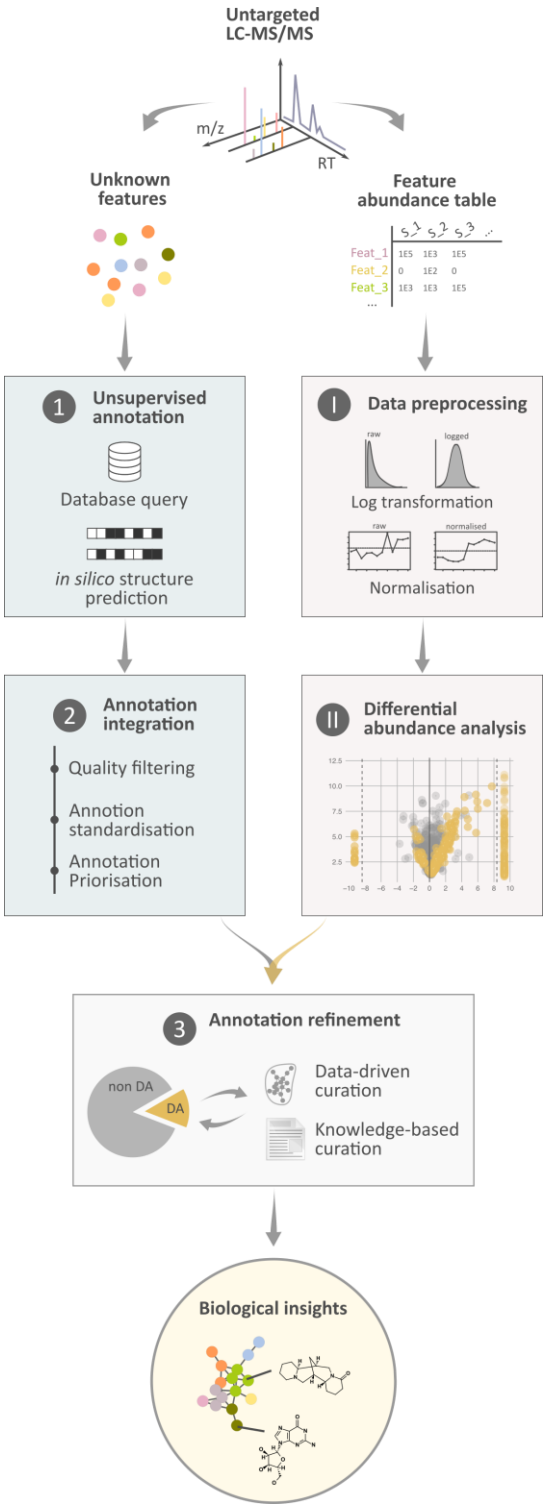

Figure 2 Metabolomic LC-MS/MS data analysis workflow.
The workflow included annotation of unknown features, differential abundance analysis, and annotation refinement of differentially abundant (DA) features. Annotation of unknown features included unsupervised annotation (1) combining database queries (GNPS public MS2 libraries, PlantCys, PhytochelatinDB, NPAtlas) and *in silico* prediction tools (SIRIUS, CSI FingerID, CANOPUS), as well as an annotation integration step (2) to select best hits within

tools, standardise annotations between tools, and prioritise high confidence MS_2 database hits over low confidence predictions. Differential abundance analysis incorporated data preprocessing steps (I) such as log transformation and EigenMS normalisation (Karpievitch et al., 2014) before differential abundance statistical analysis (II). Annotation refinement of DA features (3) used manual curation of annotation using data-driven molecular networking and knowledge-based curation from published sources. This workflow adopted manual curation efforts focused on a subset of differentially abundant metabolites of biological relevance, thereby minimising manual annotation while enabling effective extraction of biological insights across the entire untargeted LC-MS/MS metabolomics dataset.

Results

Willow and lupin arsenic phenotype and contaminant fate

Lupin (*Lupinus albus*) and willow (*Salix miyabeana*) were cultivated in 6 L pots for 62 and 67 days, respectively. Plants were either treated with arsenic (As) or left untreated as controls (n=6; 24 plants in total; **Figure 3a**). Stomatal conductance (gs) was measured at 55, 58 and 60 days after planting. Willow had significantly higher gs at all measurement timepoints, with mean gs values of 0.286 ± 0.036 mol m^{-2} s^{-1} in willow and 0.055 ± 0.008 mol m^{-2} s^{-1} in lupin (**Figure 3b**). Arsenic treatment did not significantly impact gs in either species, except in willow at one timepoint with a significant decrease from 0.276 ± 0.04 mol m^{-2} s^{-1} to 0.177 ± 0.021 mol m^{-2} s^{-1} at day 55 in controls versus As-treated (**Figure 3**).

At harvest, willow produced significantly greater biomass than lupin, with mean root dry weights of 46.5 ± 3.6 g and 1.8 ± 0.3 g, respectively. Similarly, mean shoot dry weights were 27.1 ± 1.6 g for willow compared to 2.3 ± 0.3 g for lupin. Arsenic treatment did not affect biomass, except for a reduction in willow aboveground biomass from 29.7 ± 1.6 g in controls to 24.5 ± 1.6 g in As-treated plants. No morphological symptoms of As phytotoxicity were observed. Arsenic concentrations in roots of arsenic treated plants were comparable between species, averaging 152 ± 31.6 μg g^{-1} in lupin and 144 ± 28.1 μg g^{-1} in willow (**Figure 3d**). However, As concentrations were significantly higher in As-treated lupin stems and leaves compared to As-treated willow, with mean values of 8 ± 0.5 μg g^{-1} and 26.1 ± 2.4 μg g^{-1} in lupin versus 3.7 ± 0.4 μg g^{-1} and 8.8 ± 0.4 μg g^{-1} in willow stems and leaves, respectively.

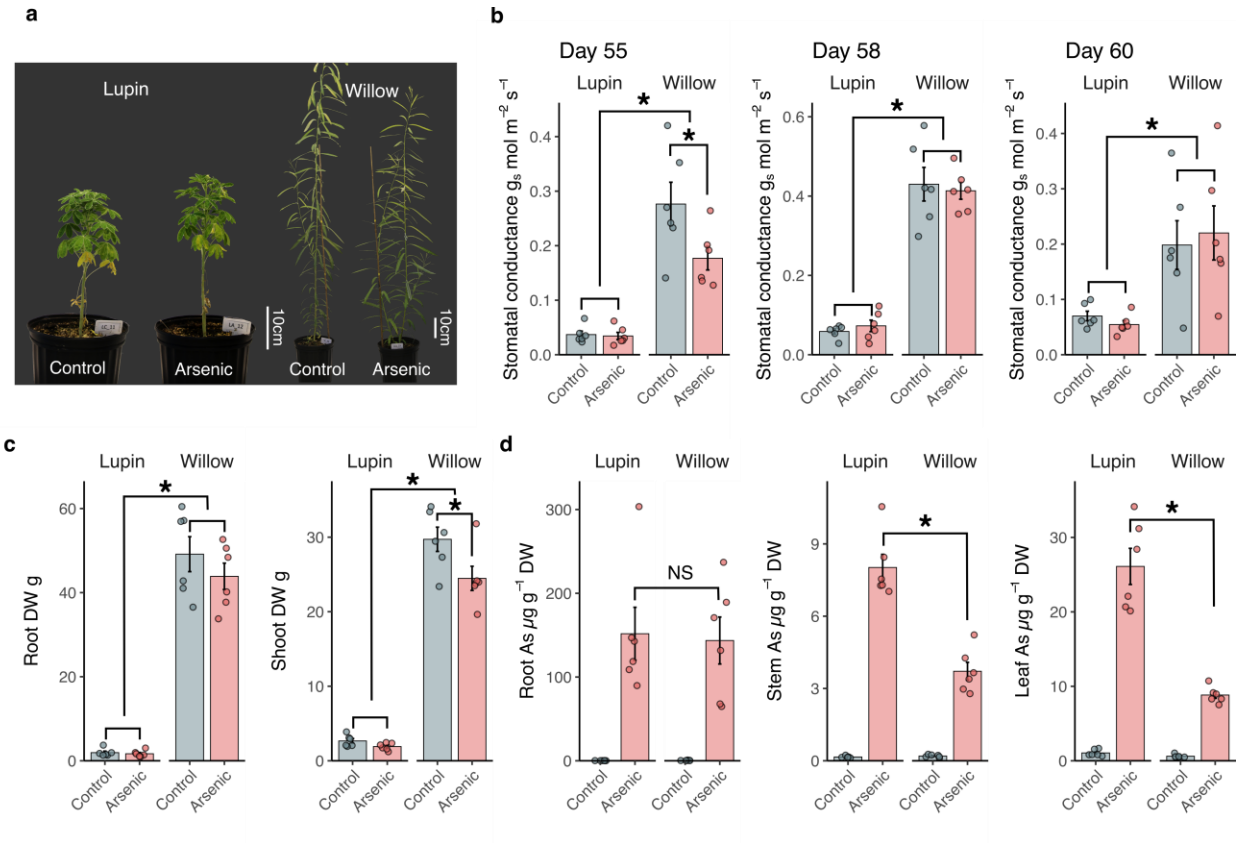

Figure 3 Physiological response and arsenic distribution in lupin and willow after arsenic exposure.

a Representative photograph of lupin and willow at harvest. **b** Stomatal conductance of lupin and willow measured on days 55, 58 and 60 during arsenic exposure. **c** Root and shoot dry weight of lupin and willow measured at harvest (day 61 for lupin, day 67 for willow). **d** Arsenic concentrations in roots, stems and leaves at harvest presented on a dry weight basis. Data show means ± SE (n=6). Asterisks indicate significant differences between treatments ($P<0.05$, T-test). NS: non-significant ($P>0.05$, T-test).

Belowground metabolome

Lupin and willow pot trial metabolomic overview

Lupin and willow root endosphere, rhizosphere and unplanted bulk soil were sampled and extracted for liquid chromatography-tandem mass spectrometry (LC-MS/MS) analysis). Alignment of metabolite features across all 70 samples revealed a total of 41,164 features, which were filtered to 16,477 features after minimum occurrence filtering and removal of contaminant features. Of the 16,477 belowground features, 5,400 were unknown due to a lack of similar database record or ambiguous annotation. The remaining 11,077 features could be putatively annotated, with 3,438 at the class level and 7,639 at the compound level (**Figure 4a**) with varying levels of confidence (Data S1). Annotated

features were classified as belonging to seven pathways: shikimates and phenylpropanoids, amino acids and peptides, alkaloids, polyketides, carbohydrates, terpenoids and fatty acids. In endosphere and rhizosphere (control and arsenic-treated samples), 13,747 features were present in lupin, 13,549 in willow, with 10,891 shared between lupin and willow (**Figure 4b**). Lupin and willow had similar proportions of all metabolic pathways; the most prevalent pathways were shikimates and phenylpropanoids, accounting for 2,331 and 2,483 features, alkaloids, accounting 1,892 and 1,760 features, and amino acids and peptides, accounting for 1,661 and 1,661 features, in lupin and willow, respectively. In lupin, alkaloids had higher relative intensity, accounting for 24.4%, compared to willow, where the relative intensity was 18.6%. Conversely, the relative intensity of features in the shikimates and phenylpropanoids, and the terpenoid pathways were higher in willow, accounting for 23.1% and 4% respectively, compared to 19% and 1.8% in lupin (**Figure 4c**).

Molecular network analysis of endosphere and rhizosphere features revealed 16 putative molecular families. Seven lupin-dominated and six willow-dominated molecular families as well as three molecular families that were common between species (**Figure 4d**). Lupin-dominated molecular families comprised 185 features and were primarily annotated as flavonoids and quinolizidine alkaloids (**Figure 4d, e**). Willow-dominated molecular families comprised 220 features and were mainly annotated as proanthocyanidins and simple phenolic acids. While common molecular families comprised 73 features, primarily annotated as small peptides and nucleosides.

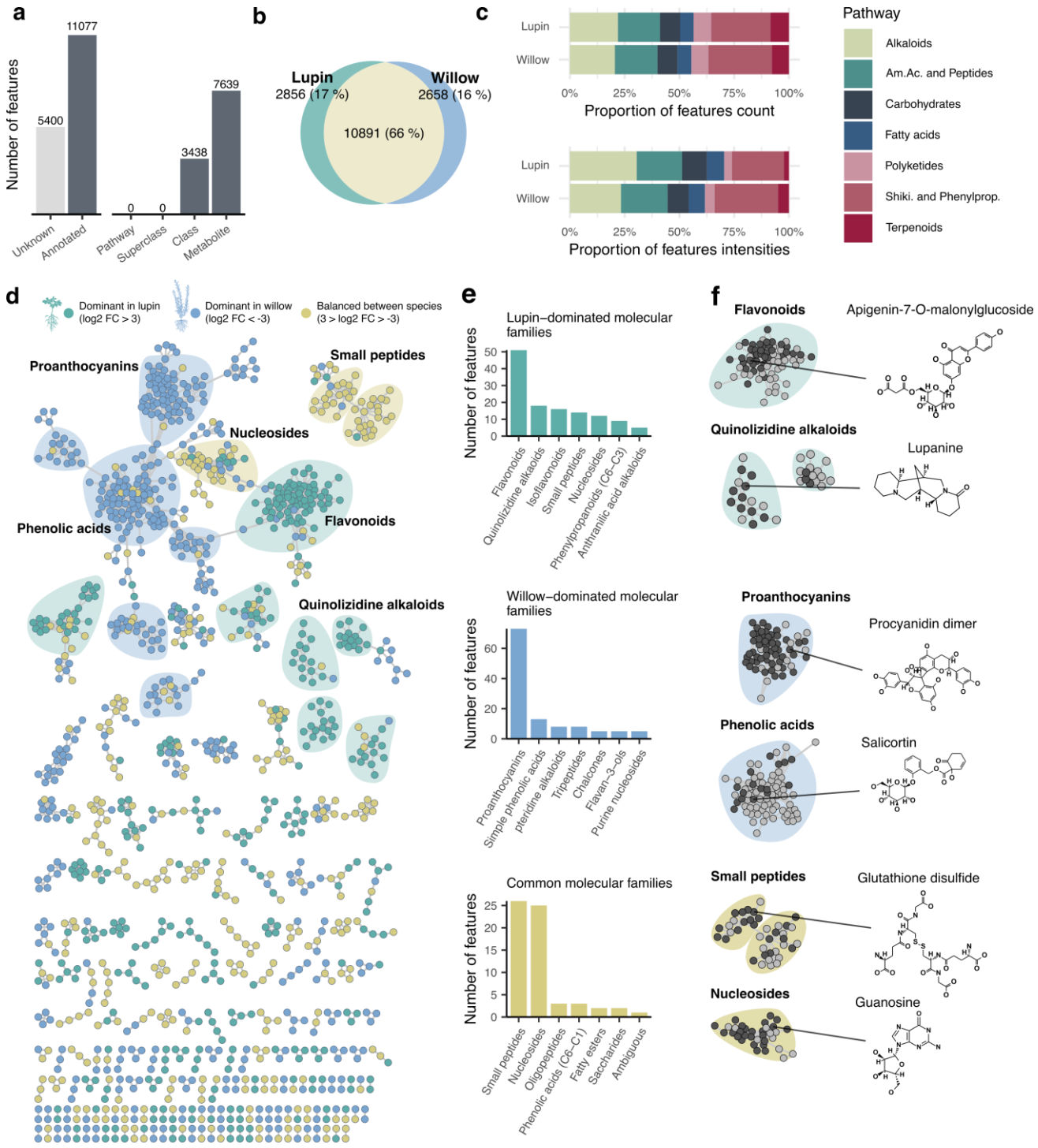

Figure 4 Metabolomic overview of lupin and willow belowground environments.

a Number and annotation levels of the detected metabolite features, classified using the NPC ontology (Kim et al., 2021). Full annotation and confidence levels of each feature is available in Data S1. **b** Venn diagram showing unique and shared features between the two plant species. **c** Proportional contribution of metabolite pathways in lupin and willow. Proportions are based on the total number of features and on total intensities. **d** Molecular network based on MS^2 spectral similarities, with features represented as dots and coloured by their species association. Species association was defined from log_2 FC values as either

dominant in lupin ($\log_2$ FC > 3), dominant in willow ($\log_2$ FC < -3), or balanced between the two species (3 > $\log_2$ FC > -3). Related features are circled as molecular families, further classified as lupin-dominated (green), willow-dominated (blue) or common (yellow). **e** Superclass composition of the molecular families, showing the seven most abundant superclasses. **f** Key molecular families with example high-confidence metabolite structures from the major superclasses. Features from the corresponding superclass are coloured in dark grey.

Metabolite partitioning across belowground compartments.

Metabolomic profiles of the endosphere, rhizosphere and bulk soil were first compared from untreated lupin and willow plants. Principal component analysis (PCA) using features separated samples according to belowground fraction in both lupin and willow (**Figure 5a**), with significant differences ($p < 0.05$, PERMANOVA on Bray-Curtis distances, Data S1) illustrated a clear, gradual shift from a similar soil metabolome to more distinct rhizosphere and endosphere profiles. Comparison of Shannon's α diversity index between belowground fractions showed a significant sequential decrease between endosphere, rhizosphere and bulk soil, in both lupin and willow (ANOVA, Tukey HSD, $\alpha < 0.05$) except between willow endosphere and rhizosphere (**Figure 5b**).

As the zone of interface between roots and soil, the rhizosphere was compared to the endosphere and unplanted bulk soil for lupin and willow. This revealed that 82.1% of features were significantly differentially abundant (DA) between fractions in lupin, and 67.2% in willow, in at least one pairwise comparison. Of the 11,492 features with differential abundance between lupin fractions, 8,752 were enriched in the endosphere, including 3,155 endosphere-unique features; 930 were enriched in the rhizosphere in both pairwise comparisons, with 182 rhizosphere-unique features; and 622 were enriched in bulk soil, including 111 soil-unique features (**Figure 5c, d**). In willow, 10,062 features showed differential abundance among fractions, including 4,788 endosphere-enriched features with 1,246 endosphere-unique features; 1,503 rhizosphere-enriched features in both pairwise comparisons, with 206 rhizosphere-unique features; and 1,193 bulk soil-enriched features, including 171 soil-unique features (**Figure 5c, d**).

Lupin endosphere-enriched compounds primarily belonged to tripeptides, purine nucleosides, cinnamic acids and derivatives, and dipeptides (**Figure S2**). The most enriched included the tripeptide glutathione (GSH) with 13.9-fold change (FC, $\log_2$), flavonoid and isoflavonoids glycosides such as apigenin 7−O−malonylglucoside and sophoricoside, coumarin glycosides such as fraxin, lysine alkaloids such as hydroxylupanine, angustifoline, lupanine and 13α-acetoxylupanine. Compounds

present only in the endosphere included the flavonoid glycoside apigenin 4',7-diglucoside the tryptophan alkaloid gramine and lysine alkaloid lupinine (**Figure 5e**, Data S1).

In willow, endosphere-enriched compounds primarily belonged to proanthocyanins, tripeptides, purine nucleosides, and simple phenolic acids (**Figure S2**). The most enriched included the tripeptide glutathione, procyanidin dimers and trimers, and phenolic acids, such as salicortin, salicin 6'-acetate and the cinnamic acid derivative syringin as well as flavonoid glycosides such as apigenin 4',7-diglucoside. High intensity compounds present only in the endosphere included the phenolic acid omega-salicoyisalicin (**Figure 5e**, Data S1).

Lupin rhizosphere-enriched compounds primarily belonged to dipeptides, amino acids, purine alkaloids, and aminosugars (**Figure S2**). The most enriched included small peptides such as leucylisoleucine, valylleucine, and theonylleucine, nucleosides such as thymidine, hypoxanthine, and thymine, fatty acids such as 3,4-methyleneazelaic acid, and 6-nonenal, carbohydrates such as trehalose and the alkaloid nicotinic acid. Compounds present only in the rhizosphere included the peptidoglycan N-acetyl-D-glucosaminyl-(1-4)-N-acetylmuramic acid and nucleosides such as 2'-deoxyinosine and 2'-deoxyuridine (**Figure 5e**, **Figure S3**).

In willow, rhizosphere-enriched compounds primarily belonged to tripeptides, amino acids, simple phenolic acids, and dipeptides (**Figure S2**). The most enriched included the dipeptide succinylproline, the nucleosides adenosine and cytidine, fatty acids such as 3,4-methyleneazelaic acid and nonenal, and the phenolic acid salicylic acid. Compounds present only in the rhizosphere included the terpenoid glycoside geniposidic acid (**Figure 5e**, **Figure S3**).

To examine the potential contributions of microbes to rhizosphere metabolite composition, the proportions of likely microbial-derived compounds were compared among metabolites enriched in the endosphere, rhizosphere, and bulk soil. Analysis using microbeMASST suggested substantial microbial contributions to rhizosphere-enriched metabolites in both lupin (37.8% microbial-derived) and willow (13.3% microbial-derived). In contrast, endosphere-enriched metabolites contained <10% of microbial inputs (**Figure S3**). The rhizosphere-enriched compounds of potential microbial origin included the peptidoglycan precursor N-acetyl-D-glucosaminyl-(1-4)-N-acetylmuramic acid, enriched in lupin rhizosphere and willow bulk soil. Other microbial-derived compounds included 6−nonenal, enriched in the rhizosphere of both species, hypoxanthine enriched in lupin rhizosphere and willow bulk soil, levocarnitine enriched in lupin and willow bulk soil compared to rhizosphere and hydroxyectoine enriched in lupin and willow rhizosphere compared to endosphere but not DA when compared to bulk soil (**Figure 5e**, Data S1).

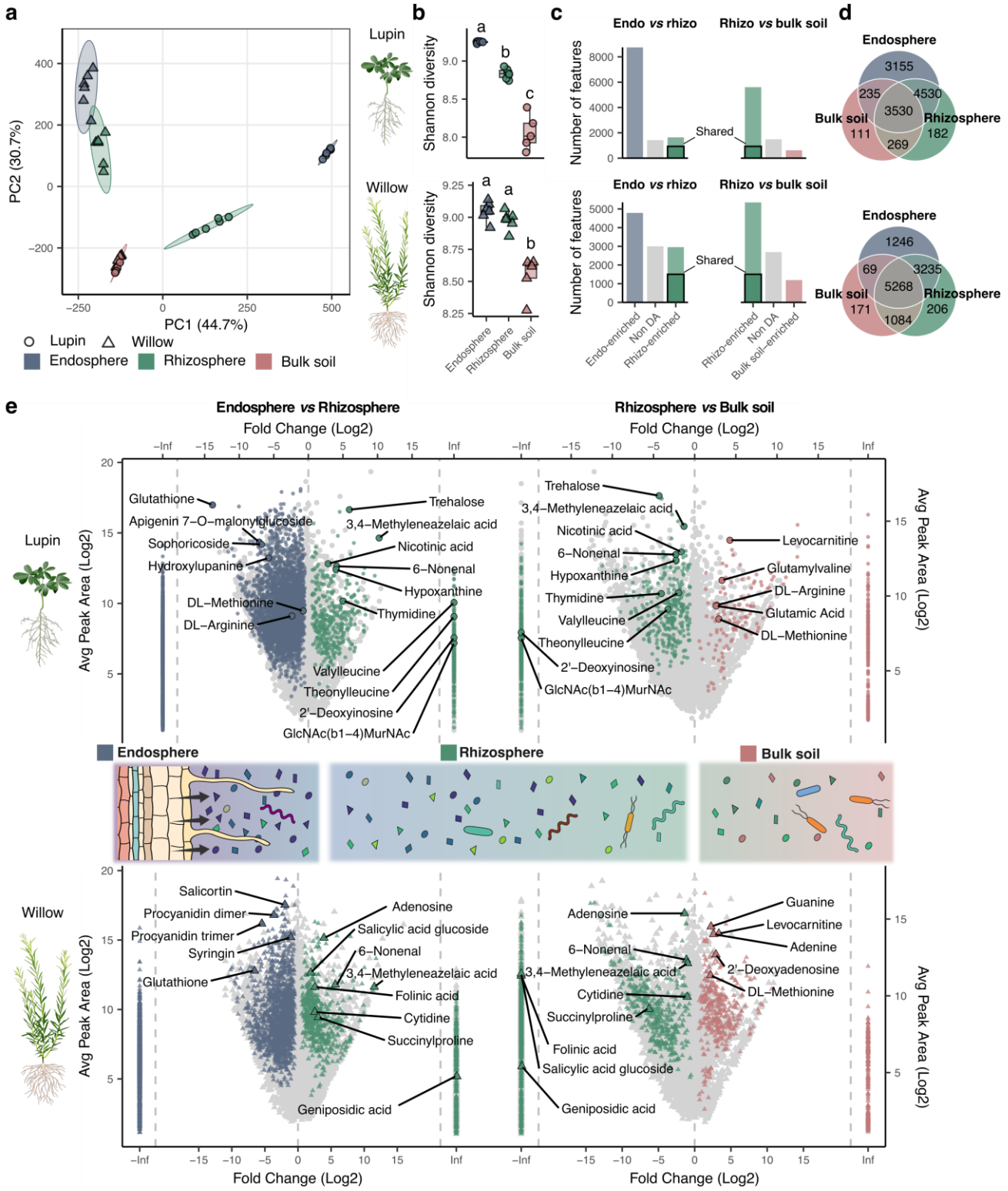

Figure 5 Metabolomic comparison of belowground fractions.

a Principal components analysis (PCA) depicting variation in metabolite composition of the untreated lupin and willow root endosphere, rhizosphere and bulk soil. Ellipses denote 95% confidence intervals (n = 6). **b** Shannon's index showing α diversity of metabolites from the different belowground fractions. For boxplots, the bottom and top of the boxes correspond to the lower and upper quartiles and the center line marks the median (n = 6). Different letters indicate significant differences between fractions

(ANOVA with Tukey HSD test, $\alpha < 0.05$). **c** Number of differentially abundant (DA) features ($p < 0.05$, $n = 6$) comparing endosphere *versus* rhizosphere and rhizosphere *versus* bulk soil for lupin and willow. Shared features were rhizosphere-enriched in both comparisons. **d** Venn diagrams indicating unique and common metabolites among belowground fractions for lupin and willow. **e** MA plots comparing differential abundance of metabolites between root fractions for lupin and willow. Coloured points denote DA features ($p < 0.001$); while other DA ($0.001 < p < 0.05$) and non-DA are coloured in grey. Labels highlight putative identifications of key differentially abundant metabolites ($p < 0.01$) in at least one comparison between fractions.

Metabolomic response to arsenic

Metabolomic profiles were compared between samples treated with 60 μM arsenate (As(V)) and untreated controls. PCA illustrated that samples segregated according to arsenic treatments within endosphere and rhizosphere of both lupin and willow, with significant difference in beta diversity ($p < 0.05$, PERMANOVA), but did not separate between treatments in bulk soil ($p > 0.05$, PERMANOVA, **Figure 6a**, **Figure S4**). Comparison of α diversity between treatments in lupin and willow showed a significant increase between control and arsenic ($p < 0.05$, ANOVA) in endosphere of lupin and willow, and in the rhizosphere of lupin, but no significant difference in rhizosphere of willow and in bulk soil ($p > 0.05$, ANOVA, **Figure 6b**, **Figure S4**).

Comparisons between control and arsenic treatment in both the endosphere and rhizosphere identified 3,041 differentially abundant (DA) features in lupin and 4,981 in willow (T-test or Mann-Whitney U-test, with adjusted p value < 0.05). In the endosphere of lupin, 775 features were significantly depleted, while 1,686 features were significantly enriched in arsenic-treated plants compared to controls (**Figure 6c**). In the rhizosphere of lupin, 225 features were depleted and 995 were enriched. In willow, 200 features were depleted, and 2,861 features were enriched in the endosphere, while 1,926 features were depleted and 1,234 features were enriched in the rhizosphere.

Lupin-specific arsenic metabolomic response

When comparing DA compounds due to arsenic treatment between plant species, 1,884 were exclusively DA in lupin (**Figure 6d**). Of these, depleted compounds in the endosphere were predominantly tripeptides (21) and amino acids (19), while depleted rhizosphere compounds were primarily amino acids (13), and tripeptides (9) (**Figure S5**). Enriched endosphere compounds were primarily tripeptides (44) and fatty acyl CoAs (32), while arsenic-enriched rhizosphere exudates were primarily tripeptides and purine nucleosides with 23 and 17 compounds, respectively. Comparing the endosphere and rhizosphere, coumarins were enriched in both compartments of lupin, with a mean

fold change of 1.4 log_2FC in the endosphere and 3.1 log_2FC in the rhizosphere (**Figure 6e**). There was also mixed depletion and enrichment of flavonoids and nucleosides in the endosphere, but overall enrichment of both classes in the rhizosphere.

Other lupin-exclusive depleted DA compounds included endosphere flavonoids such as isorhamnetin 3−galactoside and apigenin 7-O-malonylglucoside. Enriched compounds within the endosphere included putative flavonoid kaempferol-3-O-hexoxyl-hexoside, as well as the coumarins sideretin, fraxin and dihydroxy dimethoxycoumarin. In the rhizosphere, enriched compounds included the putative flavonoid luteolin 3"-methyl ether 7-glucoside, the amino acid hydroxyectoine, the small peptides alpha-glutamylaspartic acid and cysteinylglycine and the coumarins fraxin and dihydroxy dimethoxycoumarin (**Figure S6**, Data S1).

Willow-specific arsenic metabolomic response

When comparing DA compounds due to arsenic treatment between plant species, 3,824 were exclusively DA in willow (**Figure 6d**). Of these, depleted endosphere compounds were predominantly composed of tripeptides (6), and amino acids (5), while in the rhizosphere, depleted compounds were primarily classified as amino acids acids (64), and proanthocyanins (59) (**Figure S5**). Enriched endosphere compounds were primarily amino acids (91) and proanthocyanins (75), while in the rhizosphere, enriched compounds were primarily composed of amino acids (38), tripeptides and fatty acyl CoAs (27). Comparing the endosphere and rhizosphere, phenolic acids, cinnamic acids and derivatives as well as proanthocyanins were also enriched in the endosphere, while in the rhizosphere, these same compound classes were consistently depleted upon arsenic exposure, with mean FC ranging from -1 to -3.1 (log_2) (**Figure 6e**).

Other willow-exclusive depleted DA compounds in the endosphere included furofuranoid lignan such as pinoresinol diglucoside. While in the rhizosphere, flavonoids such as proanthocyanidin dimers, trimers, and tetramers and phenolic acids such as 2'−acetylsalicortin and 3−hydroxybenzoic acid were depleted in response to arsenic. Enriched compounds in the endosphere included flavonoids such as the proanthocyanidin dimers, trimers, and tetramers, the amino acid tryptophan, as well as in the rhizosphere, dipeptides such as valylleucine and the alkaloids cytisine and nicotinic acid (**Figure S7**, Data S1).

Species-shared metabolomic arsenic response

In total, 1,157 DA compounds were shared in response to arsenic in both species, either in the endosphere, rhizosphere, or both compartments (**Figure 6d**). Among these, 47 were consistently

depleted, 754 were consistently enriched, and 147 showed opposite responses between lupin and willow. The depleted endosphere compounds predominantly comprised amino acids (7) and cinnamic acids and derivatives (4), while the arsenic-depleted compounds in the rhizosphere were dominated by amino acids and tripeptides with six and five compounds, respectively (**Figure S5**). Enriched endosphere compounds primarily included tripeptides (70) and amino acids (25), which also dominated the arsenic-enriched exudates in the rhizosphere, with 49 and 13 compounds, respectively.

Dipeptides and tripeptides were predominantly enriched in the endosphere with mean log_2 FC of 2.4 and 6.1, respectively, and showed mixed depletion and enrichment in the rhizosphere of both species with mean log_2 FC of -1.1 and 4.5, respectively (**Figure 6e**). Tripeptides were primarily composed of phytochelatins, which exhibited consistent enrichment by arsenic with mean log_2 FCs of 6.3 in the endosphere and 6.6 in the rhizosphere.

Depleted DA compounds shared between both species included endosphere peptides glutathione disulfide (GSSG), oxidised cysteinylglycine (ox.CysGly) and amino acid 5-oxoproline (5OP). These peptides were strongly depleted in the endosphere of lupin and in the rhizosphere of lupin and willow with a log_2 FC ranging from -1.17 to -2.31 but not in the endosphere of willow, where they were stable or slightly depleted (**Figure S8**). Arsenic-enriched compounds from both species included phytochelatin 2 (PC_2), PC_2 oxidised (ox.PC_2), phytochelatin 3 (PC_3), PC_3 oxidised (ox.PC_3), phytochelatin 4 with two disulfide bridges (ox.PC_4), S-glutathionyl-L-cysteine, γ-glutamylcysteine (γ-GluCys) and glutathione (GSH). These compounds were all enriched in the rhizosphere and endosphere of both species, except for γ-GluCys which was present but not enriched in willow rhizosphere, and GSH which was present but not enriched in lupin endosphere and in willow rhizosphere (**Figure S8**, Data S1). Some phytochelatins were exclusively detected in arsenic treated conditions such as PC_3, ox.PC_3 and ox.PC_4 in the rhizosphere (**Figure S8**, Data S1).

A total of 863 DA features in lupin and 768 features in willow were consistently present in arsenic-treated plants but absent (or below detection) from untreated controls, and 53 features were not detected in arsenic treated lupin and 96 in willow (only present in control plants) (**Figure S9**). Of the compounds present only in arsenic-treated lupin and willow plants, 992 remained unknown, while 147 were classified as tripeptides and 144 as phytochelatins (**Figure 6e**).

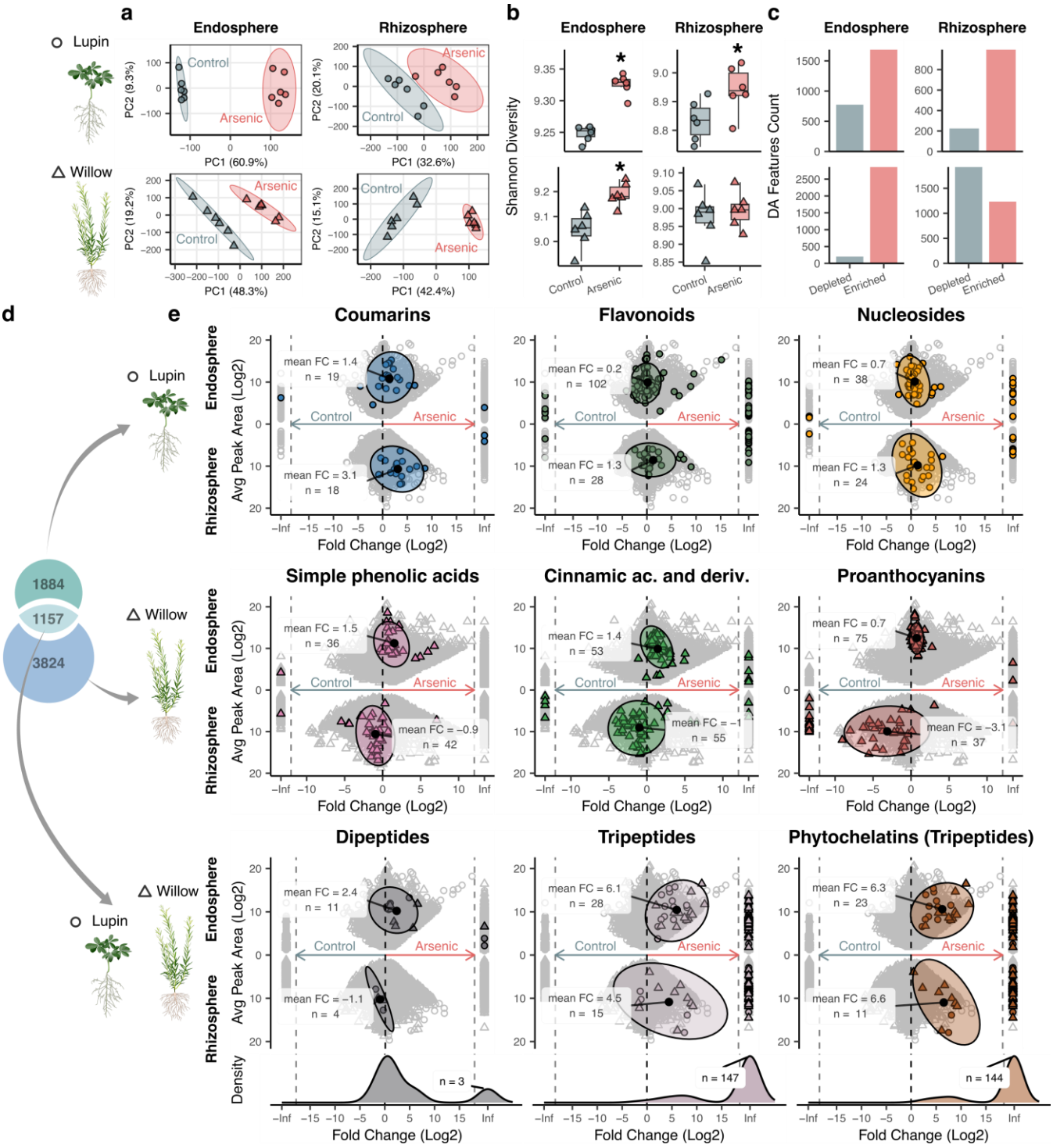

Figure 6 Arsenic-Induced Metabolomic Response.

a Principal component analysis (PCA) illustrating variations in metabolomic profiles between control and arsenic-treated endosphere and rhizosphere fractions of lupin and willow. **b** Shannon's index of α diversity from control and arsenic-treated endosphere and rhizosphere fractions of lupin and willow. For boxplots, the bottom and top of the boxes correspond to the lower and upper quartiles and the center line marks the median (n = 6). Asterisks indicate significant differences (T-test, $p < 0.05$). **c** Number of

significantly differentially abundant (DA) features between control and arsenic-treated endosphere and rhizosphere fractions of lupin and willow (n = 6). **d** Venn diagram showing unique and shared endosphere and rhizosphere DA features between lupin and willow. **e** MA-plots based on logged mean area and log_2 fold change (FC) showcasing the key metabolite classes response to arsenic treatment in endosphere and rhizosphere fractions from lupin and willow. The final panel presents MA plots of common responsive classes in lupin and willow, along with the distribution of log_2 FC values.

Arsenic chelating compounds

Based on their occurrence only in arsenic-treated conditions, 53 putative arsenic complexes were detected with an m/z corresponding to a potential arsenic-bound (halo form; **Figure 7a**) of one or several of the 195 putative chelator compounds identified in lupin and willow (**Figure 7b**). These candidate chelating compounds were mainly classified as tripeptides (13), flavonols (8), and disaccharides (5).

After confirmation of As-containing formulae, eleven arsenic complexes were identified as As(III) coordinated to ten different tripeptide chelators (**Figure 7b**). Eight of these complexes could be confidently annotated (**Figure 7c,d**). The dominating species included As(III) complexed to phytochelatin 3 (As(III)-PC_3), phytochelatin 3 with terminal Glu (As(III)-PC_3-Glu), phytochelatin 3 without terminal Gly (As(III)-des-Gly-PC_3), phytochelatin 4 (As(III)-PC_4), two phytochelatin 2 molecules (As(III)-$(PC_2)_2$), one glutathione and one phytochelatin 2 molecule (As(III)-GS-PC_2), as well as hydroxylated As(III) bound to phytochelatin 2 (As(III)(OH)-PC_2) and to homophytochelatin 2 (As(III)(OH)-hPC_2, with terminal amino acid Ala). These compounds were present in arsenic-treated lupin and willow endosphere and rhizosphere, except for As(III)-$(PC_2)_2$, As(III)-GS-PC2 and As(III)(OH)-PC_2, only present in lupin endosphere, and As(III)-PC_4, strictly endospheric in both species. Of these, As(III)-PC_3, As(III)-$(PC_2)_2$, As(III)-GS-PC_2 and As(III)(OH)-PC_2 were further confirmed using authentic standards. Other arsenic complexes could only be partially characterised from formula and compound class prediction as dimethyl As(III)-tripeptide complex (DMAs(III)), $C_{25}H_{41}AsN_{14}O_{11}$, found specifically in willow endosphere and rhizosphere, and two complexes of As(III) bound to unknown amino acids and peptides; $C_{45}H_{54}AsN_3O_{12}S_3$, present in both species endosphere and rhizosphere, and $C_{24}H_{35}AsN_6O_{14}S_3$, only present in willow endosphere and rhizosphere (**Figure 7c**).

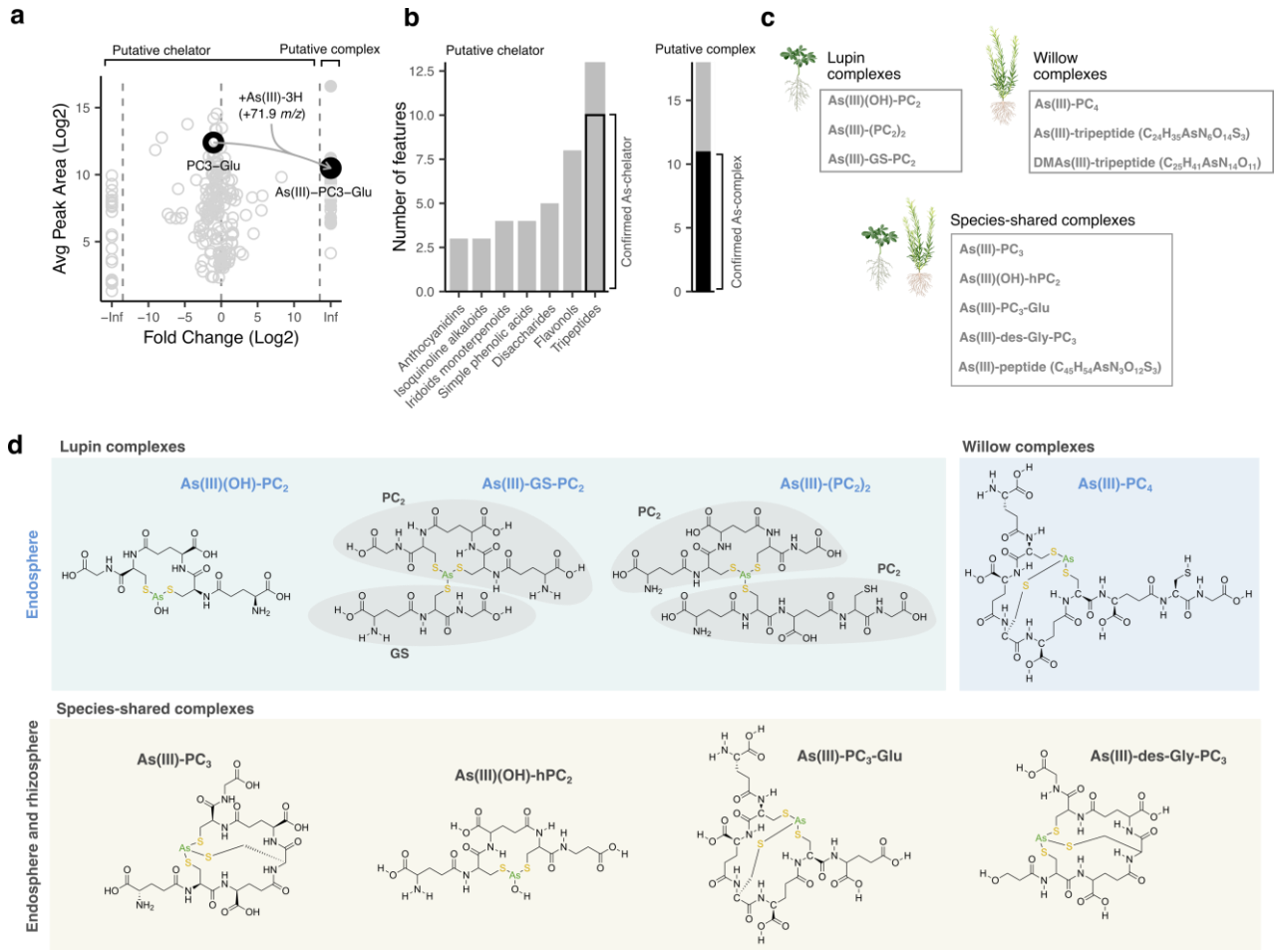

Figure 7 Identification of putative arsenic complexes in lupin and willow endosphere and rhizosphere after arsenic exposure.
a Example of mass matching between one putative arsenic chelator and one putative arsenic complex only present in arsenic-treated plants. Masses were matched across all such cases to identify candidate chelators binding arsenic and the complexes produced. **b** Composition of putative chelator classes coordinating arsenic based on fragmentation analysis of matched arsenic complex. Complexes retained had >70% MS^2 peak intensities explained by molecular formulae calculated using SIRIUS 6. **c** Putative arsenic complexes exclusively detected in root endosphere (blue) or found in both endosphere, and rhizosphere identified in lupin and willow under arsenic exposure. **d** Proposed structures of arsenic complexes in lupin and willow roots after fragmentation analysis.

Field trial belowground metabolome

To evaluate the similarity of the root endosphere and rhizosphere metabolome in real-world contaminated soil conditions, a phytoremediation field trial was sampled. Willow trees (*Salix miyabeana*) grown for four months in the contaminated or control plot (n=6) were sampled for endosphere, rhizosphere and bulk soil metabolites and assessed for growth. Plant height and main stem

diameter did not differ between plots; however, the mean number of stems was significantly lower in the contaminated plot compared to the control plot (**Figure S10**).

Alignment of metabolite features across all 36 willow field samples and those from the greenhouse trial (allowing cross-environment comparisons) revealed 11,575 quality filtered features. Comparing the metabolomic profiles of uncontaminated field samples to untreated greenhouse samples revealed significant differences between the two growth environments, with PCAs showing significant sample separation according to growth environment in endosphere, rhizosphere and bulk soil (PERMANOVA, $p < 0.05$; **Figure 8a**, Data S2). Alpha diversity analysis comparing field and greenhouse environments showed a significant increase of metabolite diversity in the endosphere compartment of the field grown plants, yet decreased metabolite diversity in the rhizosphere compartment and no significant difference in bulk soil of the field plants compared to the greenhouse pot trial (T.test, $p < 0.05$; **Figure 8b**).

Molecular networking of rhizosphere features from control plants revealed 13 main molecular families (groups of ≥ 15 features), with four molecular families dominated by greenhouse-specific features, and nine molecular families dominated by environment-shared features, while field-specific features did not dominate in any molecular family (**Figure 8c**). Greenhouse-dominated molecular families were primarily composed of proanthocyanins and flavanols, while shared molecular families mainly comprised nucleosides and phenolic acids (**Figure 8c**). Three molecular families were dominated by features identified as metabolites of putative microbial origin, purine nucleosides, purine alkaloids, and alkaloids and ornithine alkaloids molecular families, for which 50%, 59% and 93% could be associated to one or several microbial producers, respectively. These included compounds such as the purine nucleoside deoxyguanosine and adenosine and purine alkaloid hypoxanthine (**Figure S11**). The environment-shared features had the highest proportion of microbial-derived compounds, with 20%, followed by greenhouse-specific features, with 15.8%, and field-specific features, with 15.5% (**Figure S11**).

Metabolomic response to field contamination

Principal component analysis showed no distinct clustering of samples from contaminated versus uncontaminated plots across all fractions. Furthermore, α diversity indices were not significantly different between contaminated and uncontaminated plots for any fraction (T-test, $P > 0.05$, **Figure 8d,e, Figure S12**). Differential abundance analysis revealed 2,745 DA features between contaminated and uncontaminated plots, of which 436 were in the endosphere, 1,701 in the rhizosphere and 608 in bulk soil. Of the 1,701 rhizosphere DA compounds, 179 were depleted in the contaminated rhizosphere, while 1,522 were enriched (**Figure S12**). Depleted compounds were primarily amino

acids (8) and purine nucleosides (7), while enriched compounds were primarily amino acids (92) and dipeptides (47) (**Figure S12**). Notably, the oxidised tripeptide phytochelatin 2, the amino acid pipecolic acid and tryptophan and the phenolic acid salicylic acid glucoside were among the compounds enriched in the contaminated rhizosphere (**Figure 8f**). Of the DA compounds in the contaminated field rhizosphere, 71 were of putative microbial origin, with 67 enriched under contaminated conditions. These included oxidized phytochelatin 2, tryptophan and pipecolic acid, all of which were also present in the bulk soil fraction (**Figure S12**).

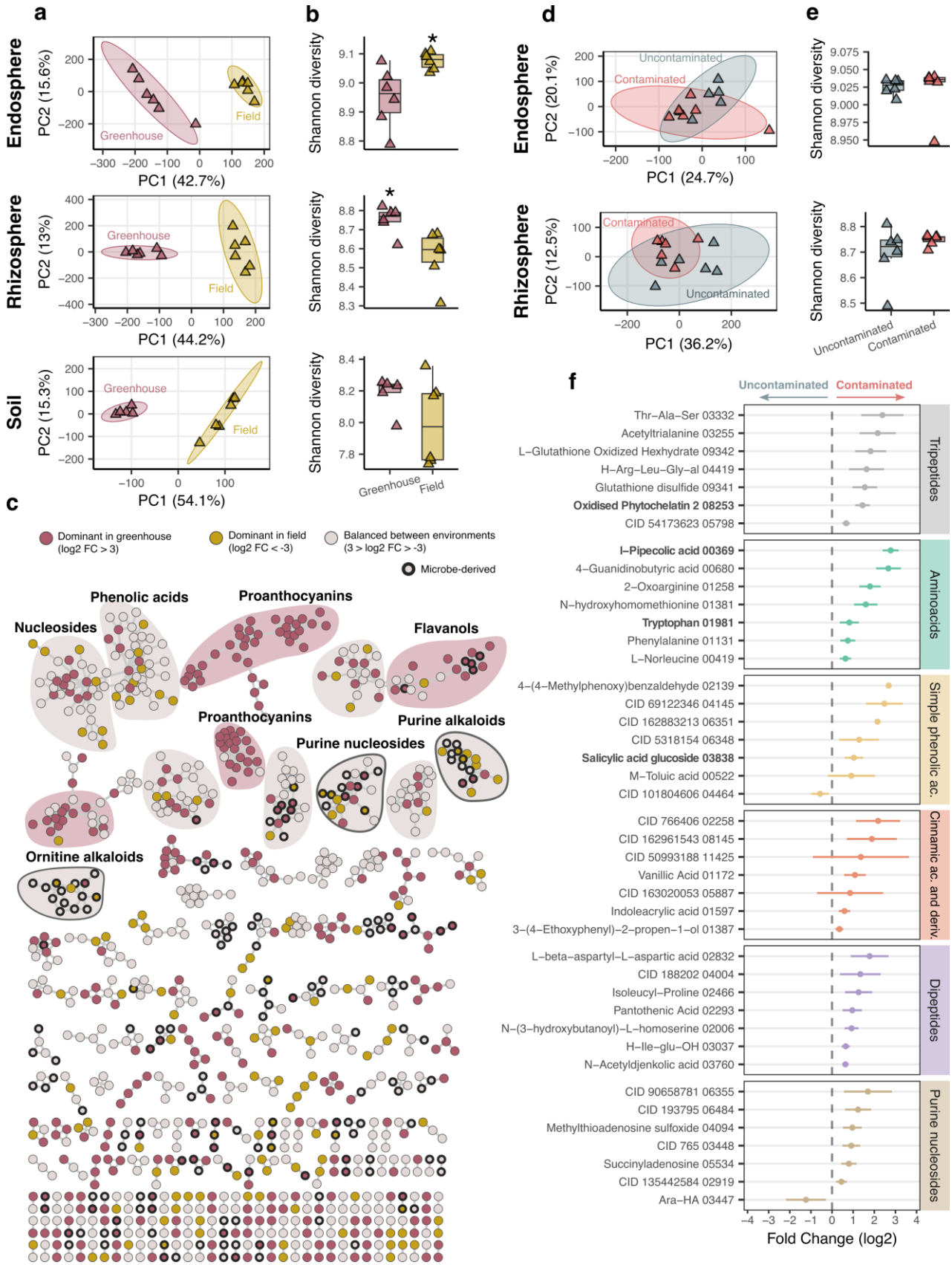
a
b
d
e
Endosphere
Rhizosphere
Soil
PC2 (15.6%)
PC1 (42.7%)
PC2 (13%)
PC1 (44.2%)
PC2 (15.3%)
PC1 (54.1%)
Greenhouse
Field
Shannon diversity
PC2 (20.1%)
PC1 (24.7%)
PC2 (12.5%)
PC1 (36.2%)
Uncontaminated
Contaminated
c
Dominant in greenhouse (log2 FC > 3)
Dominant in field (log2 FC < -3)
Balanced between environments (3 > log2 FC > -3)
Microbe-derived
Phenolic acids
Proanthocyanins
Nucleosides
Flavanols
Proanthocyanins
Purine alkaloids
Purine nucleosides
Ornitine alkaloids
f
Uncontaminated
Contaminated
Thr–Ala–Ser 03332
Acetyltrialanine 03255
L–Glutathione Oxidized Hexhydrate 09342
H–Arg–Leu–Gly–al 04419
Glutathione disulfide 09341
Oxidised Phytochelatin 2 08253
CID 54173623 05798
Tripeptides
l–Pipecolic acid 00369
4–Guanidinobutyric acid 00680
2–Oxoarginine 01258
N–hydroxyhomomethionine 01381
Tryptophan 01981
Phenylalanine 01131
L–Norleucine 00419
Aminoacids
4–(4–Methylphenoxy)benzaldehyde 02139
CID 69122346 04145
CID 162883213 06351
CID 5318154 06348
Salicylic acid glucoside 03838
M–Toluic acid 00522
CID 101804606 04464
Simple phenolic ac.
CID 766406 02258
CID 162961543 08145
CID 50993188 11425
Vanillic Acid 01172
CID 163020053 05887
Indoleacrylic acid 01597
3–(4–Ethoxyphenyl)–2–propen–1–ol 01387
Cinnamic ac. and deriv.
L–beta–aspartyl–L–aspartic acid 02832
CID 188202 04004
Isoleucyl–Proline 02466
Pantothenic Acid 02293
N–(3–hydroxybutanoyl)–L–homoserine 02006
H–Ile–glu–OH 03037
N–Acetyldjenkolic acid 03760
Dipeptides
CID 90658781 06355
CID 193795 06484
Methylthioadenosine sulfoxide 04094
CID 765 03448
Succinyladenosine 05534
CID 135442584 02919
Ara–HA 03447
Purine nucleosides
Fold Change (log2)

Figure 8 Willow belowground metabolome across controlled, field, and contaminated environments.

a Principal components analysis (PCA) showing variation in willow belowground metabolomes between uncontaminated greenhouse and field environments. **b** Shannon diversity index of metabolite α diversity in field versus greenhouse. For boxplots, the bottom and top of the boxes correspond to the lower and upper quartiles and the center line marks the median (n = 6). Asterisks denote significant differences (T-test $p < 0.05$). **c** Willow rhizosphere molecular network, dots represent features coloured by environmental association. Environment association was defined from $\log_2$ FC values as either dominant in greenhouse ($\log_2$ FC > 3), dominant in field ($\log_2$ FC < -3), or balanced between the two environments (3 > $\log_2$ FC > -3). Related features are circled as molecular families, further classified as greenhouse-dominated (red) or environment shared (grey). **d-e** PCA and diversity index showing metabolomic differentiation between field uncontaminated and contaminated plots. **f** Log_2-transformed features intensity fold changes of differentially abundant (DA) metabolites between field uncontaminated and contaminated plots, grouped by putative compound class. Only the seven most abundant DA features (average peak intensity) and the six most prevalent classes (based on number of DA feature) are shown. Data are means and standard errors (n = 6). Refer to Data S2 for full identifications and statistics.

Discussion

Plant phenotype and arsenic fate

Lupin and willow are two phytoremediation crops, used in arsenic-contaminated sites (Navazas et al., 2022; Vázquez et al., 2006a), but with limited information about their root and rhizosphere metabolomic responses to contamination (Frémont et al., 2022; Yergeau et al., 2014). Furthermore, despite divergent morphologies and physiologies, these species are thought to have similar metal-excluding strategies, preferentially restricting arsenic accumulation and stabilisation belowground (Fresno et al., 2016; Yanitch et al., 2017). Here, both lupin and willow had substantial physiological responses to arsenic treatment (**Figure 3**). Stomatal conductance and biomass were consistently higher in willow compared to lupin, corroborating willow's documented high photosynthetic and evapotranspiration abilities, exploited for diverse phytoremediation applications (Frédette et al., 2019; Jerbi et al., 2020). Arsenic did not consistently affect stomatal conductance in either species, with only a transient initial reduction in willow, indicating minimal photosynthetic impairment. This transient photosynthetic impairment in willow is likely linked with the minor aboveground biomass reduction measured at harvest but did not alter belowground biomass (**Figure 3c**). Along with the absence of visible toxicity symptoms, this indicates arsenic tolerance in lupin and willow under these conditions. In both species, arsenic preferentially accumulated in roots, with 6-39 times more arsenic retained belowground than in stems or leaves (**Figure 3d**), confirming arsenic exclusion. Despite shorter

growth and arsenic exposure, lupin stem and leaf arsenic concentrations were 2- and 3-fold higher than willow, respectively, potentially due to more efficient phosphorus acquisition in lupin, increasing uptake and translocation of the phosphorus analog arsenate (Esteban et al., 2003).

Specialised metabolism shapes belowground metabolite diversity in lupin and willow

Metabolomic analysis of lupin and willow belowground micro-environments, tentatively identified 46% (7,639) of features at the compound level (**Figure 4a**). Both species shared 66% of their belowground metabolites and all seven major metabolic pathways were captured in similar proportions in both lupin and willow, indicating conservation of the major phytochemical classes (**Figure 4b,c**). However, the relative abundance of these compounds (suggested by feature intensity) varied between lupin and willow at pathway level. Alkaloids showed greater relative abundance in lupin, while the shikimates and phenylpropanoids and the terpenoid pathways showed greater relative intensity in willow, which may underlie distinct biochemical functions in these species.

Molecular networking analysis uncovered structural diversity in the belowground metabolomes of lupin and willow (**Figure 4**). The molecular families indicate that both species produce a distinct array of metabolites with unique molecular structures. The seven lupin-dominated molecular families comprised quinolizidine alkaloids, which have roles in biotic defence, including antimicrobial, allelochemical, and herbivore-repelling properties in Fabaceae (Wink, 2013), and specifically in *Lupinus* species (Cely-Veloza et al., 2022; Tyski et al., 1988) as well as roles in abiotic stress responses such as to drought and heat (Frick et al., 2018). The six willow-dominated molecular families included proanthocyanidins and phenolic acids, which is consistent with the history of using abundant willow phenolic compounds in pharmacology (Tawfeek et al., 2021), and their potential value for biorefinery (Sas et al., 2021). Phenolic acids are associated with allelopathic plant defence against herbivory (Boeckler et al., 2011), as well as antioxidant response (Si et al., 2011). Proanthocyanidins, on the other hand, have been shown to be involved in the response to a broad range of environmental factors, serving as photo-protectants, antioxidants, and potential metal(loid) chelators (Landi et al., 2015). Contrasts between species were also observed in the higher relative abundance of alkaloids (N-rich) in lupin compared to willow, and the higher relative abundance of shikimates and phenylpropanoids as well as terpenoids (devoid of N) in willow compared to lupin (**Figure 4**). Alongside other differences in specialised metabolites which may confer specific functions, the N-rich metabolism of lupin, reflecting microbial N-fixation of the legume, and the phenolic-rich metabolome of willow, likely shape how these plants respond to environmental factors.

The three molecular families that are shared between lupin and willow (**Figure 4**) mainly consisted of small peptides and nucleosides, such as glutathione disulfide and guanosine. These compounds are widely recognized as essential components of primary plant metabolism, involved in fundamental cellular processes such as signalling, regulation of oxidative homeostasis, plant immunity and serving as precursors for less conserved specialised metabolites (Hirakawa & Sawa, 2019; Návarová et al., 2012; Queval et al., 2011). As such, these families represent constitutively produced "core" metabolites which likely provide conserved functions underlying the central metabolism of plants.

Lupin and willow belowground metabolite partitioning reveal distinct biochemical micro-environments.

The metabolite profiles of the lupin and willow endosphere were highly dissimilar, while their rhizosphere was more similar, and this was also true when subtracting compounds found in bulk soil. This pattern may reflect that rhizosphere metabolome assembly may involve conserved functions such as nutrient acquisition (Carvalhais et al., 2011) and/or recruitment of similar soil microbial producers (Reinhold-Hurek et al., 2015).

Metabolite diversity was substantially higher in the endosphere and rhizosphere than in bulk soil for both species (**Figure 5b**). This aligns with the large proportion of DA metabolites enriched in the endosphere in comparison to the rhizosphere (76.1% in lupin and 47.6% in willow; **Figure 5c**), indicating most rhizosphere metabolites follow a concentration gradient consistent with root exudation mechanisms, and are likely endosphere-derived (Frémont et al., 2022). This is further supported by the substantial overlap between fractions, with the rhizosphere sharing more than 87% of its metabolites with the endosphere in both species (**Figure 5d**), providing insight into the extent to which plants influence the rhizosphere chemistry.

Endosphere-derived metabolites had substantial overlap with the molecular families characterised as species-specific, including quinolizidine alkaloids and flavonoids in lupin, and phenolic acids and proanthocyanidins in willow (**Figure 3**). In lupin, these included the potential antifungal compound hydroxylupanine (**Figure 5e**) (Cely-Veloza et al., 2022), which though not yet reported in exudates, may contribute to shaping the lupin rhizosphere microbiota. Additionally, the (iso)flavonoids apigenin 7−O−malonylglucoside and sophoricoside, known root exudates of Lupin and other leguminous species (Cesco et al., 2010; Frémont et al., 2022), may function within nodulation signalling for recruitment of N_2-fixing rhizobacteria (Brechenmacher et al., 2010) and as antimicrobial compounds shaping the lupin rhizosphere microbial communities (Weisskopf et al., 2005). In willow, endosphere-derived metabolites included proanthocyanidins dimers and trimers, and salicortin (**Figure 5e**).

Despite not being reported as exudates, these compounds possess antioxidant and allelopathic activities that may help maintain redox homeostasis around plant roots and restrict neighbouring plant root growth (Nakano et al., 2002).

While the endosphere was the primary source of metabolite diversity in the rhizosphere, a notable proportion of metabolites were enriched only in the rhizosphere compared to both the endosphere and bulk soil (8.1% in lupin and 15% in willow, **Figure 5c**). These rhizosphere-derived metabolites may originate from diverse biotic and abiotic sources including active exudation, spontaneous chemical reactions, and microbial biosynthesis and catabolism. In lupin, rhizosphere-derived metabolites were dominated by dipeptides like valylleucine and theonylleucine, and nucleosides like thymidine and hypoxanthine. As known root exudates, these compounds and their constituent amino acids serve as key mediators of plant-microbe interactions and carbon sources for rhizosphere microbial communities (McLaughlin et al., 2023; Phillips et al., 2004; Zhalnina et al., 2018). Additional lupin rhizosphere-derived metabolites included the non-structural carbohydrate trehalose (**Figure 5e**). Produced by soil fungi and nodule-forming rhizobia, trehalose can act as an energy reserve and protectant against rhizosphere chemical stresses in legumes (Müller et al., 2001), suggesting the lupin rhizosphere can provide a niche for beneficial rhizobacteria. In willow, enriched rhizosphere metabolites included nucleosides such as cytidine, and simple phenolic acids like salicylic acid glucoside. In root exudates, these compounds can undergo rapid preferential consumption by rhizosphere microbes (Sasse et al., 2019; Zhalnina et al., 2018). Through exudation of these compounds, willow may nourish microbes capable of metabolising key exudate components to shape the rhizosphere community.

In lupin, 37.8% of rhizosphere-derived compounds were of potential microbial origin (**Figure S3**), including the peptidoglycan precursor N-acetyl-D-glucosaminyl-(1-4)-N-acetylmuramic acid, a bacterial cell wall constituent (Vollmer et al., 2008). In willow, 13.3% of rhizosphere-derived metabolites were microbially derived. These included 6-nonenal, enriched in the rhizosphere of both species (**Figure 5e**), a volatile aldehyde compound proposed to participate in belowground plant-microbe interactions (Schenkel et al., 2015), as well as the osmoprotectants hypoxanthine, either enriched in the rhizosphere or bulk soil of lupin and willow (**Figure 4e**), and known to accumulate in *Pseudomonas*, *Streptomyces* or *Rhizobium* species (C. Chen et al., 2013; Czech et al., 2018; Kol et al., 2010), including some endophytic strains (Data S1).

Delineating the rhizosphere metabolomic landscape revealed the intricate interactions between endosphere-derived compounds and soil-derived metabolites reflecting complex biotic and abiotic processes. Moreover, the extensive enrichment of rhizosphere metabolites and generation of novel

compounds unique to the rhizosphere also suggests interactions between plant roots and soil microorganisms. The rhizosphere metabolome can therefore be defined by exudate-derived metabolites, soil-derived metabolites, and these *de novo* rhizosphere-derived metabolites, which together drive plant-soil interactions underlying key belowground biochemical processes.

Arsenic-induced alterations of belowground metabolome

Arsenic alters metabolome diversity.

Arsenic drove significant alterations in the metabolomes of lupin and willow in both the endosphere and rhizosphere. However, there were no significant changes in the metabolome of unplanted soil, indicating a more limited role of soil-derived metabolites in the interactions with arsenic (**Figure 6**, **Figure S4**). Exposure to arsenic increased metabolite diversity in the endosphere of both lupin and willow, as well as in the rhizosphere of lupin but not of willow. Particularly in the endosphere, arsenic triggered an increase in metabolite diversity of over 1.52% in lupin and 2.9% in willow, indicating the synthesis of new metabolites as a response to arsenic exposure. In lupin, this increase in both endosphere and rhizosphere metabolite diversity suggests at least some endosphere metabolites were destined for exudation in response to arsenic, as opposed to internal stress responses alone (**Figure 6**). The contrasting pattern in willow may indicate a lack of bespoke exudation tools in presence of arsenic. Alternatively, willow may prioritise arsenic-responsive exudates at the expense of constitutively produced exudates in a redirection of rhizosphere metabolic flux (Dong & Lin, 2021).

These differences between species are most clearly observed using differential abundance analysis, where most endosphere and rhizosphere DA metabolites (6,776 or 84%) were enriched (**Figure 6**). One explanation for this limited endosphere metabolite depletion in both species is that arsenic exposure did not disrupt intracellular metabolism, thereby maintaining minimum levels of constitutive metabolites. Given the high arsenic concentrations applied, lethal for lupin in semi-hydroponic cultivation (Frémont et al., 2022), enriched metabolites dominating lupin and willow endosphere likely include biochemical tools providing protection to the plant which enabled the observed successful arsenic tolerance (**Figure 3**). Similarly, in the rhizosphere of lupin, 81.5% of DA metabolites were enriched, whereas in willow, arsenic exposure led to a more balanced shift in metabolite intensities, which can be attributed to divergent arsenic exclusion strategies, potentially involving the selective inhibition of exudation in willow.

Arsenic enhances coumarin, flavonoid and nucleoside exudation in lupin.

The lupin-specific arsenic response revealed an extensive enrichment of coumarins in both endosphere and rhizosphere when exposed to arsenic, including fraxin and 7,8-dihydroxy-5,6-dimethoxycoumarin, suggestive of their increased biosynthesis and exudation under arsenic stress (**Figure 6**, Data S1). While coumarins are known to be exuded by *Arabidopsis thaliana* during iron deficiency to facilitate iron acquisition via metal complexation (Chutia et al., 2019; Robe et al., 2021; Stringlis et al., 2018), the mechanisms underlying coumarin-arsenic interactions remain to be elucidated but could involve iron acquisition during arsenic stress, or arsenic-coumarin complex formation to limit arsenic uptake by plant roots.

In addition to coumarins, lupin roots showed increased exudation of flavonoids such as the flavone luteolin 3"-methyl ether 7-glucoside in response to arsenic exposure. Other flavonoids like isorhamnetin 3-galactoside and kaempferol-3-O-hexoxyl-hexoside were depleted and enriched in the endosphere, respectively, but remained unchanged in the rhizosphere (**Figure S6**). Given the potential roles of these compounds in interactions with nitrogen-fixing microbes (Kapulnik et al., 1987), the observed changes could signify modified symbiotic relationships and shifts in the rhizosphere microbial community structure. Specifically, luteolin exudation has been linked to increased nodulation of *Rhizobium meliloti* in alfalfa (Peters et al., 1986), suggesting its enhanced glycosylated exudation here may help lupin recruit nitrogen-fixing bacteria to counter arsenic's documented detrimental effects on nodulation (Talano et al., 2013). Another metabolite enriched in the rhizosphere of arsenic-exposed lupin was the amino acid hydroxyectoine (**Figure S6**). In the rhizosphere, hydroxyectoine can protect diverse microbes like beneficial rhizobia (e.g. *Rhizobium, Sinorhizobium* or *Bradyrhizobium*) against osmotic stress (Czech et al., 2018). This arsenic-induced hydroxyectoine enrichment could thus promote rhizobacteria activity, impacting lupin's long-term fitness on contaminated soils (Pajuelo et al., 2019).

Arsenic inhibits exudation of phenolic acids, cinnamic acids, and proanthocyanins in willow.

The willow-specific arsenic response was characterised by the predominant enrichment of endosphere compounds, contrasted with extensive metabolite depletion in the rhizosphere (**Figure 6**). These differences were largely driven by the consistent enrichment of phenolic acids, cinnamic acids, and proanthocyanins in the endosphere. In contrast, the rhizosphere displayed an inverse pattern, with the same metabolite classes showing consistent depletion in response to arsenic, including compounds such as proanthocyanidin dimers, trimers, and tetramers, salicortin, and salicylic acid glucoside (**Figure 6**, **Figure S7**). The antagonistic enrichment and depletion patterns of these phenolic compounds suggest strict regulation of root exudation in willow under arsenic stress. Phenolic

compounds, such as proanthocyanins are thought to be exported across membranes by ABC transporters that could facilitate their exudation into the rhizosphere (Cesco et al., 2010; Zhao, 2015). Downregulation of ABC transporter gene expression observed in arsenic-exposed willow roots (Yanitch et al., 2017) suggests a limitation in proanthocyanin exudation, explaining intracellular accumulation and extracellular depletion here (**Figure 6**). The exact functions and subcellular localisations of distinct ABC transporters governing exudation remain unclear, so further research is needed to elucidate their contributions to arsenic tolerance. Given the antioxidant (Arikan et al., 2022) and potential metal(loid) complexing (Ahammed & Yang, 2022) activities of phenolic compounds, their apparent redirection from constitutive rhizosphere exudation to intracellular accumulation may represent a key arsenic stress adaptation for intracellular detoxification and extracellular exclusion in willow.

Arsenic induces shared metabolite response in lupin and willow.

In addition to species-specific responses, arsenic exposure induced shared metabolomic changes in lupin and willow. Notably, tripeptides accounted for >6% of the differentially abundant (DA) metabolites common to both species, with overall enrichment suggesting these compounds comprise conserved arsenic tolerance metabolites accumulated intracellularly and exuded into the rhizosphere of lupin and willow. This was particularly striking for phytochelatins (PCs) and their biosynthesis intermediates glutathione (GSH) and γ-glutamylcysteine (γ-GluCys), with significant and substantial (>5 FC (log_2)) enrichment in arsenic-treated endosphere and rhizosphere (**Figure 6e**, **Figure S8**). PCs were also over-represented among metabolites exclusively detected in arsenic-treated samples in the endosphere and rhizosphere of both species. As major metal(loid) detoxification metabolites, largely accumulated intracellularly under arsenic stress (Cobbett & Goldsbrough, 2002), the observed significant and substantial increase in PCs, along with their exudation in the rhizosphere, suggests that a crucial mechanism of extracellular arsenic tolerance and detoxification only previously reported in lupin (Frémont et al., 2022) also exists in willow.

Interestingly, arsenic exposure also induced depleted levels of glutathione disulfide (GSSG), cysteinylglycine disulfide (Cys-Gly disulfide), and the amino acid 5-oxoproline (5OP) in the endosphere and rhizosphere (**Figure 6**, **Figure S8**). As essential intermediates in GSH metabolism (Noctor et al., 2012; Ohkama-Ohtsu et al., 2008), the arsenic-triggered reduction in these metabolites likely stems from increased demand for GSH-derived PCs, as previously proposed (Frémont et al., 2022). This coordinated GSH pathway regulation may confer an effective intracellular and extracellular response to arsenic, whereby both species appear to increase GSH synthesis, GSSG

recycling to GSH, and PC production, thereby assembling a diverse metabolic toolkit for arsenic detoxification and tolerance.

Novel arsenic tolerance equipment

Both the endosphere and rhizosphere of lupin and willow comprised many metabolites which were repeatedly observed as unique to arsenic treated plants across biological replicates, the majority of which remained uncharacterised (77% unknown). This proportion is not uncommon in untargeted metabolomics (Aksenov et al., 2017) and represents important yet-to-be-characterised candidate metabolites likely to have important biological function for metal tolerance. Some of these metabolites with chelating activity could contain coordinated arsenic, resulting in the detection of new metabolites, unique to arsenic treatment, with a molecular mass gain corresponding to an arsenic atom (74.92 Da). This is observed with organic acids, siderophores, metallothionein and phytochelatins, which can form complexes with metal(loids) such as Al, Fe, Cd, and As (Álvarez-Fernández et al., 2014). However, in complex compound mixtures, such as the rhizosphere, the diversity of potential arsenic-binding metabolites is substantial, limiting characterisation of arsenic-metabolite complexes and database entries on holo (bound) *versus* apo (unbound) metal-binding compounds (Aron et al., 2021). A list of putative arsenic-chelating molecules was identified here (**Figure 7**, Data S2) and the candidate structures were scrutinised.

Untargeted metabolomics, combined with this As-complex search, enabled characterisation of eight distinct arsenic complexes comprising different combinations of seven chelating metabolites, namely PC_2, hPC_2, PC_3, PC_3-Glu, $desGlyPC_3$, PC_4, and GSH (**Figure 7c,d**). Four of these arsenic species were also detected in the rhizosphere of both lupin and willow, with the dominant As(III)-PC_3 complex verified by comparing MS^2 spectra to those of complexes synthesized *in vitro* from authentic standards. While previous studies have identified several arsenic-phytochelatin complexes in tissue extracts of various plant species like *Helianthus annuus* (Raab et al., 2005), this represents, to our knowledge, the second report of arsenic complexation in the rhizosphere of any plant (Frémont et al., in submission) and the first in willow. Characterisation of these rhizosphere arsenic complexes and detection of yet-to-be-characterised arsenic complex candidates here, suggests rhizosphere chelation directly constitutes a major mechanism of arsenic detoxification in phytoremediation crops.

The field rhizosphere metabolome and stress response

To determine whether any of the willow arsenic-tolerance metabolome was preserved from controlled conditions, endosphere, rhizosphere, and bulk soil samples were collected from a willow field trial in

both non-contaminated and contaminated plots for metabolomic profiling. The metabolomic profiles significantly differed between greenhouse and field settings with differences in metabolite diversity (**Figure 8a,b**). The increased endosphere metabolite diversity and decreased rhizosphere diversity in the field compared to the greenhouse indicates distinct exudation dynamics under field environmental conditions. Molecular networking-based comparative metabolomics revealed distinct greenhouse-dominated and environment-shared molecular families in the greenhouse and field willow rhizosphere (**Figure 8c**). The decreased rhizosphere diversity in the field suggests willows were exuding fewer types of metabolites when interacting with field soil microbiota and nutrient conditions. However, most molecular families, including a large phenolic acid cluster, were conserved between the greenhouse and field, implying consistent exudation of key metabolites by willow despite the overall decrease in diversity. Conversely, greenhouse-specific families, like proanthocyanins, were not found in the rhizosphere of field willows. Which is surprinsing as, in the greenhouse, proanthocyanins were abundantly exuded in control plants (**Figure 6**e), their absence in the field suggesting proanthocyanin exudation may not be constitutive. Interestingly, within the environment-shared metabolites, 20% could be identified as microbial-derived, suggesting extensive conservation of microbially-produced metabolites between greenhouse and field (**Figure 8**, **Figure S11**). This was particularly evident for the purine nucleosides, and purine alkaloids molecular families which comprise osmoprotectants and energy sources for beneficial rhizosphere microbes, such as hypoxanthine, deoxyguanosine, as well as willow rhizosphere-associated adenosine (Zheng et al., 2023).

PCA revealed no discernible separation between the metabolomes of unpolluted and polluted field rhizosphere samples (**Figure 8d,e**). This lack of clustering was consistent with considerable metabolite variation independent of soil contamination, attributable to numerous uncontrolled confounding factors present in real-world scenarios (e.g., soil physicochemistry and diverse unquantified contaminants). However, differential abundance analysis captured consistent metabolite responses to contamination in the rhizosphere, endosphere, and bulk soil (**Figure 8f**, **Figure S12**). Notably, the consistent enrichment of numerous rhizosphere metabolites in contaminated plots, comprising 89% of differentially abundant (DA) rhizosphere metabolites. Although some metabolites, such as pipecolic acid showed contradictory differential abundance responses to contamination between field and greenhouse (**Figure 8f**; Data S1) consistent enrichment of oxidised phytochelatin 2 affirmed the role of phytochelatins in rhizosphere responses to contaminants in both controlled and real-world environments.

Conclusion

Collectively, species-specific metabolic responses to arsenic exposure revealed distinct tolerance mechanisms in lupin and willow. Lupin exhibited increased exudation of coumarins into the rhizosphere, corroborating prior evidence that coumarins are involved in extracellular defence against arsenic. In contrast, arsenic appeared to suppress exudation of certain metabolites from willow roots, including phenolics with metal-chelating properties, which may facilitate intracellular detoxification in willow while limiting extracellular arsenic mobilization**.** Despite these differences, strong similarities between species revealed extensive exudation of phytochelatin is conserved in these phylogenetically divergent phytoremediation species. Both species also showed evidence of phytochelatin-arsenic complexation in the rhizosphere, which is the first report of extracellular complexation of arsenic in the rhizosphere of soil-grown plants. Field-scale assessments of willow corroborated the real-world implications of phytochelatin exudation. Collectively, these rhizosphere arsenic tolerance mechanisms in lupin and willow could inform strategies to mitigate arsenic pollution globally.

Acknowledgements

We would like to thank Ariane Lafrenière for her kind support during the greenhouse harvest, Michel Labrecque, Patrick Benoist, Noémie Legault and Amandine Bonet for enabling the field trial sampling. A special thank you is extended to Orica Canada Inc. for providing access and support to the field. We would also like to thank Dr. Benjamin Péret for graciously providing white lupin seeds.

Supplementary information

All data supporting this study may be found in the supplementary materials. The metabolomic raw data files are publicly accessible as a MassIVE [temporarily upon request] dataset and the MS^2 spectra of identified PC-As complexes synthetised *in vitro* from authentic standards can be accessed and queried in the GNPS spectral libraries.

Supplementary methods

Greenhouse plant growth conditions

Lupin seeds (*Lupinus albus* L., cv. AMIGA) were surface sterilised in consecutive baths of 70% ethanol, 1% sodium hypochlorite and sterile Milli-Q water. Seeds were soaked overnight in sterile tap water and germinated on sterile moist filter paper for two days. Willow plants (*Salix miyabeana* cv. SX. 67) were grown from 20 cm long cuttings pre-soaked in tap water for one week. Seedlings and cuttings were then transferred to 6 L pots filled with 35% commercial growing medium (OM6®, Les Tourbières Berger Ltd., QC, Canada), 25% 24-month-old mature compost (Grenier et al., 2023), 25% perlite, 15% sand and each pot supplied twice a week with 1 L of 10% strength Hoagland nutrient solution with the following concentrations: N 1,600 µM, P 200 µM, K 605 µM, Ca 400 µM, S 100 µM, Mg 100 µM, Cl 5 µM, B 2.5 µM, Mn 0.2 µM, Zn 0.2 µM, Cu 0.05 µM, Mo 0.05 µM, Fe 4.5 µM, adjusted to pH 5.5 with 1% HNO3.

Greenhouse plant measurement and arsenic quantification

Signs of canopy toxicity were monitored, and stomatal conductance was measured at three time points during the treatment period on the abaxial surface of three fully expanded leaves per plant with a porometer (LI-600, LI-COR Biosciences, Lincoln, USA), while biomass production and arsenic concentrations were measured at harvest.

Entire shoots (excluding willow cuttings) and root systems, washed from soil with tap water, were separated, oven-dried at 105°C for 48h and weighed. For total As quantification, dried shoots and roots, as well as reference material (NIST #1573a tomato leaf, for quality control), were ground and digested in nitric acid using a block digester for 6 h at 120°C and analysed by ICP-MS, following the methods described in Courchesne et al. (2017).

Field trial plant growth conditions

Prior to planting, the field site was prepared by incorporating a 10 cm layer of manure compost into the topsoil. Subplots of 8 m × 9 m were then planted with 150 cm cuttings of *Salix miyabeana* SX64

or other species (not included in this study) at a density of 1.5 m between rows and 1 m between trees within rows. The cuttings were planted to a depth of 75 cm and supplied with daily drip irrigation.

Field trial contaminant quantification and plant measurements

Soil contaminant concentrations were measured before planting (May 2021) at two depths (10-60 cm and 60-110 cm) at 10 locations per plot corresponding to the intersections of five lateral and two longitudinal transects covering each plot (**Figure S1**). Composite soil samples (pool of three for each soil depth) were collected in amber glass containers and immediately sent to an external laboratory (AGAT Laboratories Ltd., Montreal, QC, Canada) for analysis of seven trace elements (As, Cd, Cu, Sn, Mn, Pb, and Zn, **Figure S1**) by ICP-OES, following provincial methods with duplicates, blanks and certified standards (CEAEQ MA, 2020).

Fully grown plants (4 months old) were measured for growth at time of sampling (September 2021). Height (from soil to highest meristem), number of stems and total diameter at breast height (DBH) were measured on six replicate trees in each plot.

Liquid chromatography-tandem mass spectrometry (LC-MS/MS) analysis

Untargeted profiling was performed on an Agilent 1,260 Infinity HPLC system coupled to an Agilent 6530 quadrupole time-of-flight mass spectrometer with a Jet Stream ionization source. Chromatographic separation used a Zorbax Eclipse Plus C18 column (4.6 × 100 mm, 3.5 µm) at 30°C with a 0.4 mL/min flow rate. The 80 min gradient consisted of solvent A (5% methanol, 0.1% formic acid in water) and solvent B (methanol, 0.1% formic acid), starting at 100% A for 20 min, increasing linearly to 100% B over 50 min, then holding at 100% B for 10 min. Biological samples (greenhouse n = 70; field n = 36) and extraction blanks (greenhouse n = 8; field n = 4) were analysed in ESI+ mode full-scan MS1 (100-1,400 Da). Source parameters included 300°C gas temperature, 5 L/min drying gas, 45 psig nebulizer pressure, 250°C sheath gas temperature, and 11 L/min sheath gas flow. Data-dependent MS^2 acquisition was performed at 20 and 40 eV collision energies on 3 replicated samples for each sample type and treatment (greenhouse n = 36; field n = 14). Precursor isolation used an intensity threshold set to 500, with a maximum of 4 precursors per cycle and 3 spectra per precursor locked for 0.3 min.

Untargeted metabolite data preprocessing with Mzmine 3

Raw LC-MS data were processed using the open-source software package MZmine 3.3.0 (http://mzmine.github.io/ (Schmid et al., 2023)). Background noise was filtered at intensity thresholds

of 800 for MS^1 and 10 for MS^2. Chromatograms were constructed within 10 ppm mass accuracy and a minimum peak intensity of 800. Extracted ion chromatograms were deconvoluted using MZmine's minimum search algorithm. Isotope peaks were grouped within 10 ppm mass tolerance and 0.1 min retention time tolerance. Features were aligned across samples within 15 ppm mass tolerance (75% weighting) and 0.2 min retention time tolerance (25% weighting). Gaps in the feature matrix were filled within 0.8 min retention time and 5 ppm mass tolerance using the peak finder module. Contaminant filtering was applied by removing features with a sample median intensity less than three times the median intensity observed in blanks. Features eluting within < 0.2 min retention time and with peak shape correlated by >85% (Mzmine's metaCorrelate algorithm) were assigned to a feature correlation group and used for curation of adducts, complex formation, and in-source fragments (Schmid et al., 2021). MS2 spectra were matched to precursor ions within 0.02 m/z and 0.2 min retention time windows. MS2 spectra acquired at 20 and 40 eV collision energies were merged into consensus spectra after summing their intensities.

Molecular networking

To investigate the structural diversity of lupin and willow belowground metabolomes, endosphere and rhizosphere features with available MS2 spectra were grouped based on spectral similarity (cosine score > 0.6) in a molecular network. Network cluster analysis was performed using the walktrap algorithm (Pons & Latapy, 2005) in the igraph R package (Csardi & Nepusz, 2005) and clusters were named based on their prevalent metabolite class. Main clusters were identified (groups of ≥ 15 features) and further referred to as molecular families, based on the inferred structural homology between connected features (Nothias et al., 2020). To show the differences in molecular diversity between lupin and willow, the fold change (FC, log2) of lupin versus willow was calculated. Features were then categorised as either dominant in lupin (log2 FC > 3), dominant in willow (log2 FC < -3), or balanced between the two species (3 > log2 FC > -3). Molecular families with over 50% of features that were dominant in lupin, dominant in willow, or balanced between the species were defined as lupin-dominated, willow-dominated, or common molecular families respectively.

Annotation confidence level assignment

A system of confidence level assignments was implemented to denote the reliability of metabolite identification based on Sumner et al., (2007). Level 1 corresponds to matches with retention time (RT), mass spectrum (m/z), and MS^2 spectrum (if available) of authentic standards analysed under identical conditions. Level 2 denotes matches with high-resolution MS^2 spectra from public databases and/or manually inspected unambiguous *in-silico* MS^2 annotations. Level 3 is assigned to tentative

annotations derived from ambiguous spectral matching to public MS^2 databases or from *in-silico* MS^2 predictions alone. Level 4 represents annotations of metabolite class, superclass, or pathway from *in silico* predictions, whereas Level 5 indicates annotations obtained solely from MS^1 database matches.

Characterisation of microbial metabolites

To identify microbial-derived metabolites and the putative producer organism taxonomy, a curated database of natural products from more than 60,000 microbial monocultures was queried using microbeMASST MS/MS-based tool. All experimental MS/MS spectra were searched in a batch using a custom python script of microbeMASST with a delta parent ion mass +/- 0.02 Da, a cosine similarity threshold of > 0.7 and a minimum of 4 matched peaks. For compounds with multiple matches to different microbial producers, the most recurrent hit was retained.

Characterisation of arsenic complexes

To identify arsenic-chelating metabolites, a targeted search was conducted that used m/z (mass-to-charge ratio) of unknown arsenic-elicited metabolites (categorised as potential arsenic adducts) to calculate theoretical m/z of different protonated (unbound) forms. These included seven arsenite As(III) coordination schemes, namely As(III)(X), $As(III)(X)_2$, $As(III)(X)_3$, As(III)(OH)(X), DMAs(III)(X), $MMAs(III)(X)_{1-2}$. The results were then matched with the m/z of annotated metabolites from control and arsenic-treated plants (delta m/z < 5ppm), generating a list of potential arsenic-chelating molecules that could serve as novel arsenic tolerance tools.

Arsenic complex candidates were first confirmed using raw formula prediction with SIRIUS 6. Complex candidate formulae that explained > 70% of peak intensity were retained as confident arsenic complexes. Further confirmation used authentic standards of PC2, PC3 (Anaspec, CA) and GSH (Fisher scientific) mixed with arsenite (As(III)) at different S:As molar ratios, namely 3:1, 1:3, 1:6, to produce $As\text{-}(PC_n)_n$, $As\text{-}PC_n\text{-}GS$ and $As\text{-}GS_n$ complexes in 0.1% FA MilliQ water, following Schmied-Tobies et al. (2014). In vitro complexes were then analysed using LC-MS/MS with the same parameters as for plant samples (see methods section 3.5). The spectra produced were then uploaded as new library entries (CCMSLIB00010011905, CCMSLIB00010011906, CCMSLIB00010011948, CCMSLIB00010011949, CCMSLIB00010173329, CCMSLIB00010173330s) to the GNPS platform (Wang et al., 2016) and compared to experimental complex candidates. Hits with MS2 similarity > 0.8 cosine and delta retention time (RT) < 1 min were marked as level 1 identification (Sumner et al., 2007).

Supplementary figures

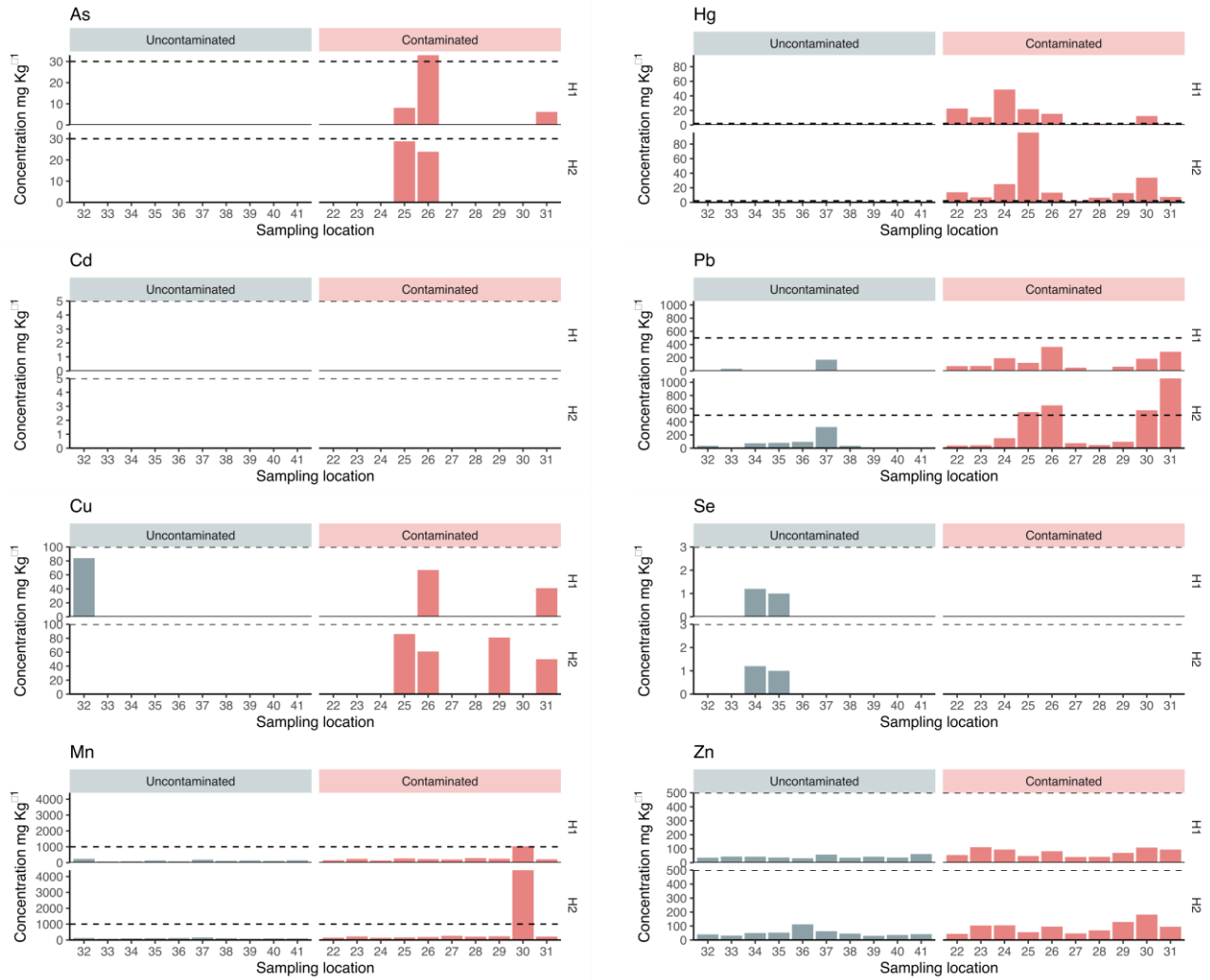

Figure S1 Field contaminant concentrations.
Concentrations of the main investigated trace elements in uncontaminated and contaminated field plots. Quantifications were evaluated at ten sampling locations in each plot and at two depths (H1: 10-60 cm; H2: 60-110 cm). Dashed lines indicate Quebec province level A-B limits for contaminated soil (Beaulieu et al., 2019).

Metabolite partitioning across belowground compartments.

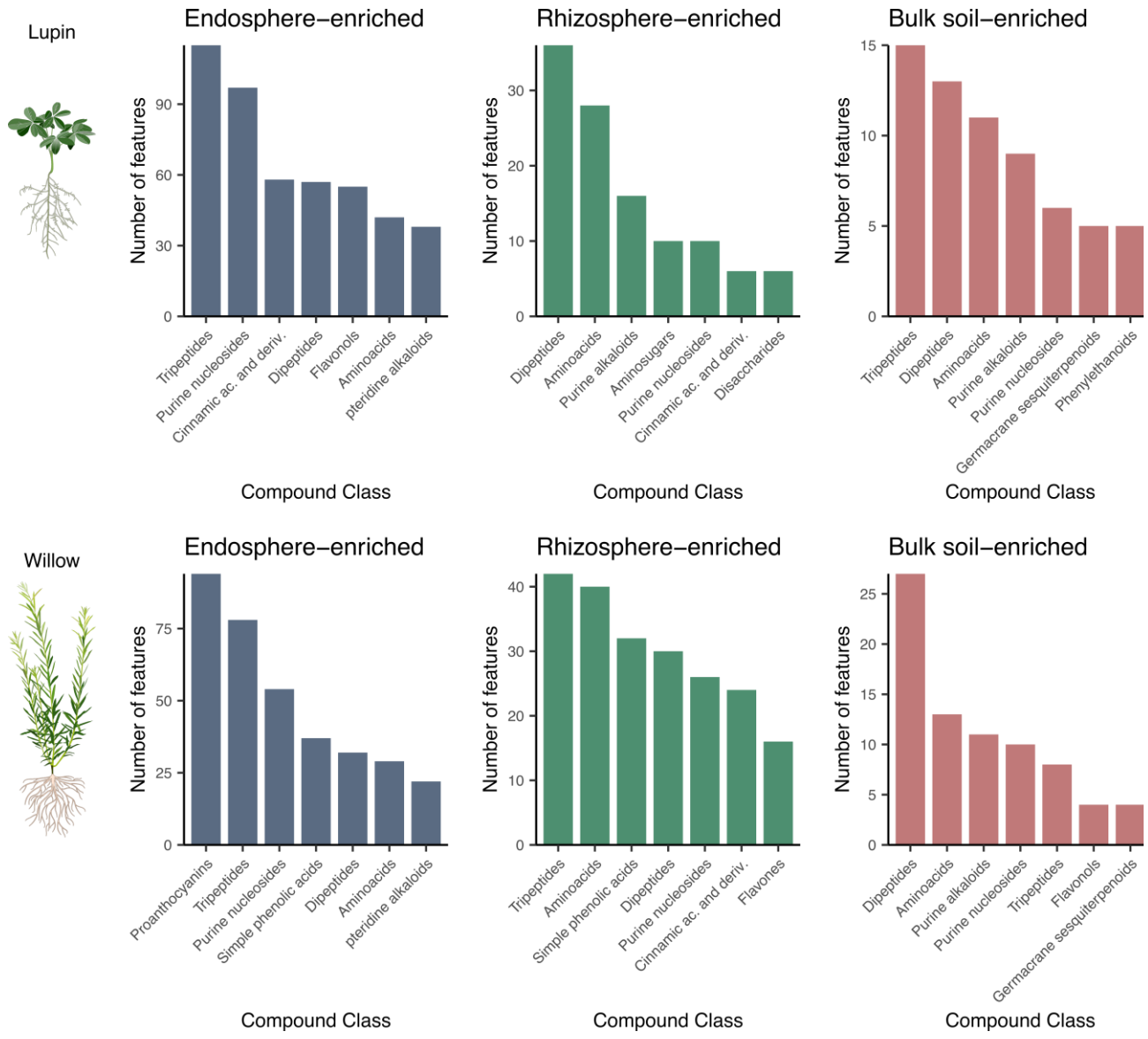

Figure S2 Compound class partitioning across belowground fractions in lupin and willow. Number of features enriched in the endosphere, rhizosphere and bulk soil grouped according to compound class for lupin and willow. Rhizosphere-enriched features, represent differentially abundant (DA) features that were shared in both pairwise comparisons (endosphere vs rhizosphere and endosphere vs bulk soil). Only the top seven classes (based on number of DA features) are shown. For full annotation of DA features between fraction, refer to Data S1.

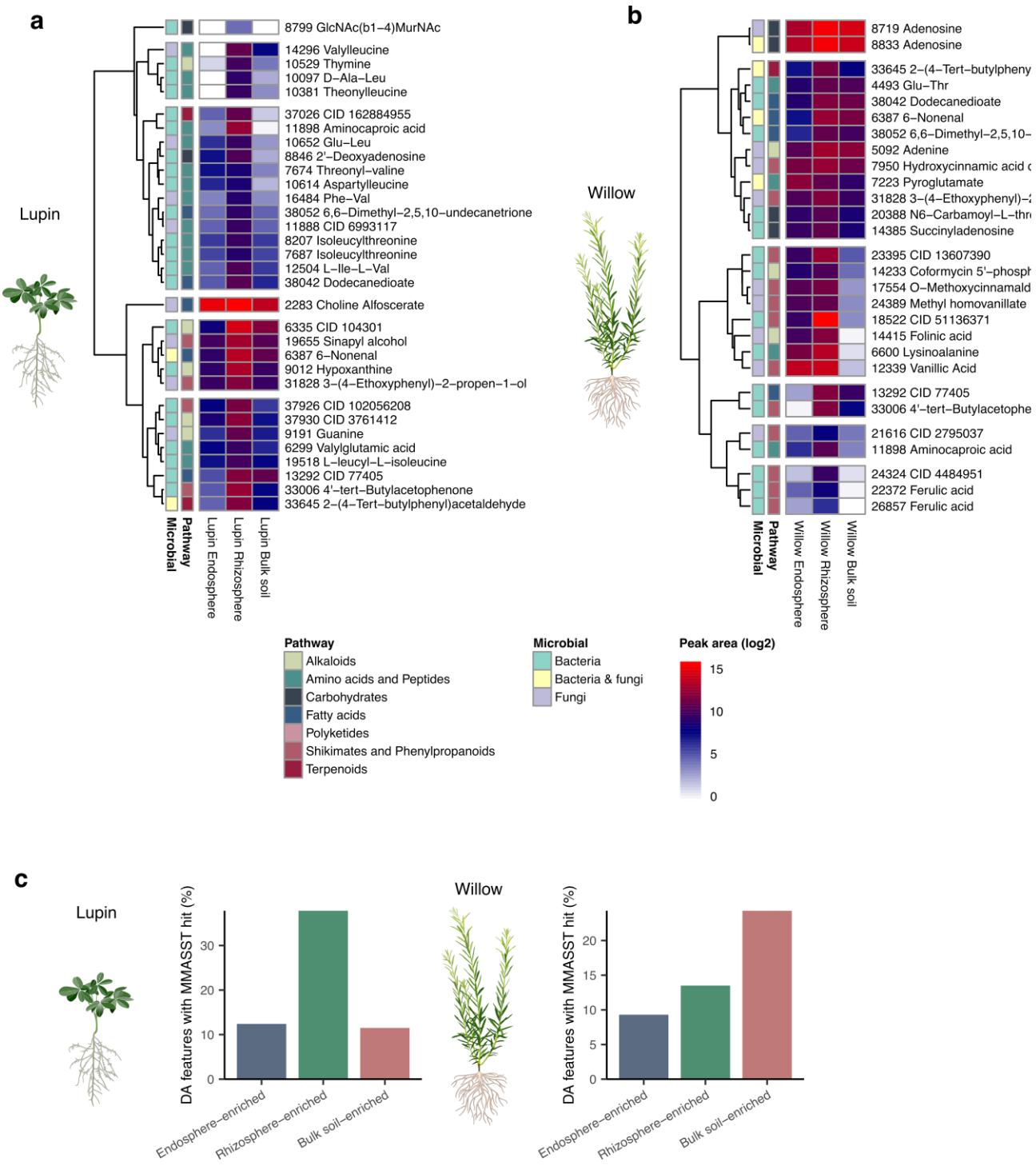

Figure S3 Rhizosphere enriched metabolites.

a-b Hierarchical clustering of rhizosphere-enriched metabolites from lupin and willow with a hit to MicrobeMASST database. **c** Proportion of differentially abundant (DA) features with a MicrobeMASST hit to a putative microbial producer for lupin and willow. Refer to Data S1 for full annotation, statistics, and full microbial hit table.

Pot trial metabolomic response to arsenic

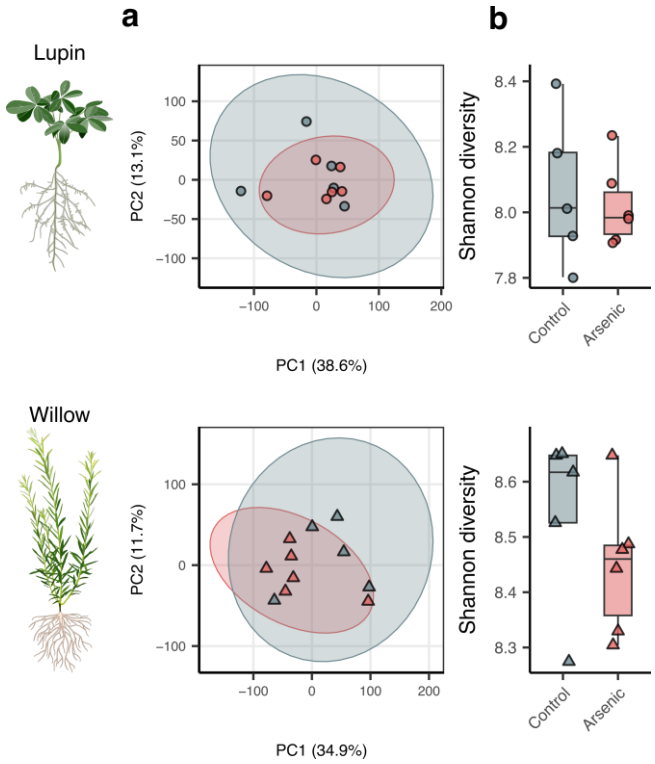

Figure S4 Bulk soil metabolome in response to arsenic.
a Principal component analysis (PCA) illustrating variations in metabolomic profiles between control and arsenic-treated bulk soil for lupin and willow. **b** Shannon's index of α diversity from control and arsenic-treated endosphere and rhizosphere fractions of lupin and willow.

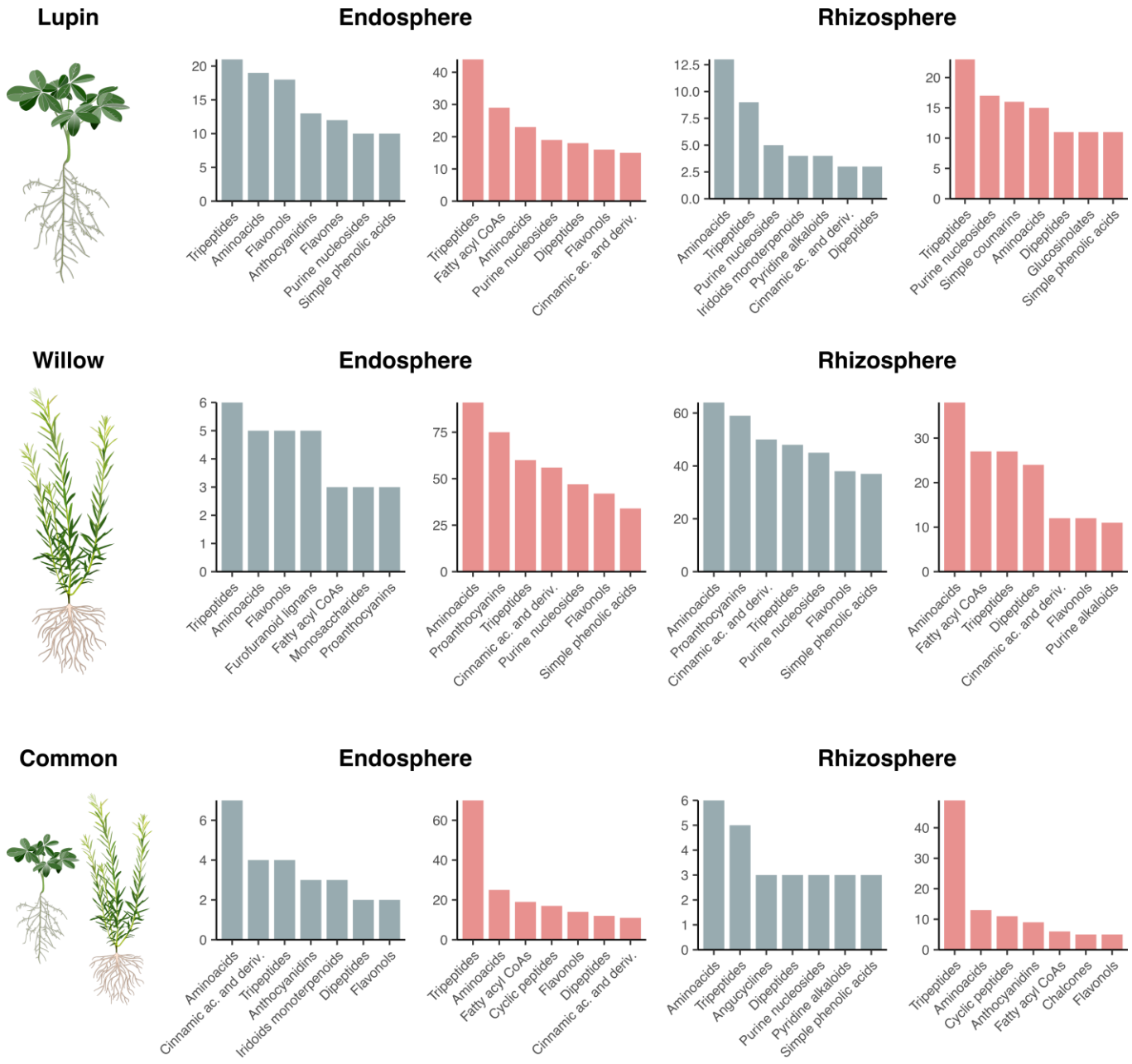

Figure S5 Specific and common arsenic-responsive compound classes.
Number of features depleted and enriched in response to arsenic, specific to lupin, willow and common between species. Differentially abundant (DA) features from the endosphere and the rhizosphere are grouped according to compound class and only the top seven classes (based on number of DA features) are shown. For full annotation of DA features between fraction, refer to Data S1.

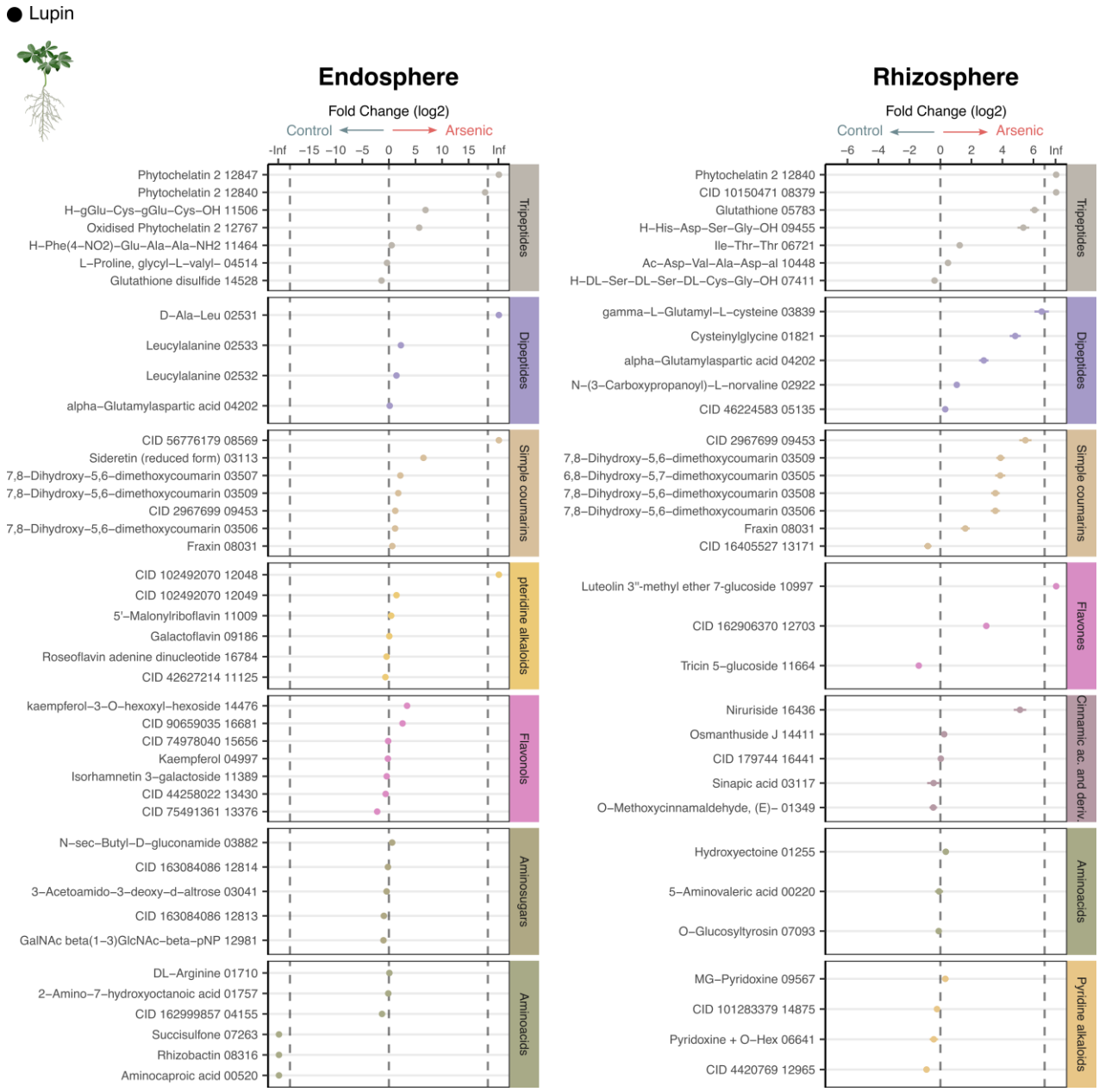

Figure S6 Lupin-specific arsenic response.

Log_2-transformed features intensity fold changes of differentially abundant (DA) metabolites between control and arsenic-treated plants, grouped by putative compound class. Only the seven most abundant DA features (average peak intensity) and the six most prevalent classes (based on number of DA feature) are shown. Data are means and standard errors (n = 6). Refer to Data S1 for full identifications and statistics.

Figure S7 Willow-specific arsenic response.

Log_2-transformed features intensity fold changes of differentially abundant (DA) metabolites between control and arsenic-treated plants, grouped by putative compound class. Only the seven most abundant DA features (average peak intensity) and the six most prevalent classes (based on number of DA feature) are shown. Data are means and standard errors (n = 6). Refer to Data S1 for full identifications and statistics.

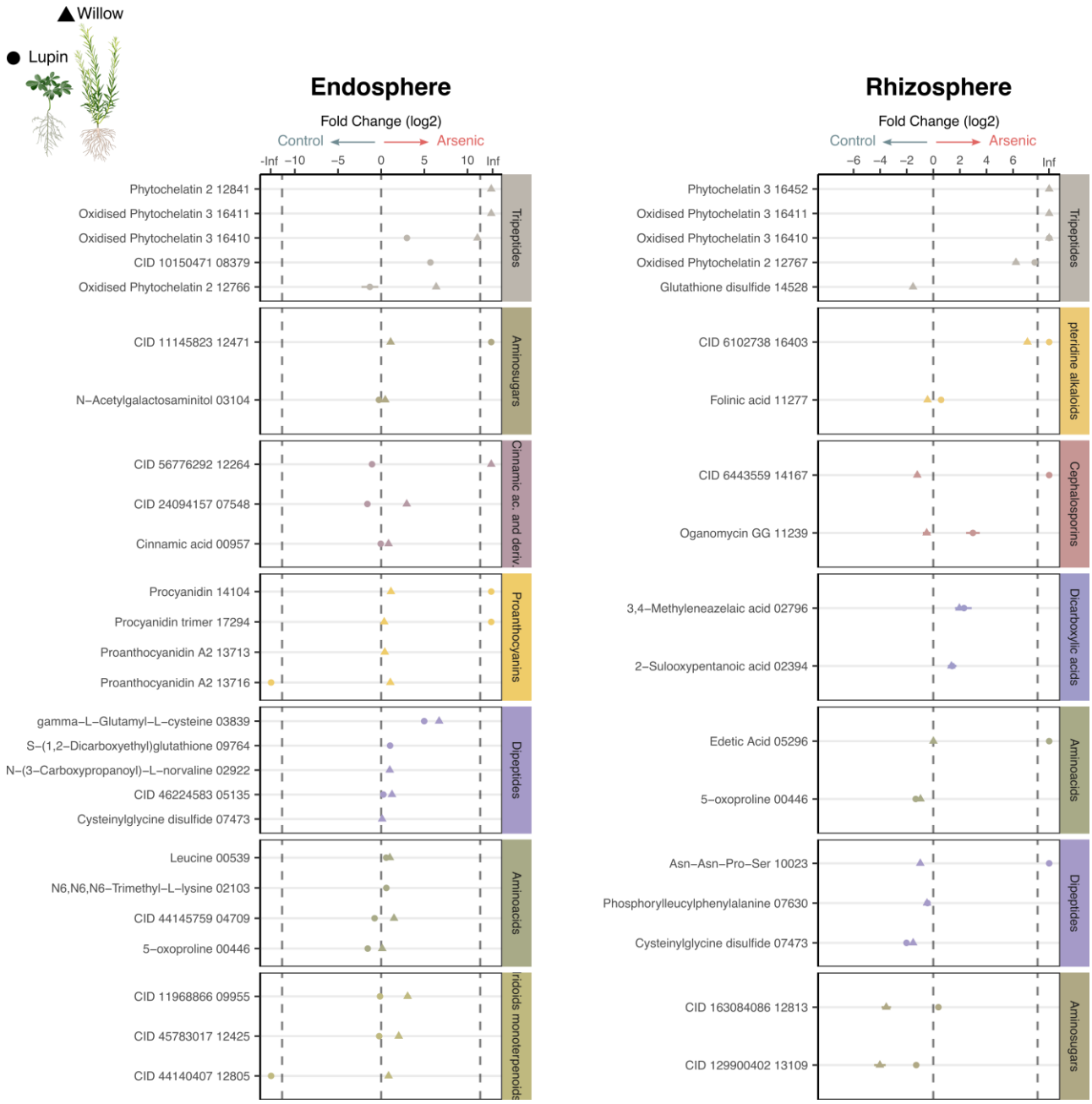

Figure S8 Species-shared arsenic response.

Log_2-transformed features intensity fold changes of differentially abundant (DA) metabolites between control and arsenic-treated plants, grouped by putative compound class. Only the seven most abundant DA features (average peak intensity) and the six most prevalent classes (based on number of DA feature) are shown. Data are means and standard errors (n = 6). Refer to Data S1 for full identifications and statistics.

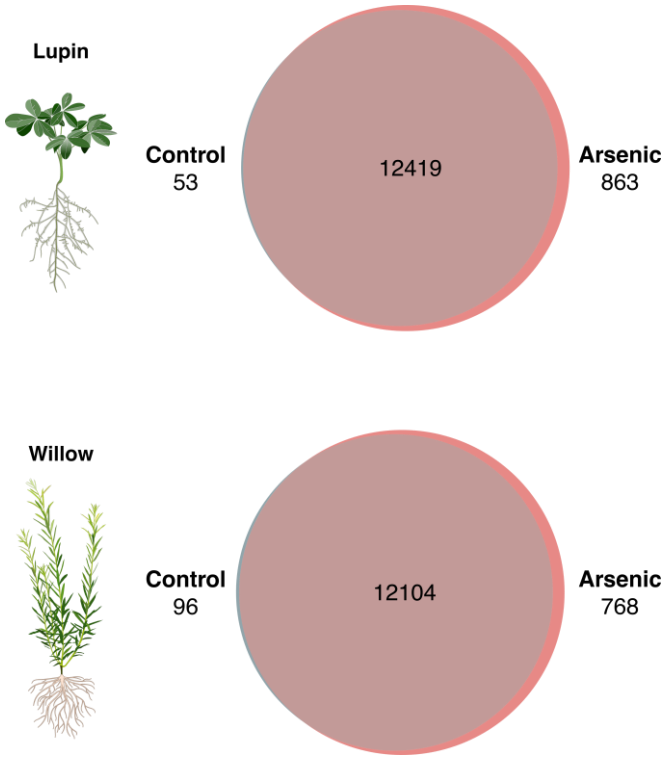

Figure S9 Arsenic-suppressed and arsenic-elicited features.
Proportional Venn diagram of the number of features unique or shared between control and arsenic-treated lupin and willow endosphere and rhizosphere samples.

Field trial physiological response

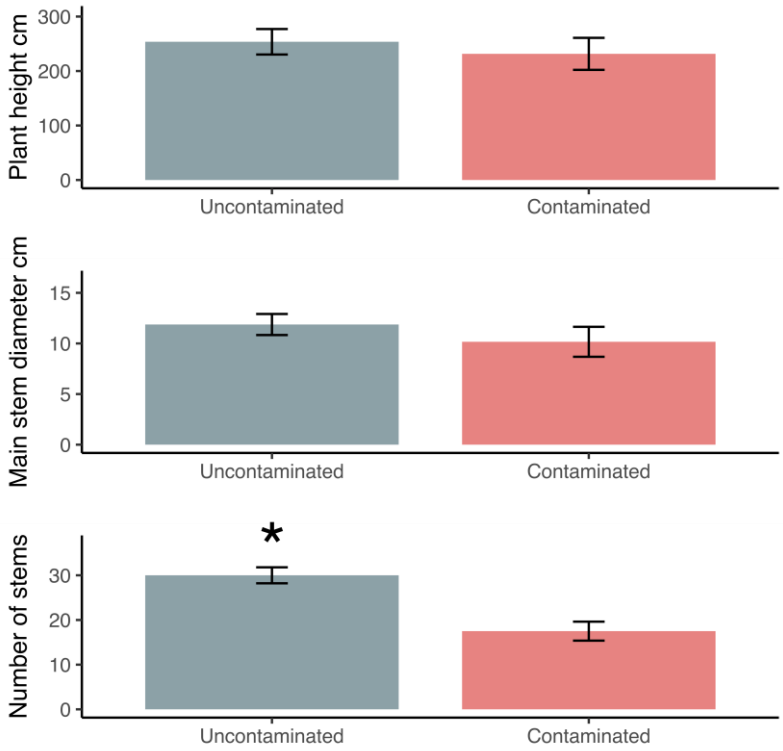

Figure S10 Physiological response of a willow plantation to soil contamination.
Data are means and standard errors (n = 6). Asterisks indicate significant differences (T-test, $p < 0.05$)

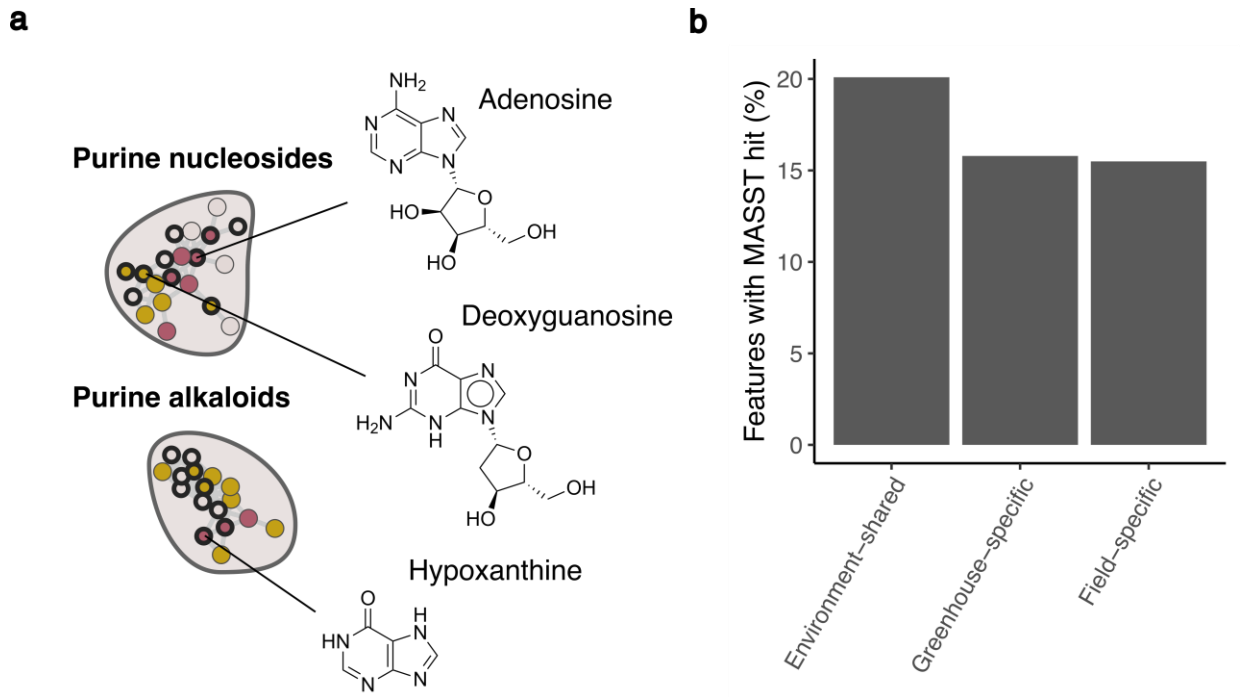

Figure S11 Microbially derived metabolites from greenhouse and field rhizosphere metabolome.

a Example structures of high confidence annotated microbe-derived metabolites. **b** Proportion of environment-shared, greenhouse-specific, and field-specific features with a microbeMASST hit to a putative microbial producer. For full annotation and full microbeMASST hit table, refer to Data S2.

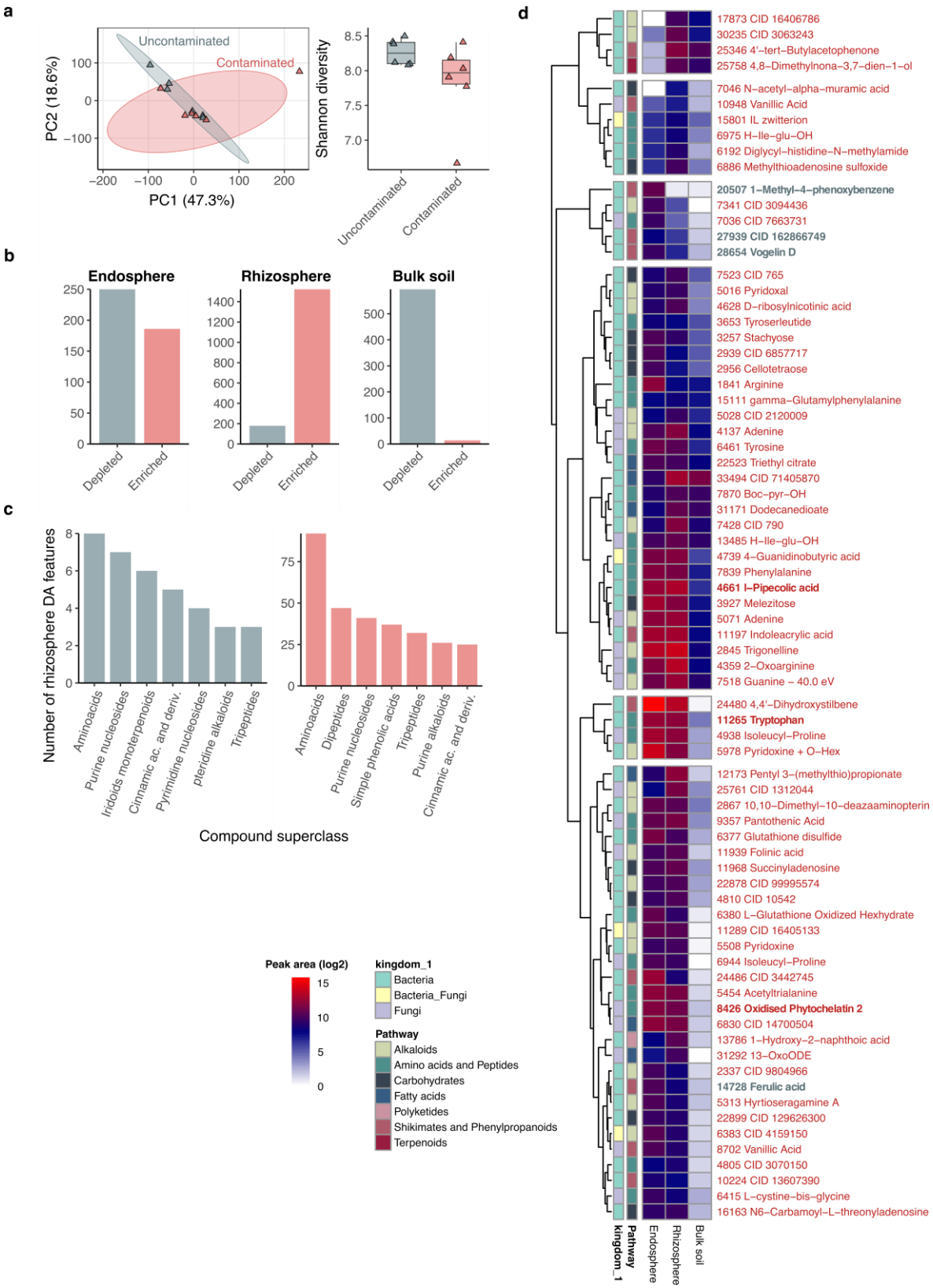

Figure S12 Field metabolomic response to soil contamination.

a Principal components analysis **(**PCA) and Shannon diversity index showing metabolomic differentiation between field uncontaminated and contaminated plots. **b** Number of significantly differentially abundant (DA) features between uncontaminated and contaminated endosphere,

rhizosphere and bulk fractions. **c** Number of features enriched in the rhizosphere grouped according to compound superclass. Only the top seven superclasses (based on number of DA features) are shown. **d** Hierarchical clustering of arsenic-enriched (red) and arsenic-depleted (blue) metabolites showing their partitioning between fractions in the contaminated plot. Only compounds with a microbeMASST hit to a putative microbial producer are shown. For full annotation statistics and full microbeMASST hit table, refer to Data S2.

Conclusion

Dans l'optique d'approfondir la compréhension des mécanismes de phytoremédiation, cette thèse s'est concentrée sur les relations entre les racines et les contaminants, au niveau moléculaire, dans la rhizosphère. Pour décrire et comprendre cet environnement complexe à l'interface entre les racines et le sol, cette thèse s'est placée à trois échelles expérimentales, passant d'un environnement contrôlé en chambre de croissance (Chapitre 1 et 2), à la mise en place d'expériences en serre, et de l'échantillonnage sur le terrain d'une plantation de phytoremédiation en conditions réelles (Chapitre 3) (**Figure 1**).

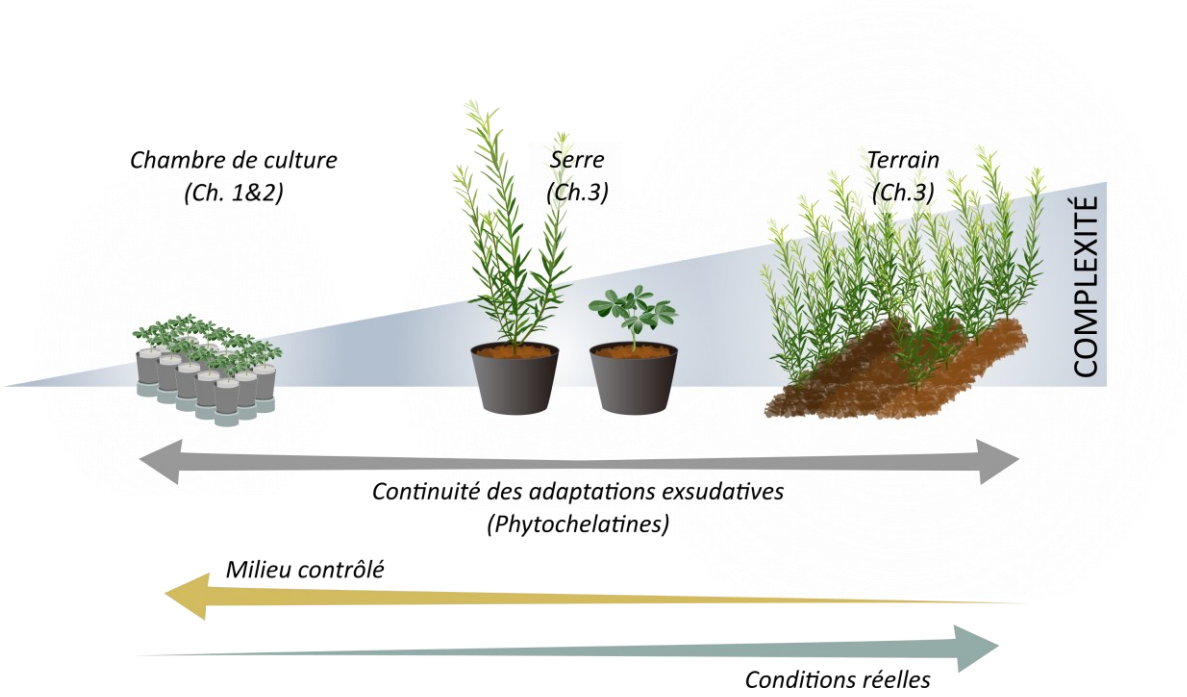

Figure 1 Cadre expérimental de la thèse.
Cette thèse adopte une approche expérimentale à trois niveaux de complexité croissante, afin d'étudier les mécanismes d'exsudation racinaire et leur modulation en réponse à l'As. Le Chapitre 1 et 2 présentent une approche en conditions contrôlées en chambre de culture. Ce système permet de caractériser précisément les mécanismes d'exsudation racinaire, de maîtriser finement les apports en nutriments et d'appliquer divers traitements de façon hautement réplicable. Le Chapitre 3 adopte une approche en conditions semi-contrôlées se rapprochant des conditions réelles de phytoremédiation. L'utilisation de plantes matures et de sols naturels introduit une complexité accrue de l'environnement chimique des racines.

Principales conclusions du Chapitre 1

Accéder à la rhizosphère et en extraire les molécules présentes est considéré dans certains cas comme une mission impossible (Oburger & Jones, 2018). Les principaux défis pour caractériser ce microenvironnement sont tout d'abord liés à l'extraction de la rhizosphère sans endommager les racines et en limitant les risques d'interférence par les constituants du sol. Ensuite, les extraits doivent être concentrés pour permettre leur analyse par des techniques de détection extrêmement sensibles, et enfin, il reste le défi majeur de l'analyse et de l'interprétation de l'information générée par les milliers de molécules présentes dans la rhizosphère.

Pour m'affranchir de ces obstacles, je présente, dans le Chapitre 1, un système de croissance et une méthodologie d'extraction qui permet de capturer les exsudats en utilisant du sable de silice comme substrat inerte, limitant ainsi les dommages causés aux racines et éliminant les problèmes d'interférence du sol. Grâce à ce système, j'ai pu tester l'effet d'une gamme de concentrations et de différentes formes d'arsenic sur le lupin blanc, *Lupinus albus.* Après extraction et concentration des extraits de rhizosphère, j'ai utilisé la chromatographie liquide couplée à la spectrométrie de masse pour établir le profil des molécules présentes de façon non ciblée.

A partir des centaines de signatures spectrales générées, et après l'analyse bioinformatique, incluant des bases de données, des réseaux moléculaires, et des outils d'annotation utilisant l'apprentissage profond, j'ai pu caractériser les structures moléculaires d'une large diversité d'exsudats libérés par le lupin en réponse à l'arsenic. Ces métabolites incluaient des composés phénoliques, comme certains flavonoïdes, impliqués dans les relations des plantes avec les microorganismes fixateurs d'azote (Cesco et al., 2010), des coumarines, connues pour leurs activités chélatrices de Fe (Robe et al., 2021), ou encore des saponines, composés aux activités antimicrobiennes qui favorisent l'établissement de certains microorganismes dans la rhizosphère (Tsuno et al., 2018). En comparant les abondances de chaque molécule exsudée, avec ou sans arsenic, les résultats ont révélé l'enrichissement de composés inattendus dans les exsudats racinaires du lupin en réponse à l'arsenic, comme les coumarines et les phytochélatines (PCs), ces dernières capables de complexer l'arsenic sous une forme non toxique pour les cellules (Schmöger et al., 2000). Face à ce résultat inattendu de l'exsudation de PCs, jusqu'alors jamais observé, une expérience de validation durant laquelle les racines ont été strictement exclues des exsudats échantillonnés *via* l'utilisation de poches en nylon insérées dans le milieu de croissance a été conduite. Celle-ci a permis de confirmer l'exsudation de PCs par le lupin, validant ainsi ce résultat.

L'exsudation de PCs pourrait expliquer en partie la capacité du lupin à tolérer de fortes concentrations d'arsenic, notamment par sa complexation directement dans la rhizosphère. Cela neutraliserait sa

toxicité et préviendrait potentiellement l'absorption d'arsenic par les racines, reflétant ainsi le caractère excluant vis-à-vis de l'arsenic du lupin. Une autre hypothèse, émise dans le Chapitre 1, interroge la possibilité de l'exsudation de complexes As-PCs comme adaptation racinaire limitant l'accumulation d'As dans les racines. Jusque-là inconnue chez les plantes, cette adaptation pourrait expliquer la partie manquante de l'efflux d'arsenic hors des racines, dont seuls 20% peuvent être expliqués selon le modèle présent (Li et al., 2016).

Principales conclusions du Chapitre 2

Dans le Chapitre 2, j'ai décidé de m'intéresser de façon ciblée aux mécanismes qui participent à l'exsudation de PCs dans la rhizosphère, ainsi qu'aux produits de l'interaction des exsudats avec l'As, et j'ai tenté d'apporter des réponses aux hypothèses soulevées dans le Chapitre 1. Pour cela, je prends avantage des méthodes d'analyses développées précédemment et d'une meilleure compréhension de la réponse exsudative du lupin.

Dans un premier temps, j'ai utilisé deux inhibiteurs chimiques, l'un inhibant la synthèse de PCs et l'autre inhibant l'activité des transporteurs de type ATP-binding cassette (ABC), impliqués dans le transport des complexes As-PCs vers les vacuoles et possiblement impliqués dans leur exsudation vers l'extérieur des racines. Ceci m'a permis de montrer que la synthèse de PCs et l'activité des transporteurs ABC sont essentiels pour la survie du lupin en présence d'As. De plus, les résultats développés dans ce chapitre montrent que les transporteurs ABC pourraient être responsables d'une partie de l'exsudation de PCs par le lupin. Dans un deuxième temps, j'ai entrepris la synthèse de complexes As-PCs *in vitro* dans le but de caractériser les différents composés pouvant être formées lors de l'interaction des exsudats avec l'As et de déterminer leurs signatures spectrales. Cela m'a permis de mettre en évidence la première observation de complexes As-PCs directement dans la rhizosphère. De plus, grâce à l'utilisation des inhibiteurs, j'ai pu montrer que l'interruption des transporteurs ABC inhibe totalement l'exsudation de complexes mais pas leur synthèse dans les racines. Ces résultats indiquent que l'exsudation de As-PCs chez le lupin représente un mécanisme d'efflux actif qui emprunte les transporteurs ABC présents sur la membrane plasmique. Ce nouveau mécanisme de détoxification par exsudation de complexes As-PCs des racines pourrait informer de nouvelles stratégies pour la phytoremédiation de l'arsenic.

Principales conclusions du Chapitre 3

Les résultats obtenus dans les Chapitres 1 et 2 ont été recueillis en conditions contrôlées, dans un système de croissance qui limite l'influence des microorganismes et du sol, et chez seulement une

espèce. Dans le Chapitre 3, mon but était de me rapprocher des conditions réelles et d'élargir les connaissances acquises vers d'autres espèces d'intérêt en phytoremédiation. J'ai donc décidé d'inclure le saule, *Salix miyabeana*, qui représente une espèce d'intérêt central en phytoremédiation pour sa croissance rapide et sa tolérance accrue aux contaminations élevées du sol (Jerbi et al., 2020; Yanitch et al., 2017). J'ai d'abord mis en place une expérience en serre, réunissant le lupin blanc et le saule, afin d'étudier les adaptations exsudatives en réponse à l'As qui sont conservées entre espèces et celles uniques à chacune des deux espèces.

Les résultats obtenus témoignent de la complexité métabolomique de la rhizosphère. Plus de 7000 métabolites ont pu être identifiés, chacun témoignant du métabolisme primaire, comme les acides aminés et les nucléotides, partagés entre espèces, ou du métabolisme spécialisé, comme les terpénoïdes, les flavonoïdes ou les alcaloïdes, uniques à chaque espèce. De plus, la répartition des métabolites entre les racines, la rhizosphère et le sol a permis de révéler des micro-environnements biochimiques distincts. La rhizosphère étant enrichie en certains composés volatiles comme le nonenal, pouvant servir de signal chimique pour les microorganismes (Schenkel et al., 2015) ou encore de métabolites comme la thymidine ou l'acide salicylique pouvant agir comme source d'énergie pour certaines rhizobactéries (Zhalnina et al., 2018). Mais principalement, ce chapitre révèle les adaptations spécifiques à chaque espèce en réponse à l'arsenic. Chez le lupin, l'arsenic induit l'enrichissement global des coumarines dans la rhizosphère, confirmant l'un des principaux résultats du Chapitre 1. De plus, en présence d'arsenic, le lupin libère des flavonoïdes, comme la lutéoline, pouvant participer au recrutement de bactéries fixatrices d'azote dans les racines (Peters et al., 1986), tout en libérant des molécules capables d'offrir une protection aux bactéries contre les stress chimiques de la rhizosphère comme l'hydroxyectoine (Czech et al., 2018). Chez le saule, l'As induit une large réponse des composés phénoliques comme les proanthocyanines ou les acides cinnamiques, dont l'exsudation racinaire est fortement réprimée en présence d'As, au profit de leur accumulation dans les racines. Ce phénomène pourrait participer à réduire la mobilisation d'As dans la rhizosphère du saule en réprimant l'activité mobilisatrice de métaux de ces composés. Enfin, la découverte centrale du Chapitre 3 est la conservation, chez ces deux espèces, de l'exsudation d'un arsenal de phytochélatines (PC_2, hPC_2, PC_3, *etc.*) dans la rhizosphère. De plus, chez les deux espèces, une large proportion de métabolites, la plupart inconnues, étaient présentes uniquement dans les exsudats des plantes traitées à l'arsenic. Après une recherche ciblée de ces métabolites comme potentiellement issues de la complexation entre une molécule chélatrice et l'As, j'ai pu identifier la présence de huit complexes As-PC dans la rhizosphère du lupin et du saule. Cette découverte représente à ce jour la deuxième observation de complexes As-PC dans la rhizosphère du lupin (après celle faite dans le Chapitre 2), et la première observation de ces

complexes dans la rhizosphère du saule. Pour valider ces observations et les confronter aux conditions réelles de terrain, le Chapitre 3 termine par l'évaluation de la réponse exsudative des saules dans une plantation de phytoremédiation. Les résultats confirment l'enrichissement de PC2 dans les exsudats du saule en réponse à la contamination, ce qui appuie l'importance de cette adaptation pour la tolérance à l'arsenic, chez plusieurs espèces, et au travers des multiples environnements testés.

Synthèse générale

L'approche adoptée tout au long de ce projet de doctorat a permis d'obtenir une vision approfondie de la réponse exsudative du lupin blanc à différentes doses d'arsenic, et de décrire un nouveau mécanisme d'exsudation pour sa détoxification dans la rhizosphère. Les connaissances acquises ont ensuite été transférées pour l'étude des adaptations exsudatives en réponse à l'arsenic dans des environnements plus complexes chez le lupin et le saule. Les résultats obtenus montrent une continuité des adaptations au travers des systèmes étudiés.

Les PCs, une classe de molécules initialement connues pour leur rôles intracellulaires de complexation de l'As, ont été dévoilées ici comme composantes majeures des adaptations exsudatives à l'As, aussi bien chez le lupin que chez le saule. Cette thèse apporte une nouvelle compréhension du rôle des PCs et pose la question de sa présence chez d'autres espèces. Premièrement, cette thèse montre que les PCs pourraient participer à l'efflux actif d'As complexé hors des racines. Deuxièmement, la diversité des formes de complexes As-PC observés dans la rhizosphère du lupin et du saule suggère des rôles diversifiés, chaque forme de PC et de complexes As-PC produits pouvant opérer différentes fonctions dans la rhizosphère.

En revanche, d'autres adaptations montrent une forte spécificité à l'espèce étudiée, comme l'exsudation de coumarines, qui est conservée chez le lupin en réponse à l'arsenic dans l'ensemble des systèmes étudiés, ou encore l'inhibition de l'exsudation et l'accumulation intracellulaire de composés phénoliques en réponse à l'As, qui semble être une adaptation spécifique du saule.

Limites et perspectives

Les découvertes du **Chapitre 1** ouvrent sur l'importance de deux classes de métabolites exsudées en réponse à l'As, les PCs et les coumarines. Cette thèse fait le choix de continuer dans l'investigation du rôle des PCs dans la rhizosphère pour son caractère surprenant et pour leurs potentielles applications concrètes pour la stabilisation de l'arsenic dans les sols. Cependant, le rôle des coumarines dans la rhizosphère en réponse à l'As reste un mystère non résolu, renforcé par les résultats du Chapitre 3 qui confirment l'importance des coumarines dans la réponse du lupin à l'As. Récemment, les coumarines

ont été décrites comme déterminantes centrales dans la nutrition en Fe et l'immunité en présence de pathogènes (Stringlis et al., 2019). Notamment, chez *Arabidopsis thaliana*, les coumarines interviennent dans la complexation du Fe dans la rhizosphère, dans le recrutement de bactéries bénéfiques et la défense contre les pathogènes (Robe et al., 2021; Stringlis et al., 2018). L'étude approfondie des coumarines induites lors de la réponse exsudative, à travers l'identification précise de ces composés par des approches telles que la résonance magnétique nucléaire (RMN), puis par le criblage de leurs activités biotiques et abiotiques en présence d'arsenic (As), par exemple par l'ajout *in vitro* de coumarines purifiées et le suivi des variations des communautés microbiennes du sol, pourrait permettre de décrire avec précision le rôle de ces coumarines dans la rhizosphère en présence d'As.

Le **Chapitre 2** montre l'existence d'un mécanisme de détoxification de l'arsenic par l'exsudation de complexes As-PC chez le lupin. Dans de futures recherches, l'exploration de la diversité des formes complexées d'arsenic, produites ou exsudées dans la rhizosphère, pourrait mettre à jour d'autres mécanismes de détoxification et, à terme, offrir des cibles d'amélioration des plantes d'intérêt agronomique pour réduire l'accumulation de l'arsenic dans les parties comestibles. De plus, la détection de complexes As-PC dans la rhizosphère vient également supporter le rôle probable des phytochélatines pour stabiliser l'arsenic dans le sol. De futures recherches pour l'application de ces découvertes en phytoremédiation devront explorer la mobilité et la stabilité des complexes dans les sols. Bien que l'identification des formes d'arsenic complexées dans un système biologique comme la rhizosphère reste un défi technique, les avancées analytiques des dernières années permettent de connaitre de mieux en mieux la diversité des complexes organométalliques dans les milieux biologiques (Aron et al., 2021; Flis et al., 2016). Par exemple, de récentes recherches ont révélé qu'un mécanisme d'efflux d'arsenic complexé, similaire à celui décrit dans le Chapitre 2, existe chez les microorganismes (Chen et al., 2016). Pour pousser la recherche en phytoremédiation dans ce sens, certaines méthodes d'analyses utilisées dans les disciplines niches comme la métallomique pourraient être appliquées à la rhizosphère (Mounicou et al., 2009). Les méthodes basées sur la spectrométrie de masse, comme l'infusion post-colonne, permettrait par exemple de dévoiler la diversité des complexes organométalliques dans une diversité de conditions chimiques, pouvant imiter le pH intracellulaire ou celui de la rhizosphère (Aron et al., 2021). En effet, la diversité des métabolites induites par l'arsenic laisse entrevoir des fonctions potentielles de protection allant au-delà des activités antioxydantes connues. Les composés phénoliques par exemple, comme les flavonoïdes ou les coumarines, possèdent de nombreux groupements catéchols connus pour leurs capacités à complexer certains métaux comme le fer (Robe et al., 2021) et des indications préliminaires suggèrent une capacité à complexer l'arsenic (Ahammed & Yang, 2022). Explorer les activités chélatrices de ces métabolites extraits de la

rhizosphère dans diverses conditions de pH pourrait permettre la mise en évidence non équivoque de nouveaux complexes et mettre à jour de nouvelles voies de détoxification de l'arsenic.

D'autres méthodes, peu répandues, comme la chromatographie liquide couplée à la spectrométrie de masse avec plasma à couplage inductif et spectrométrie de masse avec ionisation électrospray (HPLC-ICP-MS/ESI-MS), permettent la détection parallèle, d'une part de l'arsenic (ICP-MS), et d'autre part de la molécule organique chélatrice (ESI-MS). Grâce à cette technique, l'ensemble des composés contenant de l'arsenic peuvent être détectés, identifiés et quantifiés de façon précise (Raab et al., 2005). Bien qu'utilisée principalement pour le suivi des complexes As-PC dans le milieu intracellulaire (Liu et al., 2010; Mishra et al., 2017; Raab et al., 2004, 2005), appliquée à la rhizosphère du lupin ou d'autres espèces, cette méthode pourrait permettre de quantifier et de calculer le taux d'exsudation de complexes As-PC et d'informer plus finement sur la contribution de ce mécanisme dans la détoxification de l'arsenic chez les plantes.

Les avancées développées dans le **Chapitre 3** dévoilent un environnement chimique complexe au sein de la rhizosphère, qui témoigne des multiples interactions entre les racines, les contaminants du sol et les microorganismes présents dans cet environnement. De plus, ce chapitre vient corroborer et compléter les observations des études menées en chambre de culture et dans un substrat simplifié dans les chapitres 1 et 2. Cela démontre qu'il est possible de caractériser des mécanismes de tolérance finement régulés, comme l'exsudation de coumarines ou de complexes As-PCs, même dans un environnement métabolomique complexe. Les approches de caractérisation métabolomique développées et les méthodes statistiques utilisées dans ce chapitre peuvent s'appliquer à une grande diversité de systèmes biologiques complexes, comme pour l'étude des réponses métabolomiques du microbiote intestinal (Meier et al., 2023), ou encore l'étude des exometabolites produits par les récifs coralliens (Wegley Kelly et al., 2022). Cependant, comme pour l'ensemble des approches non ciblées en métabolomique, le pipeline d'analyses présenté dans le Chapitre 3 est aussi tributaire des nombreux défis techniques rendant l'identification des métabolites particulièrement difficile, et posant un obstacle majeur dans le développement de cette discipline.

L'un des principaux avantages de l'approche non ciblée entreprise dans cette thèse est l'utilisation d'une suite d'outils récents d'annotation et leur intégration en priorisant les meilleures annotations. Cette approche est donc en constante évolution, par l'intégration d'outils toujours plus performants, et pourrait permettre à l'avenir d'offrir une nouvelle compréhension des environnements chimiques complexes qui nous entourent.

La suite logique de cette thèse réside aussi dans la compréhension plus poussée de l'importance des microorganismes rhizosphériques dans le système plante/contaminant. Les résultats du Chapitre 3 offrent une tentative intéressante pour délimiter le métabolome issus des exsudats racinaires de celui issu des microorganismes, en utilisant des outils de métabolomique récents tels que microbeMASST (Zuffa et al., 2023). Les résultats indiquent notamment qu'une proportion importante des métabolites impliqués dans la réponse à l'As dans la rhizosphère pourraient avoir une origine microbienne, ce qui témoigne du potentiel du métabolisme microbien pour la production de composés de défense contre l'As. Pour confirmer ces observations, l'une des orientations entreprises à la suite de ce projet de thèse s'intéresse à la caractérisation conjointe des communautés microbiennes et du métabolome en réponse à l'As. Ces deux approches combinées pourraient offrir la possibilité de joindre les métabolites produits en réponse à l'arsenic avec les microorganismes producteurs, et pourraient offrir de nouvelles avenues pour l'utilisation des microorganismes pour la phytoremédiation de contaminants comme l'As.

References

Agency for Toxic Substances and Disease Registry (ATSDR). (2007). *Toxicological profile for Arsenic*. Atlanta, GA: U.S. Department of Health and Human Services, Public Health Service. https://www.atsdr.cdc.gov/ToxProfiles/tp2.pdf

Ahammed, G. J., & Yang, Y. (2022). Anthocyanin-mediated arsenic tolerance in plants. *Environmental Pollution*, *292*, 118475. https://doi.org/10.1016/j.envpol.2021.118475

Ahkami, A. H., Allen White, R., Handakumbura, P. P., & Jansson, C. (2017). Rhizosphere engineering: Enhancing sustainable plant ecosystem productivity. *Rhizosphere*, *3*(Part 2), 233–243. https://doi.org/10.1016/j.rhisph.2017.04.012

Akiyama, K., Matsuzaki, K., & Hayashi, H. (2005). Plant sesquiterpenes induce hyphal branching in arbuscular mycorrhizal fungi. *Nature*, *435*(7043), 824–827. https://doi.org/10.1038/nature03608

Aksenov, A. A., da Silva, R., Knight, R., Lopes, N. P., & Dorrestein, P. C. (2017). Global chemical analysis of biology by mass spectrometry. *Nature Reviews Chemistry*, *1*(7), Article 7. https://doi.org/10.1038/s41570-017-0054

Alseekh, S., Aharoni, A., Brotman, Y., Contrepois, K., D'Auria, J., Ewald, J., C. Ewald, J., Fraser, P. D., Giavalisco, P., Hall, R. D., Heinemann, M., Link, H., Luo, J., Neumann, S., Nielsen, J., Perez de Souza, L., Saito, K., Sauer, U., Schroeder, F. C., … Fernie, A. R. (2021). Mass spectrometry-based metabolomics: A guide for annotation, quantification and best reporting practices. *Nature Methods*, *18*(7), Article 7. https://doi.org/10.1038/s41592-021-01197-1

Álvarez-Fernández, A., Díaz-Benito, P., Abadía, A., López-Millán, A.-F., & Abadía, J. (2014). Metal species involved in long distance metal transport in plants. *Frontiers in Plant Science*, *5*, 105. https://doi.org/10.3389/fpls.2014.00105

Anthony, M. A., Bender, S. F., & van der Heijden, M. G. A. (2023). Enumerating soil biodiversity. *Proceedings of the National Academy of Sciences*, *120*(33), e2304663120. https://doi.org/10.1073/pnas.2304663120

Arikan, B., Ozfidan-Konakci, C., Yildiztugay, E., Zengin, G., Alp, F. N., & Elbasan, F. (2022). Exogenous hesperidin and chlorogenic acid alleviate oxidative damage induced by arsenic toxicity in Zea mays through regulating the water status, antioxidant capacity, redox balance and fatty acid composition. *Environmental Pollution*, *292*, 118389. https://doi.org/10.1016/j.envpol.2021.118389

Aron, A. T., Petras, D., Schmid, R., Gauglitz, J. M., Büttel, I., Antelo, L., Zhi, H., Nuccio, S.-P., Saak, C. C., Malarney, K. P., Thines, E., Dutton, R. J., Aluwihare, L. I., Raffatellu, M., & Dorrestein, P. C. (2021). Native mass spectrometry-based metabolomics identifies metal-binding compounds. *Nature Chemistry*, 1–10. https://doi.org/10.1038/s41557-021-00803-1

Asher, C. J., & Reay, P. F. (1979). Arsenic Uptake by Barley Seedlings. *Functional Plant Biology*, *6*(4), 459–466. https://doi.org/10.1071/pp9790459

Badri, D. V., & Vivanco, J. M. (2009). Regulation and function of root exudates. *Plant, Cell & Environment*, *32*(6), 666–681. https://doi.org/10.1111/j.1365-3040.2009.01926.x

Bais, H. P., Weir, T. L., Perry, L. G., Gilroy, S., & Vivanco, J. M. (2006). The Role of Root Exudates in Rhizosphere Interactions with Plants and Other Organisms. *Annual Review of Plant Biology*, *57*(1), 233–266. https://doi.org/10.1146/annurev.arplant.57.032905.105159

Beaulieu, M., Bégin, R., Québec (Province), Ministère de l'environnement et de la lutte contre les changements climatiques, Québec (Province), & Direction du programme de réduction des rejets industriels et des lieux contaminés. (2019). *Guide d'intervention: Protection des sols et réhabilitation des terrains contaminés*. http://collections.banq.qc.ca/ark:/52327/3671906

Bell, T. H., Joly, S., Pitre, F. E., & Yergeau, E. (2014). Increasing phytoremediation efficiency and reliability using novel omics approaches. *Trends in Biotechnology*, *32*(5), 271–280. https://doi.org/10.1016/j.tibtech.2014.02.008

Benjamini, Y., & Hochberg, Y. (1995). Controlling the False Discovery Rate: A Practical and Powerful Approach to Multiple Testing. *Journal of the Royal Statistical Society: Series B (Methodological)*, *57*(1), 289–300. https://doi.org/10.1111/j.2517-6161.1995.tb02031.x

Bhargava, A., Carmona, F. F., Bhargava, M., & Srivastava, S. (2012). Approaches for enhanced phytoextraction of heavy metals. *Journal of Environmental Management*, *105*, 103–120. https://doi.org/10.1016/j.jenvman.2012.04.002

Bienert, G. P., Thorsen, M., Schüssler, M. D., Nilsson, H. R., Wagner, A., Tamás, M. J., & Jahn, T. P. (2008). A subgroup of plant aquaporins facilitate the bi-directional diffusion of As(OH)3 and Sb(OH)3across membranes. *BMC Biology*, *6*(1), 26. https://doi.org/10.1186/1741-7007-6-26

Bluemlein, K., Raab, A., & Feldmann, J. (2009). Stability of arsenic peptides in plant extracts: Off-line versus on-line parallel elemental and molecular mass spectrometric detection for liquid chromatographic separation. *Analytical and Bioanalytical Chemistry*, *393*(1), 357–366. https://doi.org/10.1007/s00216-008-2395-z

Bluemlein, K., Raab, A., Meharg, A. A., Charnock, J. M., & Feldmann, J. (2008). Can we trust mass spectrometry for determination of arsenic peptides in plants: Comparison of LC–ICP–MS and

LC–ES-MS/ICP–MS with XANES/EXAFS in analysis of Thunbergia alata. *Analytical and Bioanalytical Chemistry*, *390*(7), 1739–1751. https://doi.org/10.1007/s00216-007-1724-y

Boeckler, G. A., Gershenzon, J., & Unsicker, S. B. (2011). Phenolic glycosides of the Salicaceae and their role as anti-herbivore defenses. *Phytochemistry*, *72*(13), 1497–1509. https://doi.org/10.1016/j.phytochem.2011.01.038

Brechenmacher, L., Lei, Z., Libault, M., Findley, S., Sugawara, M., Sadowsky, M. J., Sumner, L. W., & Stacey, G. (2010). Soybean Metabolites Regulated in Root Hairs in Response to the Symbiotic Bacterium Bradyrhizobium japonicum. *Plant Physiology*, *153*(4), 1808–1822. https://doi.org/10.1104/pp.110.157800

Brereton, N. J. B., Gonzalez, E., Desjardins, D., Labrecque, M., & Pitre, F. E. (2020). Co-cropping with three phytoremediation crops influences rhizosphere microbiome community in contaminated soil. *Science of The Total Environment*, *711*, 135067. https://doi.org/10.1016/j.scitotenv.2019.135067

Cai, Y., Zhou, Z., & Zhu, Z.-J. (2023). Advanced analytical and informatic strategies for metabolite annotation in untargeted metabolomics. *TrAC Trends in Analytical Chemistry*, *158*, 116903. https://doi.org/10.1016/j.trac.2022.116903

Cao, Y., Feng, H., Sun, D., Xu, G., Rathinasabapathi, B., Chen, Y., & Ma, L. Q. (2019). Heterologous Expression of Pteris vittata Phosphate Transporter PvPht1;3 Enhances Arsenic Translocation to and Accumulation in Tobacco Shoots. *Environmental Science & Technology*, *53*(18), 10636–10644. https://doi.org/10.1021/acs.est.9b02082

Carvalhais, L. C., Dennis, P. G., Fedoseyenko, D., Hajirezaei, M.-R., Borriss, R., & von Wirén, N. (2011). Root exudation of sugars, amino acids, and organic acids by maize as affected by nitrogen, phosphorus, potassium, and iron deficiency. *Journal of Plant Nutrition and Soil Science*, *174*(1), 3–11. https://doi.org/10.1002/jpln.201000085

Cary, T. J., Rylott, E. L., Zhang, L., Routsong, R. M., Palazzo, A. J., Strand, S. E., & Bruce, N. C. (2021). Field trial demonstrating phytoremediation of the military explosive RDX by XplA/XplB-expressing switchgrass. *Nature Biotechnology*, 1–4. https://doi.org/10.1038/s41587-021-00909-4

Caspi, R., Billington, R., Fulcher, C. A., Keseler, I. M., Kothari, A., Krummenacker, M., Latendresse, M., Midford, P. E., Ong, Q., Ong, W. K., Paley, S., Subhraveti, P., & Karp, P. D. (2018). The MetaCyc database of metabolic pathways and enzymes. *Nucleic Acids Research*, *46*(D1), D633–D639. https://doi.org/10.1093/nar/gkx935

CEAEQ MA. (2020). Méthode d'analyse, MA. 200 – Mét. 1.2, 2020-05-21 (révision 7). *MA. 200 – Mét. 1.2*. Available online: http://www.ceaeq.gouv.qc.ca/methodes/pdf/MA200Met12.pdf

Cely-Veloza, W., Quiroga, D., & Coy-Barrera, E. (2022). Quinolizidine-Based Variations and Antifungal Activity of Eight Lupinus Species Grown under Greenhouse Conditions. *Molecules*, *27*(1), Article 1. https://doi.org/10.3390/molecules27010305

Cesco, S., Mimmo, T., Tonon, G., Tomasi, N., Pinton, R., Terzano, R., Neumann, G., Weisskopf, L., Renella, G., Landi, L., & Nannipieri, P. (2012). Plant-borne flavonoids released into the rhizosphere: Impact on soil bio-activities related to plant nutrition. A review. *Biology and Fertility of Soils*, *48*(2), 123–149. https://doi.org/10.1007/s00374-011-0653-2

Cesco, S., Neumann, G., Tomasi, N., Pinton, R., & Weisskopf, L. (2010). Release of plant-borne flavonoids into the rhizosphere and their role in plant nutrition. *Plant and Soil*, *329*(1–2), 1–25. https://doi.org/10.1007/s11104-009-0266-9

Chao, D.-Y., Chen, Y., Chen, J., Shi, S., Chen, Z., Wang, C., Danku, J. M., Zhao, F.-J., & Salt, D. E. (2014). Genome-wide Association Mapping Identifies a New Arsenate Reductase Enzyme Critical for Limiting Arsenic Accumulation in Plants. *PLOS Biology*, *12*(12), e1002009. https://doi.org/10.1371/journal.pbio.1002009

Chaparro, J. M., Badri, D. V., Bakker, M. G., Sugiyama, A., Manter, D. K., & Vivanco, J. M. (2013). Root Exudation of Phytochemicals in Arabidopsis Follows Specific Patterns That Are Developmentally Programmed and Correlate with Soil Microbial Functions. *PLOS ONE*, *8*(2), e55731. https://doi.org/10.1371/journal.pone.0055731

Chen, C., Li, S., McKeever, D. R., & Beattie, G. A. (2013). The widespread plant-colonizing bacterial species Pseudomonas syringae detects and exploits an extracellular pool of choline in hosts. *The Plant Journal*, *75*(6), 891–902. https://doi.org/10.1111/tpj.12262

Chen, J., Yoshinaga, M., Garbinski, L. D., & Rosen, B. P. (2016). Synergistic interaction of glyceraldehydes-3-phosphate dehydrogenase and ArsJ, a novel organoarsenical efflux permease, confers arsenate resistance. *Molecular Microbiology*, *100*(6), 945–953. https://doi.org/10.1111/mmi.13371

Chen, Y.-T., Wang, Y., & Yeh, K.-C. (2017). Role of root exudates in metal acquisition and tolerance. *Current Opinion in Plant Biology*, *39*(Supplement C), 66–72. https://doi.org/10.1016/j.pbi.2017.06.004

Chutia, R., Abel, S., & Ziegler, J. (2019). Iron and Phosphate Deficiency Regulators Concertedly Control Coumarin Profiles in Arabidopsis thaliana Roots During Iron, Phosphate, and

Combined Deficiencies. *Frontiers in Plant Science*, *10*. https://www.frontiersin.org/articles/10.3389/fpls.2019.00113

Clemens, S. (2006). Evolution and function of phytochelatin synthases. *Journal of Plant Physiology*, *163*(3), 319–332. https://doi.org/10.1016/j.jplph.2005.11.010

Cobbett, C., & Goldsbrough, P. (2002). Phytochelatins and Metallothioneins: Roles in Heavy Metal Detoxification and Homeostasis. *Annual Review of Plant Biology*, *53*(1), 159–182. https://doi.org/10.1146/annurev.arplant.53.100301.135154

Correa-García, S., Pande, P., Séguin, A., St-Arnaud, M., & Yergeau, E. (2018). Rhizoremediation of petroleum hydrocarbons: A model system for plant microbiome manipulation. *Microbial Biotechnology*. https://doi.org/10.1111/1751-7915.13303

Courchesne, F., Turmel, M.-C., Cloutier-Hurteau, B., Constantineau, S., Munro, L., & Labrecque, M. (2017). Phytoextraction of soil trace elements by willow during a phytoremediation trial in Southern Québec, Canada. *International Journal of Phytoremediation*, *19*(6), 545–554. https://doi.org/10.1080/15226514.2016.1267700

Csardi, G., & Nepusz, T. (2005). The Igraph Software Package for Complex Network Research. *InterJournal*, *Complex Systems*, 1695.

Czech, L., Hermann, L., Stöveken, N., Richter, A. A., Höppner, A., Smits, S. H. J., Heider, J., & Bremer, E. (2018). Role of the Extremolytes Ectoine and Hydroxyectoine as Stress Protectants and Nutrients: Genetics, Phylogenomics, Biochemistry, and Structural Analysis. *Genes*, *9*(4), 177. https://doi.org/10.3390/genes9040177

da Silva Lima, L., Olivares, F. L., Rodrigues de Oliveira, R., Vega, M. R. G., Aguiar, N. O., & Canellas, L. P. (2014). Root exudate profiling of maize seedlings inoculated with Herbaspirillum seropedicaeand humic acids. *Chemical and Biological Technologies in Agriculture*, *1*(1), 23. https://doi.org/10.1186/s40538-014-0023-z

da Silva, R. R., Dorrestein, P. C., & Quinn, R. A. (2015). Illuminating the dark matter in metabolomics. *Proceedings of the National Academy of Sciences*, *112*(41), 12549–12550. https://doi.org/10.1073/pnas.1516878112

Dakora, F. D., & Phillips, D. A. (2002). Root exudates as mediators of mineral acquisition in low-nutrient environments. *Plant and Soil*, *245*(1), 35–47. https://doi.org/10.1023/A:1020809400075

Dary, M., Chamber-Pérez, M. A., Palomares, A. J., & Pajuelo, E. (2010). “In situ” phytostabilisation of heavy metal polluted soils using Lupinus luteus inoculated with metal resistant plant-growth

promoting rhizobacteria. *Journal of Hazardous Materials*, *177*(1), 323–330. https://doi.org/10.1016/j.jhazmat.2009.12.035

Das, S., Chou, M.-L., Jean, J.-S., Yang, H.-J., & Kim, P. J. (2017). Arsenic-enrichment enhanced root exudates and altered rhizosphere microbial communities and activities in hyperaccumulator Pteris vittata. *Journal of Hazardous Materials*, *325*, 279–287. https://doi.org/10.1016/j.jhazmat.2016.12.006

Delnomdedieu, M., Basti, M. M., Otvos, J. D., & Thomas, D. J. (1994). Reduction and binding of arsenate and dimethylarsinate by glutathione: A magnetic resonance study. *Chemico-Biological Interactions*, *90*(2), 139–155. https://doi.org/10.1016/0009-2797(94)90099-X

Dennis, K. K., Uppal, K., Liu, K. H., Ma, C., Liang, B., Go, Y.-M., & Jones, D. P. (2019). Phytochelatin database: A resource for phytochelatin complexes of nutritional and environmental metals. *Database: The Journal of Biological Databases and Curation*, *2019*. https://doi.org/10.1093/database/baz083

Desjardins, D., Brereton, N. J. B., Marchand, L., Brisson, J., Pitre, F. E., & Labrecque, M. (2018). Complementarity of three distinctive phytoremediation crops for multiple-trace element contaminated soil. *Science of The Total Environment*, *610–611*, 1428–1438. https://doi.org/10.1016/j.scitotenv.2017.08.196

Dessureault-Rompré, J., Nowack, B., Schulin, R., & Luster, J. (2006). Modified micro suction cup/rhizobox approach for the in-situ detection of organic acids in rhizosphere soil solution. *Plant and Soil*, *286*(1–2), 99–107. https://doi.org/10.1007/s11104-006-9029-z

Dessureault-Rompré, J., Nowack, B., Schulin, R., Tercier-Waeber, M.-L., & Luster, J. (2008). Metal Solubility and Speciation in the Rhizosphere of Lupinus albus Cluster Roots. *Environmental Science & Technology*, *42*(19), 7146–7151. https://doi.org/10.1021/es800167g

Dhankher, O. P., Rosen, B. P., McKinney, E. C., & Meagher, R. B. (2006). Hyperaccumulation of arsenic in the shoots of Arabidopsis silenced for arsenate reductase (ACR2). *Proceedings of the National Academy of Sciences*, *103*(14), 5413–5418. https://doi.org/10.1073/pnas.0509770102

Dinkelaker, B., Römheld, V., & Marschner, H. (1989). Citric acid excretion and precipitation of calcium citrate in the rhizosphere of white lupin (Lupinus albus L.). *Plant, Cell & Environment*, *12*(3), 285–292. https://doi.org/10.1111/j.1365-3040.1989.tb01942.x

Djoumbou Feunang, Y., Eisner, R., Knox, C., Chepelev, L., Hastings, J., Owen, G., Fahy, E., Steinbeck, C., Subramanian, S., Bolton, E., Greiner, R., & Wishart, D. S. (2016). ClassyFire:

Automated chemical classification with a comprehensive, computable taxonomy. *Journal of Cheminformatics*, *8*(1), 61. https://doi.org/10.1186/s13321-016-0174-y

Dong, N.-Q., & Lin, H.-X. (2021). Contribution of phenylpropanoid metabolism to plant development and plant–environment interactions. *Journal of Integrative Plant Biology*, *63*(1), 180–209. https://doi.org/10.1111/jipb.13054

Dührkop, K., Fleischauer, M., Ludwig, M., Aksenov, A. A., Melnik, A. V., Meusel, M., Dorrestein, P. C., Rousu, J., & Böcker, S. (2019). SIRIUS 4: A rapid tool for turning tandem mass spectra into metabolite structure information. *Nature Methods*, *16*(4), Article 4. https://doi.org/10.1038/s41592-019-0344-8

Dührkop, K., Nothias, L.-F., Fleischauer, M., Reher, R., Ludwig, M., Hoffmann, M. A., Petras, D., Gerwick, W. H., Rousu, J., Dorrestein, P. C., & Böcker, S. (2020). Systematic classification of unknown metabolites using high-resolution fragmentation mass spectra. *Nature Biotechnology*, 1–10. https://doi.org/10.1038/s41587-020-0740-8

Dührkop, K., Shen, H., Meusel, M., Rousu, J., & Böcker, S. (2015). Searching molecular structure databases with tandem mass spectra using CSI:FingerID. *Proceedings of the National Academy of Sciences*, *112*(41), 12580–12585. https://doi.org/10.1073/pnas.1509788112

Edwards, J., Johnson, C., Santos-Medellín, C., Lurie, E., Podishetty, N. K., Bhatnagar, S., Eisen, J. A., & Sundaresan, V. (2015). Structure, variation, and assembly of the root-associated microbiomes of rice. *Proceedings of the National Academy of Sciences*, *112*(8), E911–E920. https://doi.org/10.1073/pnas.1414592112

Elser, D., Pflieger, D., Villette, C., Moegle, B., Miesch, L., & Gaquerel, E. (2023). Evolutionary metabolomics of specialized metabolism diversification in the genus Nicotiana highlights N-acylnornicotine innovations. *Science Advances*, *9*(34), eade8984. https://doi.org/10.1126/sciadv.ade8984

Esteban, E., Carpena, R. O., & Meharg, A. A. (2003). High-affinity phosphate/arsenate transport in white lupin (Lupinus albus) is relatively insensitive to phosphate status. *New Phytologist*, *158*(1), 165–173. https://doi.org/10.1046/j.1469-8137.2003.00713.x

FAO, & ITPS. (2015). Status of the world's soil resources: Main Report. *FAO & ITPS*. http://www.fao.org/3/ a-i5199e.pdf

Faucon, M.-P., Houben, D., & Lambers, H. (2017). Plant Functional Traits: Soil and Ecosystem Services. *Trends in Plant Science*, *22*(5), 385–394. https://doi.org/10.1016/j.tplants.2017.01.005

Finnegan, P., & Chen, W. (2012). Arsenic Toxicity: The Effects on Plant Metabolism. *Frontiers in Physiology*, *3*. https://doi.org/10.3389/fphys.2012.00182

Fitz, W. J., & Wenzel, W. W. (2002). Arsenic transformations in the soil–rhizosphere–plant system: Fundamentals and potential application to phytoremediation. *Journal of Biotechnology*, *99*(3), 259–278. https://doi.org/10.1016/S0168-1656(02)00218-3

Flis, P., Ouerdane, L., Grillet, L., Curie, C., Mari, S., & Lobinski, R. (2016). Inventory of metal complexes circulating in plant fluids: A reliable method based on HPLC coupled with dual elemental and high-resolution molecular mass spectrometric detection. *New Phytologist*, *211*(3), 1129–1141. https://doi.org/10.1111/nph.13964

Frédette, C., Grebenshchykova, Z., Comeau, Y., & Brisson, J. (2019). Evapotranspiration of a willow cultivar (Salix miyabeana SX67) grown in a full-scale treatment wetland. *Ecological Engineering*, *127*, 254–262. https://doi.org/10.1016/j.ecoleng.2018.11.027

Frémont, A., Sas, E., Sarrazin, M., Brisson, J., Pitre, F. E., & Brereton, N. J. B. (n.d.). Arsenic stress triggers active exudation of arsenic-phytochelatin complexes from Lupinus albus roots. *Unpublished*.

Frémont, A., Sas, E., Sarrazin, M., Gonzalez, E., Brisson, J., Pitre, F. E., & Brereton, N. J. B. (2022). Phytochelatin and coumarin enrichment in root exudates of arsenic-treated white lupin. *Plant, Cell & Environment*, *45*(3), 936–954. https://doi.org/10.1111/pce.14163

Fresno, T., Moreno-Jiménez, E., Zornoza, P., & Peñalosa, J. M. (2018). Aided phytostabilisation of As- and Cu-contaminated soils using white lupin and combined iron and organic amendments. *Journal of Environmental Management*, *205*, 142–150. https://doi.org/10.1016/j.jenvman.2017.09.069

Fresno, T., Peñalosa, J. M., Santner, J., Puschenreiter, M., & Moreno-Jiménez, E. (2017). Effect of Lupinus albus L. root activities on As and Cu mobility after addition of iron-based soil amendments. *Chemosphere*, *182*, 373–381. https://doi.org/10.1016/j.chemosphere.2017.05.034

Fresno, T., Peñalosa, J. M., Santner, J., Puschenreiter, M., Prohaska, T., & Moreno-Jiménez, E. (2016). Iron plaque formed under aerobic conditions efficiently immobilizes arsenic in Lupinus albus L roots. *Environmental Pollution*, *216*, 215–222. https://doi.org/10.1016/j.envpol.2016.05.071

Frick, K. M., Foley, R. C., Kamphuis, L. G., Siddique, K. H. M., Garg, G., & Singh, K. B. (2018). Characterization of the genetic factors affecting quinolizidine alkaloid biosynthesis and its response to abiotic stress in narrow-leafed lupin (Lupinus angustifolius L.). *Plant, Cell & Environment*, *41*(9), 2155–2168. https://doi.org/10.1111/pce.13172

Fujimatsu, T., Endo, K., Yazaki, K., & Sugiyama, A. (2020). Secretion dynamics of soyasaponins in soybean roots and effects to modify the bacterial composition. *Plant Direct*, *4*(9), e00259. https://doi.org/10.1002/pld3.259

Gerhardt, K. E., Gerwing, P. D., & Greenberg, B. M. (2017). Opinion: Taking phytoremediation from proven technology to accepted practice. *Plant Science*, *256*, 170–185. https://doi.org/10.1016/j.plantsci.2016.11.016

Ghosh, P., Rathinasabapathi, B., & Ma, L. Q. (2011). Arsenic-resistant bacteria solubilized arsenic in the growth media and increased growth of arsenic hyperaccumulator Pteris vittata L. *Bioresource Technology*, *102*(19), 8756–8761. https://doi.org/10.1016/j.biortech.2011.07.064

Giustarini, D., Tsikas, D., Colombo, G., Milzani, A., Dalle-Donne, I., Fanti, P., & Rossi, R. (2016). Pitfalls in the analysis of the physiological antioxidant glutathione (GSH) and its disulfide (GSSG) in biological samples: An elephant in the room. *Journal of Chromatography B*, *1019*, 21–28. https://doi.org/10.1016/j.jchromb.2016.02.015

Gonzalez, E., Pitre, F. E., & Brereton, N. J. B. (2019). ANCHOR: A 16S rRNA gene amplicon pipeline for microbial analysis of multiple environmental samples. *Environmental Microbiology*, *21*(7), 2440–2468. https://doi.org/10.1111/1462-2920.14632

Gonzalez, E., Pitre, F. E., Pagé, A. P., Marleau, J., Guidi Nissim, W., St-Arnaud, M., Labrecque, M., Joly, S., Yergeau, E., & Brereton, N. J. B. (2018). Trees, fungi and bacteria: Tripartite metatranscriptomics of a root microbiome responding to soil contamination. *Microbiome*, *6*, 53. https://doi.org/10.1186/s40168-018-0432-5

Grenier, V., Gonzalez, E., Brereton, N. J., & Pitre, F. E. (2023). Dynamics of bacterial and archaeal communities during horse bedding and green waste composting. *PeerJ*, *11*, e15239. https://doi.org/10.7717/peerj.15239

Grierson, P. F. (1992). Organic acids in the rhizosphere of Banksia integrifolia L.f. *Plant and Soil*, *144*(2), 259–265. https://doi.org/10.1007/BF00012883

Grill, E., Löffler, S., Winnacker, E.-L., & Zenk, M. H. (1989). Phytochelatins, the heavy-metal-binding peptides of plants, are synthesized from glutathione by a specific γ-glutamylcysteine dipeptidyl transpeptidase (phytochelatin synthase). *Proceedings of the National Academy of Sciences*, *86*(18), 6838–6842. https://doi.org/10.1073/pnas.86.18.6838

Gu, S. L., Fuchigami, L. H., Guak, S. H., & Shin, C. (1996). Effects of short-term water stress, hydrophilic polymer amendment, and antitranspirant on stomatal status, transpiration, water loss, and growth in “better boy” tomato plants. *Journal of the American Society for Horticultural Science*, *121*(5), 831–837. https://doi.org/10.21273/JASHS.121.5.831

Gusiatin, Z. M. (2014). Tannic acid and saponin for removing arsenic from brownfield soils: Mobilization, distribution and speciation. *Journal of Environmental Sciences*, *26*(4), 855–864. https://doi.org/10.1016/S1001-0742(13)60534-3

Ha, S.-B., Smith, A. P., Howden, R., Dietrich, W. M., Bugg, S., O'Connell, M. J., Goldsbrough, P. B., & Cobbett, C. S. (1999). Phytochelatin Synthase Genes from Arabidopsis and the Yeast Schizosaccharomyces pombe. *The Plant Cell*, *11*(6), 1153–1163. https://doi.org/10.1105/tpc.11.6.1153

Haichar, F. el Z., Santaella, C., Heulin, T., & Achouak, W. (2014). Root exudates mediated interactions belowground. *Soil Biology and Biochemistry*, *77*, 69–80. https://doi.org/10.1016/j.soilbio.2014.06.017

Haldar, S., & Sengupta, S. (2015). Plant-microbe Cross-talk in the Rhizosphere: Insight and Biotechnological Potential. *The Open Microbiology Journal*, *9*, 1–7. https://doi.org/10.2174/1874285801509010001

Han, F. X., Su, Y., Monts, D. L., Plodinec, M. J., Banin, A., & Triplett, G. E. (2003). Assessment of global industrial-age anthropogenic arsenic contamination. *Naturwissenschaften*, *90*(9), 395–401. https://doi.org/10.1007/s00114-003-0451-2

Hawkins, C., Ginzburg, D., Zhao, K., Dwyer, W., Xue, B., Xu, A., Rice, S., Cole, B., Paley, S., Karp, P., & Rhee, S. Y. (2021). Plant Metabolic Network 15: A resource of genome-wide metabolism databases for 126 plants and algae. *Journal of Integrative Plant Biology*, *63*(11), 1888–1905. https://doi.org/10.1111/jipb.13163

He, H., Tang, W., Wang, W., & Crits-Christoph, P. (2014). Structural zeroes and zero-inflated models. *Shanghai Archives of Psychiatry*, *26*(4), 236–242. https://doi.org/10.3969/j.issn.1002-0829.2014.04.008

Hirakawa, Y., & Sawa, S. (2019). Diverse function of plant peptide hormones in local signaling and development. *Current Opinion in Plant Biology*, *51*, 81–87. https://doi.org/10.1016/j.pbi.2019.04.005

Hou, D., O'Connor, D., Igalavithana, A. D., Alessi, D. S., Luo, J., Tsang, D. C. W., Sparks, D. L., Yamauchi, Y., Rinklebe, J., & Ok, Y. S. (2020). Metal contamination and bioremediation of agricultural soils for food safety and sustainability. *Nature Reviews Earth & Environment*, *1*(7), Article 7. https://doi.org/10.1038/s43017-020-0061-y

Huang, Z., & Wang, C. (2022). A Review on Differential Abundance Analysis Methods for Mass Spectrometry-Based Metabolomic Data. *Metabolites*, *12*(4), Article 4. https://doi.org/10.3390/metabo12040305

ISCF, Conseil du Trésor du Canada. (2016, October 3). *Inventaire des sites contaminés fédéraux*. https://www.tbs-sct.gc.ca/fcsi-rscf/home-accueil-fra.aspx

Jerbi, A., Brereton, N. J. B., Sas, E., Amiot, S., Lachapelle-T., X., Comeau, Y., Pitre, F. E., & Labrecque, M. (2020). High biomass yield increases in a primary effluent wastewater phytofiltration are associated to altered leaf morphology and stomatal size in Salix miyabeana. *Science of The Total Environment*, *738*, 139728. https://doi.org/10.1016/j.scitotenv.2020.139728

Johansson, E. M., Fransson, P. M. A., Finlay, R. D., & van Hees, P. A. W. (2008). Quantitative analysis of root and ectomycorrhizal exudates as a response to Pb, Cd and As stress. *Plant and Soil*, *313*(1), 39–54. https://doi.org/10.1007/s11104-008-9678-1

Jozefczak, M., Remans, T., Vangronsveld, J., & Cuypers, A. (2012). Glutathione Is a Key Player in Metal-Induced Oxidative Stress Defenses. *International Journal of Molecular Sciences*, *13*(3), Article 3. https://doi.org/10.3390/ijms13033145

Jung, C., Maeder, V., Funk, F., Frey, B., Sticher, H., & Frossard, E. (2003). Release of phenols from Lupinus albus L. roots exposed to Cu and their possible role in Cu detoxification. *Plant and Soil*, *252*(2), 301–312. https://doi.org/10.1023/A:1024775803759

Kapulnik, Y., Joseph, C. M., & Phillips, D. A. (1987). Flavone Limitations to Root Nodulation and Symbiotic Nitrogen Fixation in Alfalfa 1. *Plant Physiology*, *84*(4), 1193–1196. https://doi.org/10.1104/pp.84.4.1193

Karpievitch, Y. V., Nikolic, S. B., Wilson, R., Sharman, J. E., & Edwards, L. M. (2014). Metabolomics Data Normalization with EigenMS. *PLOS ONE*, *9*(12), e116221. https://doi.org/10.1371/journal.pone.0116221

Kaul, A., Mandal, S., Davidov, O., & Peddada, S. D. (2017). Analysis of Microbiome Data in the Presence of Excess Zeros. *Frontiers in Microbiology*, *8*. https://www.frontiersin.org/articles/10.3389/fmicb.2017.02114

Kawasaki, A., Dennis, P. G., Forstner, C., Raghavendra, A. K. H., Mathesius, U., Richardson, A. E., Delhaize, E., Gilliham, M., Watt, M., & Ryan, P. R. (2021). Manipulating exudate composition from root apices shapes the microbiome throughout the root system. *Plant Physiology*, *00*(0), 17.

Kim, H. W., Wang, M., Leber, C. A., Nothias, L.-F., Reher, R., Kang, K. B., van der Hooft, J. J. J., Dorrestein, P. C., Gerwick, W. H., & Cottrell, G. W. (2021). NPClassifier: A Deep Neural Network-Based Structural Classification Tool for Natural Products. *Journal of Natural Products*, *84*(11), 2795–2807. https://doi.org/10.1021/acs.jnatprod.1c00399

Kochian, L. V. (1995). Cellular Mechanisms of Aluminum Toxicity and Resistance in Plants. *Annual Review of Plant Physiology and Plant Molecular Biology*, *46*(1), 237–260. https://doi.org/10.1146/annurev.pp.46.060195.001321

Kol, S., Merlo, M. E., Scheltema, R. A., de Vries, M., Vonk, R. J., Kikkert, N. A., Dijkhuizen, L., Breitling, R., & Takano, E. (2010). Metabolomic Characterization of the Salt Stress Response in Streptomyces coelicolor. *Applied and Environmental Microbiology*, *76*(8), 2574–2581. https://doi.org/10.1128/AEM.01992-09

Kondo, N., Isobe, M., Imai, K., & Goto, T. (1985). Synthesis of Metallothionein-like Peptides Cadystin A and B Occurring in a Fission Yeast, and Their Isomers. *Agricultural and Biological Chemistry*, *49*(1), 71–83. https://doi.org/10.1080/00021369.1985.10866670

Korenblum, E., Dong, Y., Szymanski, J., Panda, S., Jozwiak, A., Massalha, H., Meir, S., Rogachev, I., & Aharoni, A. (2020). Rhizosphere microbiome mediates systemic root metabolite exudation by root-to-root signaling. *Proceedings of the National Academy of Sciences*, *117*(7), 3874–3883. https://doi.org/10.1073/pnas.1912130117

Korenblum, E., Massalha, H., & Aharoni, A. (2022). Plant–microbe interactions in the rhizosphere via a circular metabolic economy. *The Plant Cell*, *34*(9), 3168–3182. https://doi.org/10.1093/plcell/koac163

Kosslak, R. M., Bookland, R., Barkei, J., Paaren, H. E., & Appelbaum, E. R. (1987). Induction of Bradyrhizobium japonicum common nod genes by isoflavones isolated from Glycine max. *Proceedings of the National Academy of Sciences*, *84*(21), 7428–7432. https://doi.org/10.1073/pnas.84.21.7428

Krämer, U. (2010). Metal Hyperaccumulation in Plants. *Annual Review of Plant Biology*, *61*(1), 517–534. https://doi.org/10.1146/annurev-arplant-042809-112156

Lai, Y., Liu, C.-W., Yang, Y., Hsiao, Y.-C., Ru, H., & Lu, K. (2021). High-coverage metabolomics uncovers microbiota-driven biochemical landscape of interorgan transport and gut-brain communication in mice. *Nature Communications*, *12*(1), Article 1. https://doi.org/10.1038/s41467-021-26209-8

Lambers, H., Clements, J. C., & Nelson, M. N. (2013). How a phosphorus-acquisition strategy based on carboxylate exudation powers the success and agronomic potential of lupines (Lupinus, Fabaceae). *American Journal of Botany*, *100*(2), 263–288. https://doi.org/10.3732/ajb.1200474

Lambers, H., Mougel, C., Jaillard, B., & Hinsinger, P. (2009). Plant-microbe-soil interactions in the rhizosphere: An evolutionary perspective. *Plant and Soil*, *321*(1–2), 83–115. https://doi.org/10.1007/s11104-009-0042-x

Lambers, H., Shane, M. W., Cramer, M. D., Pearse, S. J., & Veneklaas, E. J. (2006). Root Structure and Functioning for Efficient Acquisition of Phosphorus: Matching Morphological and Physiological Traits. *Annals of Botany*, *98*(4), 693–713. https://doi.org/10.1093/aob/mcl114

Landi, M., Tattini, M., & Gould, K. S. (2015). Multiple functional roles of anthocyanins in plant-environment interactions. *Environmental and Experimental Botany*, *119*, 4–17. https://doi.org/10.1016/j.envexpbot.2015.05.012

Le Quéré, C., Andrew, R. M., Friedlingstein, P., Sitch, S., Hauck, J., Pongratz, J., Pickers, P. A., Korsbakken, J. I., Peters, G. P., Canadell, J. G., Arneth, A., Arora, V. K., Barbero, L., Bastos, A., Bopp, L., Chevallier, F., Chini, L. P., Ciais, P., Doney, S. C., … Zheng, B. (2018). Global Carbon Budget 2018. *Earth System Science Data*, *10*(4), 2141–2194. https://doi.org/10.5194/essd-10-2141-2018

Lemos Batista, B., Nigar, M., Mestrot, A., Alves Rocha, B., Barbosa Júnior, F., Price, A. H., Raab, A., & Feldmann, J. (2014). Identification and quantification of phytochelatins in roots of rice to long-term exposure: Evidence of individual role on arsenic accumulation and translocation. *Journal of Experimental Botany*, *65*(6), 1467–1479. https://doi.org/10.1093/jxb/eru018

Li, N., Wang, J., & Song, W.-Y. (2016). Arsenic Uptake and Translocation in Plants. *Plant and Cell Physiology*, *57*(1), 4–13. https://doi.org/10.1093/pcp/pcv143

Lin, Y.-F., & Aarts, M. G. M. (2012). The molecular mechanism of zinc and cadmium stress response in plants. *Cellular and Molecular Life Sciences*, *69*(19), 3187–3206. https://doi.org/10.1007/s00018-012-1089-z

Liu, C.-W., & Murray, J. D. (2016). The Role of Flavonoids in Nodulation Host-Range Specificity: An Update. *Plants*, *5*(3), Article 3. https://doi.org/10.3390/plants5030033

Liu, W.-J., Wood, B. A., Raab, A., McGrath, S. P., Zhao, F.-J., & Feldmann, J. (2010). Complexation of Arsenite with Phytochelatins Reduces Arsenite Efflux and Translocation from Roots to Shoots in Arabidopsis. *Plant Physiology*, *152*(4), 2211–2221. https://doi.org/10.1104/pp.109.150862

Liu, X., Fu, J., Da Silva, E., Shi, X., Cao, Y., Rathinasabapathi, B., Chen, Y., & Ma, L. Q. (2017). Microbial siderophores and root exudates enhanced goethite dissolution and Fe/As uptake by As-hyperaccumulator Pteris vittata. *Environmental Pollution*, *223*, 230–237. https://doi.org/10.1016/j.envpol.2017.01.016

Lombi, E., Zhao, F.-J., Fuhrmann, M., Ma, L. Q., & McGrath, S. P. (2002). Arsenic distribution and speciation in the fronds of the hyperaccumulator Pteris vittata. *New Phytologist*, *156*(2), 195–203. https://doi.org/10.1046/j.1469-8137.2002.00512.x

López, J. L., Fourie, A., Poppeliers, S. W. M., Pappas, N., Sánchez-Gil, J. J., de Jonge, R., & Dutilh, B. E. (2023). Growth rate is a dominant factor predicting the rhizosphere effect. *The ISME Journal*, *17*(9), Article 9. https://doi.org/10.1038/s41396-023-01453-6

LSIP1, E. et C. climatique C. (1994). *Environnement et Changement climatique Canada—Évaluation des substances existantes—Première liste de substances d'intérêt prioritaire (LSIP1)*. https://www.ec.gc.ca/ese-ees/default.asp?lang=Fr&n=95D719C5-1

Lucas García, J. A., Barbas, C., Probanza, A., Barrientos, M. L., & Gutierrez Mañero, F. J. (2001). Low molecular weight organic acids and fatty acids in root exudates of two Lupinus cultivars at flowering and fruiting stages. *Phytochemical Analysis: PCA*, *12*(5), 305–311. https://doi.org/10.1002/pca.596

Ma, J. F., Ryan, P. R., & Delhaize, E. (2001). Aluminium tolerance in plants and the complexing role of organic acids. *Trends in Plant Science*, *6*(6), 273–278. https://doi.org/10.1016/S1360-1385(01)01961-6

Ma, J. F., Yamaji, N., Mitani, N., Xu, X.-Y., Su, Y.-H., McGrath, S. P., & Zhao, F.-J. (2008). Transporters of arsenite in rice and their role in arsenic accumulation in rice grain. *Proceedings of the National Academy of Sciences*, *105*(29), 9931–9935. https://doi.org/10.1073/pnas.0802361105

Ma, L. Q., Komar, K. M., Tu, C., Zhang, W., Cai, Y., & Kennelley, E. D. (2001). A fern that hyperaccumulates arsenic. *Nature*, *409*(6820), 579–579. https://doi.org/10.1038/35054664

Maeda, H. A., & Fernie, A. R. (2021). Evolutionary History of Plant Metabolism. *Annual Review of Plant Biology*, *72*(1), 185–216. https://doi.org/10.1146/annurev-arplant-080620-031054

Mahar, A., Wang, P., Ali, A., Awasthi, M. K., Lahori, A. H., Wang, Q., Li, R., & Zhang, Z. (2016). Challenges and opportunities in the phytoremediation of heavy metals contaminated soils: A review. *Ecotoxicology and Environmental Safety*, *126*, 111–121. https://doi.org/10.1016/j.ecoenv.2015.12.023

Mandal, B. K., & Suzuki, K. T. (2002). Arsenic round the world: A review. *Talanta*, *58*(1), 201–235. https://doi.org/10.1016/S0039-9140(02)00268-0

Manna, P., Sinha, M., Pal, P., & Sil, P. C. (2007). Arjunolic acid, a triterpenoid saponin, ameliorates arsenic-induced cyto-toxicity in hepatocytes. *Chemico-Biological Interactions*, *170*(3), 187–200. https://doi.org/10.1016/j.cbi.2007.08.001

Martínez-Alcalá, I., Walker, D. J., & Bernal, M. P. (2010). Chemical and biological properties in the rhizosphere of Lupinus albus alter soil heavy metal fractionation. *Ecotoxicology and Environmental Safety*, *73*(4), 595–602. https://doi.org/10.1016/j.ecoenv.2009.12.009

Matschullat, J. (2000). Arsenic in the geosphere—A review. *Science of The Total Environment*, *249*(1), 297–312. https://doi.org/10.1016/S0048-9697(99)00524-0

McCully, M. E. (1999). ROOTS IN SOIL: Unearthing the Complexities of Roots and Their Rhizospheres. *Annual Review of Plant Physiology and Plant Molecular Biology*, *50*, 695–718. https://doi.org/10.1146/annurev.arplant.50.1.695

McLaughlin, S., Zhalnina, K., Kosina, S., Northen, T. R., & Sasse, J. (2023). The core metabolome and root exudation dynamics of three phylogenetically distinct plant species. *Nature Communications*, *14*(1), Article 1. https://doi.org/10.1038/s41467-023-37164-x

Meharg, A. A., & Hartley-Whitaker, J. (2002). Arsenic uptake and metabolism in arsenic resistant and nonresistant plant species: Tansley review no. 133. *New Phytologist*, *154*(1), 29–43. https://doi.org/10.1046/j.1469-8137.2002.00363.x

Mei, K., Liu, J., Fan, J., Guo, X., Wu, J., Zhou, Y., Lu, H., & Yan, C. (2021). Low-level arsenite boosts rhizospheric exudation of low-molecular-weight organic acids from mangrove seedlings (Avicennia marina): Arsenic phytoextraction, removal, and detoxification. *Science of The Total Environment*, *775*, 145685. https://doi.org/10.1016/j.scitotenv.2021.145685

Meier, K. H. U., Trouillon, J., Li, H., Lang, M., Fuhrer, T., Zamboni, N., Sunagawa, S., Macpherson, A. J., & Sauer, U. (2023). Metabolic landscape of the male mouse gut identifies different niches determined by microbial activities. *Nature Metabolism*, 1–13. https://doi.org/10.1038/s42255-023-00802-1

Mishra, S., Mattusch, J., & Wennrich, R. (2017). Accumulation and transformation of inorganic and organic arsenic in rice and role of thiol-complexation to restrict their translocation to shoot. *Scientific Reports*, *7*(1), Article 1. https://doi.org/10.1038/srep40522

Miyasaka, S. C., Buta, J. G., Howell, R. K., & Foy, C. D. (1991). Mechanism of Aluminum Tolerance in Snapbeans: Root Exudation of Citric Acid. *Plant Physiology*, *96*(3), 737–743. https://doi.org/10.1104/pp.96.3.737

Moreno-Jiménez, E., Esteban, E., Fresno, T., López de Egea, C., & Peñalosa, J. M. (2010). Hydroponics as a valid tool to assess arsenic availability in mine soils. *Chemosphere*, *79*(5), 513–517. https://doi.org/10.1016/j.chemosphere.2010.02.034

Mounicou, S., Szpunar, J., & Lobinski, R. (2009). Metallomics: The concept and methodology. *Chemical Society Reviews*, *38*(4), 1119–1138. https://doi.org/10.1039/B713633C

Müller, J., Boller, T., & Wiemken, A. (2001). Trehalose becomes the most abundant non-structural carbohydrate during senescence of soybean nodules. *Journal of Experimental Botany*, *52*(358), 943–947. https://doi.org/10.1093/jexbot/52.358.943

Nakamura, S., Suzui, N., Nagasaka, T., Komatsu, F., Ishioka, N. S., Ito-Tanabata, S., Kawachi, N., Rai, H., Hattori, H., Chino, M., & Fujimaki, S. (2013). Application of glutathione to roots selectively inhibits cadmium transport from roots to shoots in oilseed rape. *Journal of Experimental Botany*, *64*(4), 1073–1081. https://doi.org/10.1093/jxb/ers388

Nakano, H., Fujii, Y., Yamada, K., Kosemura, S., Yamamura, S., Hasegawa, K., & Suzuki, T. (2002). Isolation and identification of plant growth inhibitors as candidate(s) for allelopathic substance(s), from aqueous leachate from mesquite (Prosopis juliflora (Sw.) DC.) leaves. *Plant Growth Regulation*, *37*(2), 113–117. https://doi.org/10.1023/A:1020579101938

Nakayasu, M., Ohno, K., Takamatsu, K., Aoki, Y., Yamazaki, S., Takase, H., Shoji, T., Yazaki, K., & Sugiyama, A. (2021). Tomato roots secrete tomatine to modulate the bacterial assemblage of the rhizosphere. *Plant Physiology*, *kiab069*. https://doi.org/10.1093/plphys/kiab069

Naujokas, M. F., Anderson Beth, Ahsan Habibul, Aposhian H. Vasken, Graziano Joseph H., Thompson Claudia, & Suk William A. (2013). The Broad Scope of Health Effects from Chronic Arsenic Exposure: Update on a Worldwide Public Health Problem. *Environmental Health Perspectives*, *121*(3), 295–302. https://doi.org/10.1289/ehp.1205875

Návarová, H., Bernsdorff, F., Döring, A.-C., & Zeier, J. (2012). Pipecolic Acid, an Endogenous Mediator of Defense Amplification and Priming, Is a Critical Regulator of Inducible Plant Immunity. *The Plant Cell*, *24*(12), 5123–5141. https://doi.org/10.1105/tpc.112.103564

Navazas, A., Mesa, V., Thijs, S., Fuente-Maqueda, F., Vangronsveld, J., Peláez, A. I., Cuypers, A., & González, A. (2022). Bacterial inoculant-assisted phytoremediation affects trace element uptake and metabolite content in Salix atrocinerea. *Science of The Total Environment*, *820*, 153088. https://doi.org/10.1016/j.scitotenv.2022.153088

Neumann, G., George, T. S., & Plassard, C. (2009). Strategies and methods for studying the rhizosphere—The plant science toolbox. *Plant and Soil*, *321*(1–2), 431–456. https://doi.org/10.1007/s11104-009-9953-9

Neumann, G., & Römheld, V. (1999). Root excretion of carboxylic acids and protons in phosphorus-deficient plants. *Plant and Soil*, *211*(1), 121–130. https://doi.org/10.1023/A:1004380832118

Neumann, G., & Römheld, V. (2007). The Release of Root Exudates as Affected by the Plant Physiological Status. In *The Rhizosphere: Biochemistry and Organic Substances at the Soil-Plant Interface, Second Edition*. https://doi.org/10.1201/9781420005585.ch2

Noctor, G., Mhamdi, A., Chaouch, S., Han, Y., Neukermans, J., Marquez-Garcia, B., Queval, G., & Foyer, C. H. (2012). Glutathione in plants: An integrated overview. *Plant, Cell & Environment*, *35*(2), 454–484. https://doi.org/10.1111/j.1365-3040.2011.02400.x

Nothias, L.-F., Petras, D., Schmid, R., Dührkop, K., Rainer, J., Sarvepalli, A., Protsyuk, I., Ernst, M., Tsugawa, H., Fleischauer, M., Aicheler, F., Aksenov, A. A., Alka, O., Allard, P.-M., Barsch, A., Cachet, X., Caraballo-Rodriguez, A. M., Da Silva, R. R., Dang, T., … Dorrestein, P. C. (2020). Feature-based molecular networking in the GNPS analysis environment. *Nature Methods*, *17*(9), Article 9. https://doi.org/10.1038/s41592-020-0933-6

Oburger, E., Dell'mour, M., Hann, S., Wieshammer, G., Puschenreiter, M., & Wenzel, W. W. (2013). Evaluation of a novel tool for sampling root exudates from soil-grown plants compared to conventional techniques. *Environmental and Experimental Botany*, *87*, 235–247. https://doi.org/10.1016/j.envexpbot.2012.11.007

Oburger, E., & Jones, D. L. (2018). Sampling root exudates – Mission impossible? *Rhizosphere*, *6*, 116–133. https://doi.org/10.1016/j.rhisph.2018.06.004

Oburger, E., & Schmidt, H. (2016). New Methods To Unravel Rhizosphere Processes. *Trends in Plant Science*, *21*(3), 243–255. https://doi.org/10.1016/j.tplants.2015.12.005

Ogle, D., Wheeler, P., & Dinno, A. (2020). *FSA: Fisheries Stock Analysis* [R]. https://github.com/droglenc/FSA (Original work published 2014)

Ohkama-Ohtsu, N., Oikawa, A., Zhao, P., Xiang, C., Saito, K., & Oliver, D. J. (2008). A γ-Glutamyl Transpeptidase-Independent Pathway of Glutathione Catabolism to Glutamate via 5-Oxoproline in Arabidopsis. *Plant Physiology*, *148*(3), 1603–1613. https://doi.org/10.1104/pp.108.125716

Oksanen, J., Blanchet, F. G., Friendly, M., Kindt, R., Legendre, P., McGlinn, D., Minchin, P. R., O'Hara, R. B., Simpson, G. L., Solymos, P., Stevens, M. H. H., Szoecs, E., & Wagner, H. (2019). *vegan: Community Ecology Package* (2.5-6) [Computer software]. https://CRAN.R-project.org/package=vegan

Oleszek, W., & Jurzysta, M. (1987). The allelopathic potential of alfalfa root medicagenic acid glycosides and their fate in soil environments. *Plant and Soil*, *98*(1), 67–80. https://doi.org/10.1007/BF02381728

Pajuelo, E., Rodríguez-Llorente, I. D., & Caviedes, M. A. (2019). Effect of arsenic on legumes: Analysis in the model Medicago truncatula–Ensifer interaction. In *The Model Legume Medicago truncatula* (pp. 268–280). John Wiley & Sons, Ltd. https://doi.org/10.1002/9781119409144.ch33

Pang, J., Bansal, R., Zhao, H., Bohuon, E., Lambers, H., Ryan, M. H., Ranathunge, K., & Siddique, K. H. M. (2018). The carboxylate-releasing phosphorus-mobilizing strategy can be proxied by

foliar manganese concentration in a large set of chickpea germplasm under low phosphorus supply. *New Phytologist*, *219*(2), 518–529. https://doi.org/10.1111/nph.15200

Pang, J., Ryan, M. H., Siddique, K. H. M., & Simpson, R. J. (2017). Unwrapping the rhizosheath. *Plant and Soil*, *418*(1–2), 129–139. https://doi.org/10.1007/s11104-017-3358-y

PASCF, Environnement et Changement climatique Canada. (2023, August 25). *Plan d'action pour les sites contaminés* [Résultats de programmes]. https://www.canada.ca/fr/environnement-changement-climatique/services/sites-contamines-federaux/plan-action.html

Patel, K. S., Pandey, P. K., Martín-Ramos, P., Corns, W. T., Varol, S., Bhattacharya, P., & Zhu, Y. (2023). A review on arsenic in the environment: Contamination, mobility, sources, and exposure. *RSC Advances*, *13*(13), 8803–8821. https://doi.org/10.1039/D3RA00789H

Payá Pérez, A., & Rodríguez Eugenio, N. (2018). *Status of local soil contamination in Europe: Revision of the indicator "Progress in the management contaminated sites in Europe."* Publications Office of the European Union. https://data.europa.eu/doi/10.2760/093804

Pearse, S. J., Veneklaas, E. J., Cawthray, G., Bolland, M. D. A., & Lambers, H. (2007). Carboxylate composition of root exudates does not relate consistently to a crop species' ability to use phosphorus from aluminium, iron or calcium phosphate sources. *New Phytologist*, *173*(1), 181–190. https://doi.org/10.1111/j.1469-8137.2006.01897.x

Peters, G.-J. (2018). *Userfriendlyscience (UFS): Quantitative analysis made accessible*. https://doi.org/10.17605/OSF.IO/TXEQU

Peters, N. K., Frost, J. W., & Long, S. R. (1986). A Plant Flavone, Luteolin, Induces Expression of Rhizobium meliloti Nodulation Genes. *Science*, *233*(4767), 977–980. https://doi.org/10.2307/1697901

Pétriacq, P., Williams, A., Cotton, A., McFarlane, A. E., Rolfe, S. A., & Ton, J. (2017). Metabolite profiling of non-sterile rhizosphere soil. *The Plant Journal*, *92*(1), 147–162. https://doi.org/10.1111/tpj.13639

Peuke, A. D., & Rennenberg, H. (2005). Phytoremediation. *EMBO Reports*, *6*(6), 497–501. https://doi.org/10.1038/sj.embor.7400445

Phillips, D. A., Fox, T. C., King, M. D., Bhuvaneswari, T. V., & Teuber, L. R. (2004). Microbial Products Trigger Amino Acid Exudation from Plant Roots. *Plant Physiology*, *136*(1), 2887–2894. https://doi.org/10.1104/pp.104.044222

Pilon-Smits, E. (2005). Phytoremediation. *Annual Review of Plant Biology*, *56*(1), 15–39. https://doi.org/10.1146/annurev.arplant.56.032604.144214

Pluskal, T., Castillo, S., Villar-Briones, A., & Orešič, M. (2010). MZmine 2: Modular framework for processing, visualizing, and analyzing mass spectrometry-based molecular profile data. *BMC Bioinformatics*, *11*(1), 395. https://doi.org/10.1186/1471-2105-11-395

Podar, D., & Maathuis, F. J. M. (2022). The role of roots and rhizosphere in providing tolerance to toxic metals and metalloids. *Plant, Cell & Environment*, *45*(3), 719–736. https://doi.org/10.1111/pce.14188

Podgorski, J., & Berg, M. (2020). Global threat of arsenic in groundwater. *Science*, *368*(6493), 845–850. https://doi.org/10.1126/science.aba1510

Pons, P., & Latapy, M. (2005). Computing Communities in Large Networks Using Random Walks. In pInar Yolum, T. Güngör, F. Gürgen, & C. Özturan (Eds.), *Computer and Information Sciences—ISCIS 2005* (pp. 284–293). Springer. https://doi.org/10.1007/11569596_31

Provoost, J., Cornelis, C., & Swartjes, F. (2006). Comparison of Soil Clean-up Standards for Trace Elements Between Countries: Why do they differ? *Journal of Soils and Sediments*, *6*(3), 173–181. https://doi.org/10.1065/jss2006.07.169

Queval, G., Jaillard, D., Zechmann, B., & Noctor, G. (2011). Increased intracellular H2O2 availability preferentially drives glutathione accumulation in vacuoles and chloroplasts. *Plant, Cell & Environment*, *34*(1), 21–32. https://doi.org/10.1111/j.1365-3040.2010.02222.x

R Core Team. (2020). *R: A Language and Environment for Statistical Computing* [Computer software]. https://www.R-project.org/

Raab, A., Feldmann, J., & Meharg, A. A. (2004). The Nature of Arsenic-Phytochelatin Complexes in Holcus lanatus and Pteris cretica. *Plant Physiology*, *134*(3), 1113–1122. https://doi.org/10.1104/pp.103.033506

Raab, A., Schat, H., Meharg, A. A., & Feldmann, J. (2005). Uptake, translocation and transformation of arsenate and arsenite in sunflower (Helianthus annuus): Formation of arsenic-phytochelatin complexes during exposure to high arsenic concentrations. *New Phytologist*, *168*(3), 551–558. https://doi.org/10.1111/j.1469-8137.2005.01519.x

Raab, A., Williams, P. N., Meharg, A., & Feldmann, J. (2007). Uptake and translocation of inorganic and methylated arsenic species by plants. *Environmental Chemistry*, *4*(3), 197–203. https://doi.org/10.1071/EN06079

Rahaman, Md. S., Rahman, Md. M., Mise, N., Sikder, Md. T., Ichihara, G., Uddin, Md. K., Kurasaki, M., & Ichihara, S. (2021). Environmental arsenic exposure and its contribution to human diseases, toxicity mechanism and management. *Environmental Pollution*, *289*, 117940. https://doi.org/10.1016/j.envpol.2021.117940

Read, D. B., Bengough, A. G., Gregory, P. J., Crawford, J. W., Robinson, D., Scrimgeour, C. M., Young, I. M., Zhang, K., & Zhang, X. (2003). Plant roots release phospholipid surfactants that modify the physical and chemical properties of soil. *New Phytologist*, *157*(2), 315–326. https://doi.org/10.1046/j.1469-8137.2003.00665.x

Reinhold-Hurek, B., Bünger, W., Burbano, C. S., Sabale, M., & Hurek, T. (2015). Roots shaping their microbiome: Global hotspots for microbial activity. *Annual Review of Phytopathology*, *53*, 403–424. https://doi.org/10.1146/annurev-phyto-082712-102342

Répertoire des terrains contaminés, MELCC. (2023). *Répertoire des terrains contaminés*. https://www.environnement.gouv.qc.ca/sol/terrains/terrains-contamines/recherche.asp

Robe, K., Stassen, M., Chamieh, J., Gonzalez, P., Hem, S., Santoni, V., Dubos, C., & Izquierdo, E. (2021). *Uptake of Fe-fraxetin complexes, an IRT1 independent strategy for iron acquisition in Arabidopsis thaliana* (p. 2021.08.03.454955). bioRxiv. https://doi.org/10.1101/2021.08.03.454955

Robichaud, K., Stewart, K., Labrecque, M., Hijri, M., Cherewyk, J., & Amyot, M. (2019). An ecological microsystem to treat waste oil contaminated soil: Using phytoremediation assisted by fungi and local compost, on a mixed-contaminant site, in a cold climate. *Science of The Total Environment*, *672*, 732–742. https://doi.org/10.1016/j.scitotenv.2019.03.447

Rodríguez Eugenio, N., McLaughlin, M. J., Pennock, D., & Global Soil Partnership. (2018). *Soil pollution: A hidden reality*.

Römheld, V., Müller, C., & Marschner, H. (1984). Localization and Capacity of Proton Pumps in Roots of Intact Sunflower Plants. *Plant Physiology*, *76*(3), 603–606. https://doi.org/10.1104/pp.76.3.603

Ryan, M. H., Tibbett, M., Edmonds-Tibbett, T., Suriyagoda, L. D. B., Lambers, H., Cawthray, G. R., & Pang, J. (2012). Carbon trading for phosphorus gain: The balance between rhizosphere carboxylates and arbuscular mycorrhizal symbiosis in plant phosphorus acquisition. *Plant, Cell & Environment*, *35*(12), 2170–2180. https://doi.org/10.1111/j.1365-3040.2012.02547.x

Ryan, P. R., Delhaize, and E., & Jones, D. L. (2001). Function and Mechanism of Organic Anion Exudation from Plant Roots. *Annual Review of Plant Physiology and Plant Molecular Biology*, *52*(1), 527–560. https://doi.org/10.1146/annurev.arplant.52.1.527

Sas, E., Hennequin, L. M., Frémont, A., Jerbi, A., Legault, N., Lamontagne, J., Fagoaga, N., Sarrazin, M., Hallett, J. P., Fennell, P. S., Barnabé, S., Labrecque, M., Brereton, N. J. B., & Pitre, F. E. (2021). Biorefinery potential of sustainable municipal wastewater treatment using fast-growing

willow. *Science of The Total Environment*, *792*, 148146. https://doi.org/10.1016/j.scitotenv.2021.148146

Sasaki, T., Yamamoto, Y., Ezaki, B., Katsuhara, M., Ahn, S. J., Ryan, P. R., Delhaize, E., & Matsumoto, H. (2004). A wheat gene encoding an aluminum-activated malate transporter. *The Plant Journal*, *37*(5), 645–653. https://doi.org/10.1111/j.1365-313X.2003.01991.x

Sasse, J., Kant, J., Cole, B. J., Klein, A. P., Arsova, B., Schlaepfer, P., Gao, J., Lewald, K., Zhalnina, K., Kosina, S., Bowen, B. P., Treen, D., Vogel, J., Visel, A., Watt, M., Dangl, J. L., & Northen, T. R. (2019). Multilab EcoFAB study shows highly reproducible physiology and depletion of soil metabolites by a model grass. *New Phytologist*, *222*(2), 1149–1160. https://doi.org/10.1111/nph.15662

Sasse, J., Kosina, S. M., Raad, M. de, Jordan, J. S., Whiting, K., Zhalnina, K., & Northen, T. R. (2020). Root morphology and exudate availability are shaped by particle size and chemistry in Brachypodium distachyon. *Plant Direct*, *4*(7), e00207. https://doi.org/10.1002/pld3.207

Sasse, J., Martinoia, E., & Northen, T. (2017). Feed Your Friends: Do Plant Exudates Shape the Root Microbiome? *Trends in Plant Science*. https://doi.org/10.1016/j.tplants.2017.09.003

Scheller, H. V., Huang, B., Hatch, E., & Goldsbrough, P. B. (1987). Phytochelatin Synthesis and Glutathione Levels in Response to Heavy Metals in Tomato Cells. *Plant Physiology*, *85*(4), 1031–1035. https://doi.org/10.1104/pp.85.4.1031

Schenkel, D., Lemfack, M., Piechulla, B., & Splivallo, R. (2015). A meta-analysis approach for assessing the diversity and specificity of belowground root and microbial volatiles. *Frontiers in Plant Science*, *6*. https://www.frontiersin.org/articles/10.3389/fpls.2015.00707

Schmid, N. B., Giehl, R. F. H., Döll, S., Mock, H.-P., Strehmel, N., Scheel, D., Kong, X., Hider, R. C., & Wirén, N. von. (2014). Feruloyl-CoA 6′-Hydroxylase1-Dependent Coumarins Mediate Iron Acquisition from Alkaline Substrates in Arabidopsis. *Plant Physiology*, *164*(1), 160–172. https://doi.org/10.1104/pp.113.228544

Schmid, R., Heuckeroth, S., Korf, A., Smirnov, A., Myers, O., Dyrlund, T. S., Bushuiev, R., Murray, K. J., Hoffmann, N., Lu, M., Sarvepalli, A., Zhang, Z., Fleischauer, M., Dührkop, K., Wesner, M., Hoogstra, S. J., Rudt, E., Mokshyna, O., Brungs, C., … Pluskal, T. (2023). Integrative analysis of multimodal mass spectrometry data in MZmine 3. *Nature Biotechnology*, 1–3. https://doi.org/c

Schmid, R., Petras, D., Nothias, L.-F., Wang, M., Aron, A. T., Jagels, A., Tsugawa, H., Rainer, J., Garcia-Aloy, M., Dührkop, K., Korf, A., Pluskal, T., Kameník, Z., Jarmusch, A. K., Caraballo-Rodríguez, A. M., Weldon, K. C., Nothias-Esposito, M., Aksenov, A. A., Bauermeister, A., …

Dorrestein, P. C. (2021). Ion identity molecular networking for mass spectrometry-based metabolomics in the GNPS environment. *Nature Communications*, *12*(1), 3832. https://doi.org/10.1038/s41467-021-23953-9

Schmid, R., Petras, D., Nothias, L.-F., Wang, M., Aron, A. T., Jagels, A., Tsugawa, H., Rainer, J., Garcia-Aloy, M., Dührkop, K., Korf, A., Pluskal, T., Kameník, Z., Jarmusch, A. K., Caraballo-Rodríguez, A. M., Weldon, K., Nothias-Esposito, M., Aksenov, A. A., Bauermeister, A., … Dorrestein, P. C. (2020). Ion Identity Molecular Networking in the GNPS Environment. *bioRxiv*, 2020.05.11.088948. https://doi.org/10.1101/2020.05.11.088948

Schmidt, P. E. (1994). Nod Factors of Bradyrhizobium japonicum and Rhizobium sp. NGR234 Induce Flavonoid Accumulation in Soybean Root Exudate. *Molecular Plant-Microbe Interactions*, *7*(3), 384. https://doi.org/10.1094/MPMI-7-0384

Schmied-Tobies, M. I. H., Arroyo-Abad, U., Mattusch, J., & Reemtsma, T. (2014). Mass spectrometric detection, identification, and fragmentation of arseno-phytochelatins. *Journal of Mass Spectrometry*, *49*(11), 1148–1155. https://doi.org/10.1002/jms.3435

Schmöger, M. E. V., Oven, M., & Grill, E. (2000). Detoxification of Arsenic by Phytochelatins in Plants. *Plant Physiology*, *122*(3), 793–802.

Schweiger, A. K., Cavender-Bares, J., Townsend, P. A., Hobbie, S. E., Madritch, M. D., Wang, R., Tilman, D., & Gamon, J. A. (2018). Plant spectral diversity integrates functional and phylogenetic components of biodiversity and predicts ecosystem function. *Nature Ecology & Evolution*, *2*(6), Article 6. https://doi.org/10.1038/s41559-018-0551-1

Shaibur, M. R., Kitajima, N., Huq, S. M. I., & Kawai, S. (2009). Arsenic–iron interaction: Effect of additional iron on arsenic-induced chlorosis in barley grown in water culture. *Soil Science and Plant Nutrition*, *55*(6), 739–746. https://doi.org/10.1111/j.1747-0765.2009.00414.x

Sharma, I. (2012). Arsenic induced oxidative stress in plants. *Biologia*, *67*(3). https://doi.org/10.2478/s11756-012-0024-y

Shi, S., Wang, T., Chen, Z., Tang, Z., Wu, Z., Salt, D. E., Chao, D.-Y., & Zhao, F.-J. (2016). OsHAC1;1 and OsHAC1;2 Function as Arsenate Reductases and Regulate Arsenic Accumulation. *Plant Physiology*, *172*(3), 1708–1719. https://doi.org/10.1104/pp.16.01332

Si, C.-L., Xu, J., Kim, J.-K., Bae, Y.-S., Liu, P.-T., & Liu, Z. (2011). Antioxidant properties and structural analysis of phenolic glucosides from bark of Populus ussuriensis Kom. *Wood Science and Technology*, *45*(1), 5–13. https://doi.org/10.1007/s00226-009-0286-x

Song, W.-Y., Mendoza-Cózatl, D. G., Lee, Y., Schroeder, J. I., Ahn, S.-N., Lee, H.-S., Wicker, T., & Martinoia, E. (2014). Phytochelatin–metal(loid) transport into vacuoles shows different

substrate preferences in barley and Arabidopsis. *Plant, Cell & Environment*, *37*(5), 1192–1201. https://doi.org/10.1111/pce.12227

Song, W.-Y., Park, J., Mendoza-Cózatl, D. G., Suter-Grotemeyer, M., Shim, D., Hörtensteiner, S., Geisler, M., Weder, B., Rea, P. A., Rentsch, D., Schroeder, J. I., Lee, Y., & Martinoia, E. (2010). Arsenic tolerance in Arabidopsis is mediated by two ABCC-type phytochelatin transporters. *Proceedings of the National Academy of Sciences*, *107*(49), 21187–21192. https://doi.org/10.1073/pnas.1013964107

Song, W.-Y., Yamaki, T., Yamaji, N., Ko, D., Jung, K.-H., Fujii-Kashino, M., An, G., Martinoia, E., Lee, Y., & Ma, J. F. (2014). A rice ABC transporter, OsABCC1, reduces arsenic accumulation in the grain. *Proceedings of the National Academy of Sciences*, *111*(44), 15699–15704. https://doi.org/10.1073/pnas.1414968111

Strehmel, N., Böttcher, C., Schmidt, S., & Scheel, D. (2014). Profiling of secondary metabolites in root exudates of Arabidopsis thaliana. *Phytochemistry*, *108*, 35–46. https://doi.org/10.1016/j.phytochem.2014.10.003

Stringlis, I. A., de Jonge, R., & Pieterse, C. M. J. (2019). The Age of Coumarins in Plant–Microbe Interactions. *Plant and Cell Physiology*, *60*(7), 1405–1419. https://doi.org/10.1093/pcp/pcz076

Stringlis, I. A., Yu, K., Feussner, K., de Jonge, R., Van Bentum, S., Van Verk, M. C., Berendsen, R. L., Bakker, P. A. H. M., Feussner, I., & Pieterse, C. M. J. (2018). MYB72-dependent coumarin exudation shapes root microbiome assembly to promote plant health. *Proceedings of the National Academy of Sciences*, *115*(22), E5213–E5222. https://doi.org/10.1073/pnas.1722335115

Su, Y. H., McGrath, S. P., Zhu, Y. G., & Zhao, F. J. (2008). Highly efficient xylem transport of arsenite in the arsenic hyperaccumulator Pteris vittata. *New Phytologist*, *180*(2), 434–441. https://doi.org/10.1111/j.1469-8137.2008.02584.x

Sumner, L. W., Amberg, A., Barrett, D., Beale, M. H., Beger, R., Daykin, C. A., Fan, T. W.-M., Fiehn, O., Goodacre, R., Griffin, J. L., Hankemeier, T., Hardy, N., Harnly, J., Higashi, R., Kopka, J., Lane, A. N., Lindon, J. C., Marriott, P., Nicholls, A. W., … Viant, M. R. (2007). Proposed minimum reporting standards for chemical analysis. *Metabolomics*, *3*(3), 211–221. https://doi.org/10.1007/s11306-007-0082-2

Swenson, T. L., Jenkins, S., Bowen, B. P., & Northen, T. R. (2015). Untargeted soil metabolomics methods for analysis of extractable organic matter. *Soil Biology and Biochemistry*, *80*, 189–198. https://doi.org/10.1016/j.soilbio.2014.10.007

Sylvain, B., Mikael, M.-H., Florie, M., Emmanuel, J., Marilyne, S., Sylvain, B., & Domenico, M. (2016). Phytostabilization of As, Sb and Pb by two willow species (S. viminalis and S. purpurea) on former mine technosols. *CATENA*, *136*, 44–52. https://doi.org/10.1016/j.catena.2015.07.008

Talano, M. A., Cejas, R. B., González, P. S., & Agostini, E. (2013). Arsenic effect on the model crop symbiosis Bradyrhizobium–soybean. *Plant Physiology and Biochemistry*, *63*, 8–14. https://doi.org/10.1016/j.plaphy.2012.11.007

Tawaraya, K., Horie, R., Shinano, T., Wagatsuma, T., Saito, K., & Oikawa, A. (2014). Metabolite profiling of soybean root exudates under phosphorus deficiency. *Soil Science and Plant Nutrition*, *60*(5), 679–694. https://doi.org/10.1080/00380768.2014.945390

Tawfeek, N., Mahmoud, M. F., Hamdan, D. I., Sobeh, M., Farrag, N., Wink, M., & El-Shazly, A. M. (2021). Phytochemistry, Pharmacology and Medicinal Uses of Plants of the Genus Salix: An Updated Review. *Frontiers in Pharmacology*, *12*. https://www.frontiersin.org/articles/10.3389/fphar.2021.593856

Teng, Y., Luo, Y., Sun, X., Tu, C., Xu, L., Liu, W., Li, Z., & Christie, P. (2010). Influence of Arbuscular Mycorrhiza and Rhizobium on Phytoremediation by Alfalfa of an Agricultural Soil Contaminated with Weathered PCBs: A Field Study. *International Journal of Phytoremediation*, *12*(5), 516–533. https://doi.org/10.1080/15226510903353120

Tóth, G., Hermann, T., Da Silva, M. R., & Montanarella, L. (2016). Heavy metals in agricultural soils of the European Union with implications for food safety. *Environment International*, *88*, 299–309. https://doi.org/10.1016/j.envint.2015.12.017

Tripathi, R. D., Srivastava, S., Mishra, S., Singh, N., Tuli, R., Gupta, D. K., & Maathuis, F. J. M. (2007). Arsenic hazards: Strategies for tolerance and remediation by plants. *Trends in Biotechnology*, *25*(4), 158–165. https://doi.org/10.1016/j.tibtech.2007.02.003

Tripathi, R. D., Tripathi, P., Dwivedi, S., Dubey, S., Chakrabarty, D., & Trivedi, P. k. (2012). Arsenomics: Omics of arsenic metabolism in plants. *Frontiers in Physiology*, *3*. https://doi.org/10.3389/fphys.2012.00275

Tsednee, M., Yang, S.-C., Lee, D.-C., & Yeh, K.-C. (2014). Root-Secreted Nicotianamine from Arabidopsis halleri Facilitates Zinc Hypertolerance by Regulating Zinc Bioavailability. *Plant Physiology*, *166*(2), 839–852. https://doi.org/10.1104/pp.114.241224

Tsuno, Y., Fujimatsu, T., Endo, K., Sugiyama, A., & Yazaki, K. (2018). Soyasaponins: A New Class of Root Exudates in Soybean (Glycine max). *Plant and Cell Physiology*, *59*(2), 366–375. https://doi.org/10.1093/pcp/pcx192

Tu, S., Ma, L., & Luongo, T. (2004). Root exudates and arsenic accumulation in arsenic hyperaccumulating Pteris vittata and non-hyperaccumulating Nephrolepis exaltata. *Plant and Soil*, *258*(1), 9–19. https://doi.org/10.1023/B:PLSO.0000016499.95722.16

Tyski, S., Markiewicz, M., Gulewicz, K., & Twardowski, T. (1988). The Effect of Lupin Alkaloids and Ethanol Extracts from Seeds of Lupinus angustifolius on Selected Bacterial Strains. *Journal of Plant Physiology*, *133*(2), 240–242. https://doi.org/10.1016/S0176-1617(88)80144-5

Ullrich-Eberius, C. I., Sanz, A., & Novacky, A. J. (1989). Evaluation of Arsenate- and Vanadate-Associated Changes of Electrical Membrane Potential and Phosphate Transport in Lemna gibba G1. *Journal of Experimental Botany*, *40*(1), 119–128. https://doi.org/10.1093/jxb/40.1.119

van Dam, N. M., & Bouwmeester, H. J. (2016). Metabolomics in the Rhizosphere: Tapping into Belowground Chemical Communication. *Trends in Plant Science*, *21*(3), 256–265. https://doi.org/10.1016/j.tplants.2016.01.008

van Santen, J. A., Poynton, E. F., Iskakova, D., McMann, E., Alsup, T. A., Clark, T. N., Fergusson, C. H., Fewer, D. P., Hughes, A. H., McCadden, C. A., Parra, J., Soldatou, S., Rudolf, J. D., Janssen, E. M.-L., Duncan, K. R., & Linington, R. G. (2022). The Natural Products Atlas 2.0: A database of microbially-derived natural products. *Nucleic Acids Research*, *50*(D1), D1317–D1323. https://doi.org/10.1093/nar/gkab941

Vázquez, S., Agha, R., Granado, A., Sarro, M. J., Esteban, E., Peñalosa, J. M., & Carpena, R. O. (2006a). Use of White Lupin Plant for Phytostabilization of Cd and As Polluted Acid Soil. *Water, Air, and Soil Pollution*, *177*(1), 349–365. https://doi.org/10.1007/s11270-006-9178-y

Vázquez, S., Agha, R., Granado, A., Sarro, M. J., Esteban, E., Peñalosa, J. M., & Carpena, R. O. (2006b). Use of White Lupin Plant for Phytostabilization of Cd and As Polluted Acid Soil. *Water, Air, and Soil Pollution*, *177*(1–4), 349–365. https://doi.org/10.1007/s11270-006-9178-y

Vázquez, S., Esteban, E., & Goldsbrough, P. (2005). Arsenate-induced phytochelatins in white lupin: Influence of phosphate status. *Physiologia Plantarum*, *124*(1), 41–49. https://doi.org/10.1111/j.1399-3054.2005.00484.x

Vázquez, S., Goldsbrough, P., & Carpena, R. O. (2009). Comparative analysis of the contribution of phytochelatins to cadmium and arsenic tolerance in soybean and white lupin. *Plant Physiology and Biochemistry*, *47*(1), 63–67. https://doi.org/10.1016/j.plaphy.2008.09.010

Vázquez, S., Moreno, E., & Carpena, R. O. (2008). Bioavailability of metals and As from acidified multicontaminated soils: Use of white lupin to validate several extraction methods. *Environmental Geochemistry and Health*, *30*(2), 193–198. https://doi.org/10.1007/s10653-008-9143-3

Venuti, S., Zanin, L., Marroni, F., Franco, A., Morgante, M., Pinton, R., & Tomasi, N. (2019). Physiological and transcriptomic data highlight common features between iron and phosphorus acquisition mechanisms in white lupin roots. *Plant Science*, *285*, 110–121. https://doi.org/10.1016/j.plantsci.2019.04.026

Vezza, M. E., Llanes, A., Travaglia, C., Agostini, E., & Talano, M. A. (2018). Arsenic stress effects on root water absorption in soybean plants: Physiological and morphological aspects. *Plant Physiology and Biochemistry*, *123*, 8–17. https://doi.org/10.1016/j.plaphy.2017.11.020

Vollmer, W., Blanot, D., & De Pedro, M. A. (2008). Peptidoglycan structure and architecture. *FEMS Microbiology Reviews*, *32*(2), 149–167. https://doi.org/10.1111/j.1574-6976.2007.00094.x

Wang, C., Na, G., Bermejo, E. S., Chen, Y., Banks, J. A., Salt, D. E., & Zhao, F.-J. (2018). Dissecting the components controlling root-to-shoot arsenic translocation in Arabidopsis thaliana. *New Phytologist*, *217*(1), 206–218. https://doi.org/10.1111/nph.14761

Wang, M., Carver, J. J., Phelan, V. V., Sanchez, L. M., Garg, N., Peng, Y., Nguyen, D. D., Watrous, J., Kapono, C. A., Luzzatto-Knaan, T., Porto, C., Bouslimani, A., Melnik, A. V., Meehan, M. J., Liu, W.-T., Crüsemann, M., Boudreau, P. D., Esquenazi, E., Sandoval-Calderón, M., … Bandeira, N. (2016). Sharing and community curation of mass spectrometry data with Global Natural Products Social Molecular Networking. *Nature Biotechnology*, *34*(8), Article 8. https://doi.org/10.1038/nbt.3597

Wang, X., Zhang, J., Lu, X., Bai, Y., & Wang, G. (2023). Two diversities meet in the rhizosphere: Root specialized metabolites and microbiome. *Journal of Genetics and Genomics*. https://doi.org/10.1016/j.jgg.2023.10.004

Wegley Kelly, L., Nelson, C. E., Petras, D., Koester, I., Quinlan, Z. A., Arts, M. G. I., Nothias, L.-F., Comstock, J., White, B. M., Hopmans, E. C., van Duyl, F. C., Carlson, C. A., Aluwihare, L. I., Dorrestein, P. C., & Haas, A. F. (2022). Distinguishing the molecular diversity, nutrient content, and energetic potential of exometabolomes produced by macroalgae and reef-building corals. *Proceedings of the National Academy of Sciences*, *119*(5), e2110283119. https://doi.org/10.1073/pnas.2110283119

Weisskopf, L., Abou-Mansour, E., Fromin, N., Tomasi, N., Santelia, D., Edelkott, I., Neumann, G., Aragno, M., Tabacchi, R., & Martinoia, E. (2006). White lupin has developed a complex

strategy to limit microbial degradation of secreted citrate required for phosphate acquisition. *Plant, Cell & Environment*, *29*(5), 919–927. https://doi.org/10.1111/j.1365-3040.2005.01473.x

Weisskopf, L., Fromin, N., Tomasi, N., Aragno, M., & Martinoia, E. (2005). Secretion activity of white lupin's cluster roots influences bacterial abundance, function and community structure. *Plant and Soil*, *268*(1), 181–194. https://doi.org/10.1007/s11104-004-0264-x

Weisskopf, L., Tomasi, N., Santelia, D., Martinoia, E., Langlade, N. B., Tabacchi, R., & Abou-Mansour, E. (2006). Isoflavonoid exudation from white lupin roots is influenced by phosphate supply, root type and cluster-root stage. *New Phytologist*, *171*(3), 657–668. https://doi.org/10.1111/j.1469-8137.2006.01776.x

Wen, Z., Li, H., Shen, Q., Tang, X., Xiong, C., Li, H., Pang, J., Ryan, M. H., Lambers, H., & Shen, J. (2019). Tradeoffs among root morphology, exudation and mycorrhizal symbioses for phosphorus-acquisition strategies of 16 crop species. *New Phytologist*, *223*(2), 882–895. https://doi.org/10.1111/nph.15833

Wu, F., Xu, F., Ma, X., Luo, W., Lou, L., & Wong, M. H. (2018). Do arsenate reductase activities and oxalate exudation contribute to variations of arsenic accumulation in populations of <Emphasis Type="Italic">Pteris vittata</Emphasis>? *Journal of Soils and Sediments*, 1–9. https://doi.org/10.1007/s11368-018-1987-2

Xu, X. Y., McGrath, S. P., & Zhao, F. J. (2007). Rapid reduction of arsenate in the medium mediated by plant roots. *New Phytologist*, *176*(3), 590–599. https://doi.org/10.1111/j.1469-8137.2007.02195.x

Xun, W., Ren, Y., Yan, H., Ma, A., Liu, Z., Wang, L., Zhang, N., Xu, Z., Miao, Y., Feng, H., Shen, Q., & Zhang, R. (2023). Sustained Inhibition of Maize Seed-Borne Fusarium Using a Bacillus-Dominated Rhizospheric Stable Core Microbiota with Unique Cooperative Patterns. *Advanced Science*, *10*(5), 2205215. https://doi.org/10.1002/advs.202205215

Yan, F., Zhu, Y., Müller, C., Zörb, C., & Schubert, S. (2002). Adaptation of H+-Pumping and Plasma Membrane H+ ATPase Activity in Proteoid Roots of White Lupin under Phosphate Deficiency. *Plant Physiology*, *129*(1), 50–63. https://doi.org/10.1104/pp.010869

Yan, H., Xu, W., Zhang, T., Feng, L., Liu, R., Wang, L., Wu, L., Zhang, H., Zhang, X., Li, T., Peng, Z., Jin, C., Yu, Y., Ping, J., Ma, M., & He, Z. (2022). Characterization of a novel arsenite long-distance transporter from arsenic hyperaccumulator fern Pteris vittata. *New Phytologist*, *233*(6), 2488–2502. https://doi.org/10.1111/nph.17962

Yanitch, A., Brereton, N. J. B., Gonzalez, E., Labrecque, M., Joly, S., & Pitre, F. E. (2017). Transcriptomic Response of Purple Willow (Salix purpurea) to Arsenic Stress. *Frontiers in Plant Science*, *8*. https://doi.org/10.3389/fpls.2017.01115

Yergeau, E., Sanschagrin, S., Maynard, C., St-Arnaud, M., & Greer, C. W. (2014). Microbial expression profiles in the rhizosphere of willows depend on soil contamination. *The ISME Journal*, *8*(2), 344–358. https://doi.org/10.1038/ismej.2013.163

Yergeau, E., Tremblay, J., Joly, S., Labrecque, M., Maynard, C., Pitre, F. E., St-Arnaud, M., & Greer, C. W. (2018). Soil contamination alters the willow root and rhizosphere metatranscriptome and the root–rhizosphere interactome. *The ISME Journal*, 1. https://doi.org/10.1038/s41396-017-0018-4

Zanzarin, D. M., Hernandes, C. P., Leme, L. M., Silva, E., Porto, C., Martin do Prado, R., Meyer, M. C., Favoreto, L., Nunes, E. de O., & Pilau, E. J. (2020). Metabolomics of soybean green stem and foliar retention (GSFR) disease using mass spectrometry and molecular networking. *Rapid Communications in Mass Spectrometry: RCM*, *34 Suppl 3*, e8655. https://doi.org/10.1002/rcm.8655

Zhalnina, K., Louie, K. B., Hao, Z., Mansoori, N., Rocha, U. N. da, Shi, S., Cho, H., Karaoz, U., Loqué, D., Bowen, B. P., Firestone, M. K., Northen, T. R., & Brodie, E. L. (2018). Dynamic root exudate chemistry and microbial substrate preferences drive patterns in rhizosphere microbial community assembly. *Nature Microbiology*, 1. https://doi.org/10.1038/s41564-018-0129-3

Zhang, H., & Selim, H. M. (2008). Reaction and Transport of Arsenic in Soils: Equilibrium and Kinetic Modeling. In *Advances in Agronomy* (Vol. 98, pp. 45–115). Academic Press. https://doi.org/10.1016/S0065-2113(08)00202-2

Zhao, F. J., Wang, J. R., Barker, J. H. A., Schat, H., Bleeker, P. M., & McGrath, S. P. (2003). The role of phytochelatins in arsenic tolerance in the hyperaccumulator Pteris vittata. *New Phytologist*, *159*(2), 403–410. https://doi.org/10.1046/j.1469-8137.2003.00784.x

Zhao, F.-J., Ago, Y., Mitani, N., Li, R.-Y., Su, Y.-H., Yamaji, N., McGrath, S. P., & Ma, J. F. (2010a). The role of the rice aquaporin Lsi1 in arsenite efflux from roots. *New Phytologist*, *186*(2), 392–399. https://doi.org/10.1111/j.1469-8137.2010.03192.x

Zhao, F.-J., Ago, Y., Mitani, N., Li, R.-Y., Su, Y.-H., Yamaji, N., McGrath, S. P., & Ma, J. F. (2010b). The role of the rice aquaporin Lsi1 in arsenite efflux from roots. *New Phytologist*, *186*(2), 392–399. https://doi.org/10.1111/j.1469-8137.2010.03192.x

Zhao, F.-J., McGrath, S. P., & Meharg, A. A. (2010). Arsenic as a Food Chain Contaminant: Mechanisms of Plant Uptake and Metabolism and Mitigation Strategies. *Annual Review of Plant Biology*, *61*(1), 535–559. https://doi.org/10.1146/annurev-arplant-042809-112152

Zhao, J. (2015). Flavonoid transport mechanisms: How to go, and with whom. *Trends in Plant Science*, *20*(9), 576–585. https://doi.org/10.1016/j.tplants.2015.06.007

Zhao, Ma, J. F., Meharg, A. A., & McGrath, S. P. (2009). Arsenic uptake and metabolism in plants. *New Phytologist*, *181*(4), 777–794. https://doi.org/10.1111/j.1469-8137.2008.02716.x

Zheng, Q., Hu, Y., Kosina, S. M., Van Goethem, M. W., Tringe, S. G., Bowen, B. P., & Northen, T. R. (2023). Conservation of beneficial microbes between the rhizosphere and the cyanosphere. *New Phytologist*, *240*(3), 1246–1258. https://doi.org/10.1111/nph.19225

Zhu, X. F., Zheng, C., Hu, Y. T., Jiang, T., Liu, Y., Dong, N. Y., Yang, J. L., & Zheng, S. J. (2011). Cadmium-induced oxalate secretion from root apex is associated with cadmium exclusion and resistance in Lycopersicon esulentum. *Plant, Cell & Environment*, *34*(7), 1055–1064. https://doi.org/10.1111/j.1365-3040.2011.02304.x

Zhu, Y.-G., & Rosen, B. P. (2009). Perspectives for genetic engineering for the phytoremediation of arsenic-contaminated environments: From imagination to reality? *Current Opinion in Biotechnology*, *20*(2), 220–224. https://doi.org/10.1016/j.copbio.2009.02.011

Ziegler, J., Schmidt, S., Chutia, R., Müller, J., Böttcher, C., Strehmel, N., Scheel, D., & Abel, S. (2016). Non-targeted profiling of semi-polar metabolites in Arabidopsis root exudates uncovers a role for coumarin secretion and lignification during the local response to phosphate limitation. *Journal of Experimental Botany*, *67*(5), 1421–1432. https://doi.org/10.1093/jxb/erv539

Zu, Y., Li, Z., Mei, X., Wu, J., Cheng, S., Jiang, Y., & Li, Y. (2018). Transcriptome analysis of main roots of Panax notoginseng identifies genes involved in saponin biosynthesis under arsenic stress. *Plant Gene*, *16*, 1–7. https://doi.org/10.1016/j.plgene.2018.08.001

Zuffa, S., Schmid, R., Bauermeister, A., Gomes, P. W. P., Caraballo-Rodriguez, A. M., Abiead, Y. E., Aron, A. T., Gentry, E. C., Zemlin, J., Meehan, M. J., Avalon, N. E., Cichewicz, R. H., Buzun, E., Terrazas, M. C., Hsu, C.-Y., Oles, R., Ayala, A. V., Zhao, J., Chu, H., … Dorrestein, P. C. (2023). *A Taxonomically-informed Mass Spectrometry Search Tool for Microbial Metabolomics Data* (p. 2023.07.20.549584). bioRxiv. https://doi.org/10.1101/2023.07.20.549584